STRENGTHENING OF POST-TENSIONED AND REINFORCED CONCRETE BEAMS BY BONDING EXTERNAL STEEL PLATES

by

WEIMIN LUO

B.E. (Hons) (P.R. China)

Thesis submitted for the degree of
Master of Engineering Science
at the University of Adelaide
(Department of Civil Engineering)
Australia

- January 1993 -

CONTENTS

Synopsis

This is a preliminary study of both post-tensioned and reinforced concrete beams that were strengthened by bonding external steel plates to their soffits, and reinforced concrete beams that were strengthened by bonding plates to their sides and soffits. Four post-tensioned plated beams, in which the degrees of the prestressing forces were varied, were tested to failure. A computer program was developed to carry out parametric studies on this type of beam. The results of the analytical models were compared with the experimental test results. Thirteen plated reinforced concrete beams were tested to failure in shear. Conditions varied consisted of: the thickness of the soffit plate, the length of the side plate, the thickness of the side plate and the areas of the tensile reinforcement. The effects of these parameters on the shear strength of reinforced concrete beams and their debonding moments were investigated.

STATEMENT OF ORIGINALITY

This work contains no material which has been accepted for the award of any other degree or diploma in any university or other tertiary institution and, to the best of my knowledge and belief, contains no material previously published or written by another person, except where due reference has been made in the text.

I give consent to this copy of my thesis , when deposited in the University Library, being available for loan and photocopying.

SIGNED: **DATE:** Jan. 28 1993

ACKNOWLEDGMENTS

The work described in thesis was carried out at the University of Adelaide under the supervision of Dr. Deric J. Oehlers. The author is deeply indebted to Dr. Oehlers for his excellent guidance and enthusiastic supervision throughout this research, and for his review of the thesis. The work is impossible without his interest and dedication.

The author is thankful for the help of the staff in the Civil Engineering and Laboratory, and for the valuable friendship provided by fellow post-graduate students over the period of his candidature.

The author is extremely grateful to his parents, brother and his uncle, Mr. W.H. Yen, for their love, encouragement and continual support throughout the years.

Finally, the author wishes to thank all his friends, whose support and friendship made this possible.

Notation

A_{ci} = area of a concrete layer

A_g = gross area of concrete section

A_p = area of steel plate

A_{ps} = area of prestressing steel

A_{sc} = cross-sectional area of compressive reinforcement

A_{st} = cross-sectional area of tensile reinforcement

b = the width of beam

b_p = the width of steel plate

C_1 = a coefficient

C_2 = a moment ratio

d = the depth of beam

d_c = the depth of the resultant forces of the concrete layers

d_{ci} = the depth of a concrete layer

d_e = the effective depth of reinforced concrete beam

d_{ni} = depth to neutral axis of strain

d_p = depth to steel plate

d_{ps} = depth to prestressing steel

d_{sc} = depth to compression reinforcement

d_{sec} = the depth of the resultant forces of reinforcements and concrete layers

d_{st} = depth to tensile reinforcement

d_t = depth of transformed concrete section

D_b = diameter of tension reinforcement

D_t = diameter of compression reinforcement

D_{ps} = diameter of prestressing tendon

E_c = modulus of elasticity of concrete

E_p = modulus of elasticity of steel plate

E_{ps} = modulus of elasticity of prestressing steel

E_s = modulus of elasticity of steel

$(EI)_b$ = flexural rigidity of beam

$(EI)_{sp}$ = flexural rigidity of reinforced concrete beam with both soffit and side plates based on the linear elastic analysis, ie., the tensile strength of concrete is zero

$(EI)_{sec}$ = secant bending stiffness

f_b = Brazilian tensile strength of concrete

f_c = compressive strength of concrete

f_{ci} = force in a concrete layer

f_{cu} = the cube strength of plain concrete

f_f = flexural tensile strength of concrete

f_t = split tensile strength of concrete

F_p = force in steel plate

F_{ps} = force in prestressing steel

F_{res} = resultant force in section

F_{sec} = resultant forces of concrete layers

F_{sc} = force in compressive reinforcement

F_{st} = force in tensile reinforcement

h = distance from neutral axis to the interface of concrete and plate

I_g = second moment of area of gross concrete section

I_t = second moment of area for the transformed concrete section

k_a = longitudinal or axial constant

k_c = curvature constant

k_{up} = constant

L_o = length of test concrete beam

L_1 = effective span of tested concrete beam

L_p = length of soffit plate

L_{sp} = the length of side plate

m_p = modular ratio, E_p/E_c

m_{ps} = modular ratio, E_{ps}/E_c

m_s = modular ratio, E_s/E_c

M = bending moment in the middle of beam

M_d = debonding moment

M_e = moment at the end of steel plate

M_G = dead load moment

M_{pl} = predicted peeling moment

M_{sc} = characteristic predicted serviceability peeling moment

M_{sp} = the ultimate peeling moment of reinforced concrete beam with both soffit and side plates

M_{sec} = bending moment for segment n

M_{uc} = characteristic predicted ultimate peeling moment

M_{ue} = experimentally determined ultimate peeling moment

M_{up} = the ultimate peeling moment at the plate-end

n = number of layers in section

P_i = force in prestressing steel just after transfer

P_v = the vertical component of the prestressing force

S_s = longitudinal shear at the interface of the soffit plate and concrete beam

t_p = thickness of the soffit steel plate

t_{sp} = thickness of the side plate

$(V_{in})_{st}$ = the increase in shear strength of the reinforced concrete beam due to the full soffit plating

$(V_{in})_{sp}$ = the increase in shear strength of the reinforced concrete beam due to the side plates

V_o = the shear force which would occur at the section when the bending moment at that section was equal to the decompression moment, Mo,

which is the moment that causes the concrete stress in the bottom fibre to reduce to zero

V_p = shear force in a beam when beam was failed

V_{sp} = shear strength of reinforced concrete beam with external side plates

V_{uc} = shear strength of reinforced concrete beam without stirrups

$(V_{uc})_o$ = average shear strength of beam without vertical reinforcements in tests

$(V_{uc})_p$ = shear strength of the fully plated reinforced concrete beam in terms of AS 3600

$(V_{up})_{st}$ = shear strength of the fully plated reinforced concrete beam without stirrups

y_i = distance from concrete layer i to reference axis

y_p = distant from centroid of the soffit plate to neutral axis of the plated section

y_{sec} = depth of resultant forces of concrete layers

σ_b = stress in concrete bottom fibre

σ_c = stress in concrete

σ_{ci} = average stress in a concrete layer

σ_p = stress in steel plate

σ_{ps} = stress in prestressing steel

σ_{sc} = stress in compressive reinforcing steel

σ_{st} = stress in tensile reinforcing steel

σ_t = stress in concrete top fibre

ε = strain

ε_b = strain in bottom fibre of concrete

ε_o = strain of concrete when ultimate stress f_c is reached

ε_c = strain in concrete

ε_{ce} = concrete strain at the tendon level due to effective prestressing force

ε_{ci} = average strain in a concrete layer

ε_{crack} = strain of concrete at cracking

ε_{ct} = tensile strain in the concrete

ε_{cu} = ultimate compressive strain in concrete

ε_{cps} = concrete strain at the tendon level due to the applied moment

ε_i = initial strain in the top fibre of section due to the initial prestressing forces

ε_p = strain in steel plate

ε_{ps} = tensile strain in prestressing steel

ε_s = strain in steel reinforcement

ε_{sc} = strain in compressive reinforcing steel

ε_{st} = strain in tensile reinforcing steel

ε_t = strain in top fibre of concrete

ε_y = yield strain of steel reinforcement

θ = curvature

θ_i = initial curvature in the section due to the prestressing force

θ_o = curvature at zero moment for prestressing beam

ρ = steel reinforcement ratio in the section

$\Delta\theta_i$ = the change in curvature after the external soffit plate has been bonded to the prestressed concrete beam

Chapter One

Literature Review

1.1 INTRODUCTION

Existing concrete structures may, for a variety reasons, be found to be unsatisfactory. Research has shown that over one half of the approximately 600,000 bridges in the United States are more than 30 years old, with a large number of them needing rehabilitation and twelve thousand of these bridges, on average, attain their 50 year design life every year [1]. The technique of strengthening concrete structures in situ by bonding external steel plates to concrete surfaces using epoxy resins is recognised to be an effective and convenient method because the operations can be carried out relatively quickly and simply even though the structure is still in use, as shown in Fig.1-1. It can be used not only to improve the flexural performance of structures as it increases the strength and rigidity, but also reduces the flexural crack width in the concrete. This technique has been used widely in various parts of the world, such as South Africa, Japan, Switzerland, Poland, France, Belgium and United Kingdom [2].

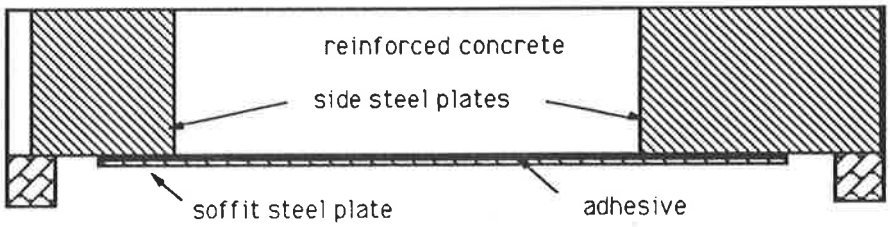

Fig.1-1 Plated reinforced concrete beam

A problem associated with this technique is peeling at the either end of the soffit steel plate due to stress concentrations induced by the discontinuity of the plate, as shown in Fig.1-2. In general, there are two distinct forms of peeling that can occur in reinforced concrete beam with externally soffit plate; flexural peeling which is induced by increasing curvature and associated with a gradual separation of the steel plate; and shear peeling which is induced by the formation of shear diagonal cracks

and associated with rapid separation of the soffit plate [3]. Much research [2-14] has gone into studying premature failure due to separation between the steel plate and the reinforced concrete member which will be refereed to as debonding.

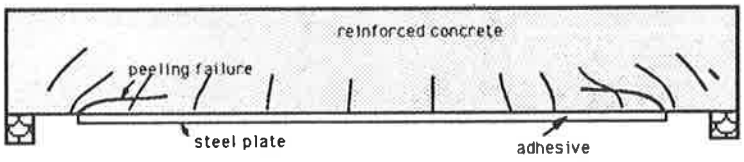

Fig.1-2 Reinforced concrete beam with soffit plate

1.2. RESEARCH OF PLATED REINFORCED CONCRETE MEMBERS

1.2.1. Research by Deric John Oehlers and John Paul Moran [3]

Oehlers and Moran studied the flexural peeling stresses on the serviceability and ultimate strength of upgraded concrete beams. The forces at the steel-plate/concrete-beam interface that cause the plate to debond are shown in Fig.1-3.

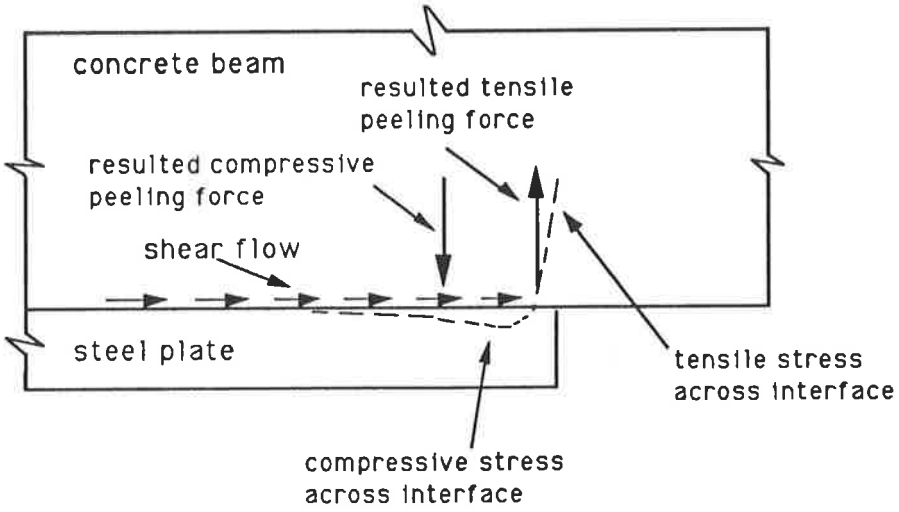

Fig.1-3 Debonding forces

The theoretically derived flexural peeling moment at which the flexural peeling starts and the plate separates from the reinforced concrete beam is based on isotropic material properties. This method, which depends on the flexural rigidity of the plated cracked concrete beam, the thickness of the plate, and the tensile strength of concrete, can be used to adjust the size of and the extent of plating so that the flexural peeling does not occur under the design load.

The predicted ultimate peeling moment, which is associated with the separation of the soffit plate from the reinforced concrete beam, is given by the following equation:

$$M_{up} = \frac{(EI)_{cp} f_b}{0.474 E_p t_p} \tag{1-1}$$

where, $(EI)_{cp}$ is the flexural rigidity of cracked plated section that is based on a linear elastic analysis and assumes that the tensile strength of the concrete is zero, f_b is Brazilian tensile strength of concrete, E_p is Young's modulus of plate steel and t_p is thickness of the plate. The only physical limitation of equation (1-1) is that the width of steel plate must be not great than that of the flexural member.

It should be noted that loads resisted by the reinforced concrete beam whilst it is being plated do not contribute to the ultimate peeling moment, M_{up}.

The probability of flexural peeling occurring can be reduced by ensuring that the external moment at the end of the plate does not exceed the following ultimate and serviceability characteristic strength which are based on the 5% probability of failure level.

$$M_{uc} = \frac{(EI)_{cp} f_b}{0.901 E_p t_p} \tag{1-2}$$

$$M_{sc} = \frac{(EI)_{cp} f_b}{1.86 E_p t_p} \tag{1-3}$$

Results of forty-four plated beams tested by Moran and thirteen beams tested by Moloney as shown in Fig.1-4. In the majority of cases, plates covered the full width

of the members. The results show that the experimental scatter above Eq.(1-1) which has a coefficient of variation of 0.283.

In conclusion, it was suggested that the above equations are applicable to the plated beams subjected to shear and flexure, but not to beams in which shear diagonal cracks have occurred. The peeling strength was found to be dependent on the flexural rigidity of the cracked plated section, the tensile strength of the concrete, and the thickness of the plate, and was independent of the previous loading history of the beam, the initial curvature of the beam, and the method of clamping the plate to the beam on gluing.

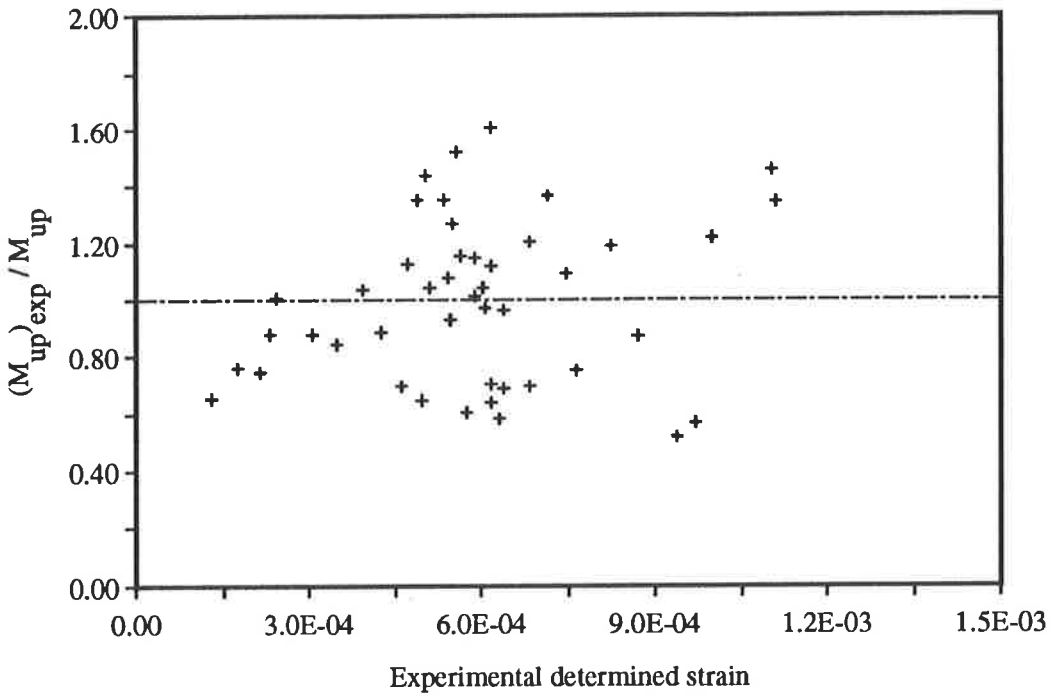

Fig. 1-4 Accuracy of ultimate peeling moment (Eq.1-1)

1.2.2. Research by D. J. Oehlers [4]

The shearing peeling and the interaction between shear and flexural peeling has been studied by Oehlers. From the experimental test results, it would suggest that the shear peeling is function of the shear strength of the concrete beam without stirrups which is a strength that can be found in most Codes of Practice. Therefore, it is the formation of the diagonal shear crack in the unplated region adjacent to the plate-end that induces shear peeling and not shear failure of the reinforced flexural beam. In other words, debonding at the plate-ends due to shear forces is neither influenced by the presence of stirrups in the section nor controlled by the shear flow along the steel-plate/concrete-beam interface. It is suggested that limiting the shear stress at the end of the interface between the steel-plate and concrete section would be a poor method of preventing debonding due to shear force. Furthermore, it has also been found that there is very strong interaction between debonding due to shear forces and peeling due to flexural forces, as shown in Fig.1-5.

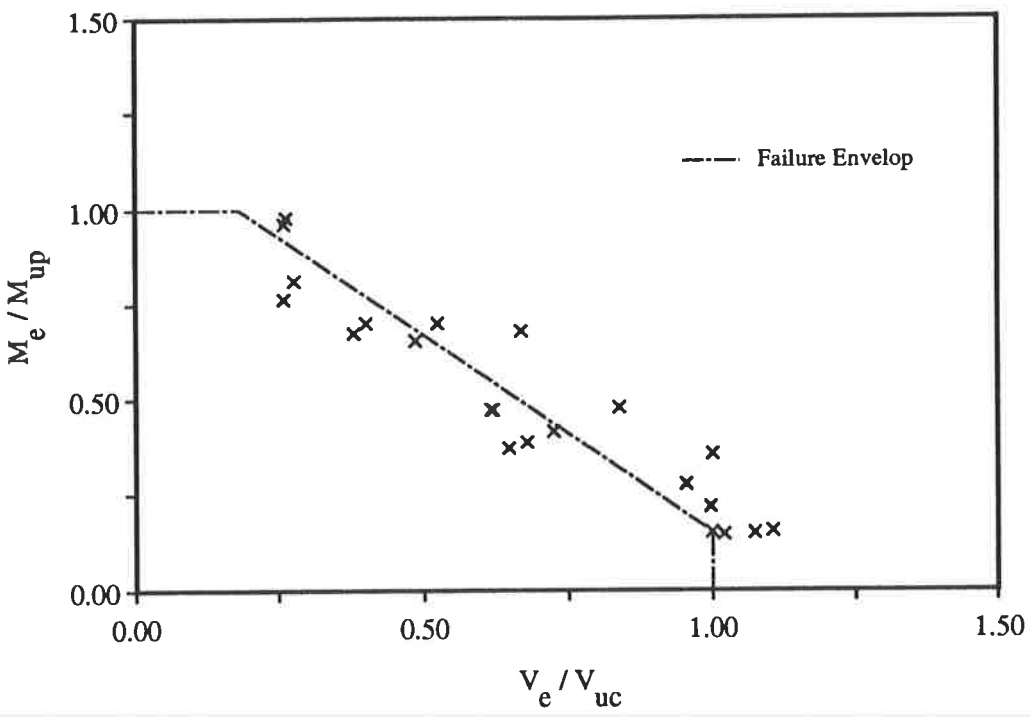

Fig. 1-5 Interaction between shear and flexural peeling

A design rule is recommended below:

$$\frac{M_e}{M_{up}} + \frac{V_e}{V_{uc}} \leq 1.17 \qquad (1\text{-}4)$$

where, M_e is the moment at the end of the plate, that is being applied to the plated reinforced beam, so that if the reinforced concrete beam was resisting a moment whilst it was being plated then this moment would not be included in M_e, V_e is the total shear force being applied to the structure at the plate-end being considered, V_{uc} is the shear strength of the flexural member without stirrups as can be determined from most Codes of Practice and M_{up} is the predicted ultimate peeling moment, as described in Sect. 1.2.1

1.2.3 Research by T. M. Roberts and H. Haji-kazemi (5-7)

An analytical solution derived from a theoretical investigation for predicting the displacements, strains and stresses in reinforced concrete beams that are strengthened on the tension faces with externally bonded steel plates, has been presented by authors. Results obtained for practical dimensions and material properties indicated that the shear and normal stress, in and adjacent to the adhesive layer, as shown in Fig.1-6, increase rapidly towards the ends of the steel plates and depend on the shear and normal stiffness of the connection and on the thickness and points of termination of the steel plates.

It was suggested that the high normal stresses in particular are consistent with the premature peeling or tensile failure of the concrete cover as the thickness of the steel plate is increased. Therefore, the use of anchor bolts would not be expected to reduce significantly the magnitude of the normal stresses nor to substantially

increase the strength of plated beams. The use of anchor bolts does, however, increase the ductility of plated beams.

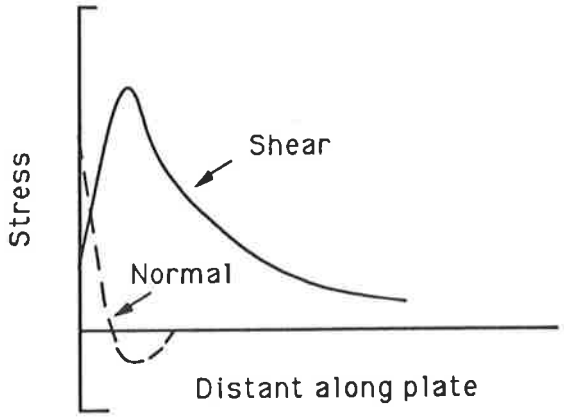

Fig.1-6 Shear and normal stresses at end of adhesive joint

Roberts suggested that it should be possible to establish simple practical failure criteria based on the predicted stress distribution due to combinations of shear, normal and axial stresses for bond failure, for failure of the adhesive and for failure of the adjacent concrete. From an analysis of the test results presented by Jones et al, the authors recommended that failure of adhesive bonded steel plates is likely to occur at shear stresses between 3 and 5 N/mm^2, combined with normal stresses between 1 and 2 N/mm^2, but these limits depend on the strength of concrete, epoxy adhesive and the method of surface preparation.

1.2.4 Research by G. F. J. Monoley (8)

Moloney used an isotropic finite element analysis to determine the parameters that affect peeling and to formulate a prediction equation. It was found that the peeling forces at the end of a plate were induced by the curvature of the beam and by the

longitudinal strain in the concrete adjacent to the plate. The predicted peeling moment could be derived from the following equation:

$$M_{pl} = \frac{(EI)_{cp} f_t}{k_c E_p t_p + k_a E_p h} \qquad (1\text{-}5)$$

where $(EI)_{cp}$ is the flexural rigidity of the plated cracked section, f_t is the indirect tensile strength of the concrete (splitting strength), k_c is the curvature constant, k_a is the longitudinal or axial constant and h is the distance from the neutral-axial to the interface of the concrete and the steel plate. The ultimate peeling moment is defined as the moment at which a horizontal crack caused the plate to completely separate from the reinforced concrete section and the serviceability peeling moment is defined as the moment at which the horizontal peeling crack first formed through the width of the beam.

Twenty plated reinforced concrete beams, in which the width of the soffit steel plates was the same as that of beams, were tested in flexural. The external steel plate was terminated in constant moment region. From a comparison of the constants k_c and k_a that were derived from the experimental tests, it was concluded that the effect of curvature on peeling was much more significant than the longitudinal effect. It was felt that this occurred because the flexural cracks adjacent to the plate-end reduced significantly the longitudinal strain in the concrete adjacent to the plate, so that the above prediction equation can be reduced to:

$$M_{pl} = \frac{(EI)_{cp} f_{ct}}{k_c E_p t_p} \qquad (1\text{-}6)$$

1.2.5 Research by R. P. Johnson and C. J. Tait [9]

The influence on the short-term ultimate strength of plated concrete beams, of the stress concentration that occurs in the concrete adjacent to each end of the plate has been studied by Johnson and Tait. The main variable investigated in the tests was the ratio of the length of the plate to the length of the cantilever reinforced concrete beam. Sixteen plated reinforced concrete beams , which were subjected to bending and shear and axial tension, were tested by Tait.

They recommend that for a member with a linear bending moment diagram between the points of zero and maximum moment, the plate should extend over eighty per cent of the region in tension. Because the stress concentration at the end of the plate weaked the beam at that cross-section and a vertical crack always formed in this region.

Tests showed that the stress concentration at the end of a plate reduced the shear strength of the section. Tait recommended that the ACI-ASCE design method [10] for determining ultimate strength in vertical shear of the concrete member at the plate-end was unsafe for the plated members because of the stress concentration induced by the plate-end. Therefore, the shear strength of a beam at the end of a plate may be reduce to half the value of the unplated beam.

1.2.6 Research by R. N. Swamy, R. Jones et al [2, 11-14]

Research had been carried out in order to investigate the behaviour of plated beams under short-term loading and to establish design criteria by authors. The main parameters of the plated reinforced concrete beams that were investigated were: plate thickness, glue thickness, layered plates, lapped plates, variations in glue thickness, and the presence of stress concentration in the adhesive. The beams were tested in

flexure to failure with all the plates extending beyond the constant moment region. The test results showed that the addition of a plate increased the range of the elastic behaviour, increased the ultimate flexural capacity and increased the ductility at flexural failure, and also enhanced flexural stiffness while controlling cracking and deformation at all loads level until failure. For a given concrete section and glue thickness, it was suggested that there is a limiting area of plate beyond which a flexural failure will change into shear or combined flexural-shear failure. With a short shear spans (shear span-effective depth ratio less than two), steel plates glued to the tension face of beam increase stiffness, but do not improve the shear capacity. In order to ensure that premature brittle shear/bond failure does not occur before the fully flexural strength is reached and also to ensure ductility, two tentative design criteria are presented for the plated reinforced concrete beams:

$$\frac{b_p}{t_p} > 50 \qquad (1\text{-}7)$$

and

$$\frac{d_n}{d_e} < 0.4 \qquad (1\text{-}8)$$

where b_p is the width of the plate, t_p is the thickness of the plate, d_n is the depth of the neutral axial and d_e is the effective depth of section.

The authors also pointed out that the anchorage zone at the ends of the soffit plates has played a critical role in determining the failure load. The rate of plate strain build-up in the anchorage zone increased as the plate thickness was reduced. The use of bolts did not prevent debonding and glued anchor plates produce the best performance with thick plates. The results from the tests showed that at the ends of the plates interface stress concentrations exist, which have limiting peak values in the region of $\sqrt{2} \times$ tensile splitting strength of the concrete. However, theoretical interface bond stresses, based on simple elastic behaviour, are found to have no

consistent relationship to the measured peak values. In order to achieve the full theoretical flexural strength, together with ductile behaviour, they suggest that more detailed research into the mechanism of glued anchor plates is required.

1.2.7 Research by M. D. Macdonald [15]

A series of 3.5m long reinforced concrete beams, which were subjected to 4-point bending, have been studied by Macdonald. From experimental results, it was suggested that narrow plates permitted the development of sufficient horizontal shear stress to cause a concrete beam failure. However wide plates remained bonded to the beam at the maximum sustained load and produce a soft failure because wide plates not only reduced the horizontal shear stress in the concrete but also reduced peeling stress due to their lower inherent stiffness. In general, the external plates increased the maximum sustained load by 40 per cent for both plated as-cast and plated precracked. It was found that an average increase in stiffness of the plated precracked reinforced concrete beams is approximately 1.3 times than that of the plated as-cast beams. Macdonald recommended that the type of failure caused by rapid shear failure of the concrete can be prevented by the selection of plate with suitable width and thickness, namely, the plate proportion (b_p/t_p) had a optimum value for these test beams of

$$\frac{b_p}{t_p} = 60 \qquad (1\text{-}9)$$

1.3 Comparison of design criteria and recommendations

All of researchers agreed that as the thickness of steel plate increased, failure by the separation between the reinforcement concrete and the plate more readily occurred. A comparison of the design criteria and recommendations are given in Table 1.1 below:

Table 1.1 A Comparison of design Rules

Authors	Design criteria and recommendations
D.J. Oelhers [3]	$M_{up} = \frac{(EI)_{cp} f_b}{0.474 E_p t_p}$ (flexural) $\frac{M_e}{M_{up}} + \frac{V_e}{V_{uc}} \geq 1.17$ (flexural/shear) $V_p < V_{uc}$ (shear)
M. Roberts [6]	Limiting the shear stresses, combined with normal stresses at the end of plate.
D. Macdonald [15]	$\frac{b_p}{t_p} = 60$
N. Swamy and R.N. Jones [2]	$\frac{b_p}{t_p} > 50$ $\frac{d_n}{d_e} < 0.4$

Chapter Two

Experimental work

2.1 Introduction

The use of bolts at the end of the soffit plate does not prevent debonding, as described in Sect.1.2.3 and Sect.1.2.6, also little benefit was achieved by the use of tapered or multiplate systems. Therefore, the following experimental work has been carried out in order to prevent debonding of the soffit plate due to peeling cracks as described in Sect. 1.2.1 and Sect.1.2.2.

The theoretical analyses described in Sect.1.2.1 and Sect.1.2.3 indicate that the steel plate separates from the soffit of the reinforced concrete beam because of the high local interface bond stresses and peeling forces at the end of the plate. Therefore, the anchorage detail at the plate-end has a considerable effect on the ultimate strength and mode of failure of reinforced concrete beam. From previous research [2], it was shown that there are two distinct forms of peeling which can occur: shear peeling, induced by the formation of the shear diagonal crack and which is associated with rapid separation of the plate; and flexural peeling, induced by increasing curvature, and associated with a gradual separation of the soffit plate. Debonding of the soffit plate, in the plated reinforced concrete beam, due to the shear forces is not influenced by the amounts of the presence of stirrups and only depends upon the shear strength of the concrete members without the stirrups.

In this experimental work, steel plates were glued to the sides and soffits of reinforced concrete beams as shown in Fig.2-1. The reason for the use of the side plates in the experimental work was to restrict the formation of inclined shear cracks in the vicinity of the end of soffit plate and hence to increase the shear strength of the concrete beam without stirrups and therefore to prevent debonding of the soffit plate by shear peeling.

Four series of plated reinforced concrete beams in the Group One were tested to failure in shear. The parameters varied consisted of: the length of the side plates; the thickness of both the side and soffit plates; and the quantity of longitudinal tensile steel reinforcement in the concrete section.

A preliminary study of the plated post-tensioned concrete beams was also carried out in the experimental work. Four post-tensioned beams in the Group Two were tested to failure in flexure. The parameter varied was the degree of the initial prestressing forces that were applied to the sections. The main aim of this series was to investigate the effect of the initial prestressing forces on the debonding moment.

2.2 Specimens and Test Rig

Two groups of plated reinforced concrete beams were tested in the experimental work. The general arrangement of the test rigs, together with the beam description are given in Fig.2-1 and in Fig.2-2. The beams were simply supported at each end as shown in Fig.2-1. The load was applied to the top of the beam by a hand pumped hydraulic jack through a load cell and knife edge bearing.

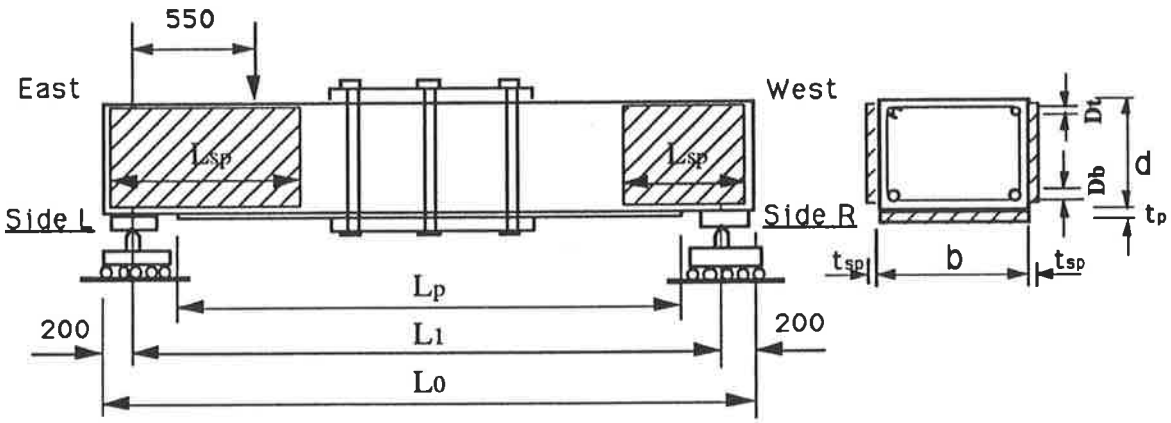

Fig.2-1 The general arrangement of the test rig and description of the beam in the group one

Thirteen plated reinforced concrete beams in Group One were divided into four series. They were tested to failure in shear. Both shear spans of the plated beams were tested, which was achieved by clamping the adjacent shear span, as shown in Fig.2-1. There was a minimal number of the stirrups in each beam; each beam had three stirrups to hold the longitudinal reinforcement in position and were placed at the ends of the beams and at mid-span so that they were well away from the peeling regions. From the geometry of the loading arrangement, the maximum shear load in the shear span beams tested is approximately 71 per cent of the total applied load. The ratio of the distant between the position of the applied load and support, ie. 550 mm in Fig.2.1, to the depth of the beam is greater than 3 in order to avoid the increase in shear strength due to short span tied arching action.

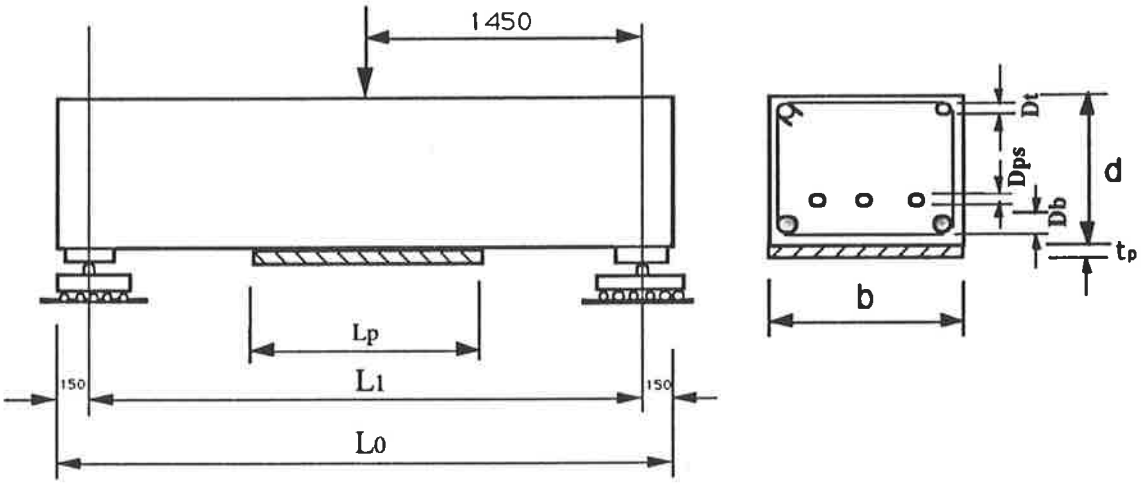

Fig.2-2 The general arrangement of the test rig and description of the beam in the group two

There were four plated post-tensioned beams in Group Two. The ends of the plate were terminated in the flexure-shear region as shown in Fig.2-2. The mild steel plates were glued to the soffits of the beams after a beam had been prestressed. The position of the applied load was in the mid-span of the beam as shown in Fig.2-2. The moment at the ends of the steel plate was approximately 65 per cent of that in the mid-span of beam section.

2.2.1 Series 1

The main aim in series 1 is to investigate the increase of the shear strength in the reinforced concrete beam due to the side plates. These beams were made without stirrups and were plated with both soffit and side plates. Four beams were tested to failure in shear. The main variation is the length of the side plates L_{sp} in Fig.2-1. The length of side plates varies from 0.0 mm, ie. without side plates, to 690.0 mm, as shown in Table 2.1. The test rig is shown in the Fig.2-1. Both shear spans of the plated reinforced concrete beam were tested and this was achieved by clamping the adjacent shear span as shown in Fig.2-1. The shear load in the shear span being tested is approximately 71 per cent of the total applied load. The position of the electrical strain gauges and displacement dial gauge is shown in Fig.2-3 and Fig 2-4, respectively.

Table 2.1 Geometric properties of the beams in the series 1

Specimen	Side	L_{sp} (mm)	b (mm)	d (mm)	D_t (mm)	D_b (mm)	t_p (mm)	L_o (mm)	L_1 (mm)	L_p (mm)	t_{sp} (mm)
SP/S1	L	0.0	130	180	10.0	16.0	5.0	2290	1890	1590	4.0
SP/S1	R	360.0	130	180	10.0	16.0	5.0	2290	1890	1590	4.0
SP/S2	L	0.0	130	180	10.0	16.0	5.0	2290	1890	1590	4.0
SP/S2	R	180.0	130	180	10.0	16.0	5.0	2290	1890	1590	4.0
SP/S3	L	90.0	130	180	10.0	16.0	5.0	2290	1890	1590	4.0
SP/S3	R	540.0	130	180	10.0	16.0	5.0	2290	1890	1590	4.0
SP/S4	L	690.0	130	180	10.0	16.0	5.0	2290	1890	1590	4.0
SP/S4	R	270.0	130	180	10.0	16.0	5.0	2290	1890	1590	4.0

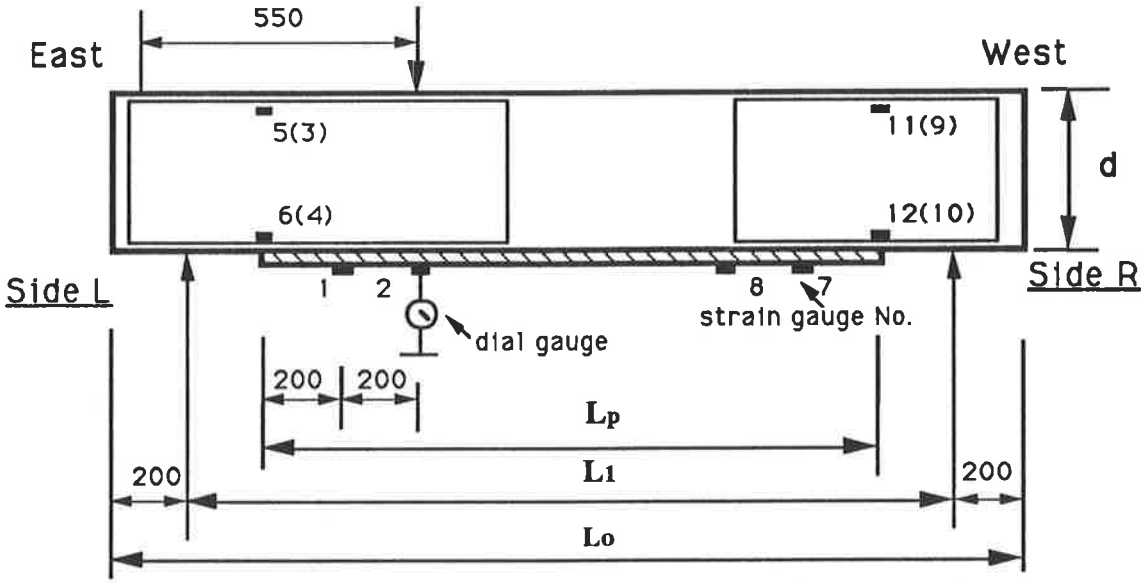

Fig.2-3 Beam geometry and instrumentations applied in the series 1

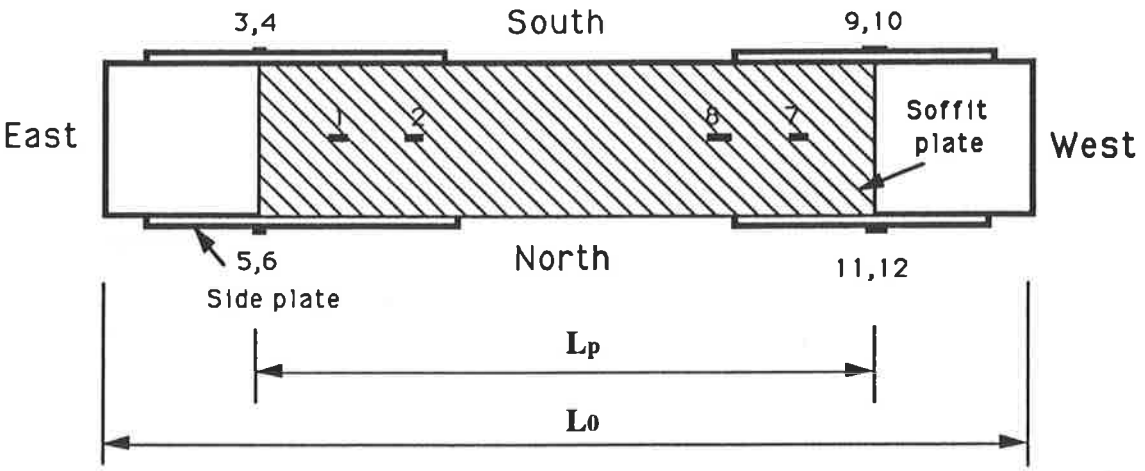

Fig.2-4 Plan of the beam in the series 1

2.2.2 Series 2

The main purpose of this series is to investigate the increase in the shear strength of reinforced concrete beams due to the external soffit plate. In order to prevent premature failure due to debonding the plates were glued along the entire length of beam as shown in Fig.2-5. Four beams were tested to failure. The main variation in the series is the thickness of the soffit plates. The geometric properties of series 2 are given in Table 2.2. Both shear spans of a beam were tested to failure and this was achieved by clamping the adjacent shear span, as shown in Fig.2-1. The position of electrical strain gauges and displacement dial gauge is shown in Fig.2-5 and Fig.2-6, respectively. The test rig is shown in the Fig.2.1.

Table 2.2 Geometric properties of the beams in the series 2

Specimen	t_p (mm)	L_{sp} (mm)	b (mm)	d (mm)	D_t (mm)	D_b (mm)	L_0 (mm)	L_1 (mm)	L_p (mm)	t_{sp} (mm)
FP/B1/L	0.0	-	130	180	10.0	16.0	2290	1890	2290	-
FP/B1/R	0.0	-	130	180	10.0	16.0	2290	1890	2290	-
FP/B2/L	3.0	-	130	180	10.0	16.0	2290	1890	2290	-
FP/B2/R	3.0	-	130	180	10.0	16.0	2290	1890	2290	-
FP/B3/L	5.0	-	130	180	10.0	16.0	2290	1890	2290	-
FP/B3/R	5.0	-	130	180	10.0	16.0	2290	1890	2290	-
FP/B4/L	10.0	-	130	180	10.0	16.0	2290	1890	2290	-
FP/B4/R	10.0	-	130	180	10.0	16.0	2290	1890	2290	-

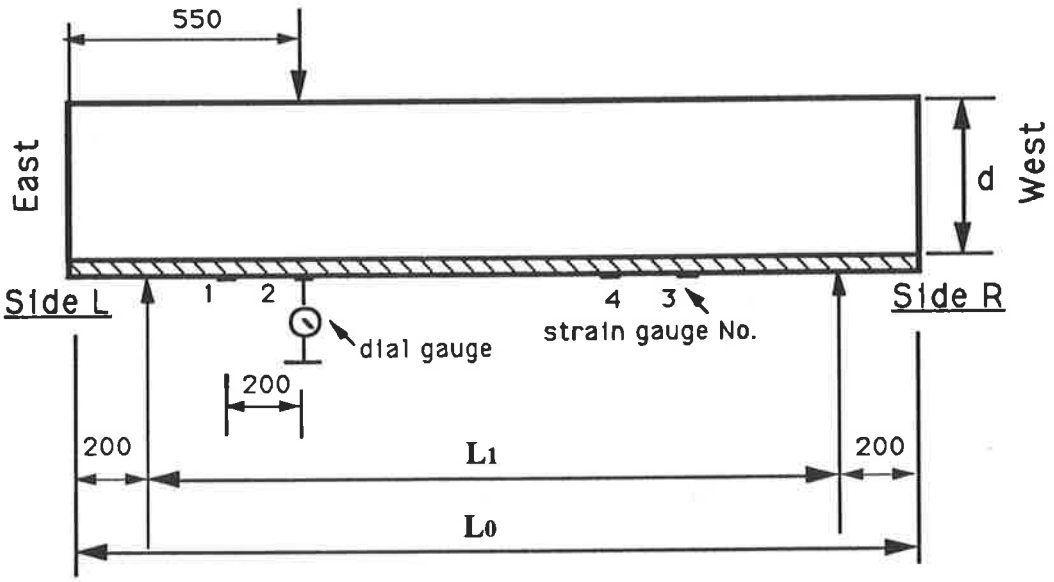

Fig.2-5 Beam geometry and instrumentations applied in the series 2

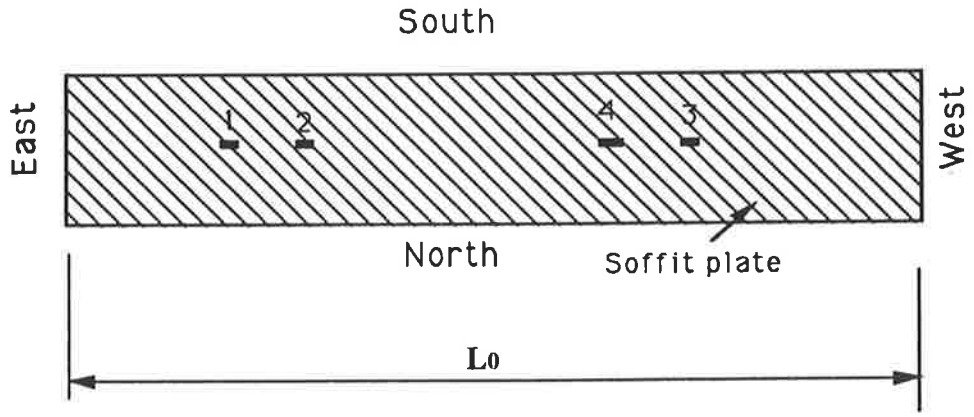

Fig.2-6 Plan of the beam in the series 2

2.2.3 Series 3

The main task of this series is to investigate the effect of varying the longitudinal reinforcement in beam with side plates. Two beams were tested to failure in shear. The length of side plates (L_{sp} = 690 mm) is constant in this series. The geometric properties of this series are given in Table 2.3. The beams tested were without stirrups. Both shear spans of the beam were tested to failure so that the strength with the side plates could be compared with the strength without the side plates. The test rig is shown in the Fig.2-1. The position of the electrical resistant strain gauges and displacement dial gauge is shown in Fig.2-7 and Fig.2-8, respectively.

Table 2.3 Geometric properties of the beams in the series 3

Specimen	A_{st} (mm^2)	L_{sp} (mm)	b (mm)	d (mm)	D_t (mm)	D_b (mm)	L_o (mm)	L_1 (mm)	L_p (mm)	t_{sp} (mm)
SP/S8/L	157	-	130	180	10.0	10.0	2290	1890	1750	-
SP/S8/R	157	690	130	180	10.0	10.0	2290	1890	1750	4.0
SP/S9/L	628	-	130	180	10.0	20.0	2290	1890	1750	-
SP/S9/R	628	690	130	180	10.0	20.0	2290	1890	1750	4.0

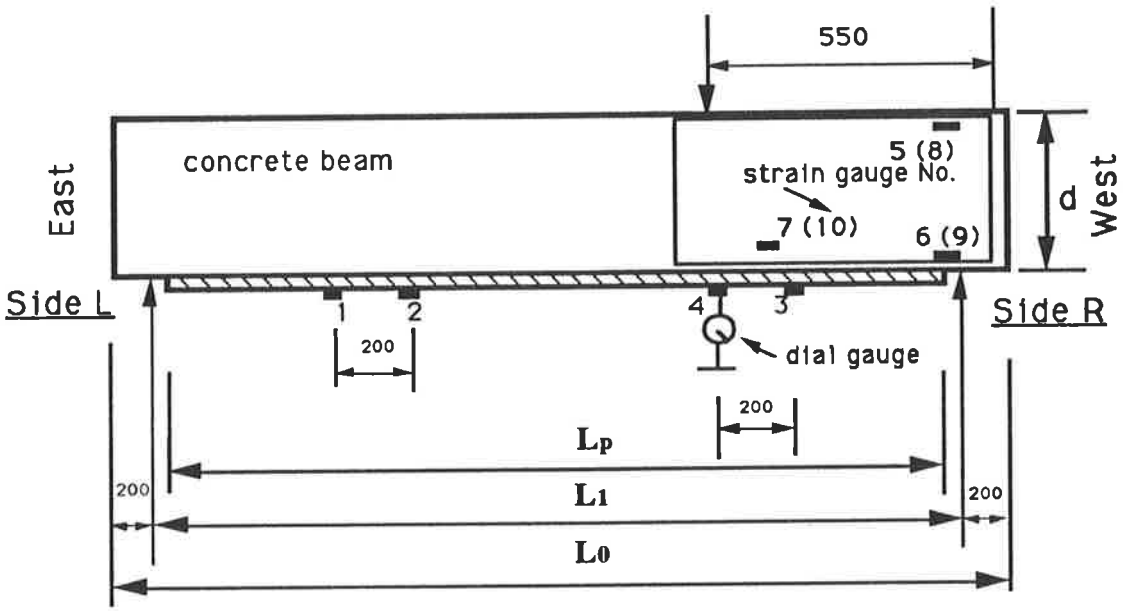

Fig.2-7 Beam geometry and instrumentations applied in the series 3

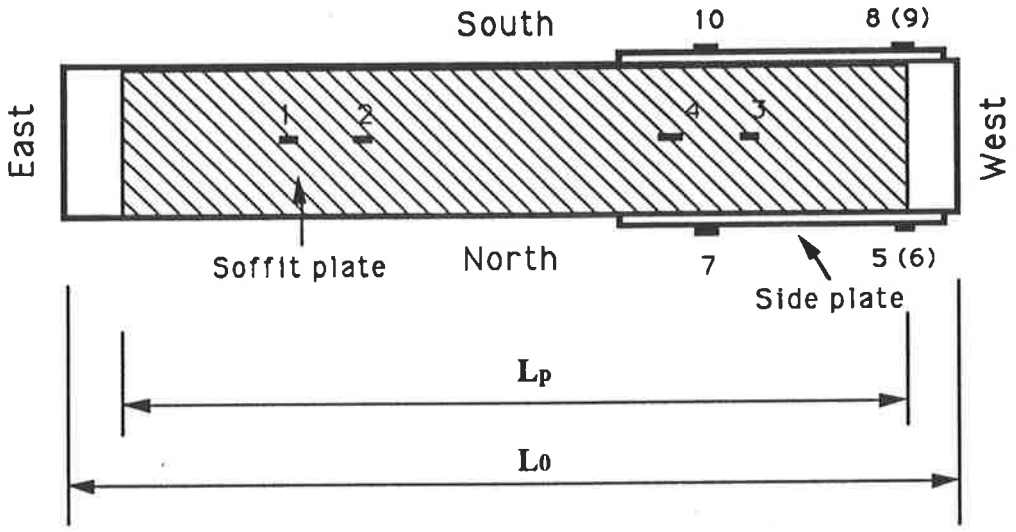

Fig.2-8 Plan of the beam in the series 3

2.2.4 Series 4

The main target of this series is to investigate the variation of the shear strength in the reinforced concrete beams due to the external side plates as shown in Fig.2-9. Three beams were tested to failure. The geometric properties of this series are given in Table 2.4. The main variation in the series is the thickness of the side plates. The plated reinforced concrete beams tested were without stirrups. The side plates shown in Fig.2-9 were extended to the middle span of the beam in order to ensure that debonding of the side plates did not occur. Also the side plates were folded round the edge of the beam end, as shown in Fig.2-10, to ensure that debonding did not take place. Both shear spans of the beam were tested to failure as in previous series. The position of the electrical resistant strain gauges and displacement dial gauge is shown in Fig.2-9 and Fig.2-10, respectively. The test rig is also shown in Fig.2-1.

Table 2.4 Geometric properties of the beams in the series 4

Specimen	Side	t_{sp} (mm)	L_{sp} (mm)	b (mm)	d (mm)	D_t (mm)	D_b (mm)	t_p (mm)	L_0 (mm)	L_1 (mm)	L_p (mm)
SP/S5	L	0.0	0.0	130	180	10.0	16.0	5.0	2290	1890	1750
SP/S5	R	1.0	1250	130	180	10.0	16.0	5.0	2290	1890	1750
SP/S6	L	0.0	0.0	130	180	10.0	16.0	5.0	2290	1890	1750
SP/S6	R	2.0	1250	130	180	10.0	16.0	5.0	2290	1890	1750
SP/S7	L	0.0	0.0	130	180	10.0	16.0	5.0	2290	1890	1750
SP/S7	R	3.0	1250	130	180	10.0	16.0	5.0	2290	1890	1750

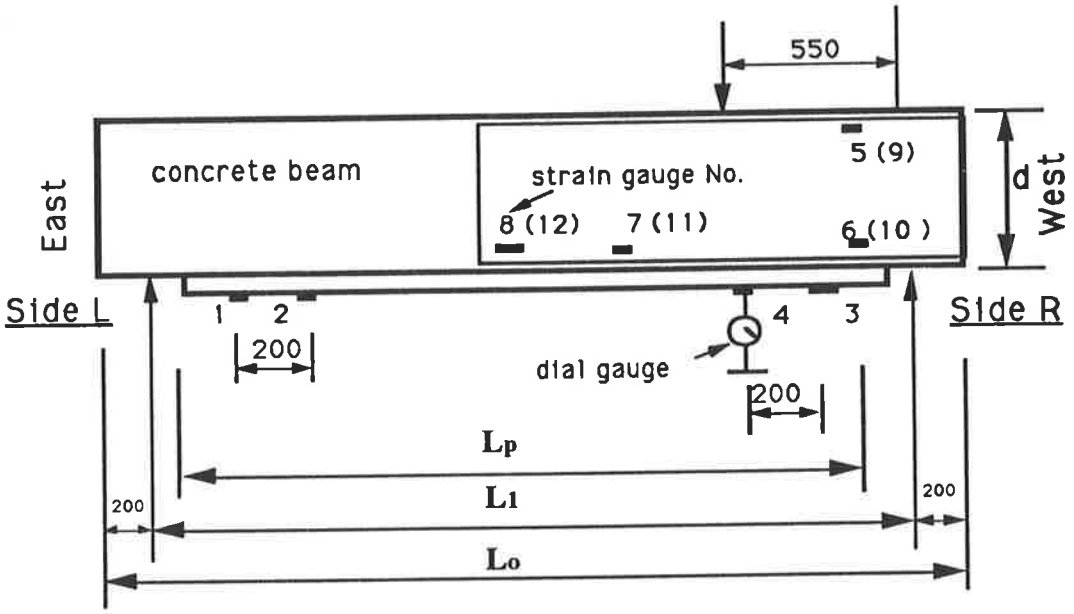

Fig.2-9 Beam geometry and instrumentations applied in the series 4

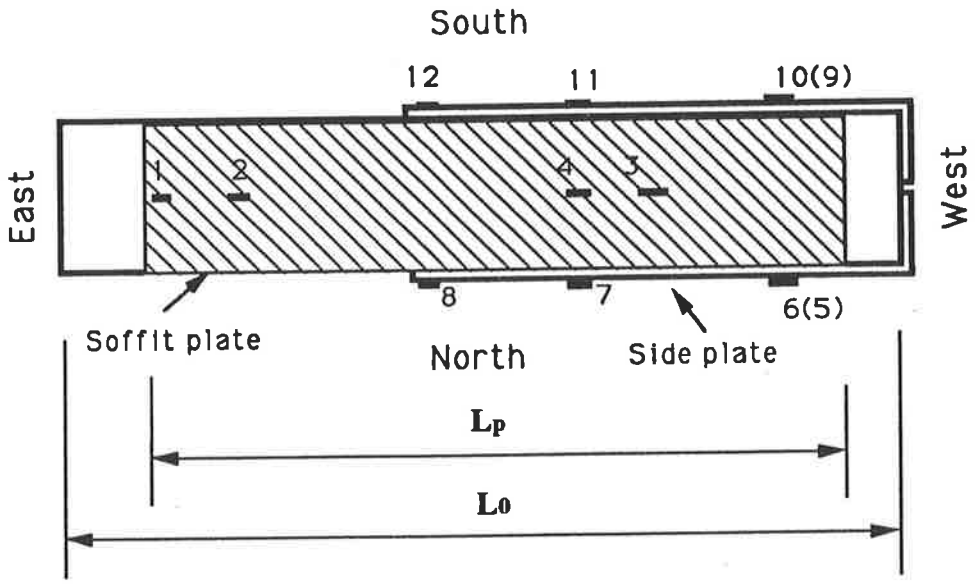

Fig.2-10 Plan of the beam in the series 4

2.2.5 Series 5

The object of this series is to study the effect of post-tensioning on the debonding beams with external soffit plates. Various degrees of the initial prestressing forces were applied to determine their effect on the debonding of soffit plates. The main variation is the degree of the prestressing forces. The post-tensioned beams were prestressed before gluing the external soffit plate. The first beam (PT1) in Table 2.5 was only prestressed by small amount in order to keep tendons tied to the section. The other beams were prestressed by varying degrees of prestressing forces that ranged from 20 to 45 per cent of the yield strength of the tendon. The beams were subjected to three points load as shown in Fig.2-2. Four beams were tested to failure. The geometric properties of this series are given in Table 2.5. The test rig is shown in the Fig.2-2. The position of the electrical resistant strain gauges and displacement dial gauge is illustrated in Fig.2-11.

Table 2.5 Geometric properties of the beams in the series 5

Specimen	P_i (kN)	b (mm)	d (mm)	D_t (mm)	D_b (mm)	D_{ps} (mm)	t_p (mm)	L_0 (mm)	L_1 (mm)	L_p (mm)
PT1	3.00	180	220	10.0	16.0	5.0	4.0	3200	2900	1000
PT2	30.0	180	220	10.0	16.0	5.0	4.0	3200	2900	1000
PT3	18.0	180	220	10.0	16.0	5.0	4.0	3200	2900	1000
PT4	42.0	180	220	10.0	16.0	5.0	4.0	3200	2900	1000

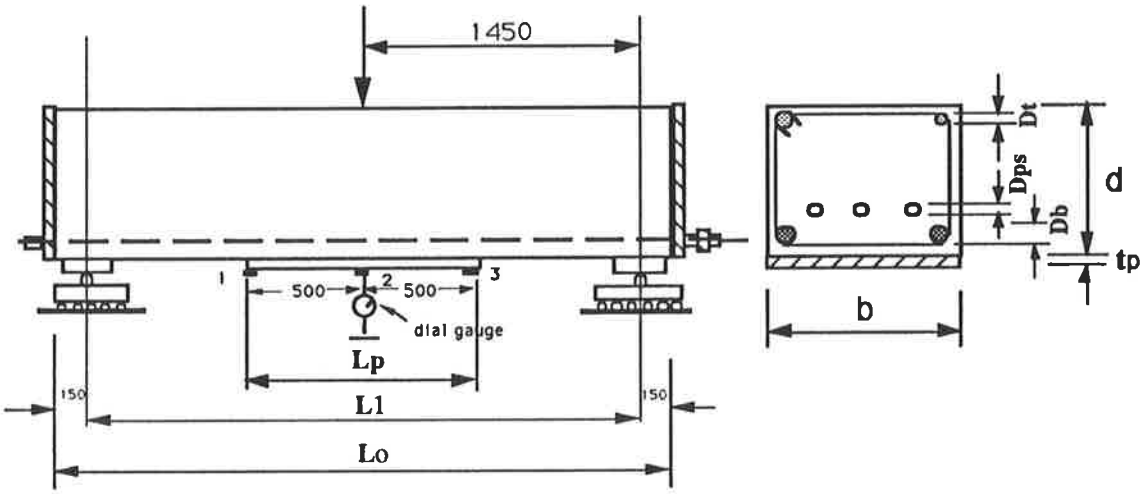

Fig.2-11 Beam geometry and instrumentations applied in the group two

2.3 Instrumentations

The positions of the electrical resistance strain gauges used in each series are illustrated in Fig.2-3, Fig.2-5, Fig.2-7, Fig.2-9 and Fig.2-11, respectively. The position of the displacement dial gauge used in the test to measure the deflection of the beam is also shown in Fig.2-3, Fig.2-5 , Fig.2-7, Fig.2-9 and Fig.2-11, respectively.

2.4 Preparation of Beams and Plates

The surfaces the reinforced concrete beams, where the plates were to be bonded, were roughed by needle gunning to expose the aggregate and the loose aggregate was removed from the surfaces as shown in P2-1 before bonding. The surfaces of the steel plates were roughened as shown in P2-1, by using either a disc grinder for the thin steel plate (ie. 1.0 mm and 2.0 mm) or sandblasting for the plate thickness of 3.0 mm, 4.0 mm, 5.0 mm and 10.0 mm. The plates surfaces were washed with a degreasing agent. The plates were glued to the reinforced concrete beams by a two-pot medium setting adhesive paste CA 273. The epoxy adhesive is manufactured by Hilti (Aust) Pty. Ltd. and has a compressive strength of 110-120 N/mm^2 and a tensile strength of 30-40 N/mm^2 after 2 days at 25 ^{o}C. The glue consisted of a resin and a hardener which were mixed at the ratio of 1:1 by weight or volume. The epoxy adhesive was spread over the surfaces of the reinforced concrete beam and steel plate, as shown in P2-2 and P2-3, respectively. The steel plates were then placed directly over the beams and pressed down with clamps or wood wedges, as shown in P2-4. The excess adhesive was extruded from the side and the air was driven out, as shown in P2-5.

The post-tensioned beams were stressed using a hand-operated hydraulic jack, as shown in P2-6. Rings were used at the beam-end in order to monitor the variation of the prestressing forces applied to the tendons, as illustrated in Fig.2-7. Two electrical resistance strain gauges were symmetrically glued onto the outside of each ring. The electrical resistance strain gauges were connected to the strain control panel shown in P2-8. Therefore, both the hydraulic prestressing forces and the corresponding tendon strains could be measured. In this way the prestressing forces applied to each of the tendon were kept approximately equal.

2.5 Material Properties

The test beams were cast as two pours. One pour was required for the beams in Group One and other pour required for the post-tensioned beams in Group Two. Details of the concrete properties in Group One are given from Table 2.7 to 2.14. The compression, indirect tensile, flexural and Young's modulus of concrete specimens were tested before and after the plated reinforced concrete beams in Group One were tested. The concrete specimens for Group Two were tested after the plated post-tensioned beams had been tested. Details of specimens in Group Two are given in Tables 2.15 to 2.18. The mean ultimate stresses of 10 mm diameter reinforcement is 590 N/mm^2. The average yield stresses and ultimate stresses of 16.0 mm diameter reinforcement is 460 N/mm^2 and 580 N/mm^2, respectively. The elastic modulus of reinforcement is 210 kN/mm^2.

In calculating concrete properties of the plated reinforced concrete beams in Group One, the compressive strength f_c, indirect tensile strength f_t and stiffness E_c of the concrete, f_c, was taken as 35.1 N/mm^2, 3.6 N/mm^2 and 34.2 kN/mm^2, respectively The compressive strength f_c, indirect tensile strength f_t and stiffness E_c of the concrete of the plated post-tensioned concrete beams in Group Two was taken as 37.2 N/mm^2, 4.0 N/mm^2 and 34.2 kN/mm^2, respectively.

The epoxy adhesive has a compressive strength of 110-120 N/mm^2 and a tensile strength of 30-40 N/mm^2 after 2 days at 25 ^{o}C.

The properties of the 5.0 mm diameter strand are given in Table 2.19. Tensile tests were performed on specimens of the mild steel plate used as external reinforcement. The material properties for these plates are summarised in Table 2.20.

Table 2.7 Results of the cylinder specimens (150 mm)

Specimen No.	P_{max} (kN)	f_c (N/mm^2)	E_c (kN/mm^2)	weight (g)	size dia/length (mm/mm)	density (kg/m^3)	Age (days)
1	587.5	31.95	-	13044.0	153.0/306.0	2318.6	96
2	626.0	34.14	24.94	12955.7	152.8/307.0	2301.4	96

The average of f_c and E_c is 33.0 N/mm^{2}and 24.9 kN/mm^2 at 96 day, respectively.

Table 2.8 Results of the cylinder specimens (150 mm)

Specimen No.	P_{max} (kN)	f_c (N/mm^2)	E_c (kN/mm^2)	weight (g)	size dia/length (mm/mm)	density (kg/m^3)	Age (days)
3	647.0	35.19	29.05	13016.0	153.0/306.0	2313.6	266
4	641.0	34.96	29.18	13072.0	152.8/308.0	2314.5	265
5	604.0	32.94	31.03	13131.4	152.8/308.0	2317.5	265
6	674.5	36.78	36.04	13055.3	152.8/306.0	2326.6	260
7	621.0	33.78	32.06	13075.8	153.0/306.0	2324.2	266
8	642.0	34.83	41.26	13079.9	153.2/308.0	2303.8	260
9	675.0	36.71	39.47	12955.7	153.0/305.0	2310.4	260
10	658.0	35.88	35.59	13058.9	152.8/306.0	2327.3	260

The average of f_c and E_c is 35.1 N/mm^{2}and 34.2 kN/mm^2 at 265 day, respectively

Table 2.9 Results of the specimens of cube (100 mm)

Specimen No.	P_{max} (kN)	f_{cu} (N/mm^2)	weight (g)	size (mm/mm)	density (kg/m^3)	Age (day)
1	390.8	37.94	2476.2	100.0/103.0	2404.1	96
2	399.0	39.31	2497.9	100.0/101.5	2461.0	96
3	351.6	34.47	2486.5	100.0/102.0	2437.7	96

The average of f_{cu} is 37.2 N/mm^2 at 96 day.

Table 2.10 Results of the specimens of cube (100 mm)

Specimen No.	P_{max} (kN)	f_{cu} (N/mm^2)	weight (g)	size (mm/mm)	density (kg/m^3)	Age (day)
4	433.0	41.21	2542.3	103.0/104.0	2444.5	265
5	434.0	41.31	2481.4	102.0/103.0	2409.1	265
6	436.5	41.55	2503.3	102.0/103.0	2429.4	265

The average of f_{cu} is 41.4 N/mm^2 at 265 day.

Table 2.11 Results of the specimens of cylinder (100 mm)

Specimen No.	P_{max} (kN)	f_c (N/mm^2)	f_t (N/mm^2)	weight (g)	size (mm/mm)	density (kg/m^3)	Age (days)
1	269.8	34.21	-	3713.5	100.2/201.0	2342.9	96
2	278.4	35.45	-	3677.6	100.0/200.0	2341.2	96
3	104.4	-	3.26	3717.0	100.4/203.0	2312.8	96
4	102.2	-	3.19	3705.3	100.4/203.0	2305.5	96
5	102.4	-	3.18	3749.9	100.6/204.0	2312.6	96

The average of f_c and f_t is 34.8 MP_a and 3.2 MP_a at the 96 day, respectively.

Table 2.12 Results of the specimens of cylinder (100 mm)

Specimen No.	P_{max} (kN)	f_c (N/mm^2)	f_t (N/mm^2)	weight (g)	size (mm/mm)	density (kg/m^3)	Age (days)
6	308.0	39.06	-	3712.0	100.2/202.0	2330.4	265
7	315.6	40.18	-	3675.5	100.0/201.0	2328.3	265
8	299.8	37.94	-	3721.4	100.3/203.0	2320.2	265
9	297.4	37.49	-	3739.4	100.5/202.0	2333.6	265
10	116.8	-	3.71	3689.4	100.2/200.0	2339.4	265
11	111.6	-	3.50	3713.7	100.7/201.5	2314.1	265
12	123.2	-	3.85	3738.0	100.8/202.0	2318.9	265
13	105.6	-	3.34	3688.7	100.1/201.0	2332.2	265
14	130.6	-	4.09	3742.0	100.7/202.0	2326.0	265
15	114.8	-	3.62	3729.6	100.5/201.0	2339.1	265
16	104.6	-	3.28	3682.4	100.4/202.0	2302.6	265
17	115.4	-	3.64	3687.8	100.3/201.0	2322.1	265
18	107.6	-	3.40	3675.0	100.2/201.0	2318.7	265

The average of f_c and f_t is 38.7 $N/mm^2$and 3.6 N/mm^2 at the 265 day, respectively

Table 2.11 Results of the specimens of a beam (500 mm)

Specimen No.	P_{max} (kN)	f_f (N/mm^2)	weight (g)	size (mm/mm/mm)	density (kg/m^3)	Age (days)
1	16.52	4.76	12043.5	100.0/102.0/500.0	2316.5	96
2	16.90	4.87	12010.9	100.0/102.0/500.0	2355.1	96

The average of f_f is 4.8 N/mm^2 at 96 day.

Table 2.14 Results of the specimens of a beam (500 mm)

Specimen No.	P_{max} (kN)	f_f (N/mm^2)	weight (g)	size (mm/mm/mm)	density (kg/m^3)	Age (days)
3	16.40	4.73	12072.9	100.0/102.0/500.0	2367.2	265
4	16.56	4.73	12144.3	100.0/102.5/500.0	2369.6	265
5	15.78	4.46	12129.1	100.0/103.0/500.0	2355.2	265
6	17.36	4.82	12162.2	100.0/104.0/500.0	2338.9	265
7	16.74	4.43	12087.5	100.0/102.0/500.0	2370.1	265
8	18.50	5.23	12318.3	100.0/103.0/500.0	2391.9	265

The average of f_f is 4.7 N/mm^2 at 265 day.

Table 2.15 Results of the cylinder specimens (150 mm)

Specimen No.	P_{max} (kN)	f_c (N/mm^2)	E_c (kN/mm^2)	Age (days)
1	700.5	38.6	36.4	220
2	672.5	36.6	24.7	220
3	745.5	40.5	37.5	220
4	607.5	32.8	38.3	220

The average of f_c and E_c is 37.1 $N/mm^2$and 34.2 kN/mm^2 at 220 day, respectively

Table 2.16 Results of the specimens of cylinder (100 mm)

Specimen No.	P_{max} (kN)	f_c (N/mm^2)	f_t (N/mm^2)	weight (g)	ρ (kg/m^3)	Age (days)
1	270.5	31.2	-	3700.3	2136.7	220
2	340.8	41.6	-	3722.0	2108.8	220
3	125.4	-	3.8	3711.0	2142.9	220
4	135.4	-	4.2	3708.0	2268.9	220
5	236.8	27.9	-	3706.0	2181.3	220
6	189.8	21.9	-	3714.0	2144.6	220
7	140.6	-	4.6	3692.5	2350.7	220
8	102.6	-	3.1	3722.0	2149.2	220

The average of f_c and f_t is 30.7 $N/mm^2$and 3.9 N/mm^2 at the 220 day, respectively

Table 2.17 Results of the specimens of cube (100 mm)

Specimen No.	P_{max} (kN)	f_{cu} (N/mm^2)	weight (g)	density (kg/m^3)	Age (day)
1	394.0	37.9	2464.4	2444.5	220
2	414.0	40.2	2459.6	2409.1	220
3	284.5	27.3	2467.2	2429.4	220
4	363.5	34.9	2478.5	2429.4	220

The average of f_{cu} is 35.1 N/mm^2 at 220 day.

Table 2.18 Results of the specimens of a beam (500 mm)

Specimen No.	P_{max} (kN)	f_f (N/mm^2)	weight (g)	density (kg/m^3)	Age (days)
1	13.00	3.90	11855.4	2371.1	225
2	15.22	4.48	12090.8	2394.2	225
3	14.22	4.27	11959.2	2391.8	225

The average of f_f is 4.2 N/mm^2 at 225 day.

Table 2.19 Properties of strands

Specimen No.	P_y (kN)	f_y (N/mm^2)	P_{max} (kN)	f_{max} (N/mm^2)	E_s (kN/mm^2)
1	29.0	1523.0	32.9	1676.0	210
2	30.0	1528.0	33.0	1680.0	210
3	30.0	1528.0	33.0	1680.0	210

Table 2.20 Properties of the steel plates

Plate thickness (mm)	P_y (kN)	P_{max} (kN)	f_y (N/mm^2)	f_{max} (N/mm^2)	E_p (kN/mm^2)	Average yield stress (N/mm^2)	Average ultimate stress (N/mm^2)	Average elastic modulus (kN/mm^2)
1.0	-	3.7	-	308.3	200.0	-	317.0	200.0
1.0	-	3.7	-	308.3	200.0			
1.0	-	4.0	-	333.3	205.0			
2.0	8.11	9.0	324.4	360.0	220.0	300.0	352.0	215.0
2.0	7.16	8.4	286.3	336.0	215.0			
2.0	7.20	9.0	288.0	360.0	205.0			
3.0	12.2	15.5	320.0	413.3	200.0	321.0	411.0	205.0
3.0	12.0	15.4	320.0	410.7	205.0			
3.0	12.1	15.3	322.6	408.0	210.0			
4.0	12.5	16.4	250.0	328.0	210.0	243.0	320.0	210.0
4.0	12.5	16.3	250.0	326.0	215.0			
4.0	11.4	15.3	228.0	306.0	205.0			
5.0	19.9	28.0	318.4	448.0	210.0	317.0	447.0	210.0
5.0	19.6	27.6	313.6	441.6	210.0			
5.0	20.0	28.2	320.0	451.2	205.0			
10.0	36.1	61.3	288.8	490.4	210.0	293.0	495.4	210.0
10.0	36.4	62.9	291.2	503.2	200.0			
10.0	37.5	61.7	300.0	492.6	210.0			

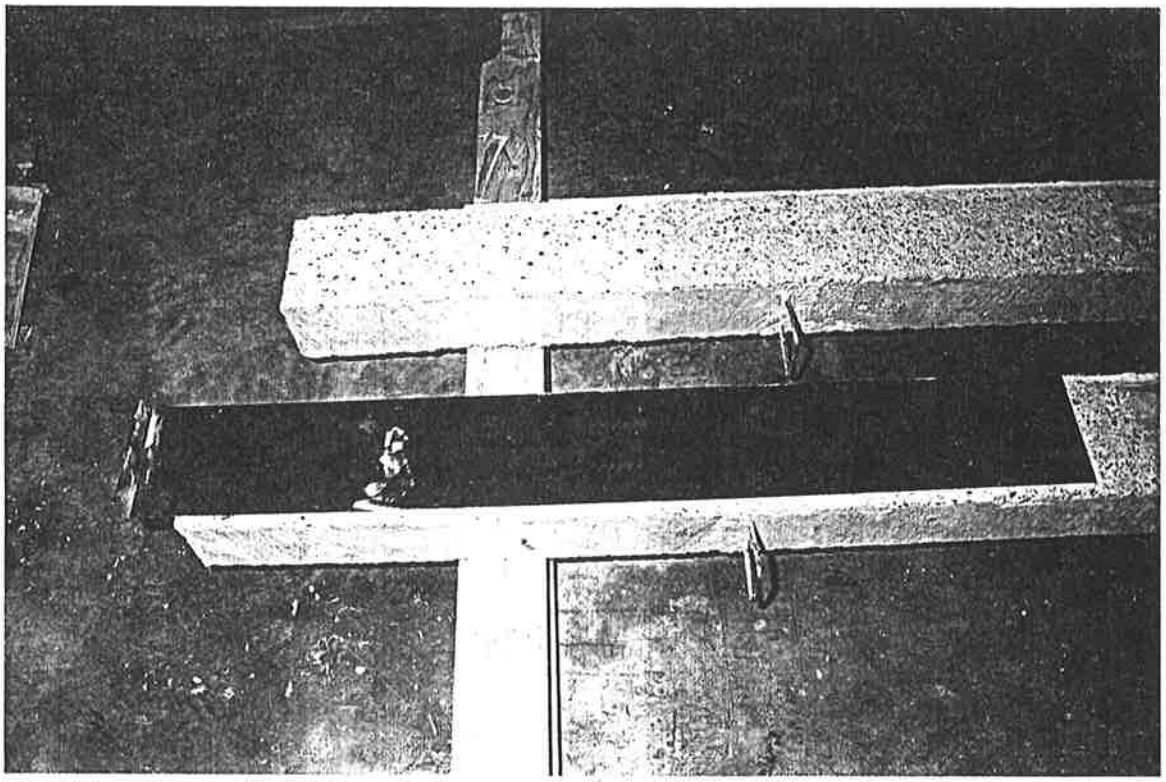

P2-1 Preparation of the surface concrete beam and steel plate

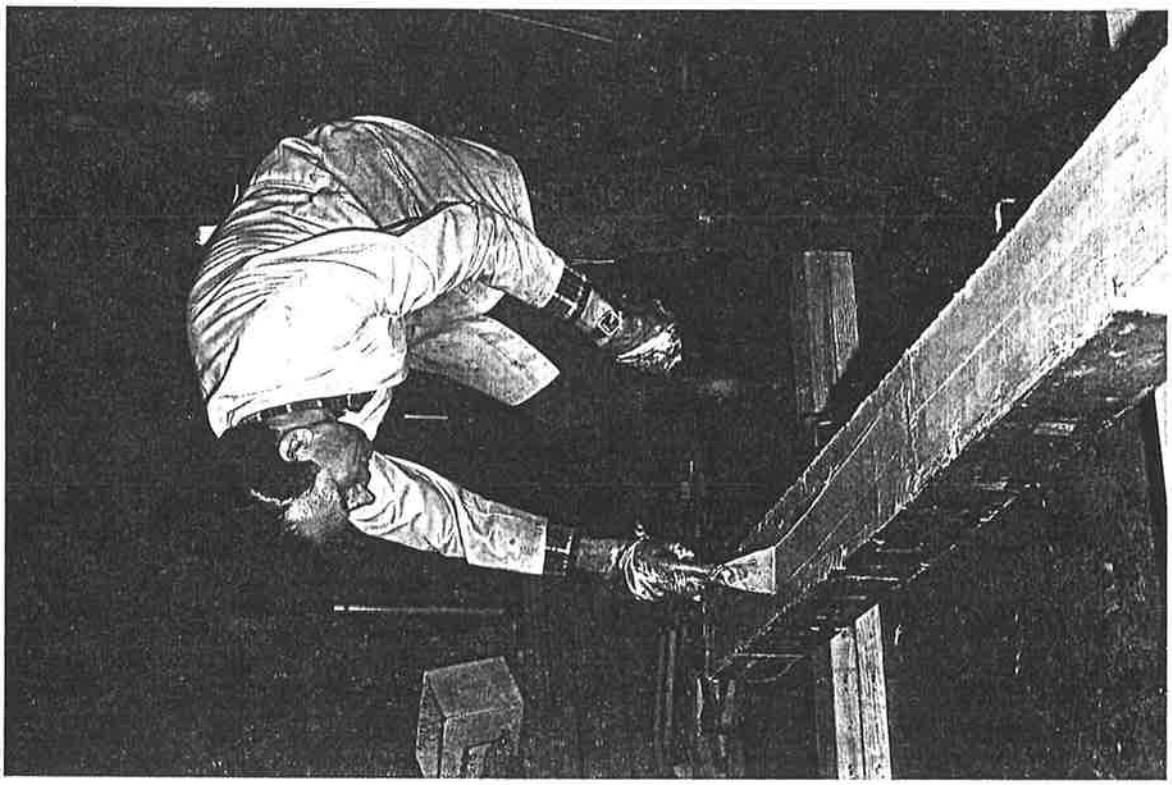

P2-2 The epoxy adhesive was spread over the surface of reinforced concrete beam

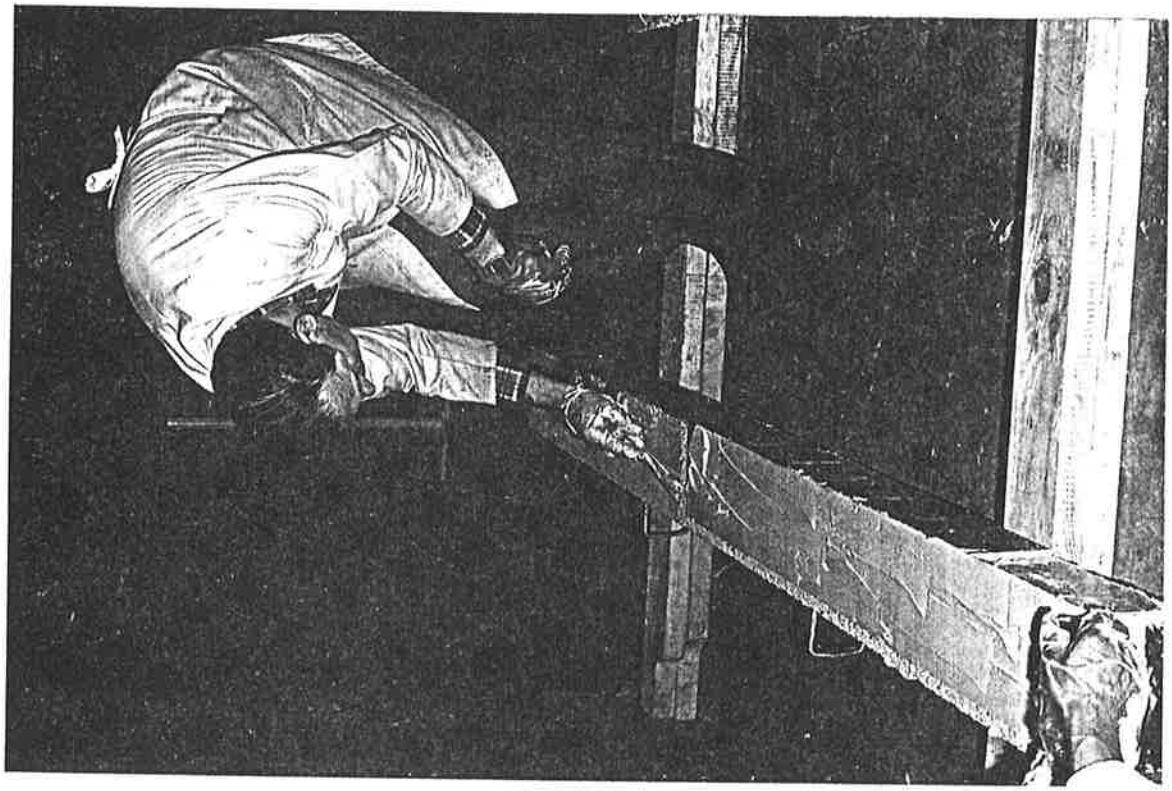

P2-3 The epoxy adhesive was spread over the surface of steel plate

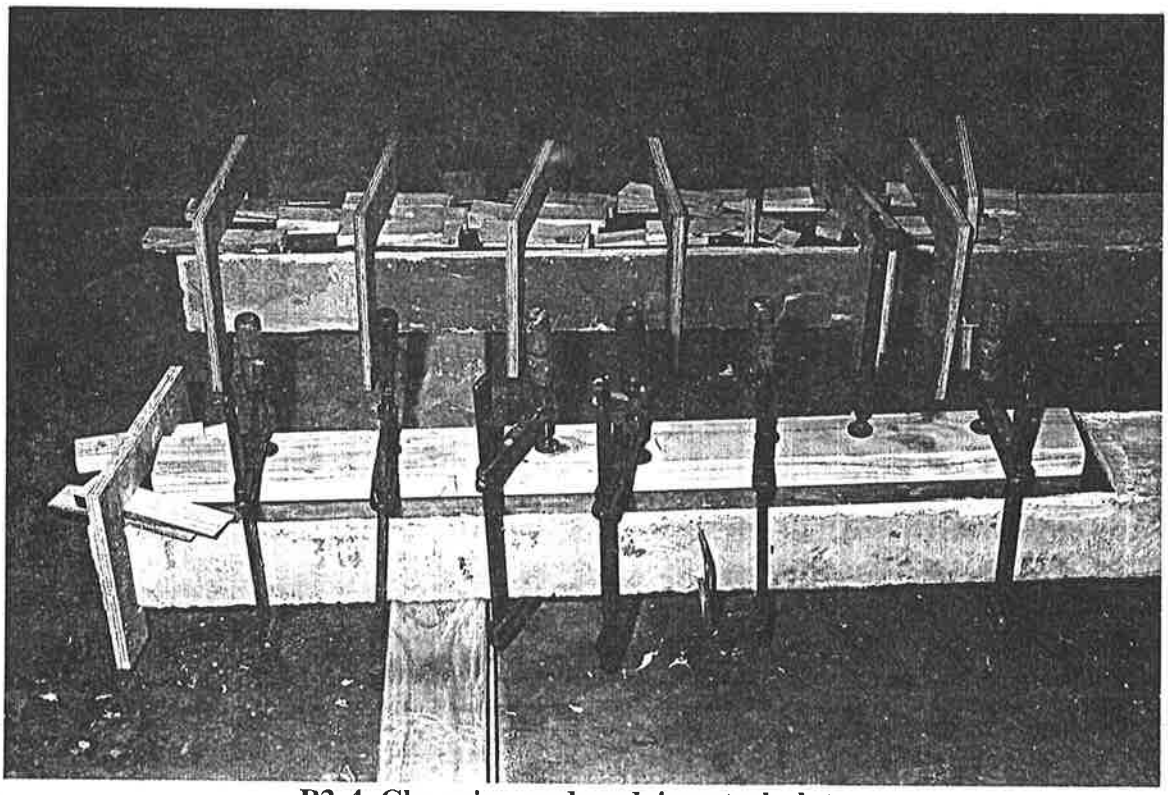

P2-4 Clamping and wedging steel plate

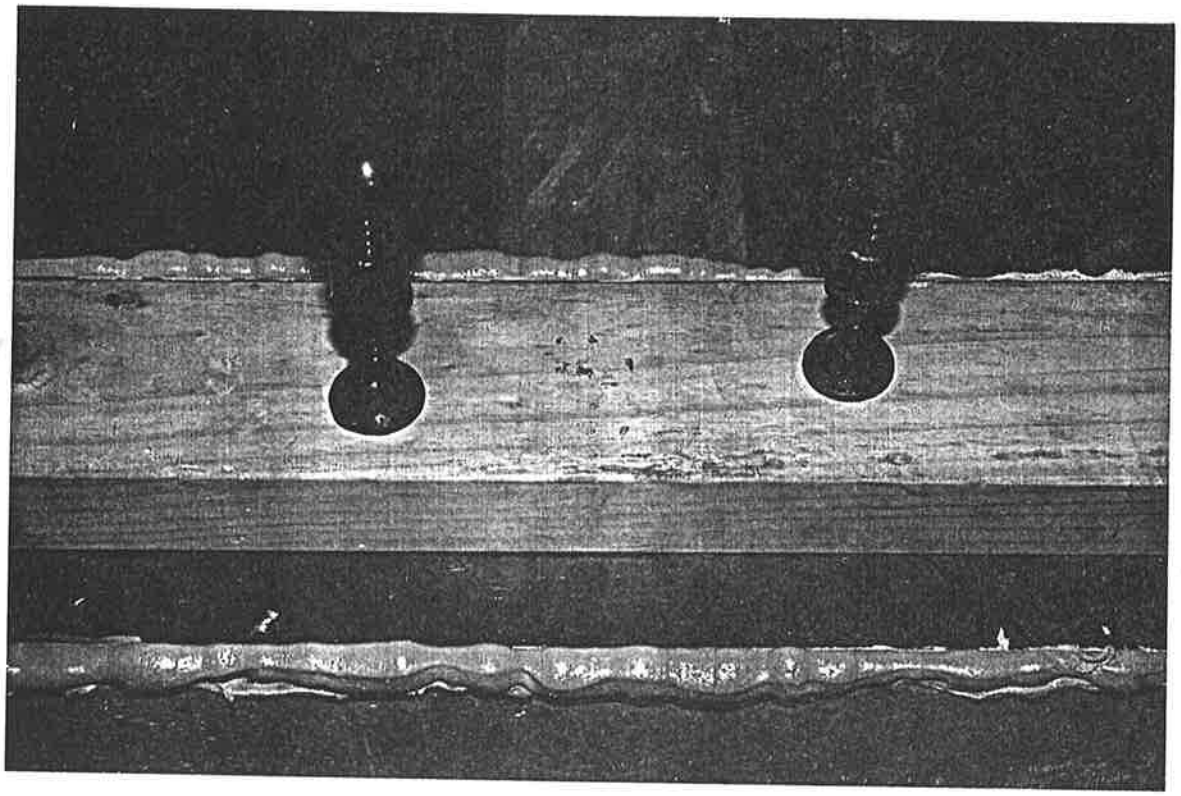

P2-5 Extruding excess adhesive

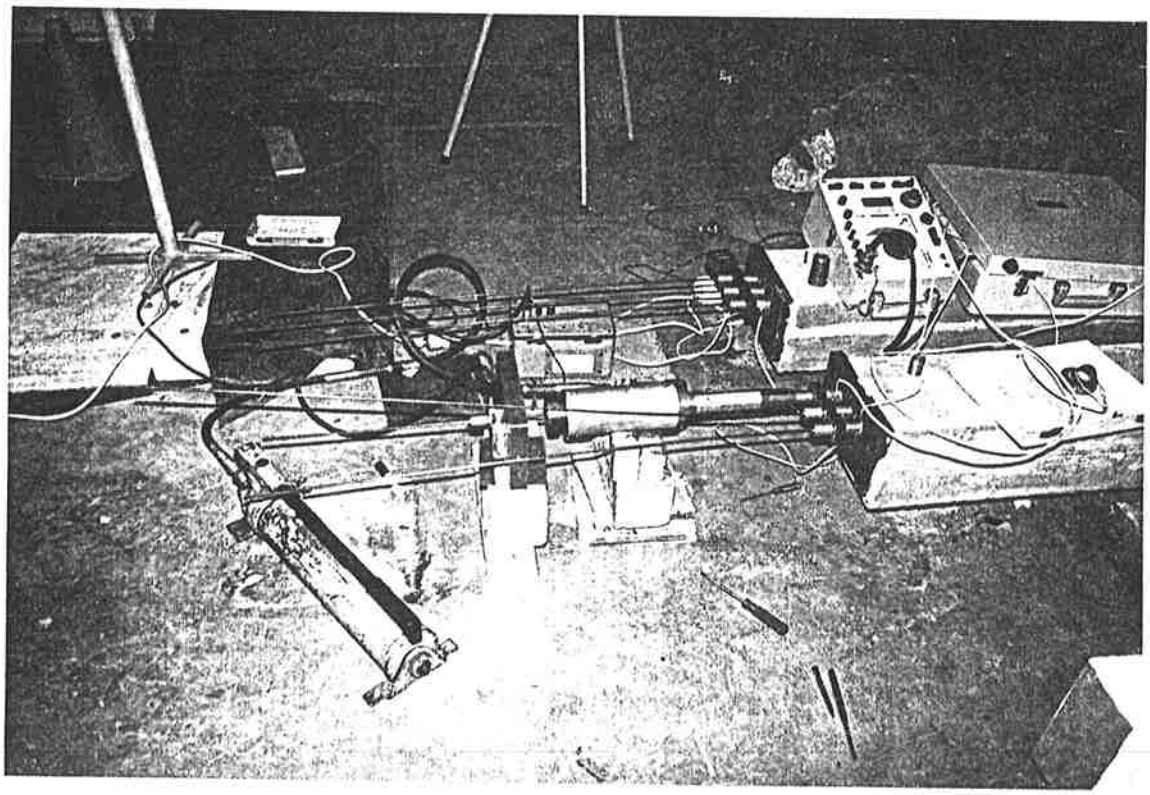

P2-6 Prestressing reinforced concrete beams

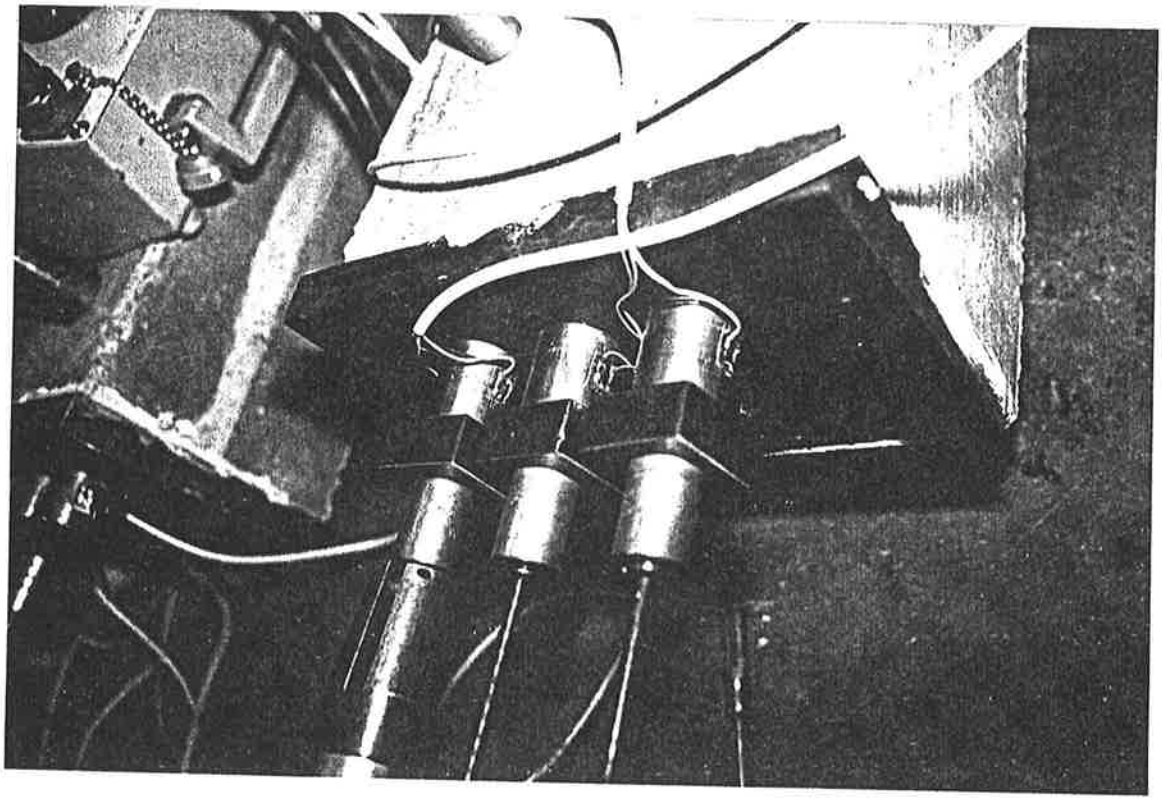

P2-7 Steel rings

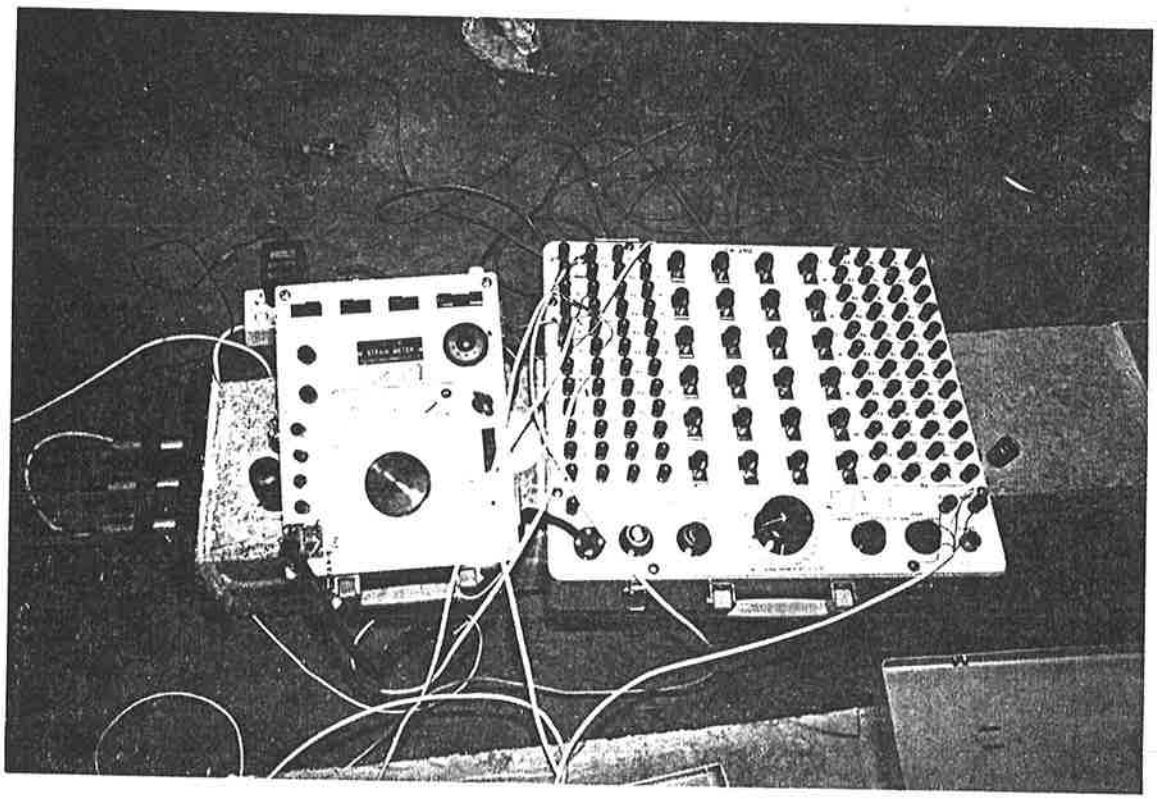

P2-8 Strain control panel

Chapter Three

Description of the Experimental Test

3.1 Introduction

A preliminary study of both reinforced concrete beams that are strengthened by bonding external steel plates, and post-tensioned beams that are strengthened by external steel soffit plates are carried out in the experimental tests. Four series of plated reinforced concrete beams and one series of plated post-tensioned concrete beams were tested, each series had the following conditions applied:

Series 1 - beams are strengthened with both soffit and side plates, the length of the side plates is varied, the thickness of the side plates and the length of the soffit plates are constant.

Series 2 - beams are plated with soffit plates, the lengths of the plates are the same as that of the reinforced concrete beams but the thickness of the soffit plates is varied.

Series 3 - beams are plated with both soffit and side plates, the area of the longitudinal tensile reinforcement are varied.

Series 4 - beams are glued with both soffit and side plates, the thicknesses of the side plates is varied.

Series 5 - post-tensioned reinforced concrete beams are strengthened with soffit plates, the initial prestressing forces are varied in each beam, and the thickness of the plates are constant.

3.2 Description of the experimental test

3.2.1 Series 1

The main aim of this series is to investigate the increase of the shear strength in the concrete beam due to the side plates; the beams are plated with both soffit and side plates and do not have stirrups. The main variation is the length of the side plates, as shown in Table 2.1. The test rig is shown in the Fig.2-1. Both shear spans of the plated reinforced concrete beam were tested and this was achieved by clamping the adjacent shear span as shown in Fig.2-1. The loads shown in the following photographs is the total applied load and is therefore proportional to the shear load; the maximum shear load in the section is 71 per cent of the total applied load. The numbers written on the beams in the following photographs is the load stage during the experimental work. The positions of the electrical strain gauges and dial gauges is shown in Fig.2-3 and in Fig 2-4.

L_{sp} = 0.0 mm

Beam SP/S1/L

The first flexural crack, which was almost vertical, occurred at the end of the soffit plate at a shear load of 16.6 kN (ie., an applied load P_a = 23.4 kN), as can be seen in P3-1. As the load was further increased, a horizontal peeling crack formed at the level of the bottom reinforcement at a shear load of 24.9 kN (ie., P_a = 35.1 kN), as shown in P3-2. When the shear load reached 26.3 kN (ie., P_a = 37.1 kN in P3-3), a web-shear crack was formed. The horizontal peeling crack extended gradually along the level of the bottom reinforcement and other inclined cracks also formed as the applied load was further increased, as can be seen in P3-4 and P3-5, respectively. Eventually, shear peeling and debonding of the soffit plate occurred simultaneously at a shear load of 33.4 kN (P_a = 47.1 kN), as are shown in P3-6

and P3-7 respectively.

Figure 3-1 shows the relationship between the shear load and the longitudinal strains in the soffit plate. It can be seen in Fig.3-1 that the longitudinal strains in the soffit plate increased almost linearly with the shear load prior to shear peeling. The horizontal peeling crack formed and developed quickly with increasing shear load. Strain gauge No.1, which is close to the end of the soffit plate, first dropped off at point **a** in Fig.3-1 before shear peeling occurred. Shear peeling and debonding of the soffit plate occurred instantaneously at a shear load of 33.4 kN. It can be seen in Fig.3-1 that the longitudinal strains in the soffit plate dropped rapidly down. Finally, the beam failed in shear at a shear load of 42.4 kN.

Beam SP/S2/L

The first inclined crack formed in the vicinity of the soffit plate-end at a shear load of 24.5 kN (P_a = 34.5 kN), as can be seen in P3-8. As the shear load further increased, the shear diagonal crack occurred at a shear load of 26.4 kN (P_a = 37.2 kN), as shown in P3-9. A further small increase in load, induced a horizontal shear peeling crack at the level of the bottom reinforcement at a shear load of 27.5 kN (P_a = 38.8 kN). The diagonal crack tended to develop rapidly towards the point of the applied load. Shear peeling and debonding of the soffit plate occurred simultaneously at a shear load of 27.5 kN (P_a = 38.8 kN) as can be seen in P3-10. Eventually, the beam failed in shear at a shear load of 37.3 kN.

The relationship between the shear load and the longitudinal strains in the soffit plate is given in Fig.3-2. It can be seen that the longitudinal strains in the soffit plate increase with the increase in shear load until debonding of the soffit plate had occur.

L_{sp} = 90.0 mm

Beam SP/S3/L

Cracks formed along the edge of the side plate on the south side of the beam, as can be seen in P3-11, when the shear load reached 24.7 kN (P_a = 34.8 kN). As the shear load was further increased up to 27.1 kN (P_a = 38.2 kN), it can be seen in P3-12 that cracks also formed along the edge of the side plate on the north side of the beam. The cracks extended towards the point of the applied load as the load further increased gradually, and then the horizontal peeling cracks formed at the level of the bottom reinforcement at a shear load of 29.4 kN (P_a = 41.5 kN) as shown in P3-13. A small further increase in load caused debonding of the soffit plate at a shear load of 30.8 kN (P_a = 43.4 kN), as shown in P3-14.

The relationship between the shear load and the strains in the side plates is illustrated in Fig.3-3. The relationship between the shear load and the longitudinal strains in the soffit plate is shown in Fig.3-4. The relationship between the shear load and deflection of the beam is given in Fig.3-5.

It can be seen in Fig.3-3 that most strains in the side plates vary linearly with the shear load up to approximately 24.0 kN, and then become non-linear until debonding of the side plate that occurred at a shear load of 27.1 kN. The changeover, from linear to non-linear, suggest that cracks may have occurred behind the side plates. Debonding of the side plates occurred at a shear load of 27.1 kN. Furthermore Figure 3-3 also shows that strain gauge No.4, on the side plate on the south side of the beam, varies linearly with the shear load up to Point a where the shear load was 20.5 kN, and then becomes non-linear. This would suggest that cracks may have formed behind this side plate when the shear load was 20.5 kN, which resulted in the side plate debonding. Debonding of this side plate occurred

when the shear load was 24.7 kN, as can be seen in Fig.3-3 where the strain in this plate reduces gradually. Figure 3-4 shows that the longitudinal strains in the soffit plate increases linearly with the shear load before debonding of the soffit plate occurred. The strain gauge No.2, which is close to the plate-end, drops off rapidly, as shown in Fig.3-4. Debonding of the soffit plate occurred at a shear load of 30.8 kN. It can be seen in Fig.3-5 that the deflection of the beam increases progressively with the shear load before debonding of the plates has occurred. The beam failed finally in shear at the shear load of 36.7 kN.

In this specimen, debonding of both side plates and soffit plate was induced by the inclined cracks and peeling cracks. However, debonding of the side plates occurred prior to debonding of the soffit plate.

L_{sp} = 180.0 mm

Beam SP/S2/R

It is shown in P3-15 that debonding of the soffit plate occurred at a shear load of 37.0 kN (P_a = 52.2 kN).

The relationship between the shear load and the strain in the side plates is illustrated in Fig.3-6. The relationship between the shear load and the longitudinal strains in the soffit plate is shown in Fig.3-7 and the relationship between the shear load and deflection of the beam is illustrated in Fig.3-8.

It can be seen in Fig.3-6 that the tensile strains in both side plates almost varies linearly with the shear load at the initial stages of loading. At a shear load of approximately 10.0 kN there is a slight change in the slope. When the shear load in the section is greater than 20.0 kN, the relationship between the shear load and the

tensile strains in the side plates then becomes non-linear. This probably suggests that cracks may have occurred behind the side plates at this stage. At a shear load of 34.0 kN, debonding of the side plate, on the north side of the beam, occurs first (the point **a** in Fig.3-6). Debonding of the soffit plate and of the side plates almost occurs instantaneously when the shear load reaches 37.0 kN, as shown in Fig.3-6 and Fig.3-7, respectively. Figure 3-7 shows that the longitudinal strains in the soffit plate vary almost linearly with the shear load until debonding of the soffit plate occurs. It can be seen in Fig.3-8 that the deflection of the beam varies linearly with the shear load until debonding of the plates occurs.

In this specimen, debonding of both the side and soffit plates were induced by the inclined cracks and by the peeling cracks. Debonding of the side plates occurred prior to the debonding of the soffit plate.

L_{sp} = 270.0 mm

Beam SP/S4/R

The crack formed at the end of the soffit plate when the shear load reached 34.4 kN (P_a = 48.5 kN), as shown in P3-16. A small further increase in load induced debonding of the soffit plates at a shear load of 35.0 kN (P_a = 49.5 kN), as can be seen in P3-17.

The relationship between the shear load and the strains in the side plates is given in Fig.3-9. Figure 3-10 shows the variation of the longitudinal strains in the soffit plate with the shear load. The relationship between the shear load and deflection of the beam is shown in Fig.3-11.

It can be seen in Fig.3-9 that the tensile strains in the side plates almost vary linearly

with the shear load at the initial stage. When the shear load is greater than 20.0 kN, it becomes non-linear. The changeover would suggest that cracks have formed behind the side plates; the local stresses in the section being redistributed due to the formation of the cracks. Debonding of the side plates occurred at a shear load of 35.0 kN. Figure 3-10 illustrates that the longitudinal strains in the soffit plate vary linearly with the shear load until debonding of the soffit plate which occurred at a shear load of 35.0 kN.

Debonding of both the side plates and the soffit plate, which was induced by the inclined cracks and the peeling cracks, occurred simultaneously in this specimen.

L_{sp} = 360.0 mm

Beam SP/S1/R

The flexural crack formed on the north side of the beam at a shear load of 36.0 kN (P_a = 50.6 kN), as shown in P3-18. It can be seen in P3-19 that the crack formed along the edge of the side plates when the shear load was 42.5 kN (P_a = 59.1 kN). After a further small increase in the load, debonding of the soffit plate occurred when the shear load reached 43.0 kN (P_a = 61.0 kN), as shown in P3-20.

The relationship between the shear load and the strains in the side plates is illustrated in Fig.3-12. The relationship between the shear load and the longitudinal strains in the soffit plate is shown in Fig.3-13. The relationship between the shear load and deflection of the beam is given in Fig.3-14.

It can be seen in Fig.3-12 that the tensile strains in the side plates vary linearly with the shear load until the shear load equals 25.0 kN, and then the variation become non-linear. It may be implied that the cracks, which had occurred behind the side

plates, formed prior to the formation of the visible flexural crack shown in P3-18. As the shear load increase gradually, debonding of the side plates occurred at a shear load of 43.0 kN. It can be seen in Fig.3-13 that the longitudinal strains in the soffit plate increases with the increase in shear load until debonding of the soffit plate occurred at the shear load of 43.0 kN. Fig.3-14 shows that the deflection of the beam increase progressively with the shear load until debonding of both plates occurred.

In this specimen, debonding of the side plates and the soffit plate were induced by the inclined cracks and peeling cracks and occurred instantaneously.

L_{sp} = 540.0 mm

Beam SP/S3/R

The flexural crack formed when the shear load reached 43.0 kN (P_a = 60.0 kN), as can be seen in P3-21. As the load increased, a few cracks occurred along both the side and soffit plates at a shear load of 49.0 kN (P_a = 69.0 kN), as is illustrated in P3-22. After a small further increase in load, debonding of the soffit plate occurred when the shear load attained 50.0 kN (P_a = 69.8 kN), as shown in P3-23.

The relationship between the shear load and the strains in the side plates is given in Fig.3-15. Figure 3-16 shows that the variation of the longitudinal strains in the soffit plate with the shear load. The relationship between the shear load and the deflection of the beam is given in Fig.3-17.

It can be seen in Fig.3-15 that initially the tensile strains in the side plates vary linearly with the shear load. However, there is a changeover, in which the relationship of tensile strains in the side plates and the shear load change from linear

to non-linear, when the shear load is approximately 20.0 kN. The formation of the cracks behind the side plates may have caused this changeover. It seems that debonding of the side plates did not occur in this specimen. Figure 3-16 shows that the longitudinal strains in the soffit plate increase gradually with the shear load until debonding of the soffit plate occurred at a shear load of 50.0 kN.

In this specimen, it was found that debonding of the soffit plate was induced only by the peeling cracks.

L_{sp} = 690.0 mm

Beam SP/S4/L

The first visible flexural crack formed in the beam at a shear load of 37.8 kN (P_a = 53.3 kN), as can be seen in P3-24. At shear loads up to 45.7 kN (P_a = 64.5 kN), as shown in P3-25, cracks formed along the edge of side plates. As the load was further increased, debonding of the soffit plate occurred at a shear load of 60.6 kN (P_a = 85.54 kN), as shown in P3-26.

The relationship between the shear load and the tensile strains in the side plates is given in Fig.3-18. Figure 3-19 shows that the variation of the longitudinal strains in the soffit plate with the shear load. The relationship between the shear load and the deflection of the beam is given in Fig.3-20.

It can be seen in Fig.3-18 that initially the tensile strains in the side plates vary linearly with the shear load. However, there is a changeover in the relationship between the tensile strains in the side plates and the shear load when the shear load is approximately 30.0 kN due to the formation of the cracks behind the side plates. It also seems that debonding of the side plates did not occur. Figure 3-19 shows

that the longitudinal strains in the soffit plate increase gradually with the shear load until debonding of the soffit plate occurred at a shear load of 60.6 kN. Eventually, the beam failed in flexure at the maximum shear load of 63.1 kN after debonding of the soffit plate had occurred. It can be seen in Fig.3-20 that the deflection of the beam varies almost linearly with the shear load until debonding of the soffit plate occurred.

In this specimen debonding of the soffit plate was induced by the peeling cracks.

Comparison of experimental results

The experimental results of this series are given in the following Table 3.1. The relationship between the length of the side plates and the shear load that caused debonding of the soffit plate is given in Fig.3-21.

Table 3.1 Experimental results of the series 1

Specimen	L_{sp} (mm)	V_{sp} (kN)	V_p (kN)	ε_p	V_{max} (kN)	failure mode
SP-S1-L	0.0	-	33.4	630	42.4	shear peeling
SP-S2-L	0.0	-	26.4	538	37.3	shear peeling
SP-S3-L	90	24.7	30.8	604	36.7	side plate debonded first
SP-S2-R	180	34.8	37.0	710	-	side plate debonded first
SP-S4-R	270	35.0	35.0	774	-	both plates debonded
SP-S1-R	360	43.2	43.2	937	-	both plates debonded
SP-S3-R	540	50.0	50.0	1239	-	soffit plate debonded only
SP-S4-L	690	60.6	60.6	1469	63.1	soffit plate debonded only

where

L_{sp} = the length of the side plates

V_{sp} = the shear load when debonding of either the side plates or the soffit plate occurs

V_p = the shear load when debonding of the soffit plate occurs

ε_p = the longitudinal strain in the soffit plate when debonding of the soffit plate occurs

V_{max} = the maximum shear load when the specimen failed in shear

3.2.2 Series 2

The main purpose of this series is to investigate the increase in the shear strength in reinforced concrete beams due to the external soffit plate when the plate is prevented from debonding through peeling. The beams did not have stirrups and were plated over the full soffit area and over the supports. The main variation in the series is the thickness of the soffit plates, as shown in Table 2.2. Both shear spans of a beam were tested to failure and this was achieved by clamping the adjacent shear span, as shown in Fig.2-1. The loads shown in the following photographs is the total applied load. The numbers indicated in the beams, in the following photographs, is the load stage during testing. The test rig is shown in the Fig.2-1. The position of electrical strain gauges and the dial gauge is shown in Fig.2-3 and Fig.2-4, respectively.

t_p = 0.0 mm

Beam FP/B1/R

The first flexural-shear crack occurred when the applied load was 19.5 kN, as shown in P3-27. The crack extended gradually towards the point of the applied load as the load further increased, as shown in P3-28. Finally, the beam failed in flexural when the maximum applied load reached 30.0 kN.

Beam FP/B1/L

The first flexural crack formed when the applied load reached 20.0 kN. At an applied load of 36.7 kN, the beam failed in flexural.

The variation of the deflection of the beam, at the position of the applied load, with the applied load is shown in Fig.3-22. It can be seen that initially the deflection of the beam almost varies linearly with the applied load until the formation of the

cracks had occurred (the point **a** in Fig.3-22). The stiffness decreased as the applied load increased in the range **ab** and **bc**. The beam failed in flexure eventually.

t_p = 3.0 mm

Beam FP/B2/L

The flexural and flexure-shear cracks formed in the beam at a shear load of 33.1 kN (P_a = 46.7 kN), as shown in P3-29. It can be seen in P3-30 that the flexure-shear cracks developed gradually as the shear load further increased. The inclined shear crack occurred when the shear load reached 38.8 kN (P_a = 54.7 kN), as shown in P3-31. The beam failed finally in shear at a shear load of 46.9 kN (P_a = 66.1 kN), as can be seen in P3-32.

Beam FP/B2/R

It can be seen in P3-33 that the flexural cracks formed at a shear load of 31.2 kN (P_a = 44.0 kN). The inclined cracks developed gradually as the shear load increased, as can be seen in P3-34. As the shear load further increased up to 43.2 kN (P_a = 61.0 kN), a diagonal crack formed, as shown in P3-35. Eventually, the beam failed in shear when the maximum shear load reached 50.1 kN (P_a = 70.6 kN), as can be seen in P3-36.

The relationship between the shear load and the deflection of the beams is illustrated in Fig.3-23. It can be seen in Fig.3-23 that the deflection of the beams initially varies linearly with the shear load. The stiffness of the beam reduces gradually with the increase in shear load prior to the beam failing in shear. Finally, the beams fails in shear at the maximum shear load of 47.0 kN and 50.1 kN, respectively.

t_p = 5.0 mm

Beam FP/B3/L

The inclined cracks first formed at a shear load of 40.1 kN (P_a = 56.5 kN), as shown in P3-37. As the load further increased, the inclined cracks developed gradually towards applied load and the support, as shown in P3-38 and P3-39, respectively. Finally, the beam failed in shear at the maximum shear load of 64.2 kN (P_a = 90.5 kN), as shown in P3-40.

The relationship between the shear load and the deflection of the beam is illustrated in Fig.3-24. The relationship between the shear load and the longitudinal strains in the soffit plate is given in Fig.3-25.

It can be seen in Fig.3-24 that the deflection of the beam almost varies linearly with the shear load prior to the formation of the inclined cracks (point **a** in Fig.3-24), and then becomes non-linear until the beam fails in shear. The stiffness of the beam decreases after the formation of the inclined cracks at a shear load of 40.1 kN, as shown in range **ab** in Fig.3-24. The relationship between the shear load and the longitudinal strain in the soffit plate is shown in Fig.3-25; the longitudinal strain in the soffit plate almost varies linearly with the shear load before the beam failed in shear. Finally, the beam fails in shear at the maximum shear load of 64.2 kN.

Beam FP/B3/R

The inclined crack occurred at a shear load of 43.0 kN (P_a = 60.6 kN), as shown in P3-41. As the shear load further increased, it can be seen in P3-42 that the inclined crack developed, and the other inclined cracks formed and extended to the points of the applied load and support. Finally, the beam failed in shear at the maximum shear load of 70.8 kN (P_a = 99.8 kN), as shown in P3-43.

The relationship between the deflection of the beam and the shear load is illustrated in Fig.3-26. The relationship between the shear load and the longitudinal strain in the soffit plate is given in Fig.3-27.

It can be seen in Fig.3-26 that deflection of the beam varies linearly with the shear load prior to the formation of the inclined crack. The shear load drops down slightly when the inclined crack occurs at a shear load of 43.2 kN, as shown by the point **a** in Fig.3-26. Also, it can be seen in Fig.3-27, the longitudinal strain in the soffit plate almost varies linearly with the shear load before the formation of the inclined crack and then slightly drops off (the point **a** in Fig.3-27). The stiffness of the beam then decreases with increasing shear load as shown in the range **ab** and **bc** in Fig.3-27. The beam failed finally in shear at a maximum shear load of 70.8 kN.

t_p = 10.0 mm

Beam FP/B4/L

It can be seen in P3-44 that the inclined crack formed at a shear load of 47.3 kN (P_a = 66.7 kN). As the load increased, the other inclined cracks formed, as shown in P3-45. As the load further increased, the inclined cracks extended gradually towards both the applied load and the support as can be seen in P3-46 and P3-47 respectively. The beam failed eventually in shear at the maximum shear load of 85.0 kN (P_a = 119.9 kN), as shown in P3-48.

The relationship between the deflection of the beam and the shear load is illustrated in Fig.3-28. The relationship between the shear load and the longitudinal strains in the soffit plate is illustrated in Fig.3-29.

It can be seen in Fig.3-28 that initially deflection of the beam varies linearly with the shear load prior to the formation of the inclined crack at a shear load of 47.3 kN (the point **a** in Fig.3-28). The stiffness of the beam then decreases gradually after the formation of the inclined crack, as shown in the range **ab** and **bc** in Fig.3-28. It is shown in Fig.3-29 that the longitudinal strains in the soffit plate vary linearly with the shear load before the beam failed in shear. Finally, the beam failed in shear at the maximum shear load of 85.0 kN.

Beam FP/B4/R

The inclined cracks formed at a shear load of 51.8 kN (P_a = 73.0 kN), as can be seen in P3-49. As the shear load further increased, the inclined cracks extended gradually toward the points of the applied load and the support, as can be seen in P3-50 and P3-51, respectively. Eventually, the beam failed in shear when the maximum shear load was 78.7 kN (P_a = 111.0 kN), as can be seen in P3-52.

The relationship between the deflection of the beam and the shear load is given in Fig.3-30. The relationship between the shear load and the longitudinal strains in the soffit plate is illustrated in Fig.3-31

It can be seen in Fig.3-30 that initially deflection of the beam varies linearly with the shear load. The stiffness decreases gradually after the formation of the inclined cracks at a shear load of 51.8 kN, as shown in the range **ab** in Fig.3-30. The longitudinal strains in the soffit plate almost vary linearly with the shear load prior to the beam failing in shear, as can be seen in Fig.3-31. Eventually, the beam failed in shear at the maximum shear load of 78.7 kN.

Comparison of experimental results

The experimental results of this series are given in Table 3.2. Comparison of the deflections are shown in Fig.3-32.

It can be seen in Table 3.2 that the failure mode of beams were different. The plated reinforced concrete beams did not fail in flexural because the soffit plates was terminated at the ends of the reinforced concrete beam; the plating action of the supports prevented the plates from debonding due to peeling.

Table 3.2 Experimental results of the series 2

Specimen	t_p (mm)	V_s (kN)	ε_p	failure mode
FP/B1/L	0.0	25.98	-	failed in flexure
FP/B1/R	0.0	25.94	-	failed in flexure
FP/B2/L	3.0	46.80	-	failed in shear
FP/B2/R	3.0	50.03	-	failed in shear
FP/B3/L	5.0	64.17	1492	failed in shear
FP/B3/R	5.0	70.76	1746	failed in shear
FP/B4/L	10.0	85.00	1144	failed in shear
FP/B4/R	10.0	78.70	933	failed in shear

where

t_p = the thickness of the soffit plate

V_s = the shear load when the specimen failed in shear

ε_p = the longitudinal strain in the soffit plate when the beam failed in shear

3.2.3 Series 3

The main variation in this series is the area of the tensile reinforcement in the concrete beam, as shown in Table 2.3. The test beams are without stirrups. Both shear spans of the beam were tested to failure and this was achieved by clamping the adjacent shear span, as shown in Fig.2-1. The test rig is shown in the Fig.2-1. The position of the electrical resistant strain gauges and dial gauges are shown in Fig.2-5 and Fig.2-6, respectively.

A_{st} = 157.0 mm² (D_b = 10.0 mm)

Beam SP/S8/L (L_{sp} = 0.0 mm)

The shear diagonal cracking took place at a shear load of 25.7 kN (ie., the applied load P_a = 36.2 kN), as can be seen in P3-53. As the load further increased, it can be seen in P3-54 that the horizontal peeling cracks formed at a shear load of 31.4 kN (P_a = 44.3 kN). After a small increase in the shear load, debonding of the soffit plate occurred at a shear load of 32.9 kN (P_a = 46.4 kN), as shown in P3-55 and P3-56 respectively.

The relationship between the longitudinal strains in the soffit plate and the shear load is given in Fig.3-33. The relationship between the shear load and the deflection of the beam is shown in Fig.3-34.

Figure 3-33 illustrates that the longitudinal strains in the soffit plate almost varies linearly with the shear load until debonding of the soffit plate occurred. As the horizontal peeling crack formed and developed quickly with increasing shear load, strain gauge No.1, which was close to the soffit plate-end, reduced gradually before the shear peeling and debonding occurred (the point **a** in Fig.3-33). Debonding of the soffit plate occurred at a shear load of 33.0 kN (ie., the applied

load reached 46.4 kN), as shown by point **b** in Fig.3-33. The maximum longitudinal strain in the soffit plate was 569 micro-strains when debonding occurred. Finally, the beam failed in shear at the maximum shear load of 41.8 kN. It can be seen in Fig.3-34 that, initially, the deflection of the beam varies linearly with the shear load. After the inclined crack formed at a shear load of 25.7 kN (the point **a** in Fig.3-34), the shear load dropped slightly. As the inclined cracks and horizontal peeling cracks further developed with increasing shear load, the stiffness of the beam decreased, as shown in range **bc** in Fig.3-34.

A_{st} = 157.0 mm^2 (D_b = 10.0 mm)

Beam SP/S8/R (L_{sp} = 690.0 mm)

The first visible flexural cracks occurred at a shear load of 37.2 kN (P_a = 52.5 kN), as shown in P3-57. At a shear load of 51.8 kN (P_a = 73.0 kN), it can be seen in P3-58 that a few cracks have formed along the edge of the side plates. As the load further increased, it can be seen in P3-59 that the cracks developed gradually along the plates. Debonding of the soffit plate took place at the maximum shear load of 62.8 kN (P_a = 88.5 kN), as shown in P3-60. Finally, the beam failed in flexure at a shear load of 50.1 kN (P_a = 70.7 kN) after debonding of the soffit plate had occurred.

The relationship between the shear load and the strains in the side plates is given in Fig.3-35. The relationship between the longitudinal strains in the soffit plate and the shear load is shown in Fig.3-36. The relationship between the shear load and the deflection of the beam is illustrated in Fig.3-37.

It can be seen in Fig.3-35 that initially the tensile strains in the side plates varied linearly with the shear load and then became gradually non-linear for shear loads

greater than approximately 37.0 kN. It could be implied that the local stresses had redistributed and that cracks may have formed behind the side plates. Figure 3-36 shows that the longitudinal strains in the soffit plate increased gradually with the shear load until debonding of the soffit plate took place at a shear load of 62.8 kN. The maximum longitudinal strain in the soffit plate was 1285 micro-strains when debonding of the soffit plate occurred. It can be seen in Fig.3-37 that the deflection of the beam varied linearly with the shear load until debonding of the soffit plate occurred. Eventually, the beam failed in flexure at the shear load of 50.1 kN after debonding the soffit plate took place.

A_{st} = 628.0 mm^2 (D_b = 20.0 mm)

Beam SP/S9/L (L_{sp} = 0.0 mm)

It should be noted in this test that the soffit plate was twisted before it was glued to the beam. Therefore, the strength of the plated reinforced concrete beam and the results of the test could have been affected.

The inclined crack and the horizontal peeling crack occurred at a shear load of 31.6 kN (P_a = 44.5 kN), as shown in P3-61. After a small increase in the shear load, debonding of the soffit plate took place at a shear load of 32.6 kN (P_a = 46.0 kN), as can be seen in P3-62. The beam failed in shear at the maximum shear load of 45.0 kN (P_a = 63.4 kN), as shown in P3-63.

The relationship between longitudinal strains in the soffit plate and the shear load is given in Fig.3-38. Figure 3-39 shows the variation between the deflection of the beam with the shear load.

It can be seen in Fig.3-38 that the longitudinal strains in the soffit plate vary linearly

with the shear load. Debonding of the soffit plate occurred at a shear load of 31.5 kN. The maximum longitudinal strain in the soffit plate was 451 micro-strains when debonding of the soffit plate took place. Figure 3-39 shows that the deflection of the beam varies linearly with the shear load until debonding of the soffit plate occurred at a shear load of 31.5 kN (the point **a** in Fig.3-39). As the shear load further increased, the stiffness of the beam decreased, as can be seen in the range **ab** and **bc** in Fig.3-39. The beam failed in shear at the maximum shear load of 45.0 kN after the soffit plate had debonded as can be seen at point **c** in Fig.3-39.

A_{st} = 628.0 mm² (D_b = 20.0 mm)

Beam SP/S9/R (L_{sp} = 690.0 mm)

The first visible crack took place along the edge of the side plates at a shear load of 48.4 kN (P_a = 68.2 kN) as can be seen in P3-64. After a further increase in the shear load, the cracks develop along the side plates as can be seen in P3-65. Soffit plate debonding occurred at the maximum shear load of 69.8 kN (P_a = 98.5 kN) as shown in P3-66. Finally, the beam failed in flexure at a shear load of 62.8 kN (P_a = 88.6 kN).

The relationship between the strains in the side plates and the shear load is illustrated in Fig.3-40. The relationship between the shear load and the longitudinal strains in the soffit plate is shown in Fig.3-41and the relationship between the shear load and the deflection of the beam is given in Fig.3-42.

It can be seen in Fig.3-40 that initially the strains in the side plates vary linearly with the shear load. At a shear load of approximately 40.0 kN, the variation in the tensile strains in the side plates becomes non-linear. The strain in strain gauge

No.7, that was positioned on the north side of the beam which is the closest to the position of the applied load, was the first to reduce with increasing the shear load. It may be suggested that the local stresses had redistributed and the cracks may had occurred behind the side plates at the shear load of 33.0 kN (the point **a** in Fig.3-40). As the shear load was further increased, the strain in strain gauge No.10, which was positioned on the south side of the beam, began to drop off gradually at a shear load of 53.0 kN (the point **b** in Fig.3-40) before debonding of the soffit plate had occurred. Figure 3-41 shows the gradual increase in the longitudinal strains in the soffit plate. Debonding of the soffit plate occurred at a shear load of 69.8 kN. The maximum longitudinal strain in the soffit plate was 1449 micro-strains when soffit plate debonding occurred. It can be seen in Fig.3-42 that the deflection of the beam varied linearly with the shear load. Debonding of the soffit plate took place at the maximum shear load of 69.8 kN. The beam failed eventually in flexure at a shear load of 62.8 kN after debonding of the soffit plate had occurred.

Comparison of experimental results

The experimental results of series 3 are given in the following Table 3.3. As mentioned before, it can be seen in Table 3.3 that the shear load that caused debonding of the plated reinforced concrete beam without side plates, SP/S9/L, is less than that in beam SP/S8/L without side plates, even though the A_{st} in beam SP/S9/L is four times that in beam SP/S8/L. It is felt that the strength of plated reinforced concrete beam SP/S9 was influenced by twist in the plate. The relationship between the shear load and the area of the tensile reinforcement in the concrete beams with plates is shown in Fig.3-43.

Table 3.3 Experimental results of the series 3

Specimen No.	A_{st} (mm^2)	L_{sp} (mm)	V_p (kN)	ε_p	V_{max} (kN)	failure mode
SP-S8-L	157.0	-	33.0	569	41.8	debonding of the soffit plate
SP-S9-L	628.0	-	31.5	451	45.0	debonding of the soffit plate
SP-S8-R	157.0	690	62.8	1285	62.8	debonding of the soffit plate
SP-S9-R	628.0	690	69.8	1449	69.8	debonding of the soffit plate

3.2.4 Series 4

The main task of this series is to investigate the variation of the shear strength in the reinforced concrete beams due to external side steel plates. The main variation in the series is the thickness of the side plates as shown in Table 2.4. The concrete beams tested were without stirrups. Both shear spans of the beams were tested to failure. The test rig is shown in Fig.2-1. The position of the electrical resistant strain gauges and the dial gauges are shown in Fig.2-7 and Fig.2-8.

t_{sp} = 0.0 mm

Beam SP/S5/L (Lsp = 0.0 mm)

The inclined crack took place at a shear load of 21.3 kN (P_a = 30.1 kN) as shown in P3-67. On further loading up to a shear load of 25.2 kN (P_a = 35.6 kN), the horizontal peeling crack had occurred at the level of the tensile reinforcement as can be seen in P3-68. Debonding of the soffit plate occurred at a shear load of 28.0 kN (P_a = 40.0 kN) as can be seen in P3-69. The beam failed in shear at the maximum shear load of 47.1 kN (P_a = 66.5 kN), as shown in P3-70.

The relationship between the shear load and the longitudinal strains in the soffit plate is shown in Fig.3-44 and the relationship between the shear load and the deflection of the beam is illustrated in Fig.3-45.

It can be seen in Fig.3-44 that the longitudinal strains in the soffit plate varied linearly with the shear load until debonding of the soffit plate took place. Debonding of the soffit plate occurred at a shear load of 28.0 kN. The maximum longitudinal strain in the soffit plate was 542 micro-strains when debonding of the soffit plate took place. The beam failed in shear at the maximum shear load of 47.1 kN. Figure 3-45 shows that the deflection of the beam varied linearly with the

shear load until debonding of the soffit plate had occurred.

t_{sp} = 1.0 mm

Beam SP/S5/R (Lsp = 1250.0 mm)

The first visible flexural crack formed at a shear load of 40.5 kN (P_a = 57.1 kN) as shown in P3-71. As the load further increased, debonding of the soffit plate occurred at the maximum shear load of 55.0 kN (P_a = 78.0 kN) as can be seen in P3-72. Eventually, the beam failed in flexure after soffit plate debonding had occurred. The side plates were then removed from the beam and it was found that debonding of the soffit plate was only induced by horizontal peeling cracks along the level of the tensile reinforcement and no inclined cracks were found in this test as shown in P3-73.

Figure 3-46 illustrates the variation of the strains in the side plates with the shear load. The relationship between the longitudinal strains in the soffit plate and the shear load is given in Fig.3-47. The relationship between the deflection of the beam and the shear load is shown in Fig.3-48. The relationship between the shear load and the strain gauges No.7 and No.11, that were positioned at the location of the applied load as shown in Fig.2-5 and Fig.2-6, in the side plates is given in Fig.3-49.

It can be seen in Fig.3-46 that initially the strains in the side plates varied linearly with the shear load. At shear loads up to approximately 17.0 kN, the strains in gauge No.7, that was positioned at the location of the applied load, increased linearly up to point **a** in Fig.3-46. At a shear load of 33.0 kN, the variation in the strains in strain gauges No.6 and No.10, which were positioned close to the soffit plate-end, become non-linear (point **b** in Fig.3-46). Further increases in the load

induced local peeling of the side plates which occurred at a shear load of 47.3 kN (point **c** in Fig.3-46). Figure 3-47 shows that the longitudinal strains in the soffit plate varied almost linearly with the shear load until debonding of the soffit plate had occurred. Debonding of the soffit plate occurred at the maximum shear load of 54.6 kN. The maximum longitudinal strain in the soffit plate was 1008 micro-strains when the soffit plate debonding had taken place.

Figure 3-48 shows that the deflection of the beam varied linearly with the shear load until debonding of the soffit plate had occurred at a shear load of 54.6 kN. The stiffness of the beam then decreased after debonding of the soffit plate, as shown in the range **ab** and **bc** in Fig.3-48. The beam failed in flexure at a shear load of 53.5 kN after soffit plate debonding had occurred. Figure 3-49 indicates that the tensile strains in the side plates almost varied linearly with the shear load until debonding of the soffit plate had occurred at the maximum shear load of 54.6 kN (point **a** in Fig.3-49), and then became non-linear until the beam failed in flexure at a shear load of 53.5 kN, as can be seen in the range **bc** and **cd** in Fig.3-49.

t_{sp} = 0.0 mm

Beam SP/S6/L (Lsp = 0.0 mm)

The inclined crack occurred at a shear load of 26.2 kN (P_a = 37.0 kN) as shown in P3-74. After a small increase in the load, it can be seen in P3-75 that the horizontal peeling crack had formed at the level of the tensile reinforcement at a shear load of 28.7 kN (P_a = 40.5 kN). Debonding of the soffit plate occurred at a shear load of 33.3 kN (P_a = 47.0 kN), as shown in P3-76. Finally, the beam failed in shear at the maximum shear load of 38.5 kN (P_a = 54.0 kN).

Figure 3-50 shows that the relationship between the longitudinal strains in the soffit

plate and the shear load. The relationship between the deflection of the beam and the shear load is given in Fig.3-51.

It can be seen in Fig.3-50 that the longitudinal strains in the soffit plate vary linearly with the shear load. At a shear load of 26.1 kN, there is a slight change in the relation due to the formation of the inclined cracks (points **a** and **b** in Fig.3-50). Debonding of the soffit plate occurred at a shear load of 33.1 kN. The maximum longitudinal strain in the soffit plate was 598 micro-strains when debonding took place. Figure 3-51 indicates that the deflection of the beam varied linearly with the shear load, and then the stiffness of the beam decreased because of the formation of the inclined cracks, as shown in the range **ab** in Fig.3-51. As the load further increased, the stiffness of the beam decreased progressively until debonding occurred, as shown in the range **bc** in Fig.3-51. The beam eventually failed in shear at the maximum shear load of 38.5 kN.

t_{sp} = 2.0 mm

Beam SP/S6/R (Lsp = 1250.0 mm)

The first visible crack formed at the end of the soffit plate at a shear load of 57.4 kN (P_a = 81.0 kN) as shown in P3-77. Debonding of the soffit plate occurred at a shear load of 64.5 kN (P_a = 91.0 kN) as can be seen in P3-78. Finally, the beam failed in flexure at the maximum shear load of 66.6 kN (P_a = 94.0 kN), as shown in P3-79.

Figure 3-52 illustrates the relationship between the strains in the side plates and the shear load. Figure 3-53 shows the variation of the longitudinal strains in the soffit plate with the shear load. The relationship between deflection of the beam and the shear load is given in Fig.3-54 and the relationship between the shear load and the

strains in strain gauges No.7 and No.11 in the side plates is given in Fig.3-55.

It can be seen in Fig.3-52 that initially the strains in the side plates varied linearly with the shear load, and then became non-linear at a shear load of approximately 32.0 kN, as shown by the point **a** in Fig.3-52. As the load further increased and the cracks developed gradually behind the side plates, local peeling of the side plate on the south and north side of the beam took place at shear loads of 57.5 kN and 63.3 kN, respectively. Figure 3-52 indicates that strains in the strain gauges No.6 and No.10, which were positioned close to the soffit plate-end in the side plate reduced (points **b** and **c** in Fig.3-52) prior to debonding of the soffit plate. The longitudinal strains in the soffit plate almost varied linearly with the shear load, as shown in Fig.3-53. Debonding of the soffit plate occurred at a shear load of 64.7 kN. The maximum longitudinal strain in the soffit plate was 1254 micro-strains when the soffit plate debonding had occurred.

Figure 3-54 indicates that the deflection of the beam varied linearly with the shear load until the occurrence of soffit plate debonding. The stiffness of the beam then decreased as the load increased, as can be seen in the range **ab** and **bc** in Fig.3-54. Debonding of the soffit plate took place at a maximum shear load of 64.7 kN. The beam failed eventually in flexure at a shear load of 66.6 kN (ie., the applied load was 94.0 kN) after soffit plate debonding had occurred. Figure 3-55 shows the relationship between the shear load and strains in the strain gauges No.7 and No.11 in the side plates. It can be seen that tensile strains in the side plates almost varied linearly with the shear load before soffit plate debonding occurred at a shear load of 64.7 kN (point **a** in Fig.3-55) and then became non-linear until the beam failed in flexure.

t_{sp} = 0.0 mm

Beam SP/S7/L (Lsp = 0.0 mm)

It can be seen in P3-80 that the crack formed at the end of the soffit plate at a shear load of 27.2 kN (P_a = 38.4 kN). The inclined cracks took place in P3-81 at a shear load of 29.8 kN (P_a = 42.1 kN). Debonding of the soffit plate occurred at a shear load of 33.0 kN (P_a = 46.1 kN), as shown in P3-82. Finally the beam failed in shear at the maximum shear load of 46.7 kN (P_a = 65.0 kN).

Figure 3-56 shows the relationship between the longitudinal strains in the soffit plate with the shear load. The relationship between the shear load and the deflection of the beam is illustrated in Fig.3-57.

It can be seen in Fig.3-56 that the longitudinal strains in the soffit plate vary linearly with the shear load until debonding of the soffit plate occurred. Debonding of the soffit plate occurred at a shear load of 33.0 kN. The maximum longitudinal strain in the soffit plate was 552 micro-strains when debonding took place. The beam failed in shear at the maximum shear load of 46.7 kN after debonding of the soffit plate had occurred. Figure 3-57 shows that the deflection of the beam almost varied linearly with the shear load until debonding of the soffit plate had occurred.

t_{sp} = 3.0 mm

Beam SP/S7/R (Lsp = 1250.0 mm)

The first visible cracking had formed along the edge of the side plates at a shear load of 63.1 kN (P_a = 89.0 kN), as shown in P3-83. Debonding of the soffit plate occurred at a shear load of 72.6 kN in P3-84 (P_a = 102.4 kN).

Figure 3-58 shows the variation of the strains in the side plates with the shear load

and Figure 3-59 illustrates how the longitudinal strains in the soffit plate varied with the shear load. The relationship between the shear load and the deflection of the beam is given in Fig.3-60 and the relationship between the shear load and the strains in the strain gauges No.7 and No.11 in the side plates is shown in Fig.3-61.

It can be seen in Fig.3-58 that initially the strains in the side plates vary linearly with the shear load, and then become non-linear at a shear load of 40.0 kN approximately (point **a** in Fig.3-58). As the shear load further increased and the cracks developed progressively behind the side plates, local peeling of the side plates took place at the shear load of 68.7 kN and 71.3 kN respectively. It can be seen in Fig.3-58 that the strains in the strain gauges No.6 and No.10, which were positioned close to the end of the soffit plate, in the side plates dropped off (points **b** and **c** in Fig.3-58) prior to debonding of the soffit plate. Debonding of the soffit plate occurred at a shear load of 72.6 kN. It can be seen in Fig.3-59 that the longitudinal strains in the soffit plate almost vary linearly with the shear load until debonding of the soffit plate occurred. The maximum longitudinal strain in the soffit plate was 1310 micro-strains when debonding of the soffit plate took place at a shear load of 72.6 kN.

Figure 3-60 shows that the deflection of the beam varied linearly with the shear load until debonding of the soffit plate occurred at a shear load of 72.6 kN (point **a** in Fig.3-60). The stiffness of the beam then decreased with increasing load after debonding of the soffit plate had taken place, as can be seen in the range **bc** in Fig.3-60. Finally, the beam failed in flexure at a shear load of 65.5 kN (point **c** in Fig.3-60). Figure 3-61 indicates the relationship between the shear load and the strains in strain gauges No.7 and No.11 in the side plates. It can be seen that the tensile strains in the side plates almost varied linearly with the shear load before debonding of the soffit plate occurred at the shear load of 64.7 kN, and then the

variation became non-linear until the beam failed in flexure.

Comparison of the experimental results

The experimental results of series 4 are given in the following Table 3.4. The relationship between the thickness of the side plates and the debonding shear load is shown in Fig.3-62.

Table 3.4 Experimental result of the series 4

Specimen	t_{sp} (mm)	L_{sp} (mm)	V_{sp} (kN)	ε_p	V_{max} (kN)	failure mode
SP-S5-L	-	-	27.9	542	47.1	debonding of the soffit plate
SP-S5-R	1.0	1250.0	54.6	1008	54.6	debonding of the soffit plate
SP-S6-L	-	-	33.1	598	38.5	debonding of the soffit plate
SP-S6-R	2.0	1250.0	64.7	1254	64.7	debonding of the soffit plate
SP-S7-L	-	-	33.0	552	46.7	debonding of the soffit plate
SP-S7-R	3.0	1250.0	72.6	1310	72.6	debonding of the soffit plate

3.2.5 Series 5

The object of this series is to determine the effect of prestressing on the debonding of the soffit plate by varying the degrees of the prestressing forces in a post-tensioned beam. The tested beams were subjected to three points load as shown in Fig.2-2. The geometric properties of this series are given in Table 2.5. The test rig is shown in the Fig.2-2 and the positions of the electrical resistant strain gauges and dial gauges are shown in Fig.2-11.

Beam PT1 (P_i = 3.0 kN)

It can be seen in P3-85 that the flexural cracks formed at an applied moment of 11.2 kNm (P_a = 15.4 kN). Flexure-shear cracks occurred at both ends of the soffit plate at an applied moment of 16.2 kNm (P_a = 22.3 kN at the load stage 6), as can be seen in P3-86 and P3-87. The horizontal peeling cracks took place at an applied moment of 19.2 kNm and 20.7 kNm (ie., load stages 8 and 9), as shown in P3-87 and P3-88 respectively. As the applied moment further increased, it can be seen in P3-88 that the peeling cracks developed gradually along the level of the bottom reinforcement. Debonding of the soffit plate occurred at an applied moment of 27.8 kNm (P_a = 39.0 kN), as shown in P3-89. It can be seen in P3-90 that the beam finally failed in flexure at an applied moment of 29.2 kNm (P_a = 40.2 kN).

Figure 3-63 illustrates that the variation of the longitudinal strain in the middle of the soffit plate with the applied moment. Figure 3-64 shows that the relationship between the average strain at the both ends of the plate and the applied moment. Figure 3-65 gives the moment-deflection curve for the beam.

It can be seen in Fig.3-63 that the longitudinal strain in the centre of the soffit plate varied linearly with the applied moment until debonding of the soffit plated occurred

at an applied moment of 27.8 kNm. Figure 3-64 shows that the average strain, at the both ends of the soffit plate, initially varied linearly with the applied moment and then the strain reduced after flexural cracks had formed at an applied moment of 11.2 kNm (point **a** in Fig.3-64). As the applied moment further increased, horizontal peeling cracks formed at both ends of the plate at applied moments of 19.2 kNm and 20.7 kNm. It can be seen that the average strain, at the ends of the plate, reduced again at points **b** and **c** in Fig.3-64. Figure 3-65 shows the relationship between the deflection in the centre of the beam and the applied moment. It can be seen that the stiffness of the beam decreases with increasing applied moment after debonding of the soffit plate has taken place, as shown the range **bc** in Fig.3-65.

Beam PT2 (P_l = 30.0 kN)

It can be seen in P3-91 that flexural cracks occurred at an applied moment of 12.5 kNm (P_a = 17.2 kN at load stage 4). The horizontal peeling crack formed at the applied moment of 23.4 kNm (P_a = 32.3 kN at load stage 9), as shown in P3-92. As the applied moment further increased, it can be seen in P3-93 that the horizontal peeling crack developed progressively along the level of the bottom reinforcement, and flexure-shear cracks extended towards the compressive region of the concrete. Debonding of the soffit plate took place at an applied moment of 32.3 kNm (P_a = 44.5 kN), as shown in P3-94. Eventually, the beam failed in flexure at the maximum applied moment of 32.5 kNm (P_a = 44.8 kN), as shown in P3-95.

Figure 3-66 shows how the longitudinal strain in the middle of the soffit plate varies with the applied moment. Figure 3-67 illustrates the variation of the average strain, at both ends of the plate, with the applied moment and Figure 3-68 shows the relationship between the deflection in the centre of a beam and the applied

moment.

It can be seen in Fig.3-66 that the longitudinal strain in the middle of the soffit plate varied linearly with the applied moment and then the strain dropped down rapidly when debonding of the soffit plate had taken place at an applied moment of 32.3 kNm. Figure 3-67 gives the variation of the average strains, at both ends of the soffit plate, with the applied moment. It can be seen that the strain drops slightly when the flexural cracks form at the ends of the soffit plate at an applied moment of 12.5 kNm (point **a** in Fig.3-67). The horizontal peeling cracks took place at an applied moment of 23.4 kNm (point **b** in Fig.3-67), and then the strains dropped off rapidly with further increasing in the applied moment(point **c** in Fig.3-67) before debonding of the soffit plate occurred. Figure 3-68 illustrates the variation of the deflection in the centre of a beam with the applied moment. It can be seen that the stiffness of the beam decreased with increasing applied moment after debonding of the soffit plate occurred (range **bc** in Fig.3-68). Finally, the beam failed in flexure.

Beam PT3 (P_i = 18.0 kN)

It can be seen in P3-96 the sequence of the crack formation during the testing. The first visible flexural crack occurred at the end of the soffit plate at the load stage 8 (ie., the applied moment was 11.8 kNm and P_a = 16.3 kN), and then the horizontal peeling crack formed at load stage 14 (ie., the applied moment was 23.0 kNm and P_a = 31.7 kN). Debonding of the soffit plate occurred at load stage 23 (ie., the applied moment reached 30.8 kNm and P_a = 42.4 kN). At last, the beam failed in flexure at the maximum applied moment of 32.4 kNm (P_a = 44.6 kN).

Figure 3-69 shows the variation of the longitudinal strain, in the middle of the soffit

plate, with the applied moment. Figure 3-70 illustrates the variation of the average strain, at both ends of the plate, with the applied moment. Figure 3-71 gives the relationship between the deflection in the centre of a beam and the applied moment.

It can be seen in Fig.3-69 that the longitudinal strain in the middle of the soffit plate varied linearly with the applied moment, and then dropped rapidly down when debonding of the soffit plate had taken place at the applied moment of 30.8 kNm. Figure 3-70 shows the variation of the mean strain, at both ends of the soffit plate, with the applied moment. Initially, the strain varied linearly with the applied moment up to 7.4 kNm (point **a** in Fig.3-70) and then dropped down rapidly. It could be implied that the cracks had already occurred at this stage before the first visible crack, which is shown in P3-96 (ie., the load stage 8), had been observed. The strain then dropped down slightly when the horizontal peeling cracks formed at the applied moment of 23.0 kNm, as shown at point **b** in Fig.3-70. As the applied moment further was increased the cracks extended progressively; the average strain, at both ends of the soffit plate, dropped off rapidly before debonding of the soffit plate had taken place (point **c** in Fig.3-70). Figure 3-71 illustrates the variation of the deflection in the centre of a beam with the applied moment. It can be seen that the stiffness of a beam decreased with increase in the applied moment after debonding of the soffit plate occurred at an applied moment of 30.8 kNm, as shown in the range **bc** in Fig.3-71. Finally, the beam failed in flexure at the maximum applied moment of 32.4 kNm (ie., the applied load was 44.6 kN).

Beam PT4 (P_i = 42.0 kN)

It can be seen in P3-97 the crack pattern after the horizontal peeling crack had formed. The first flexural crack occurred at load stage 9 (ie., the applied moment was 13.2 kNm and P_a = 18.1 kN), and the horizontal peeling crack formed at load

stage 17 (ie., the applied moment was 23.6 kNm and P_a = 32.5 kN). It can be seen in P3-98 that the beam failed eventually in flexure after debonding of the soffit plate had occurred at load stage 21 (ie. the applied moment reached 31.8 kNm and P_a = 43. 8 kN).

Figure 3-72 gives the variation of the longitudinal strain, in the middle of the soffit plate, with the applied moment. Figure 3-73 shows the relationship between the average strain, at both ends of the plate, and the applied moment. Figure 3-74 illustrates the relationship between the deflection in the centre of a beam and the applied moment.

It can be seen in Fig.3-72 that the longitudinal strain in the middle of the soffit plate varied linearly with the applied moment, and then dropped off at the applied moment of 31.8 kNm when debonding of the soffit plate had occurred (point **a** in Fig.3-72). Figure 3-73 shows the variation of the mean strain, at both ends of the plate, with the applied moment. It can be seen that the strain dropped off when the crack formed at the end of the plate at an applied moment of 13.2 kNm (point **a** in Fig.3-73). When the horizontal peeling cracks had occurred at the applied moment of 23.6 kNm, the strain dropped gradually down as the applied moment was further increased (ie., point **b** in Fig.3-73). Figure 3-74 illustrates the variation of the deflection in the centre of a beam with the applied moment. It can be seen that the stiffness of the beam decreased as the applied moment further increased after debonding of the soffit plate had occurred (range **bc** in Fig.3-74). Finally, the beam failed in flexure at the maximum applied moment of 34.9 kNm (ie., the applied load reached 48.1 kN).

Comparison of the experimental results

The experimental results of the series 5 are given in the following Table 3.5. The relationship between the varying degrees of the prestressing forces in a reinforced concrete beam and the cracking moment, peeling moment and debonding moment is shown in Fig.3-75.

Table 3-5 Experimental results of the series 5

Specimen No.	P_i (kN)	M_{cr} (kNm)	M_{pl} (kNm)	M_d (kNm)	ε_p
PT1	0.00	11.2	19.2	27.8	630
PT3	18.0	11.8	23.0	30.8	608
PT2	30.0	12.5	23.4	32.3	705
PT4	42.0	13.2	23.6	31.8	612

where

M_{cr} = cracking moment

M_{pl} = peeling moment

M_d = debonding moment

3.3 Summary of the experimental results

For series 1, in which the length of the side plates was varied, the test results, in Table 3.1, showed that the shear strength of the reinforced concrete beams, without stirrups, increases with increasing the length of the side plates, as shown in Fig.3-21. Also the debonding moment of the plated reinforced concrete beams increases as the length of the side plates increases.

For series 2, in which the thickness of the soffit plate varied, the test results, in Table 3.2, showed that the shear strength increases with the increase in the thickness of the soffit steel plate.

For series 3, in which the area of the longitudinal tensile reinforcement was varied, the experimental test results show that the debonding moment increases with the greater area of the longitudinal tensile reinforcement.

For series 4, in which the thickness of the side plates varies, the increase in the shear strength of the reinforced concrete beams, without stirrups, is the result of the thickness of the side plate increasing, as shown in Table 3.4 and in Fig.3-62, respectively.

For series 5, in which the degree of the initial prestressing force is varied, the experimental results show that debonding moment increases generally with the prestressing forces, as can be seen in Table 3.5 and Fig.3-75, respectively.

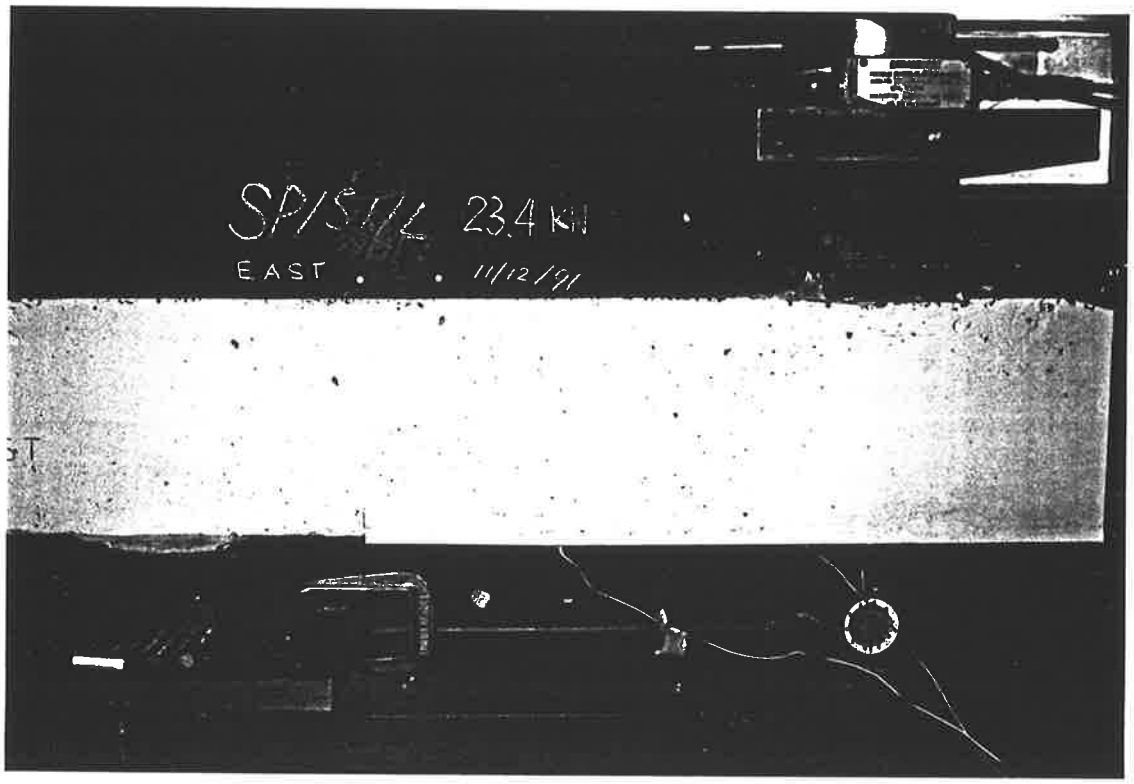

P3-1 The flexural crack formed

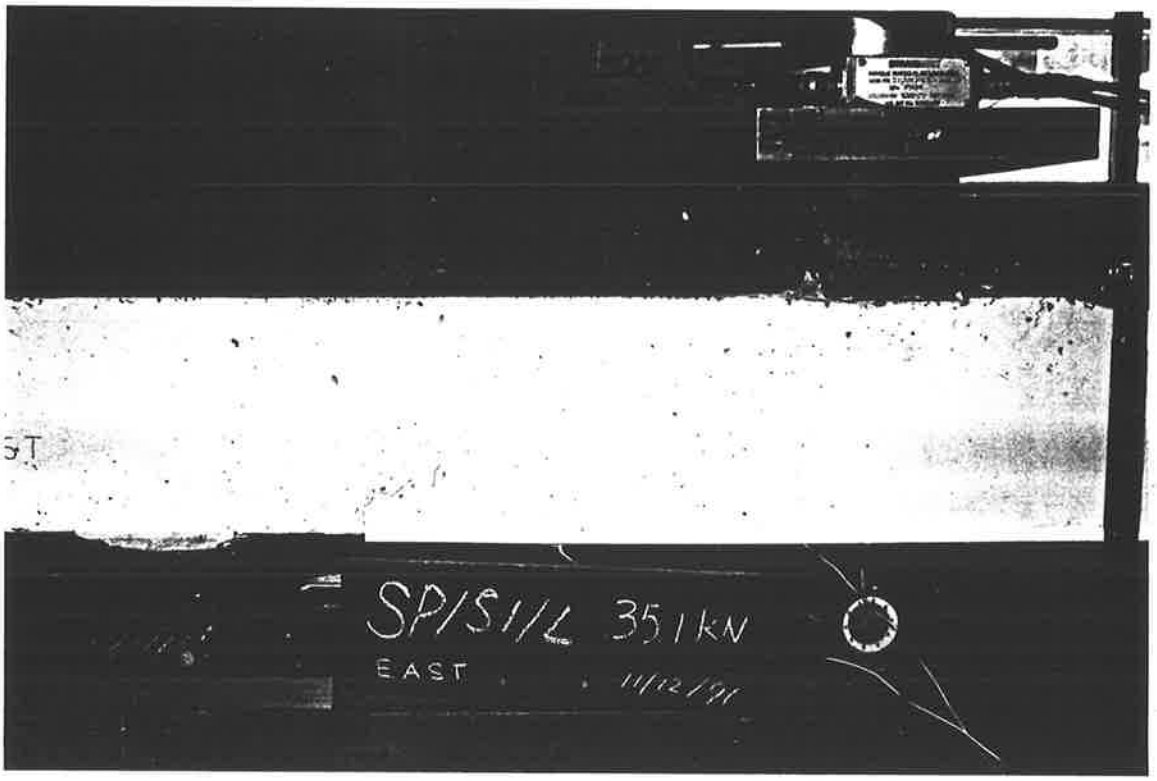

P3-2 The horizontal peeling crack formed at the level of the bottom reinforcement

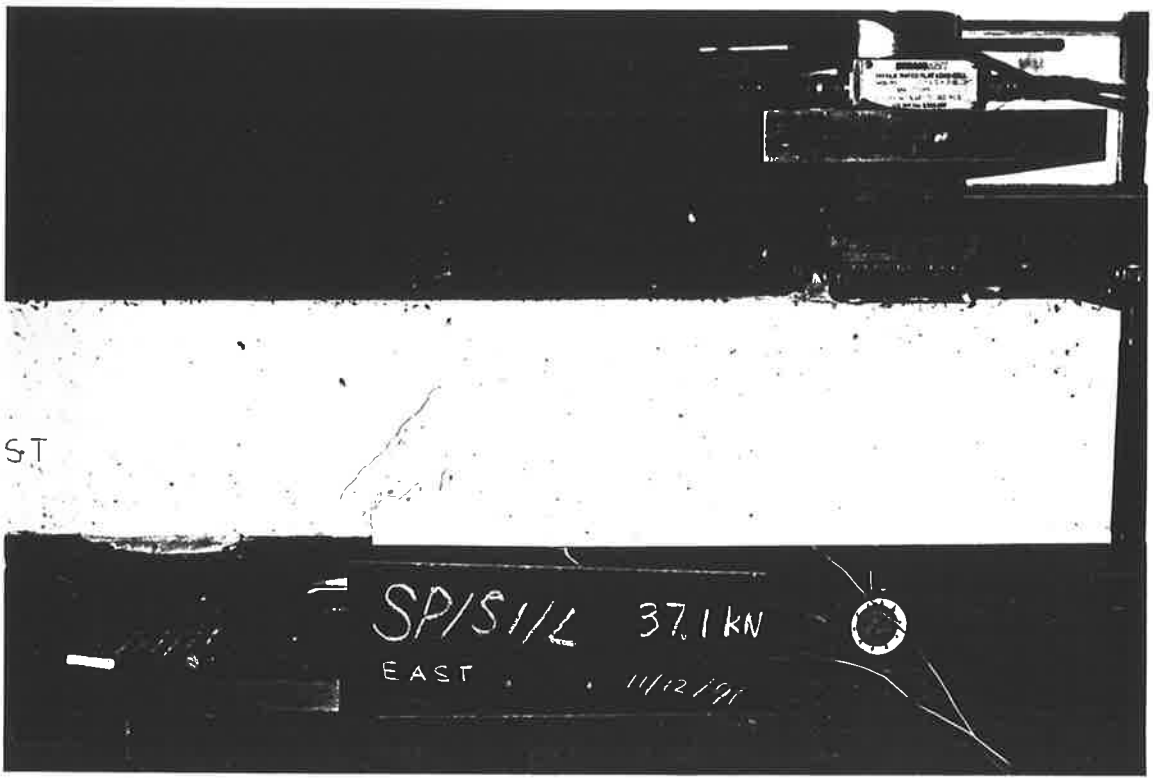

P3-3 The web crack formed

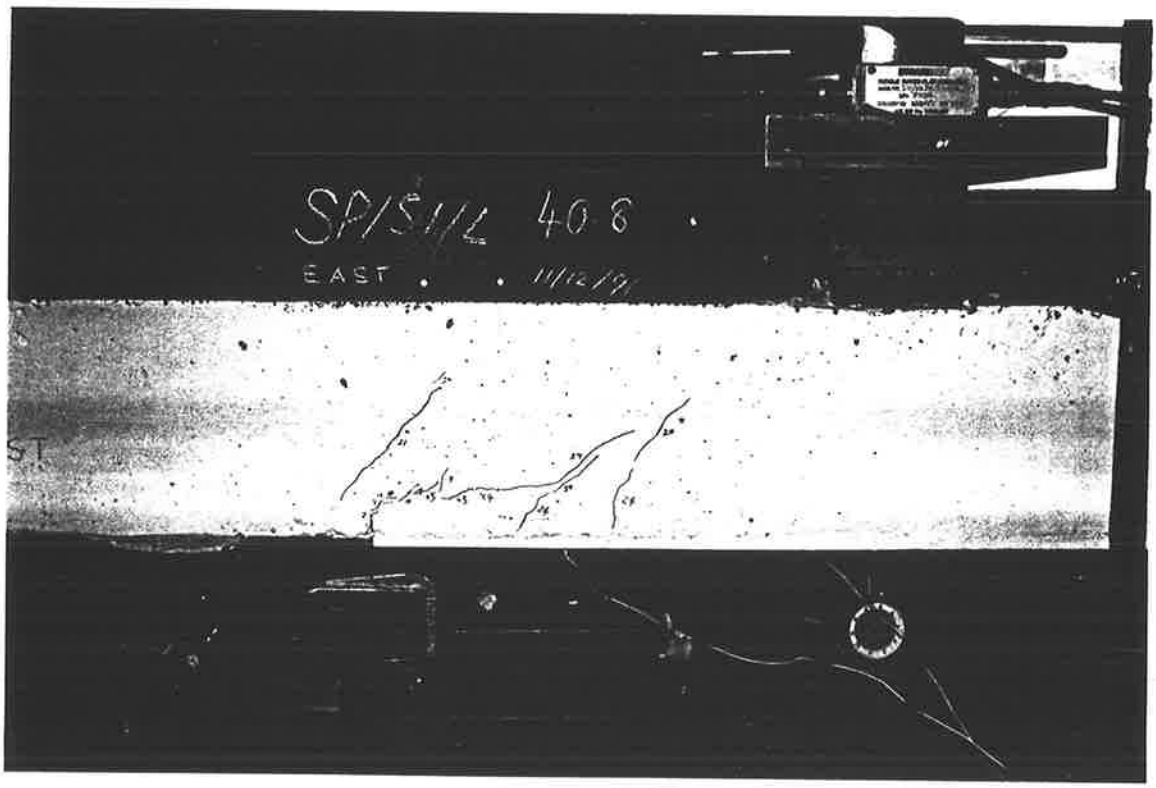

P3-4 The cracks developed

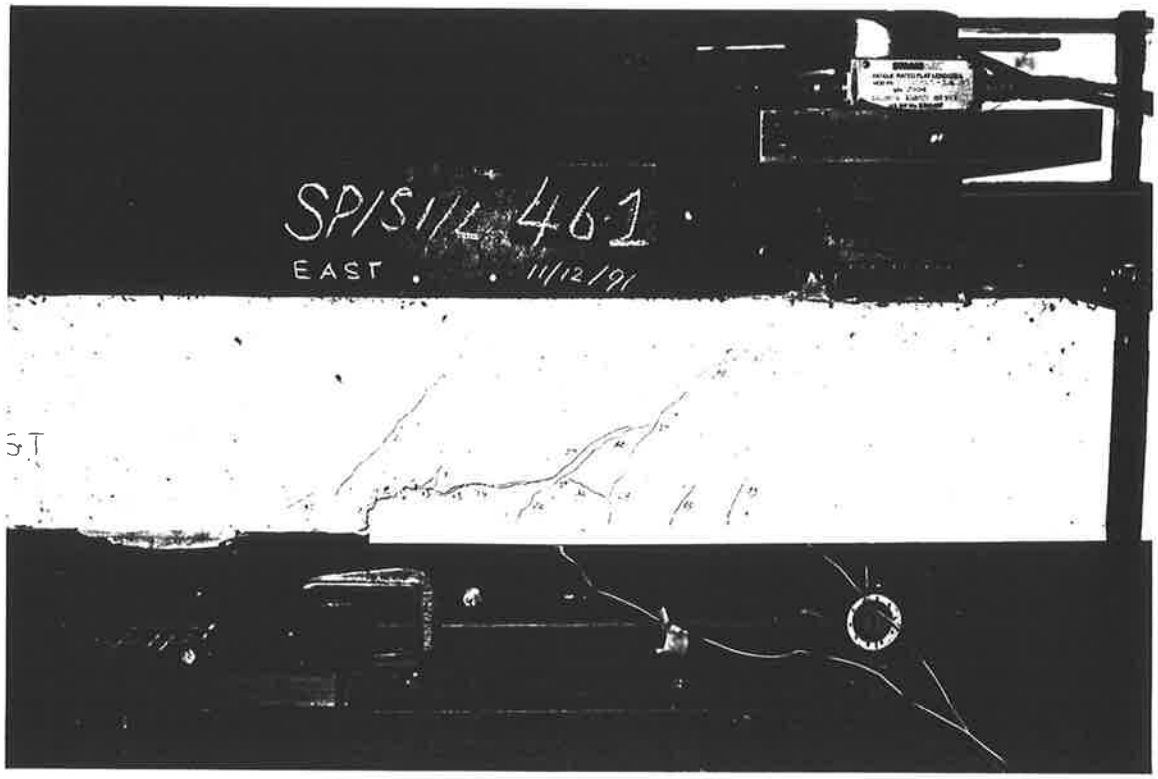

P3-5 The peeling crack extended along the level of the bottom reinforcement

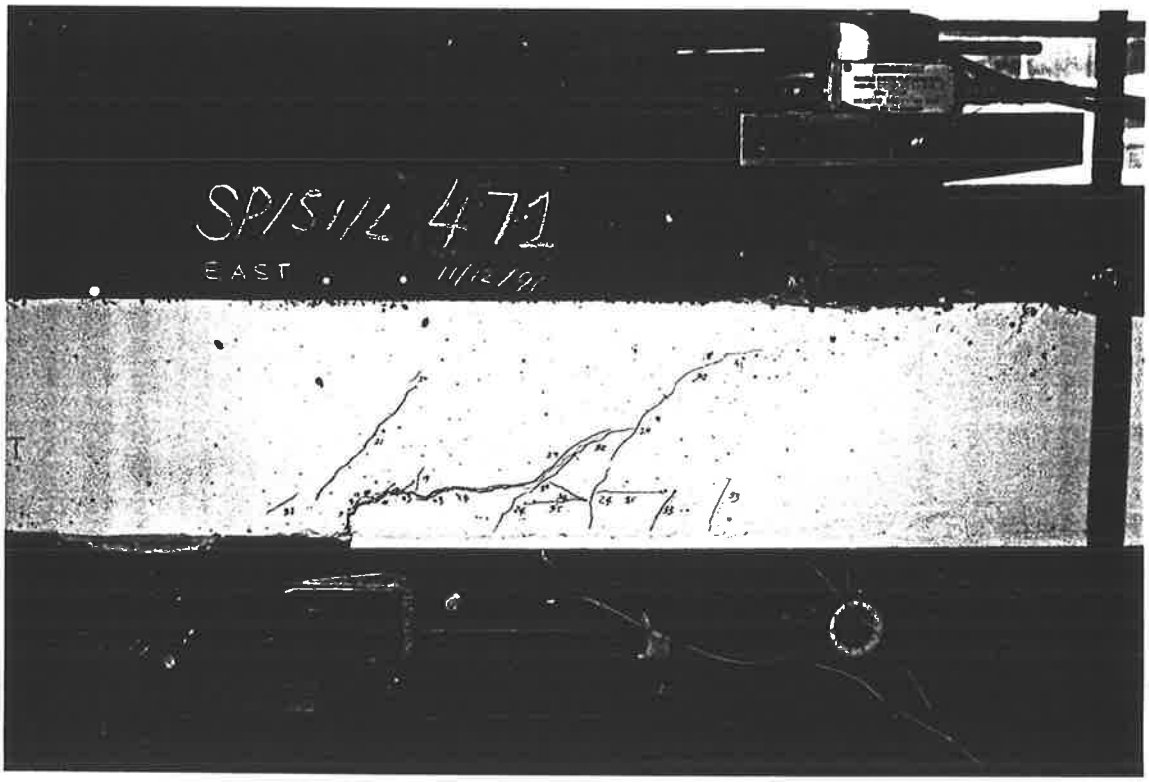

P3-6 Debonding of the soffit plate

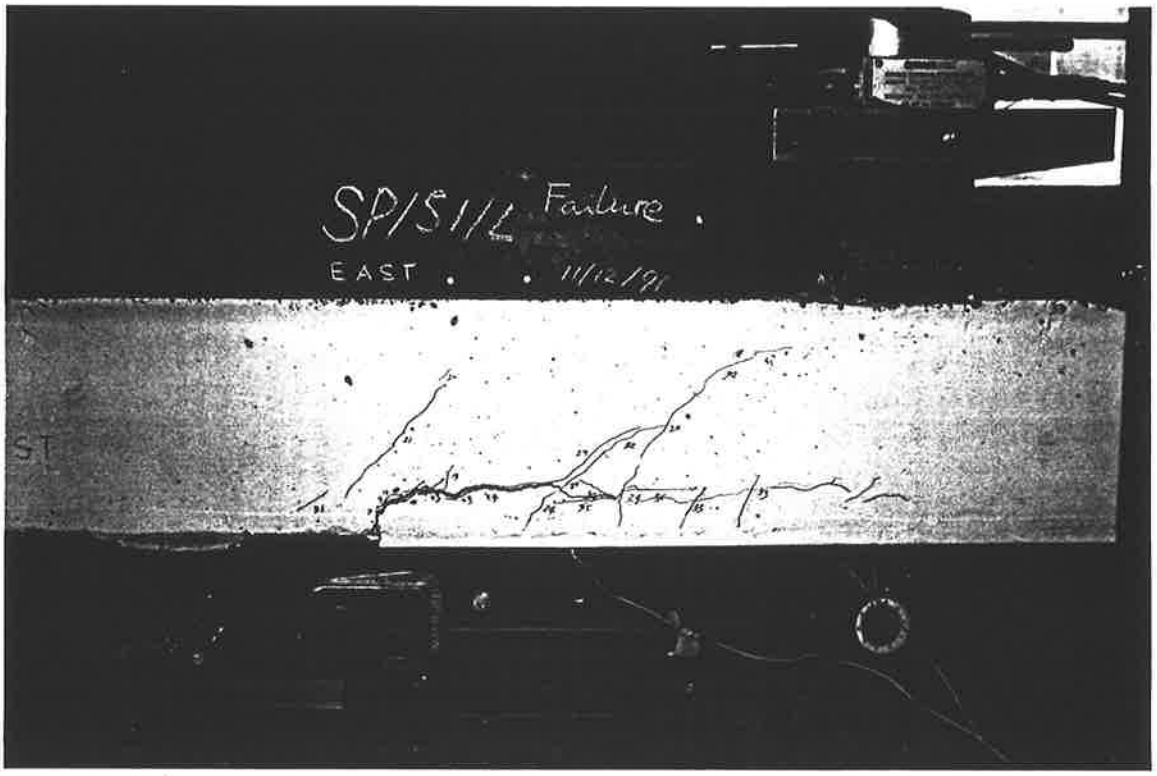

P3-7 Premature failure

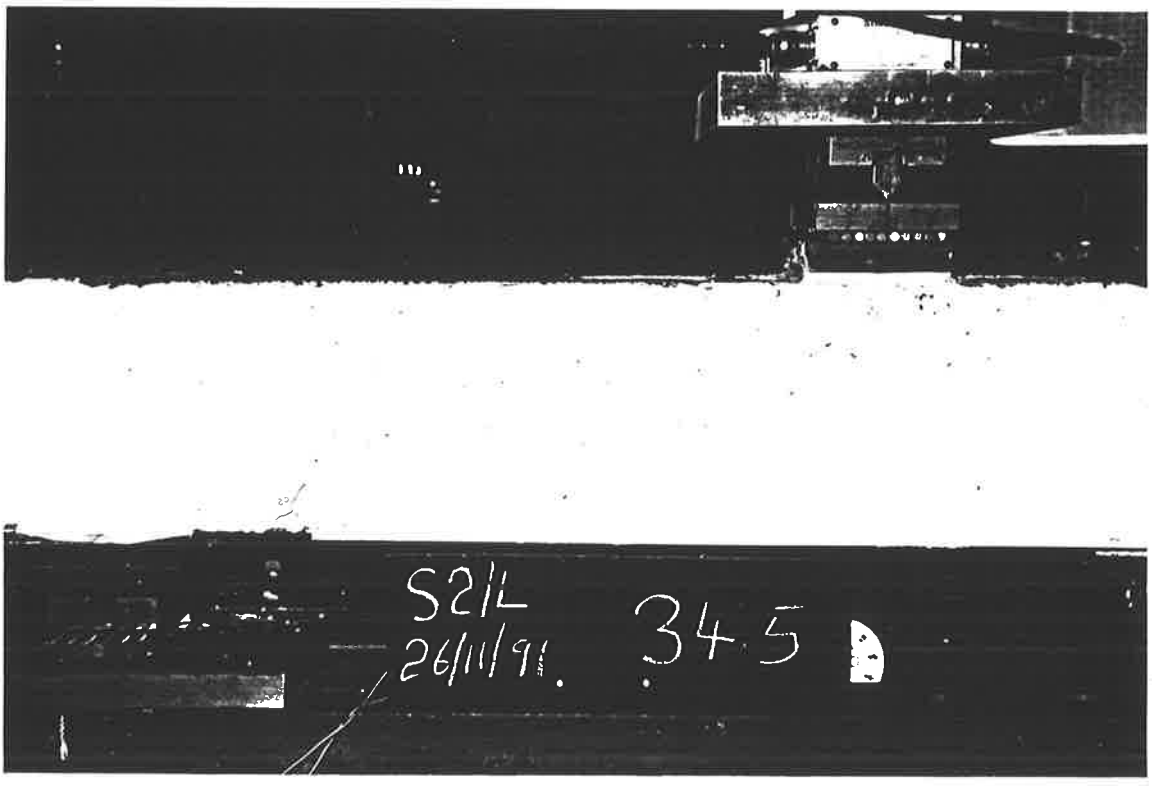

P3-8 The inclined cracks occurred in the vicinity of the soffit plate

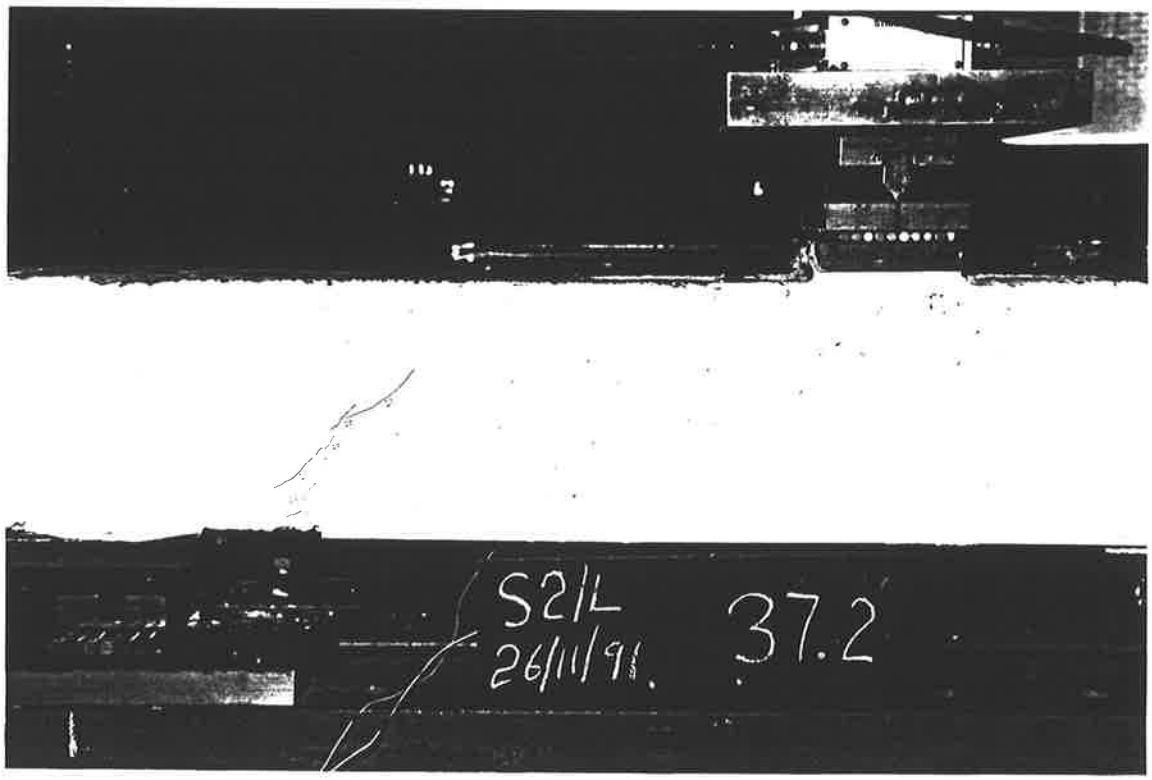

P3-9 The shear diagonal crack formed

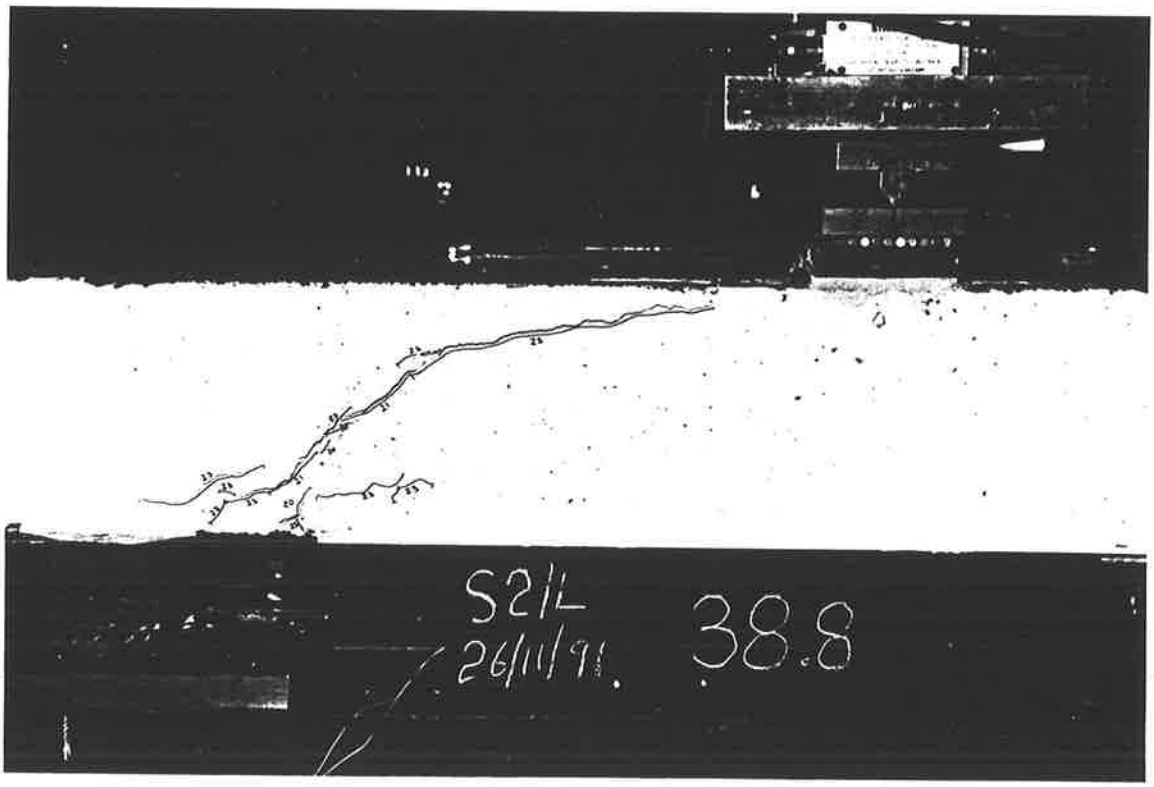

P3-10 The shear peeling and shear failure

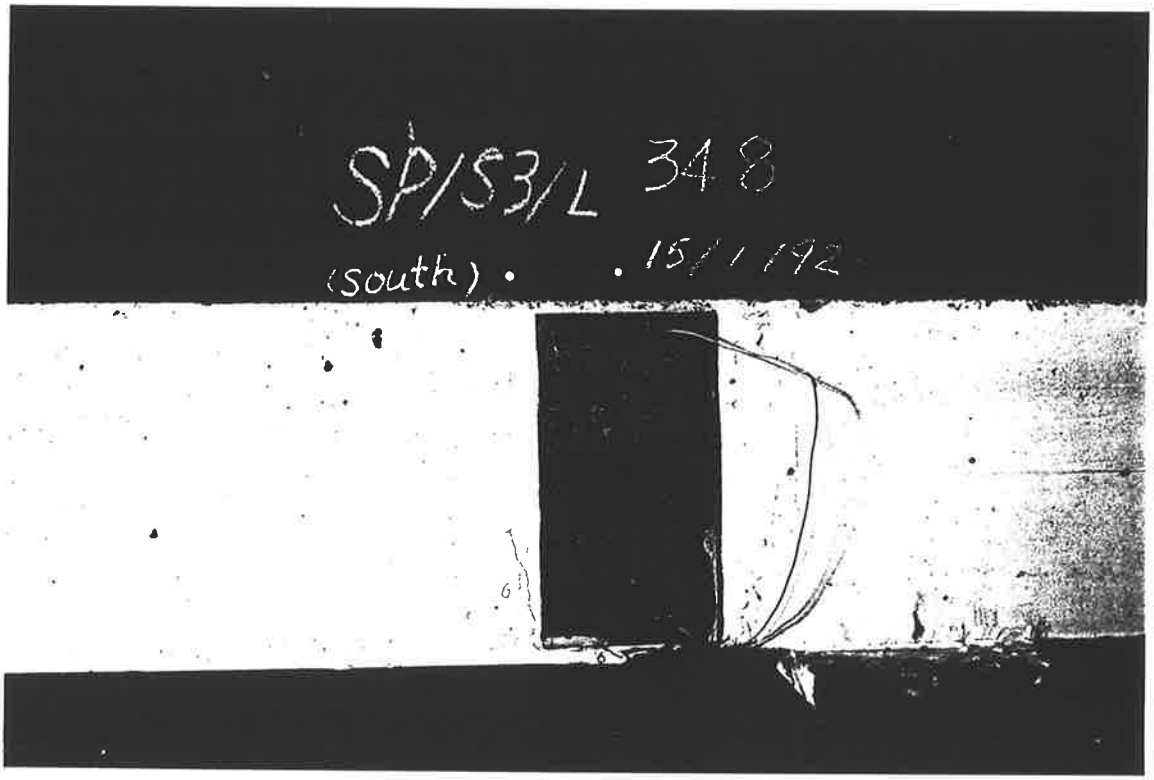

P3-11 Cracks formed along the edge of the side plate in south

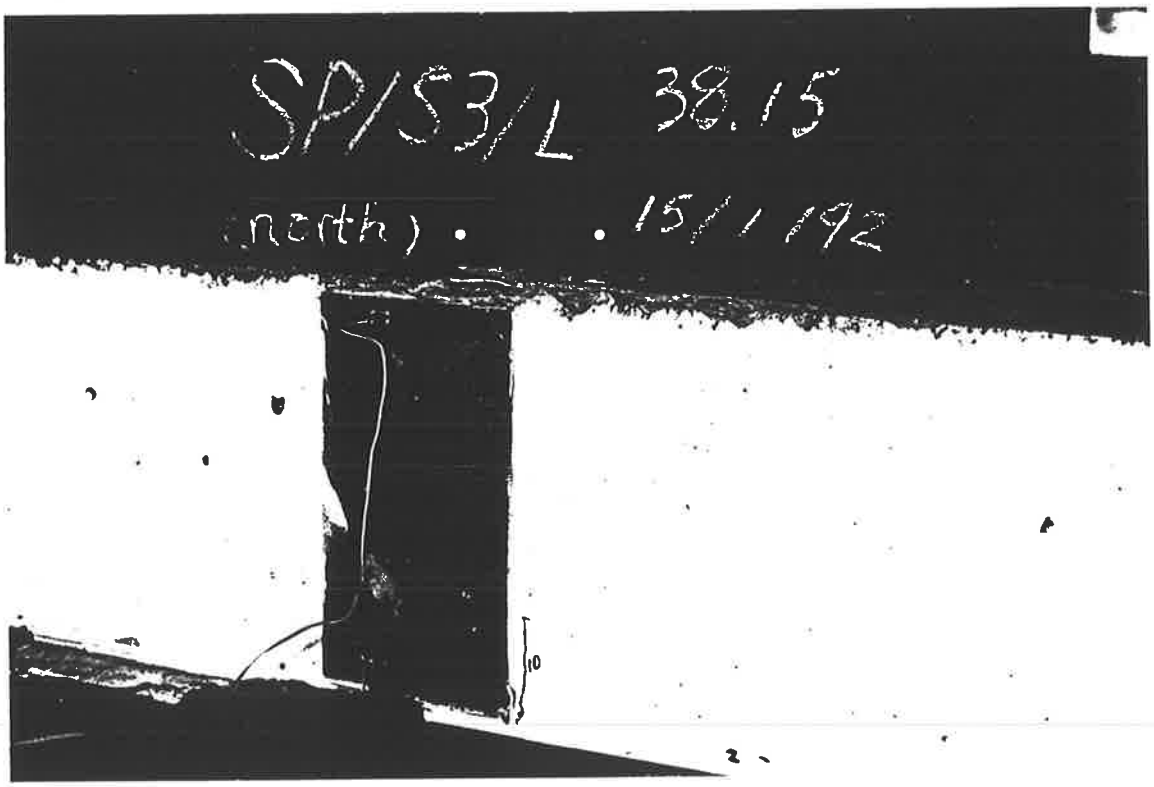

P3-12 Cracks formed along the edge of the side plate in north

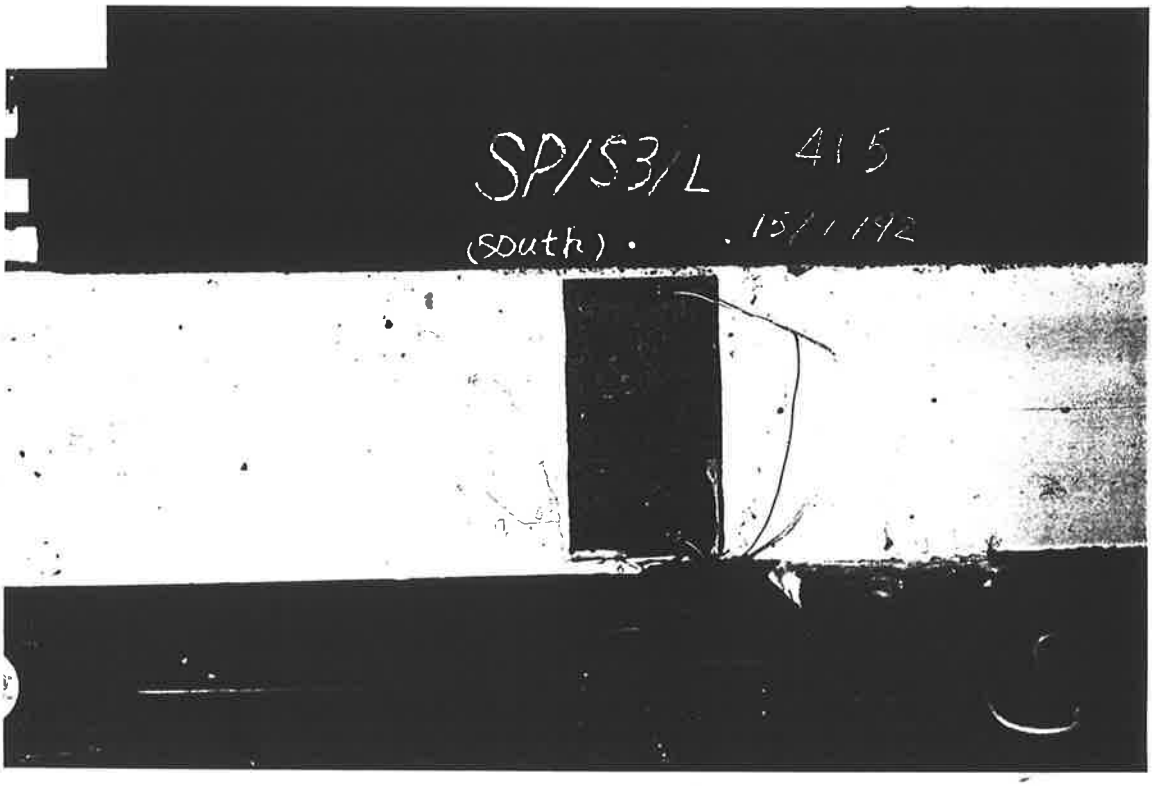

P3-13 Cracks extended and peeling crack formed at the level of the bottom reinforcement

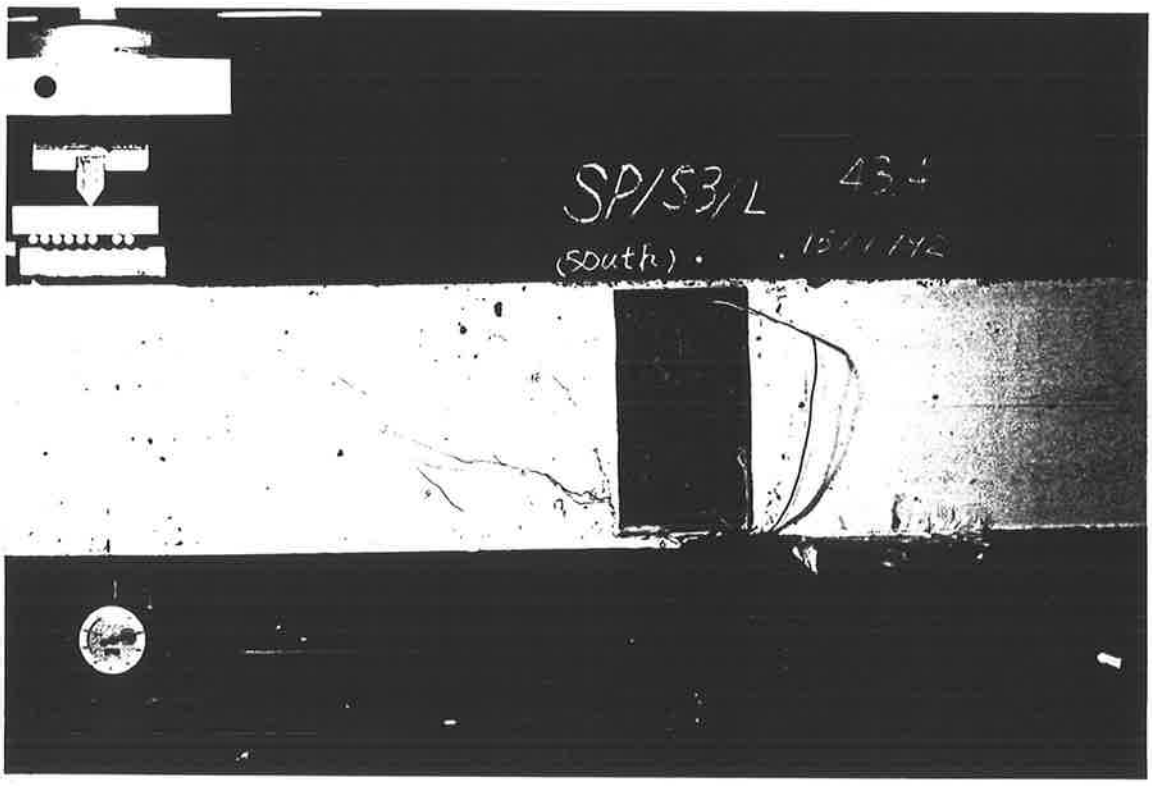

P3-14 Debonding of the soffit plate

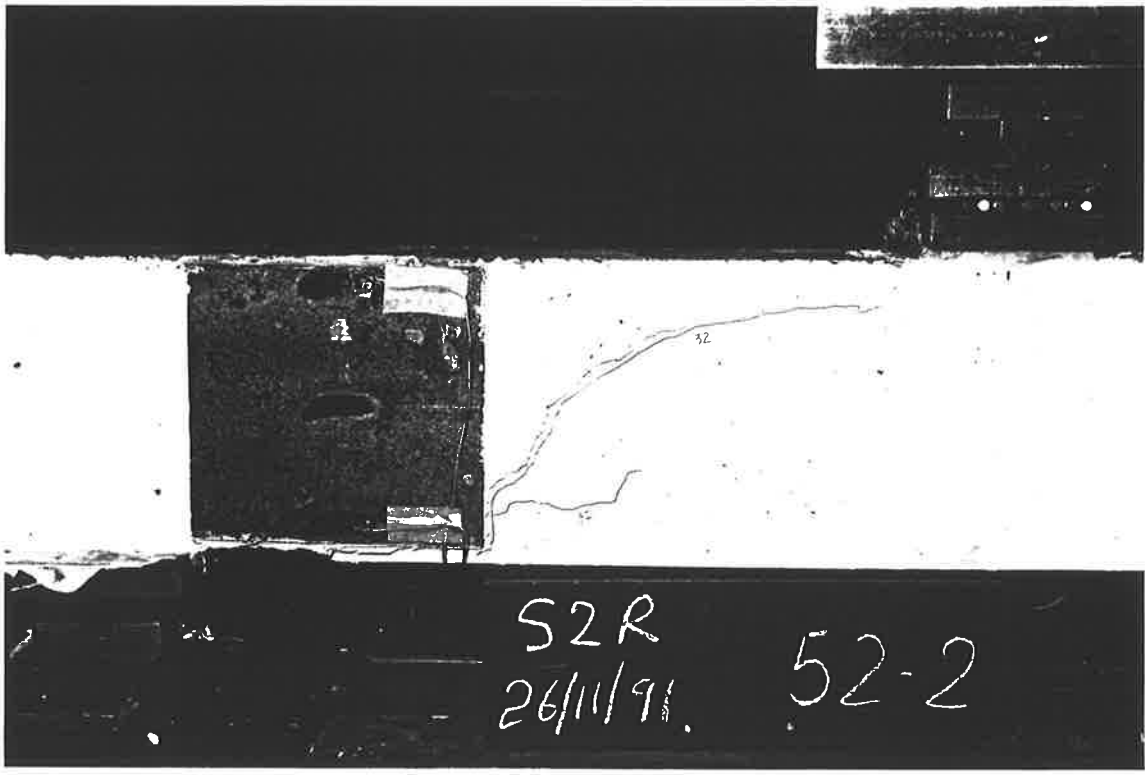

P3-15 Debonding of the soffit plate

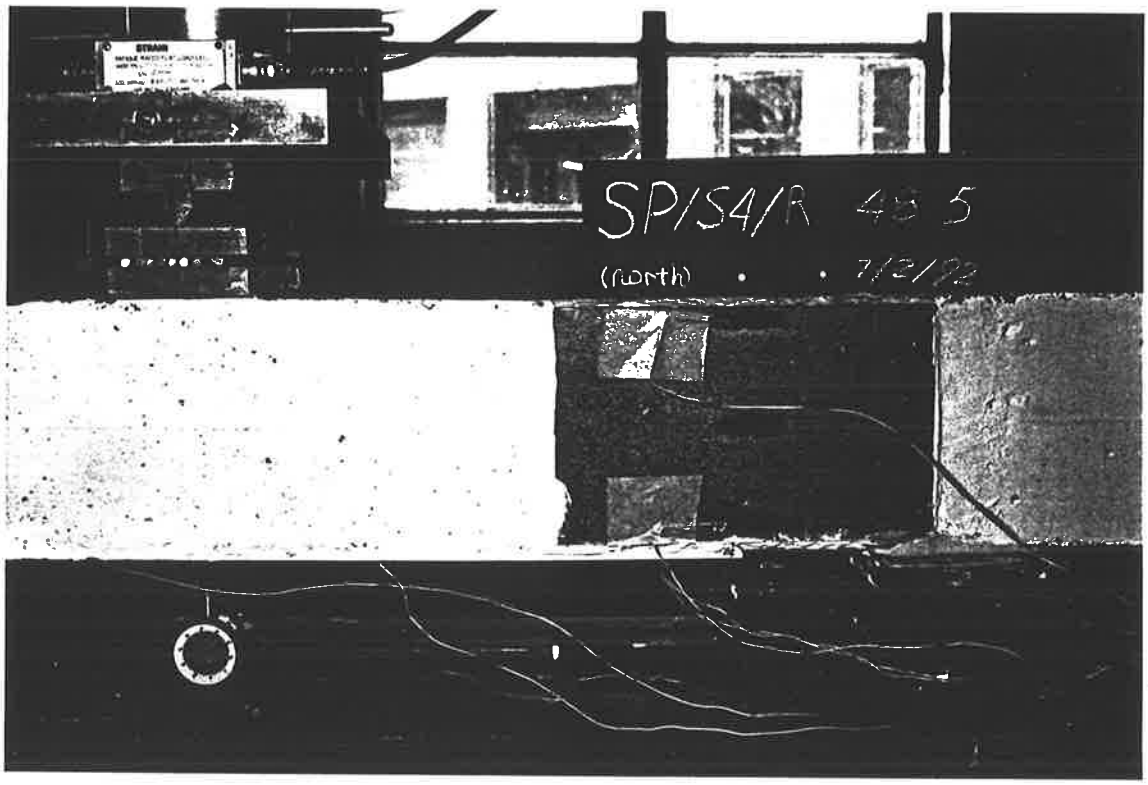

P3-16 The crack formed at the soffit plate-end

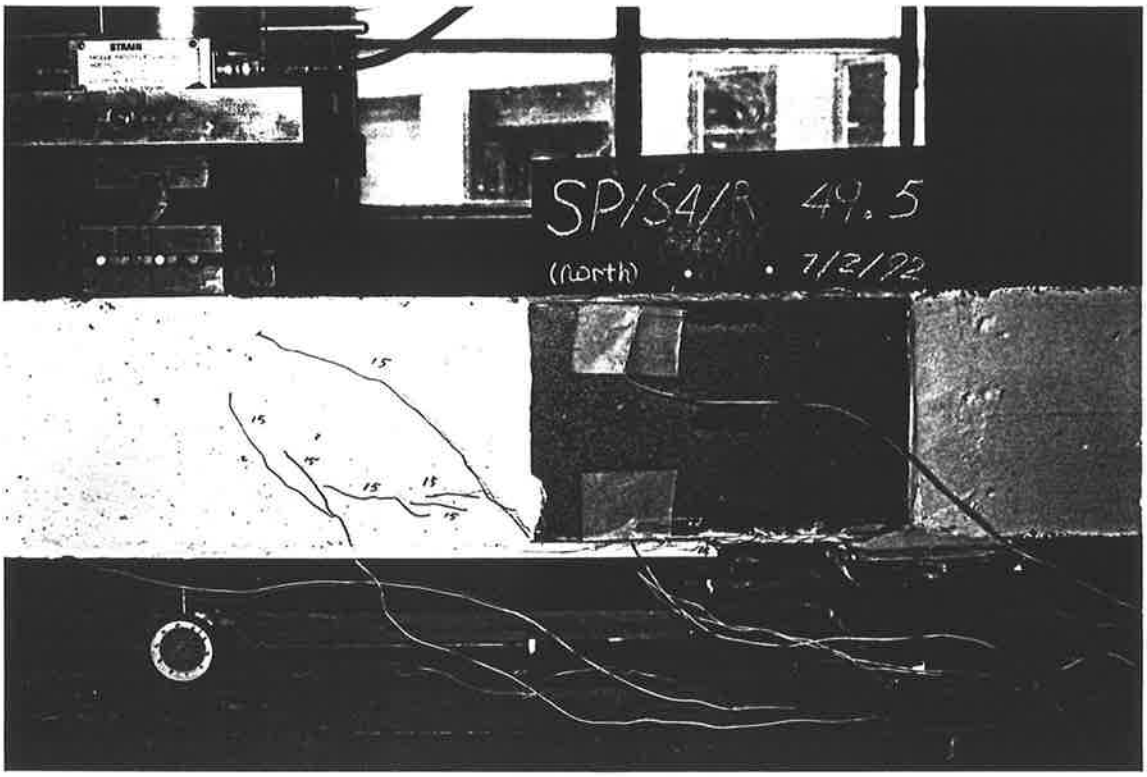

P3-17 Debonding of the both side and soffit plate occurred

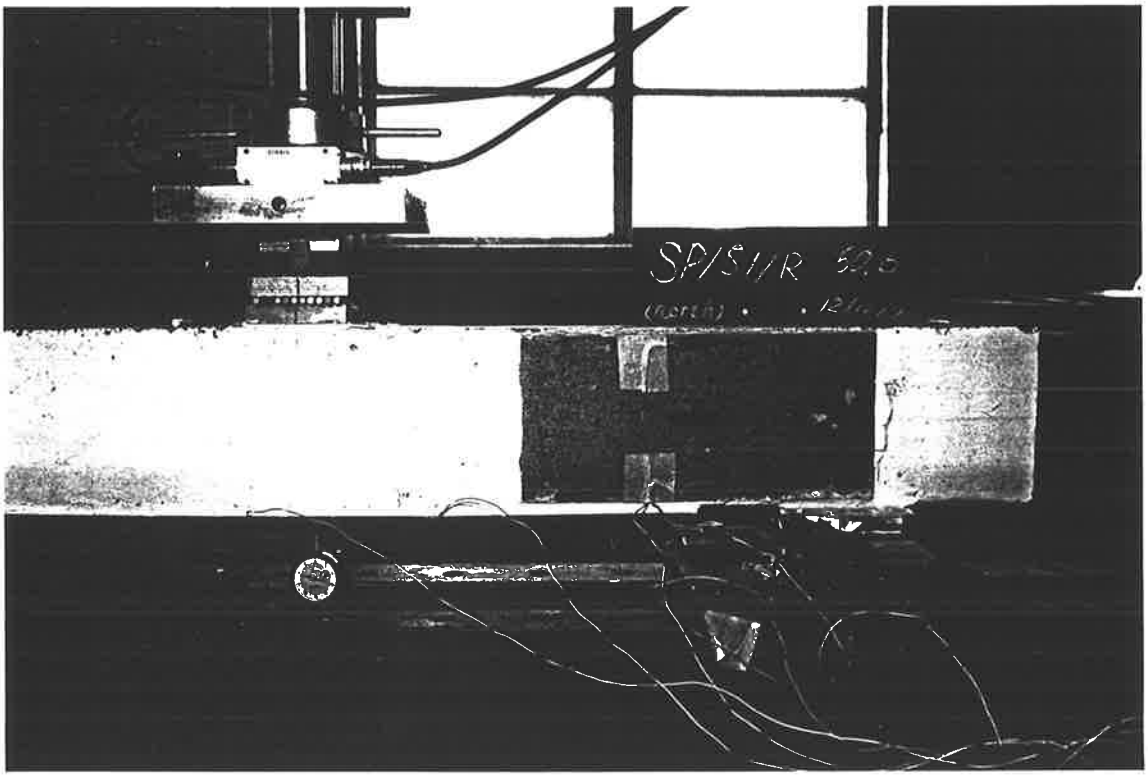

P3-18 The flexure crack formed

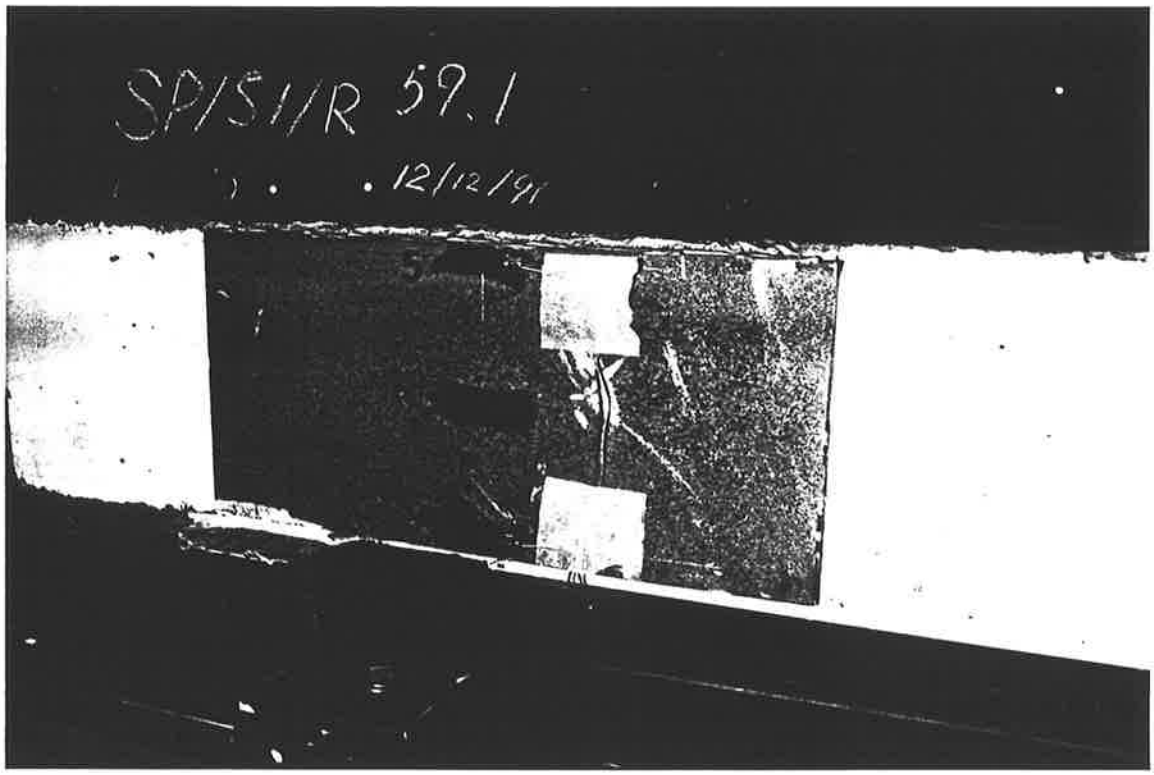

P3-19 The cracks formed along the edge of the plates

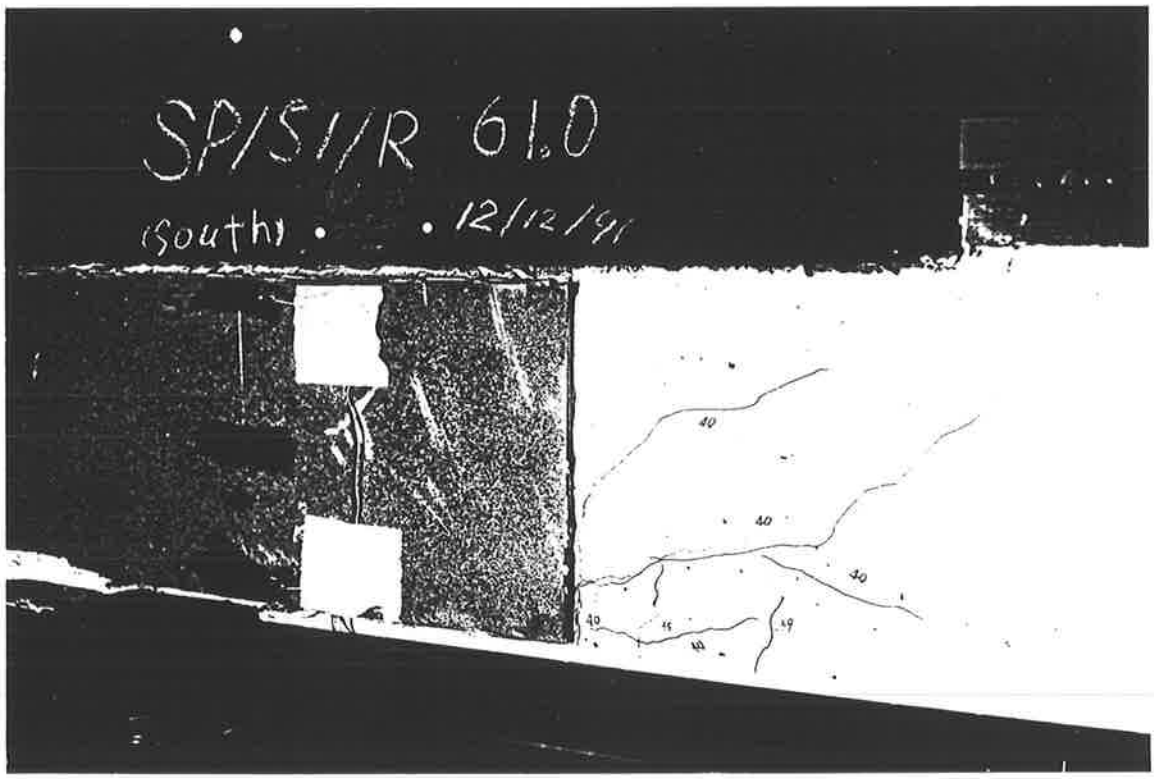

P3-20 Debonding of the side and soffit plates

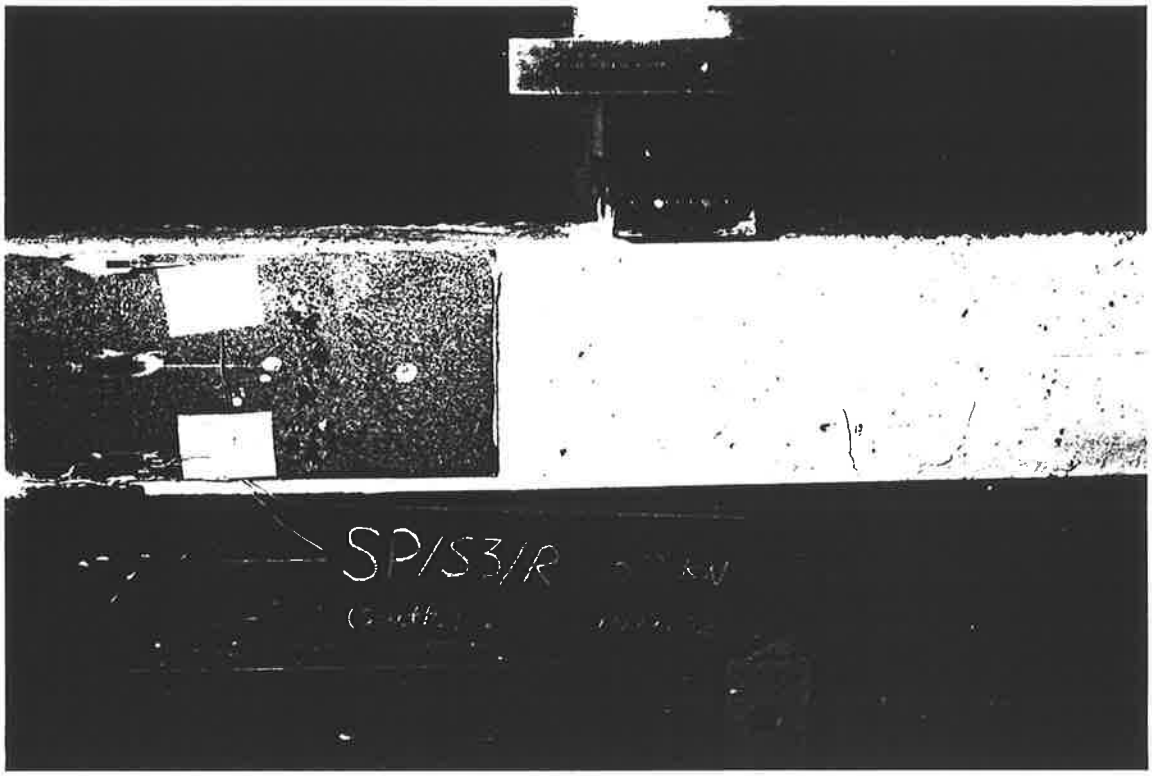

P3-21 The flexural crack formed

P3-22 Cracks occurred along the edge of the plates

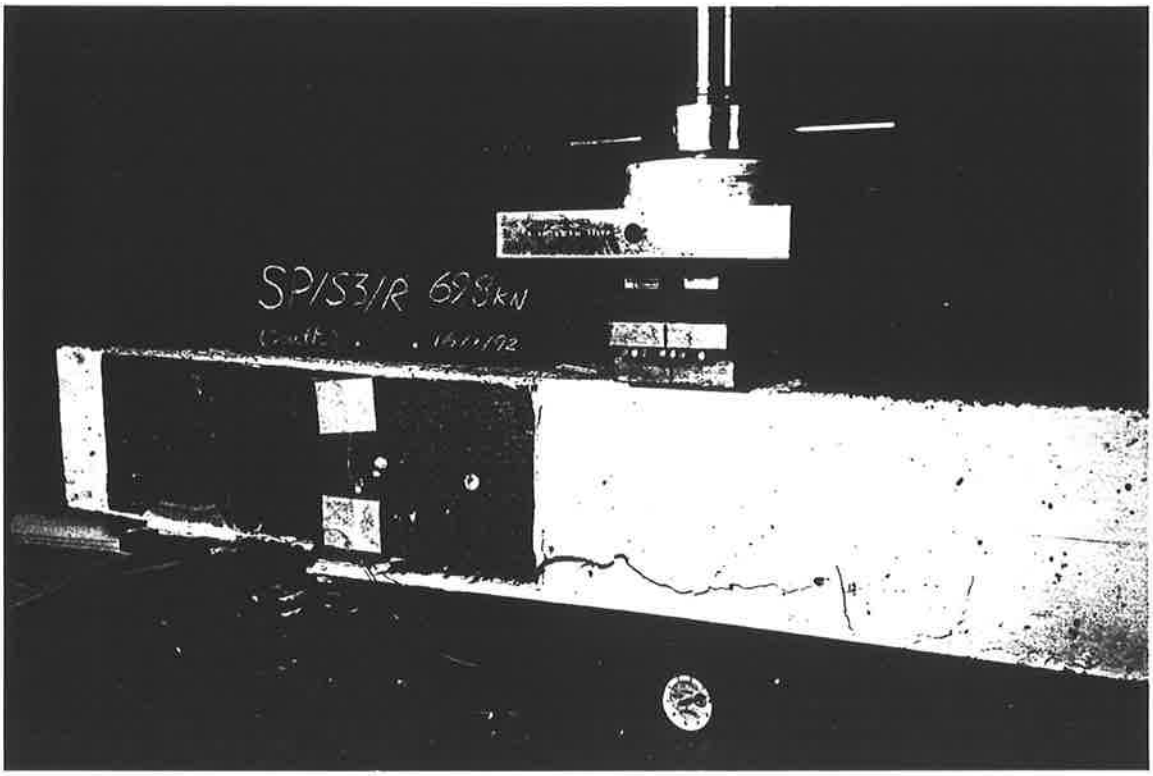

P3-23 Debonding of the soffit plate

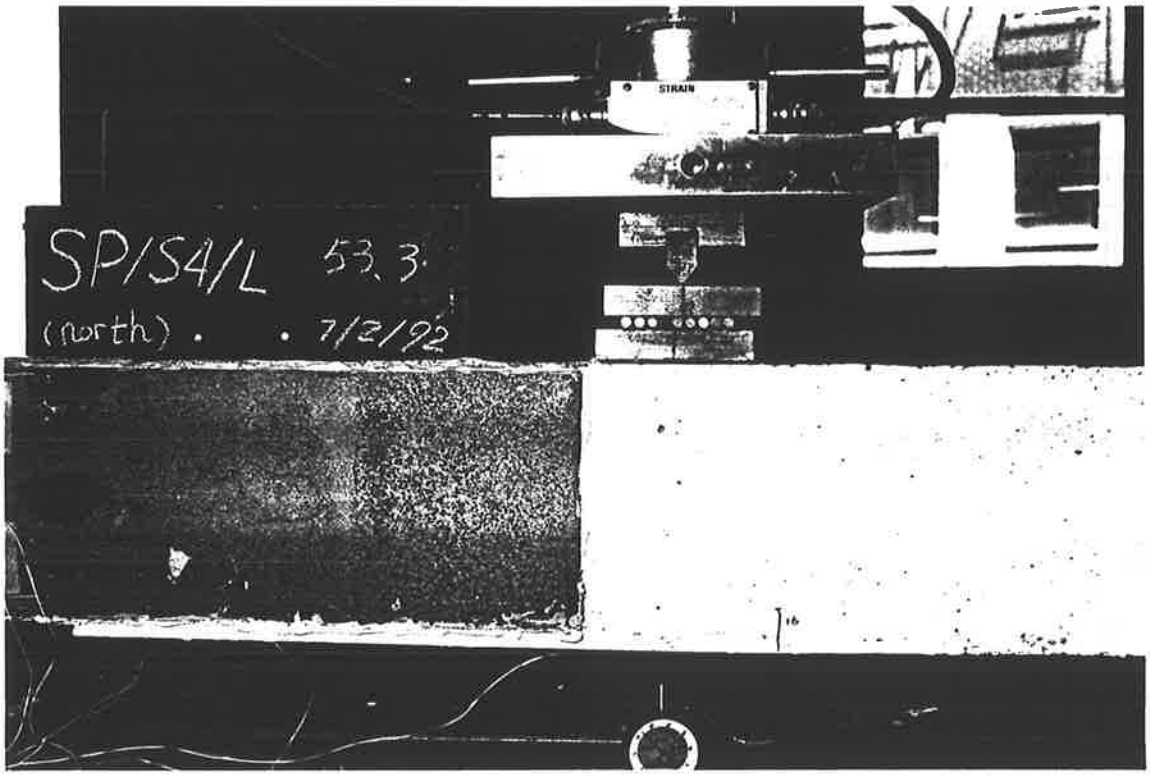

P3-24 The flexural crack occurred

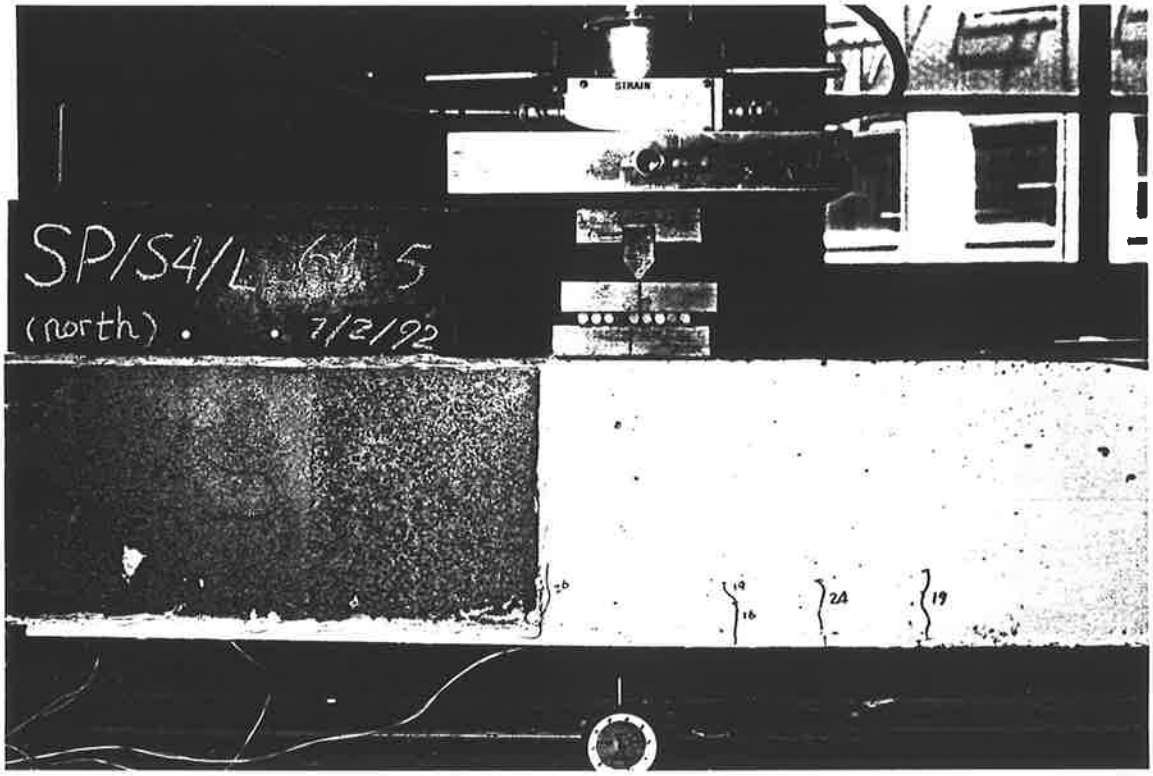

P3-25 Cracks formed along the edge of the plates

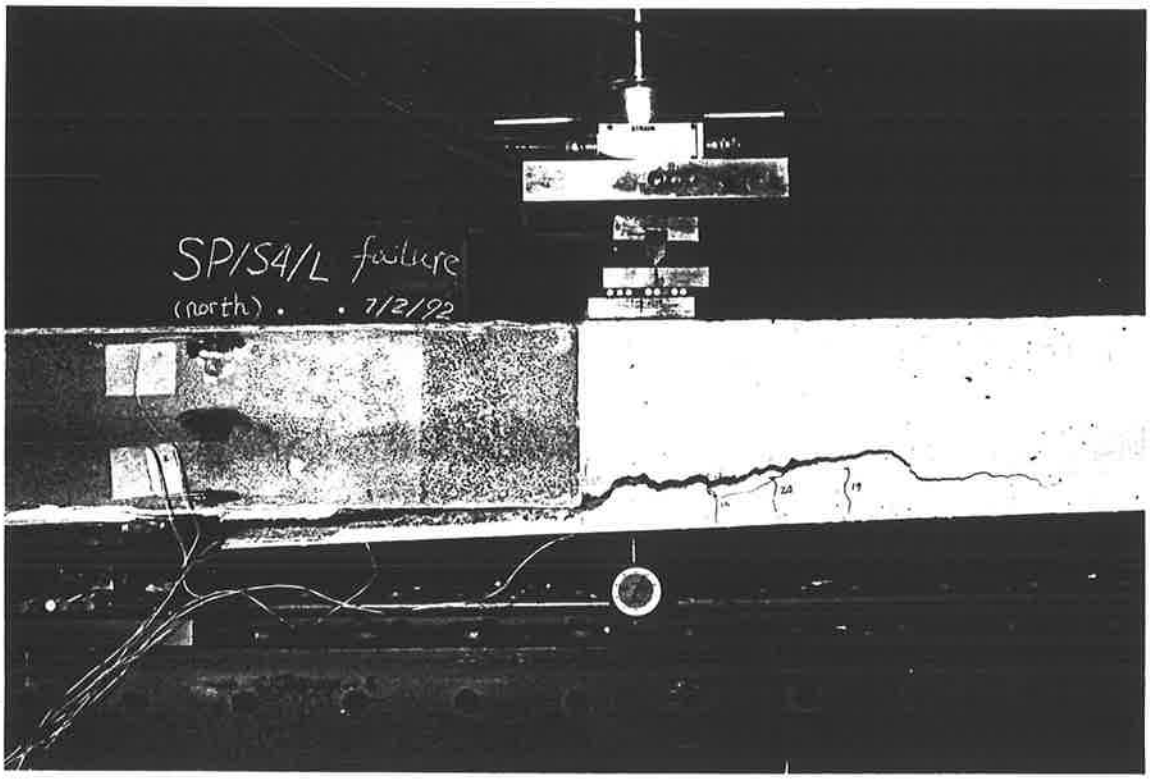

P3-26 Debonding of the soffit plate

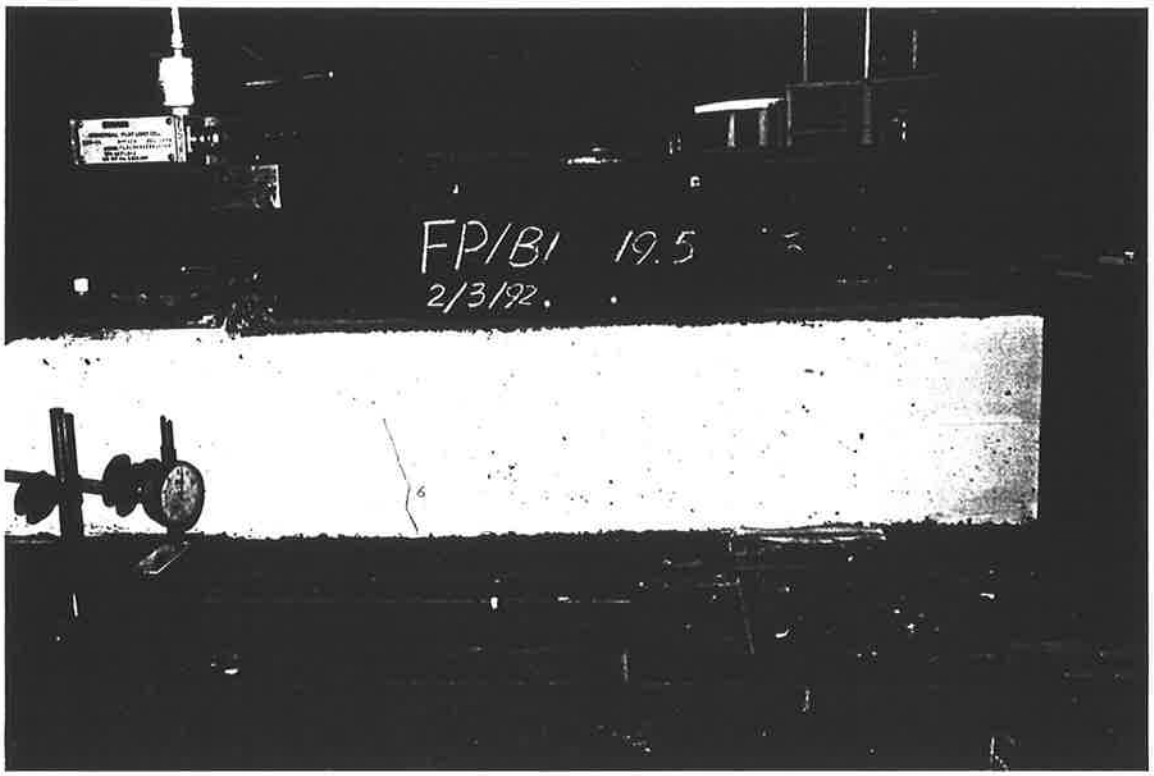

P3-27 The flexural crack formed

P3-28 Crack extended toward a point of the applied load

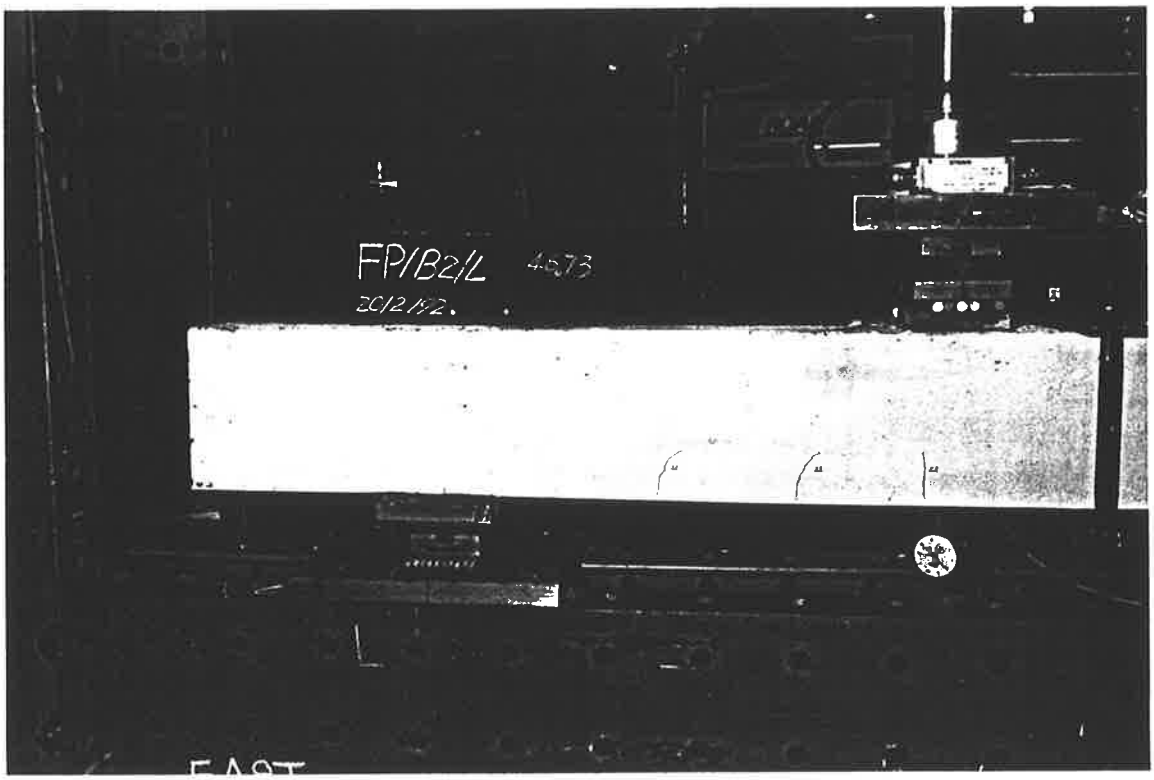

P3-29 The flexural and flexure-shear cracks formed

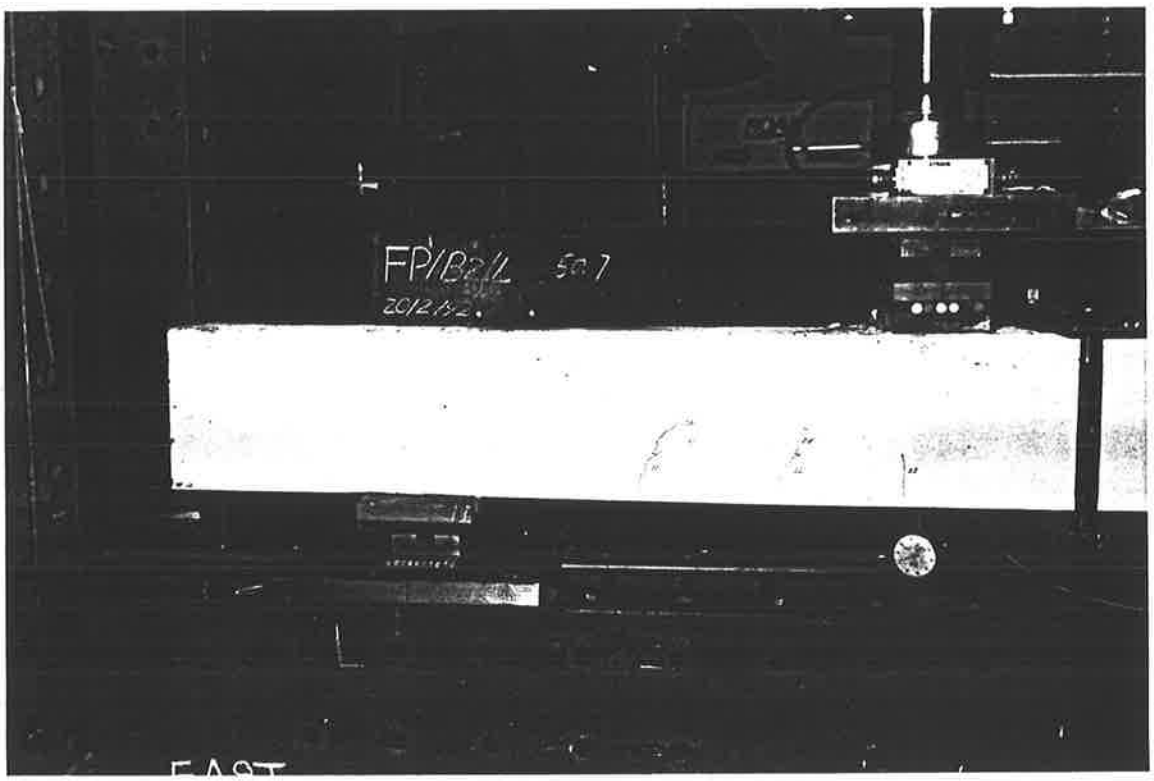

P3-30 The cracks developed gradually

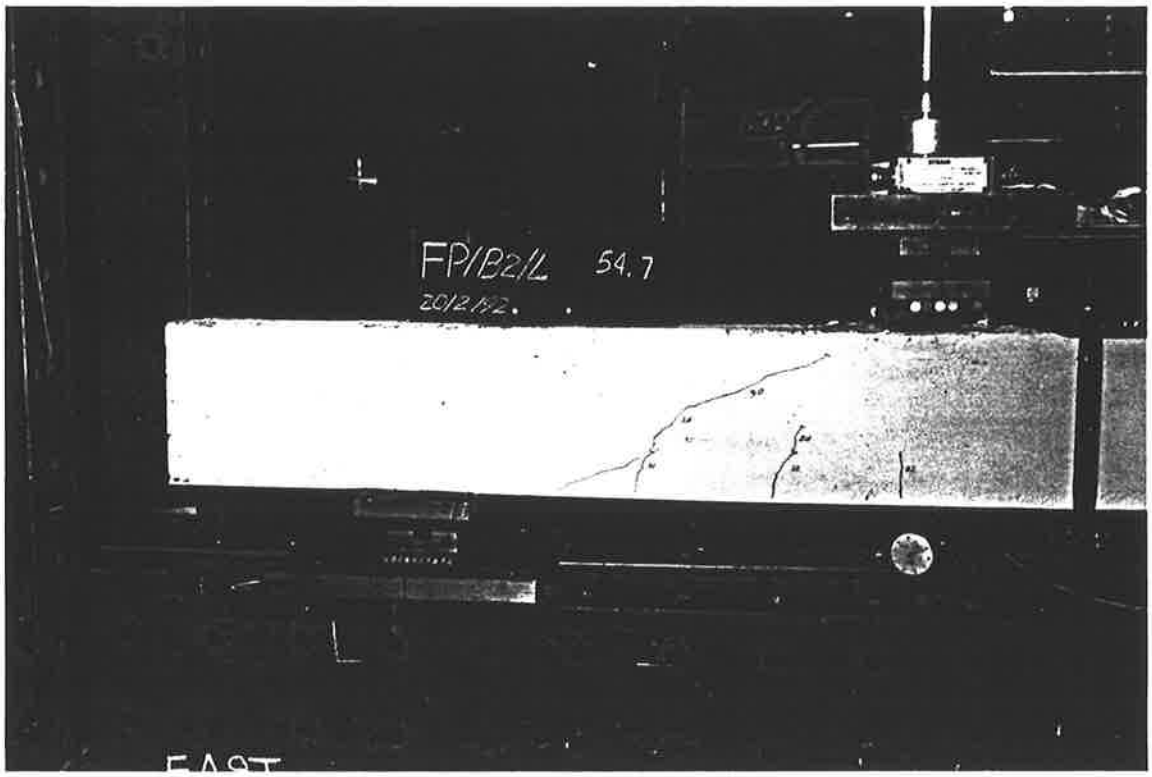

P3-31 A shear diagonal crack formed

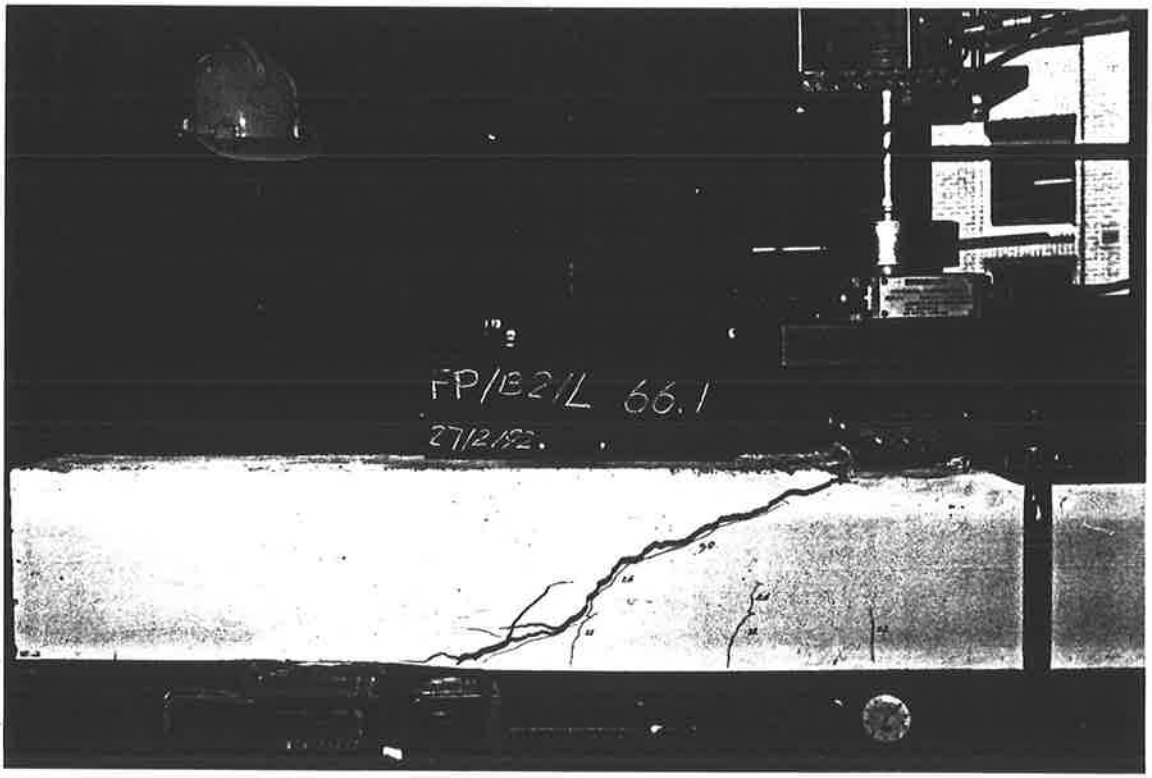

P3-32 A beam failed in shear

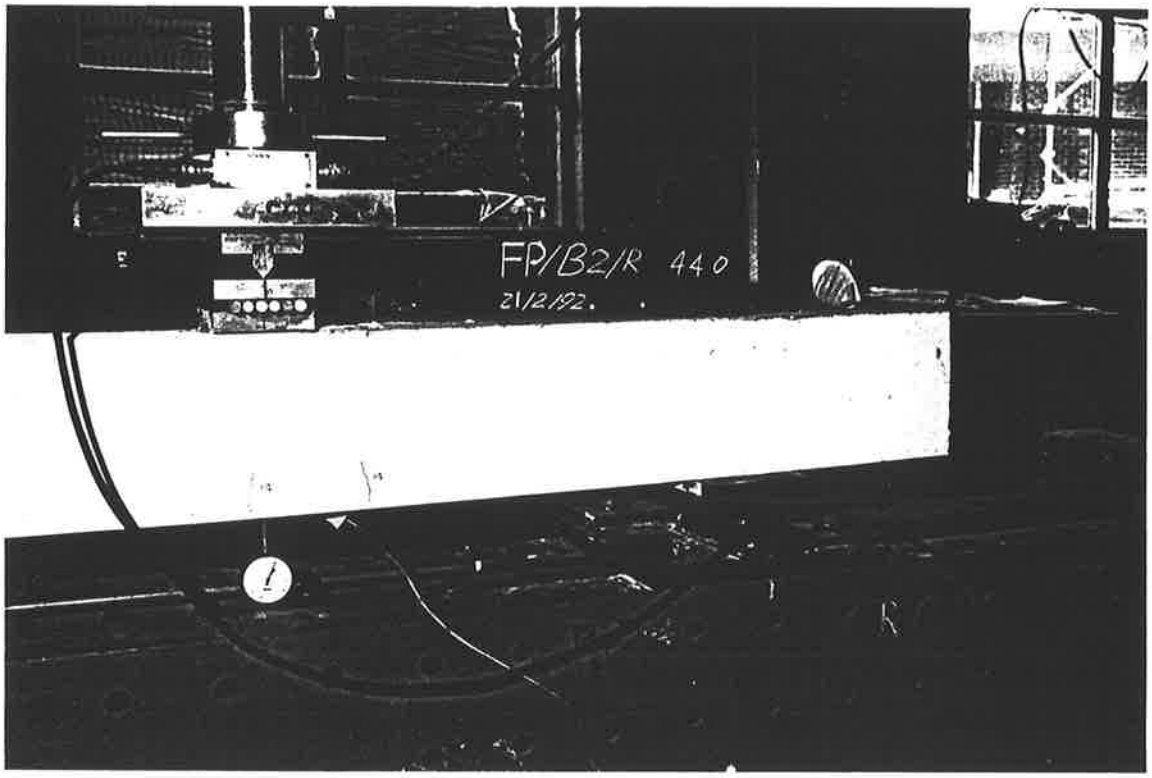

P3-33 The flexural crack occurred

P3-34 The inclined crack formed

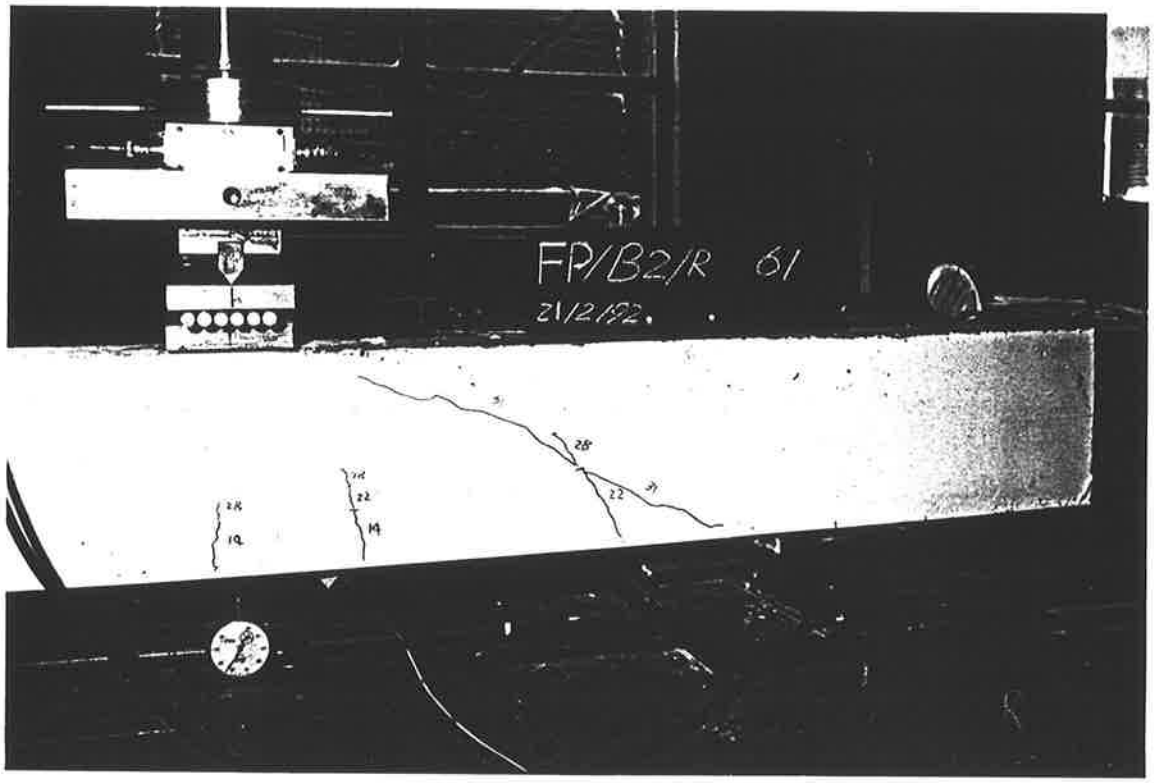

P3-35 A shear diagonal crack occurred

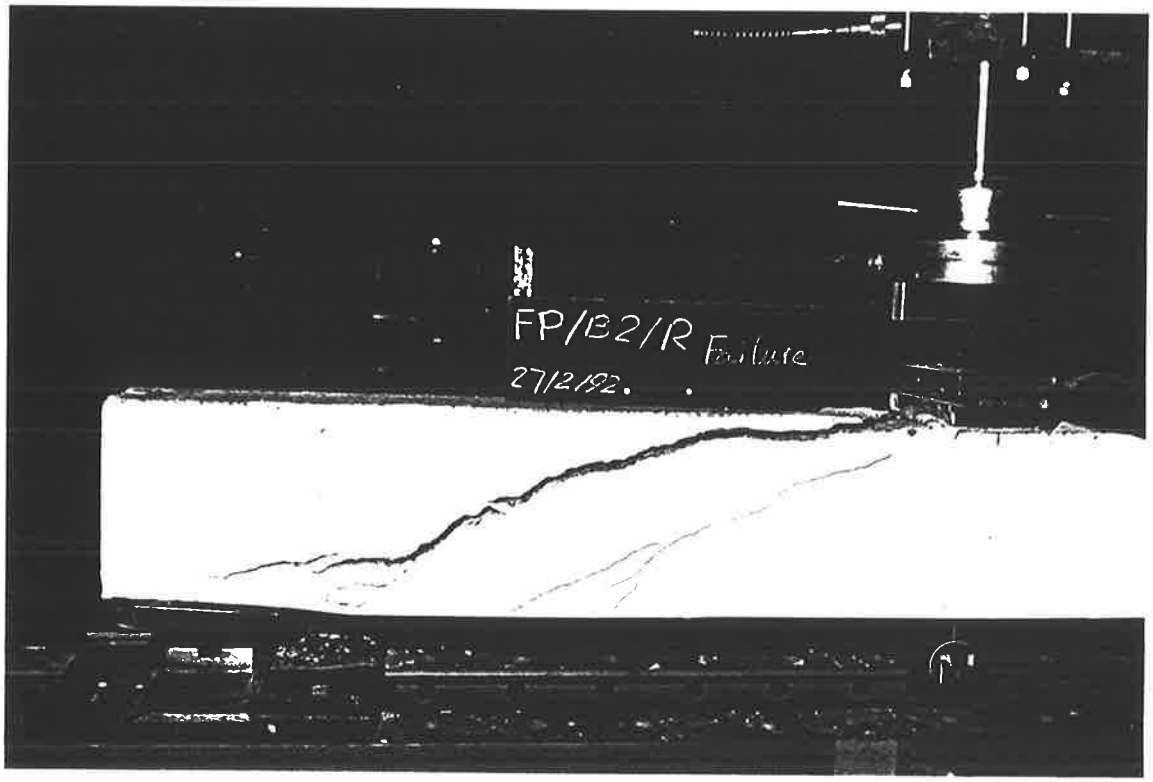

P3-36 A beam failed in shear

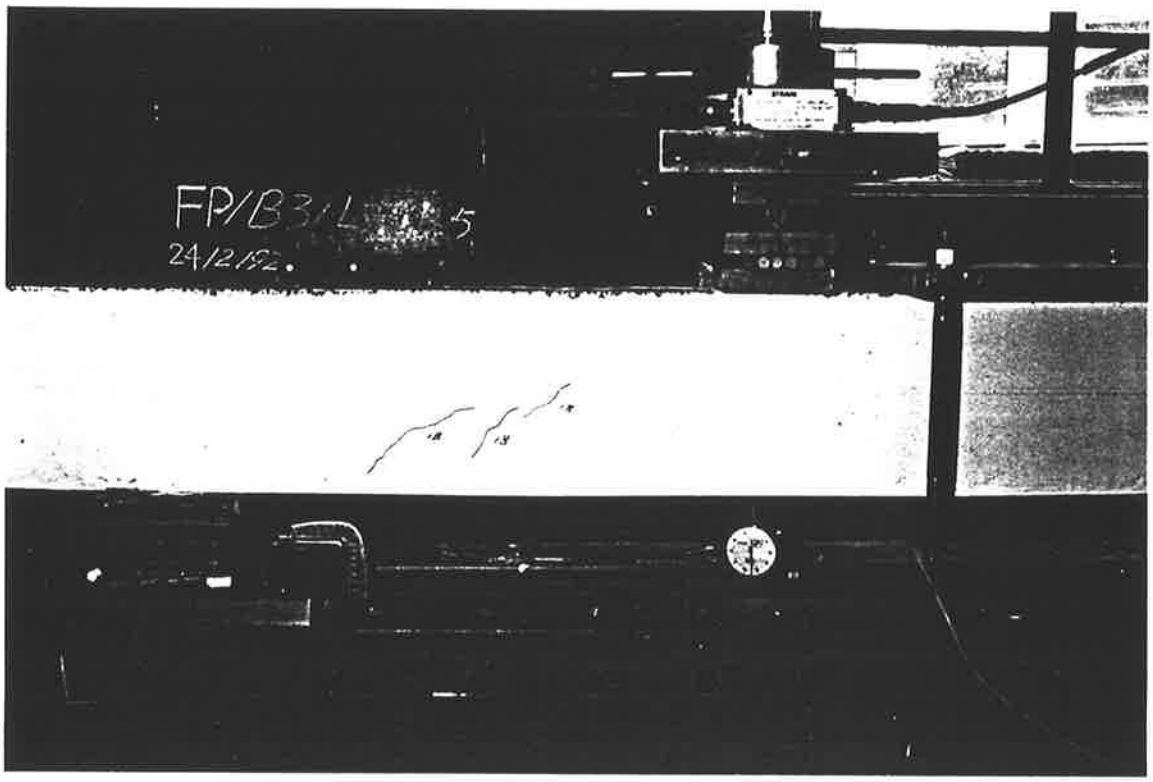

P3-37 The inclined cracks formed

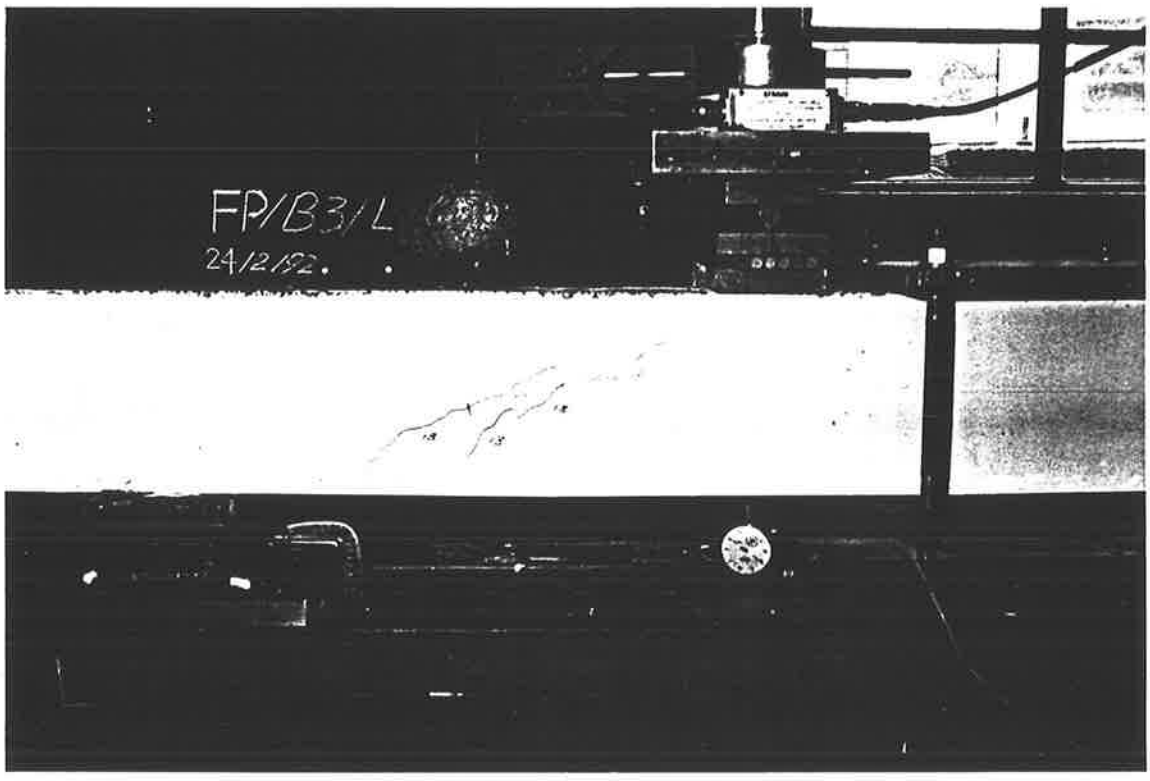

P3-38 The inclined crack developed gradually

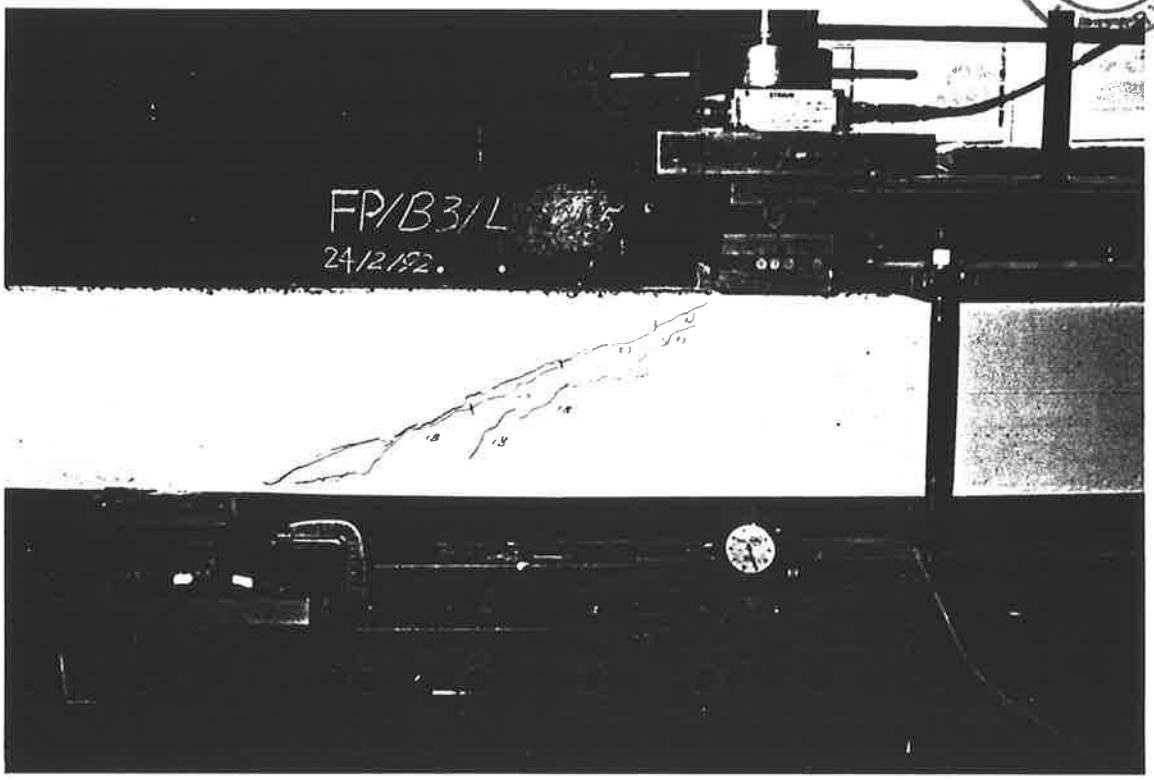

P3-39 The inclined cracks extended toward the points of the applied load and support

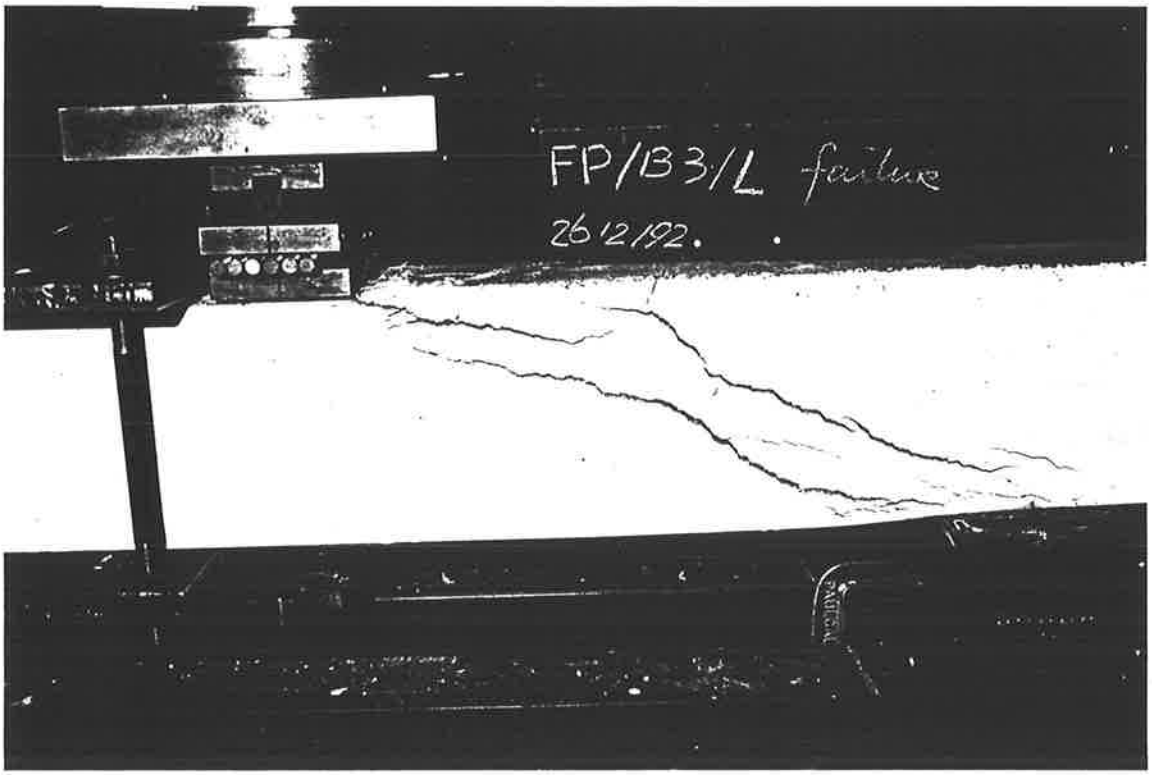

P3-40 A beam failed in shear

P3-41 The inclined crack formed

P3-42 A diagonal crack occurred and the cracks extended toward the points of the applied load and support

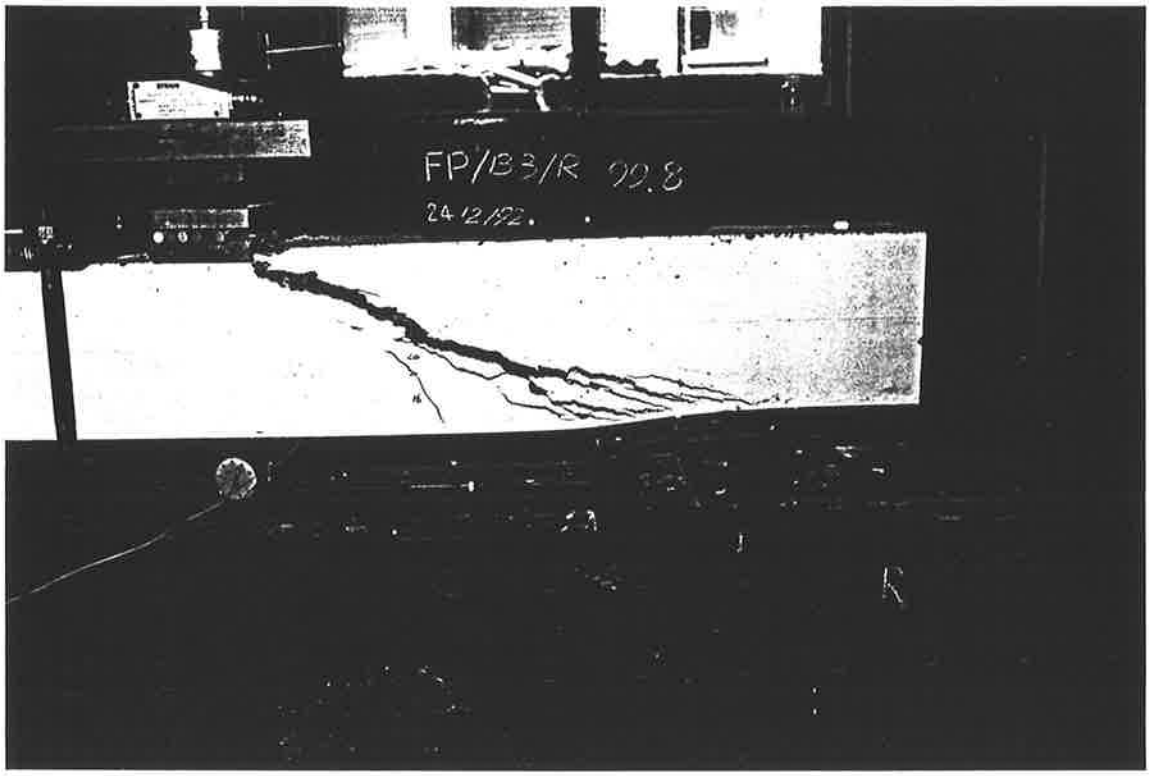

P3-43 A beam failed in shear

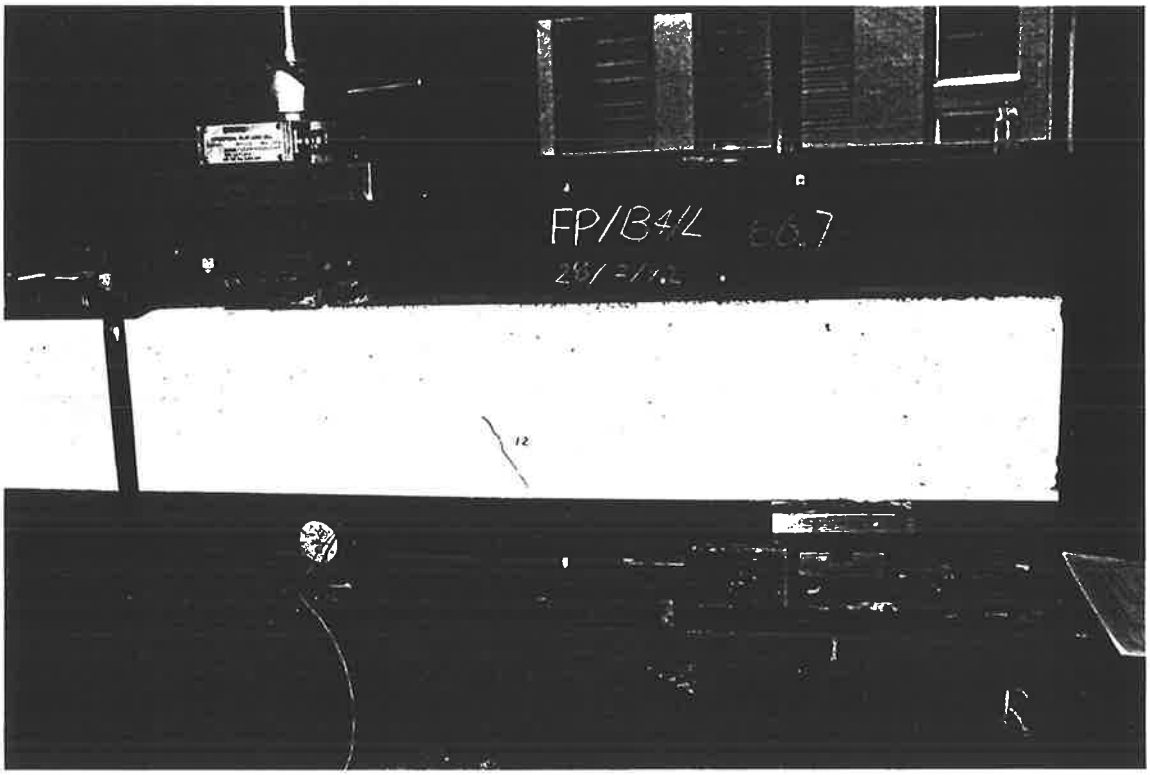

P3-44 The inclined crack formed

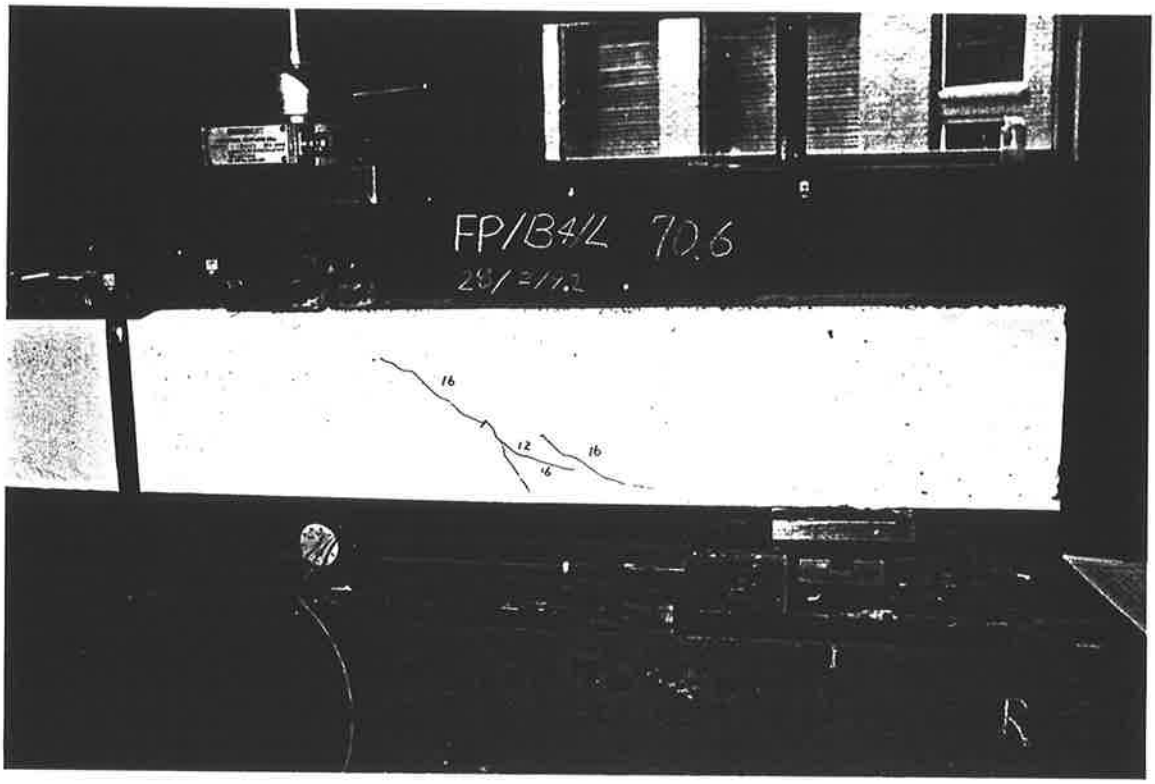

P3-45 A diagonal crack formed

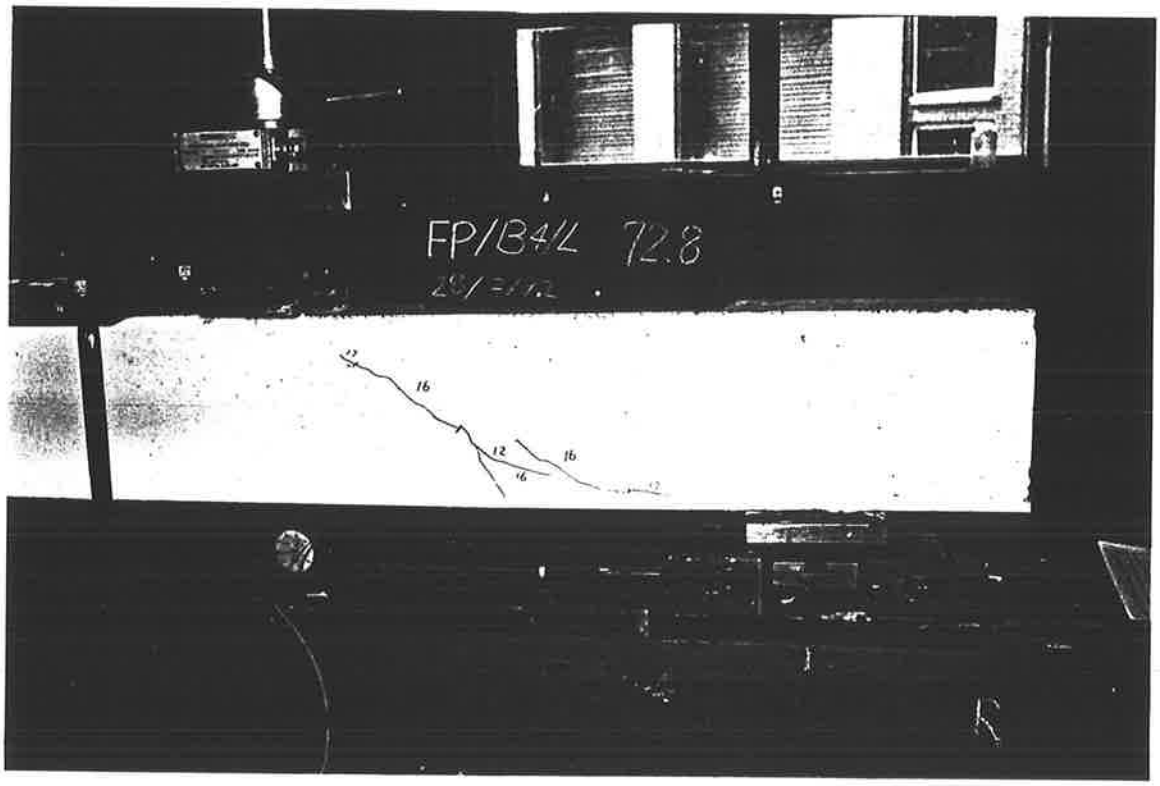

P3-46 The cracks developed gradually

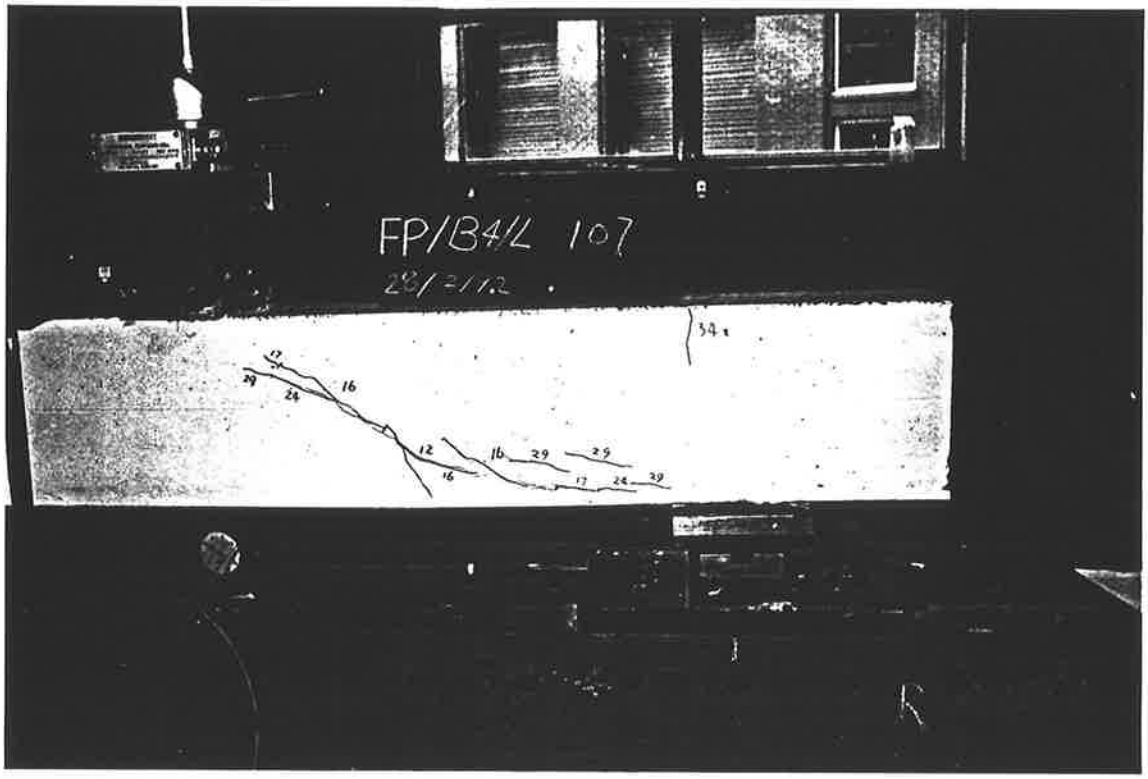

P3-47 The cracks extended toward the points of the applied load and support

P3-48 A beam failed in shear

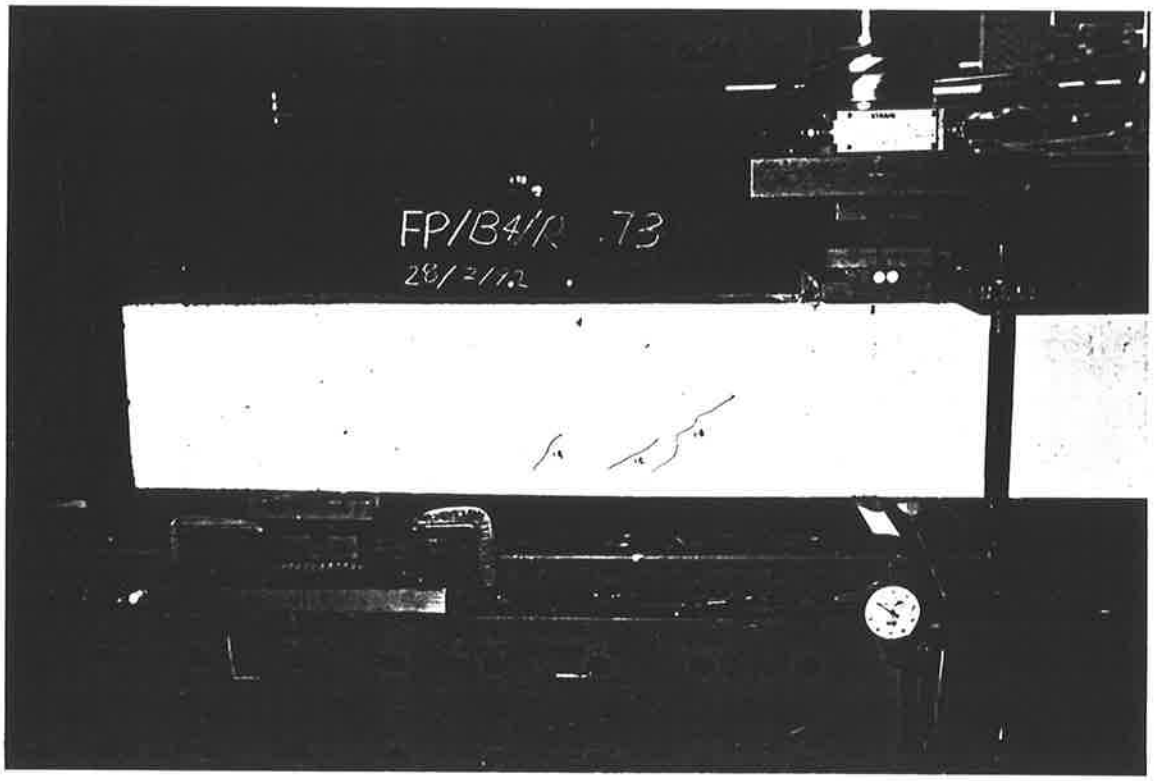

P3-49 The inclined cracks formed

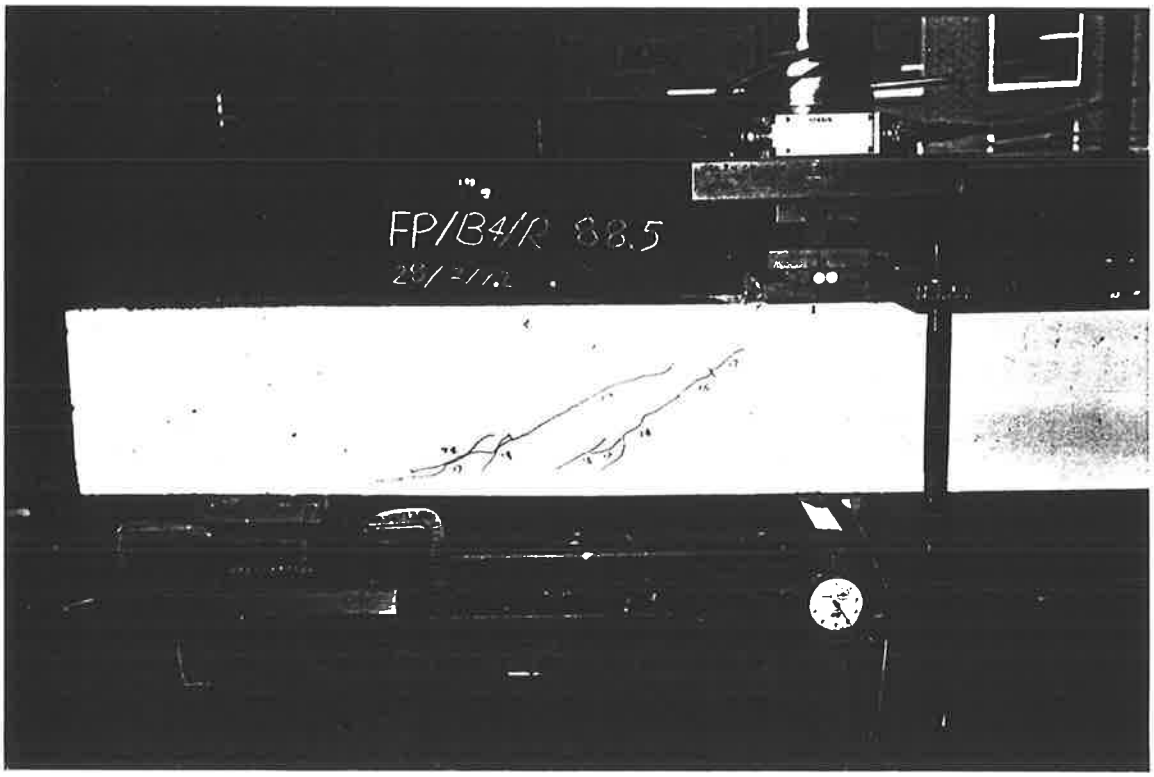

P3-50 The inclined cracks developed gradually

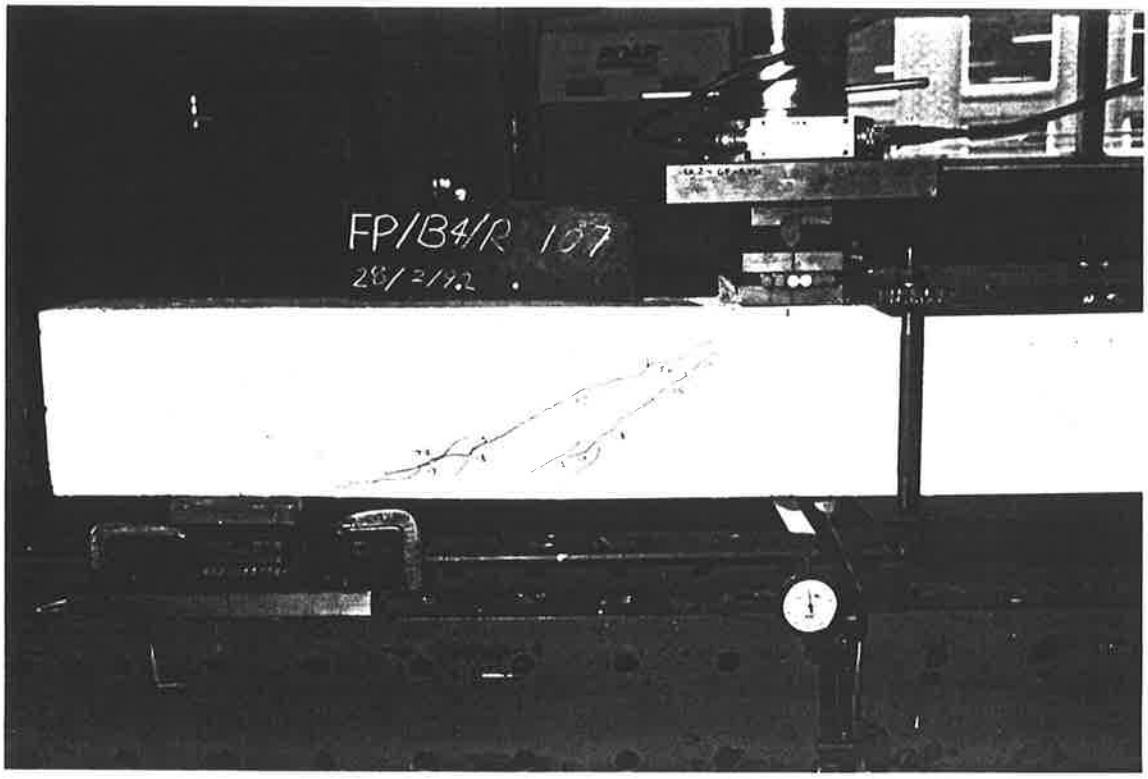

P3-51 The inclined cracks extended toward the points of the applied load and support

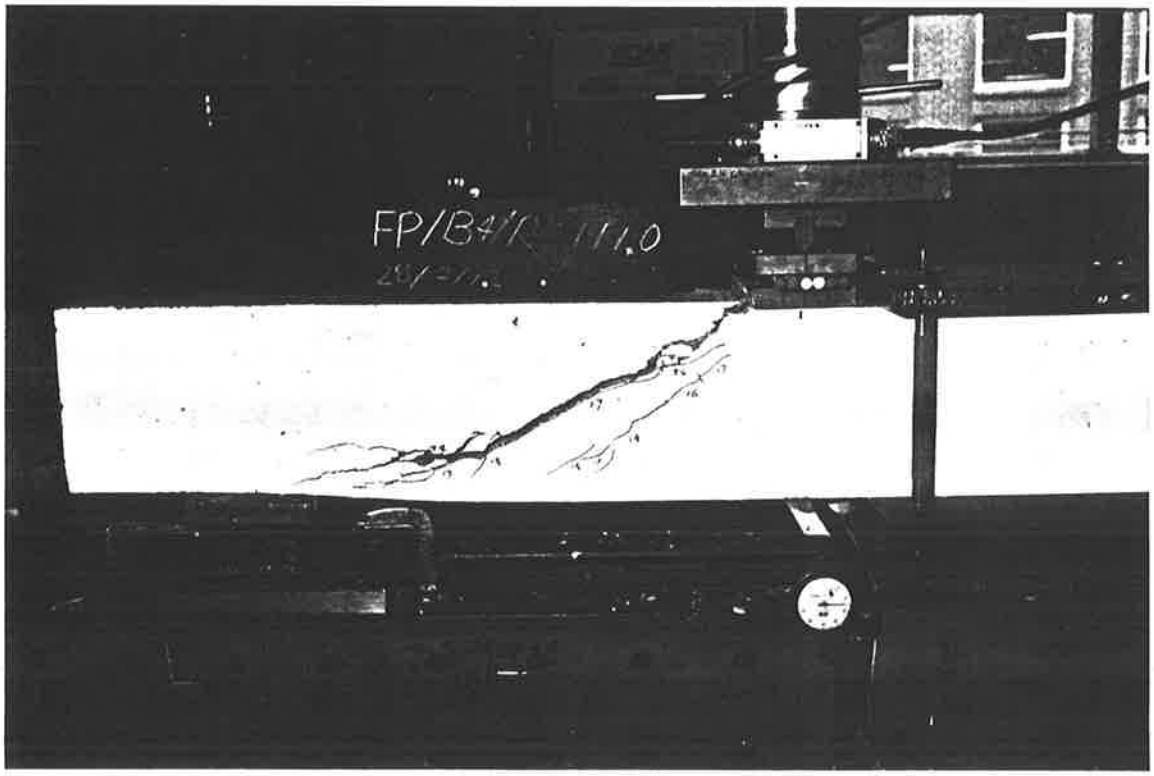

P3-52 A beam failed in shear

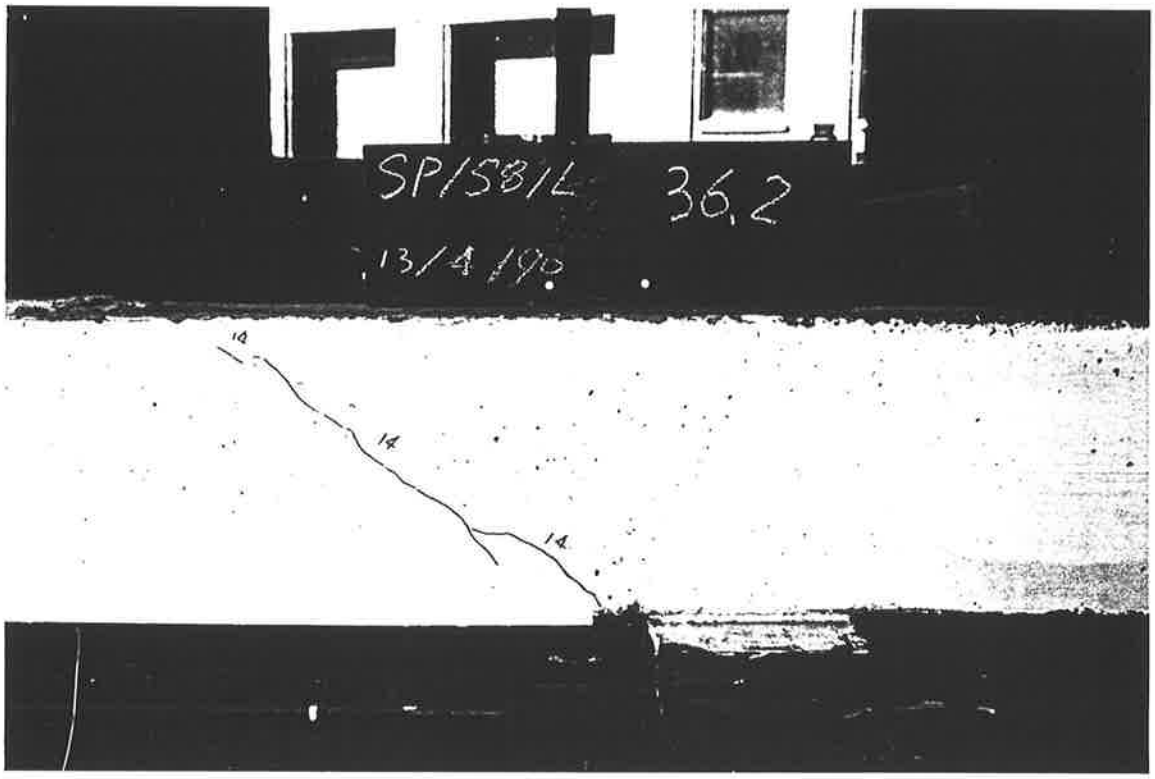

P3-53 The inclined crack formed

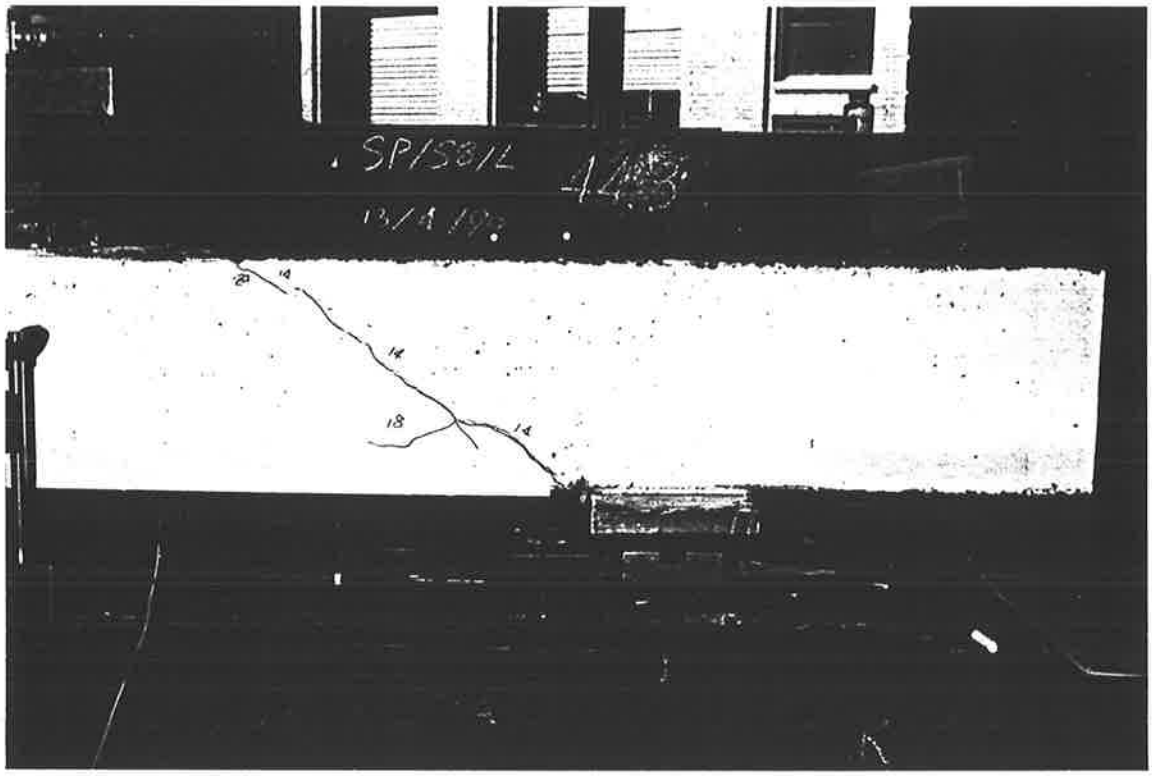

P3-54 The horizontal peeling cracks formed at the level of the tensile reinforcement

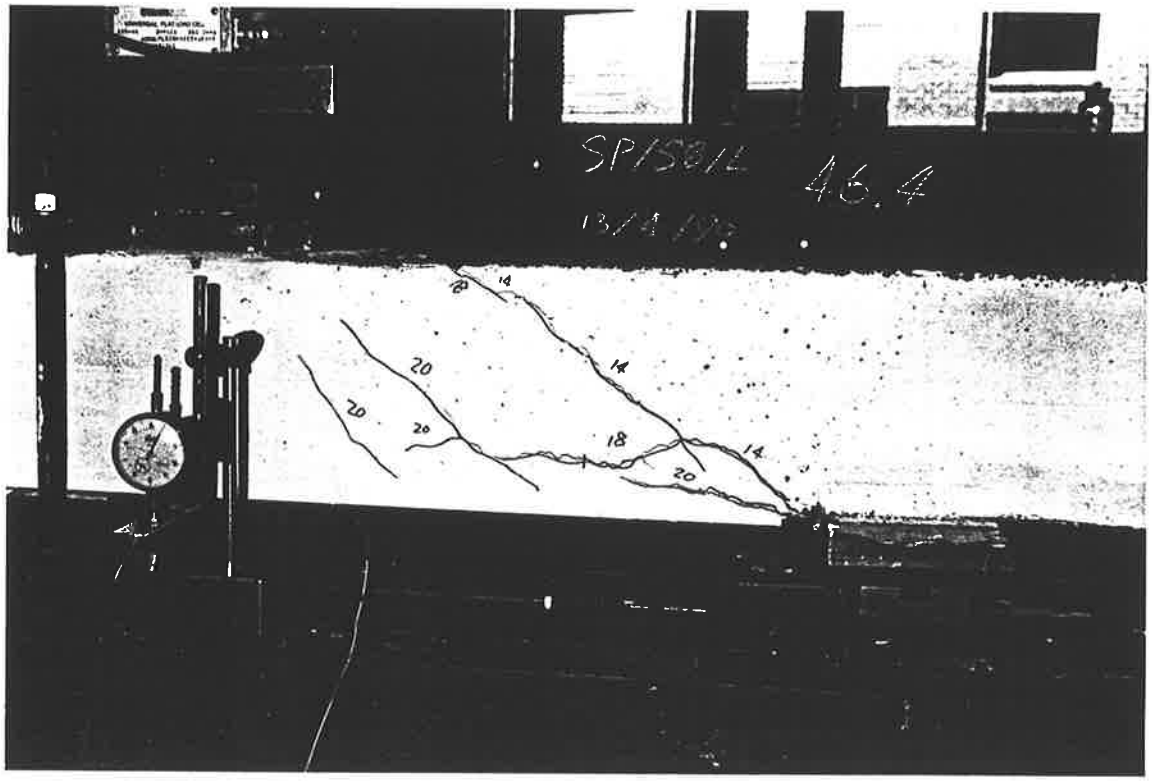

P3-55 The shear peeling occurred

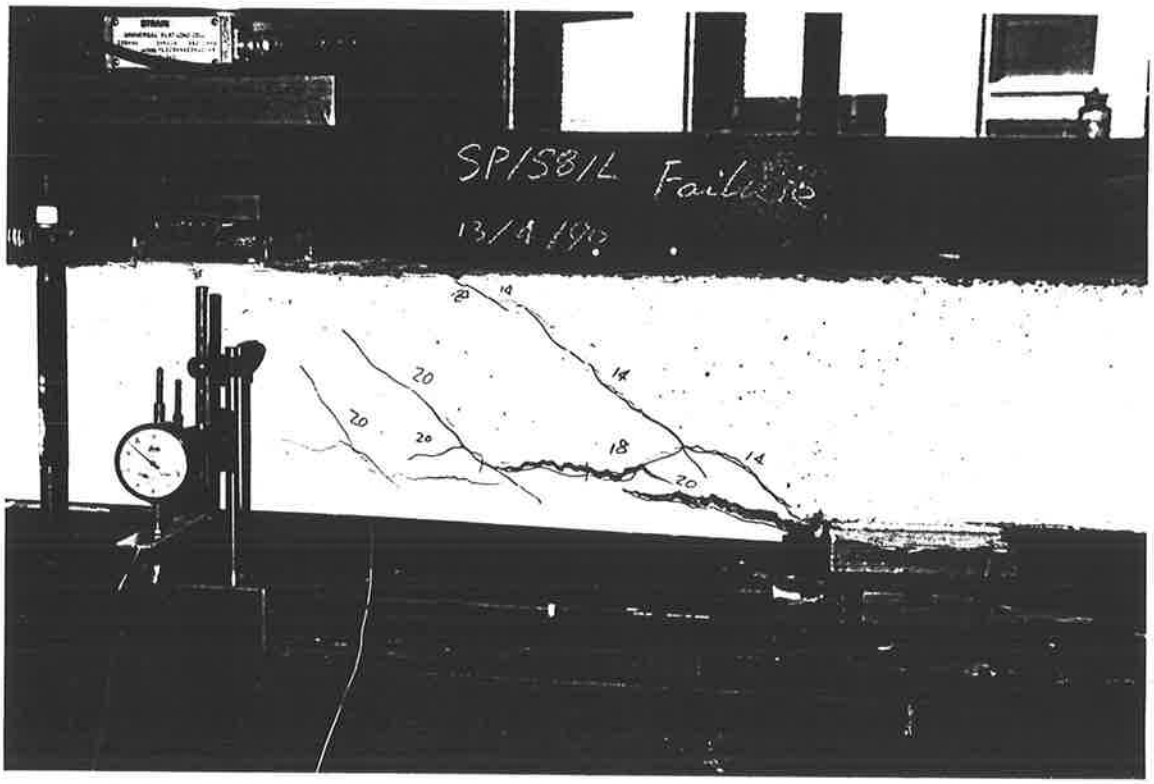

P3-56 Debonding of the soffit plate

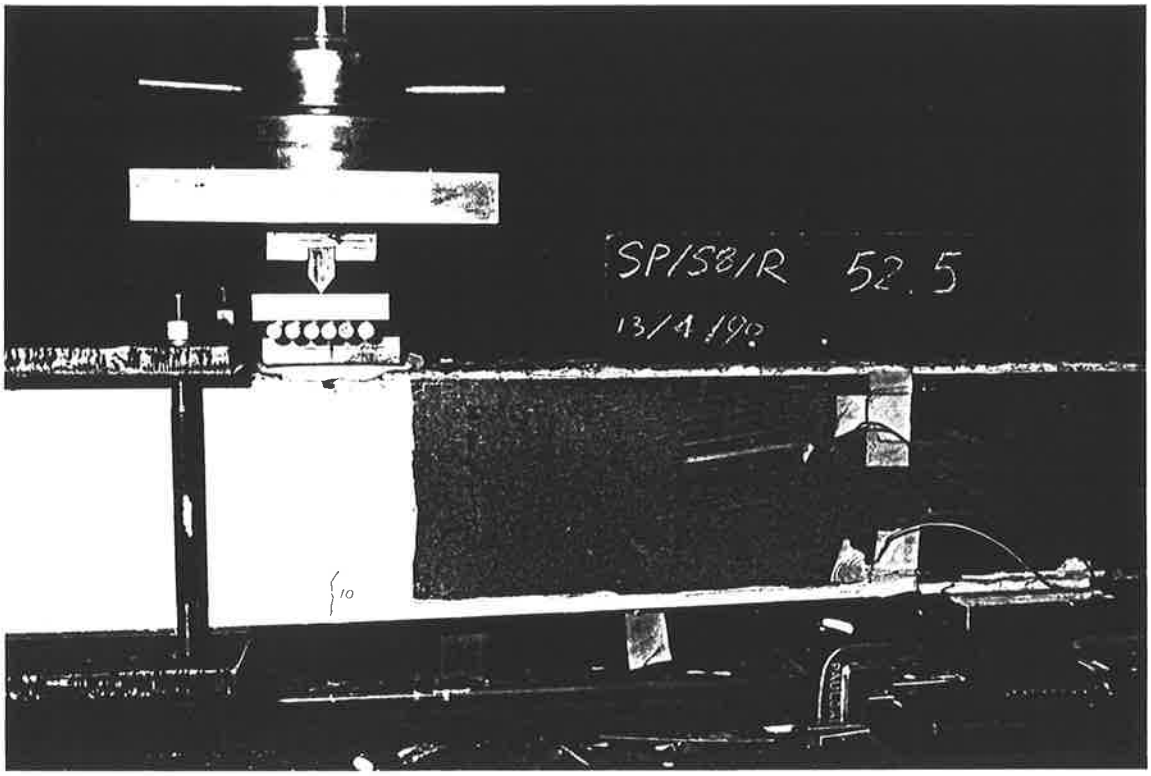

P3-57 The first visible crack formed in a beam

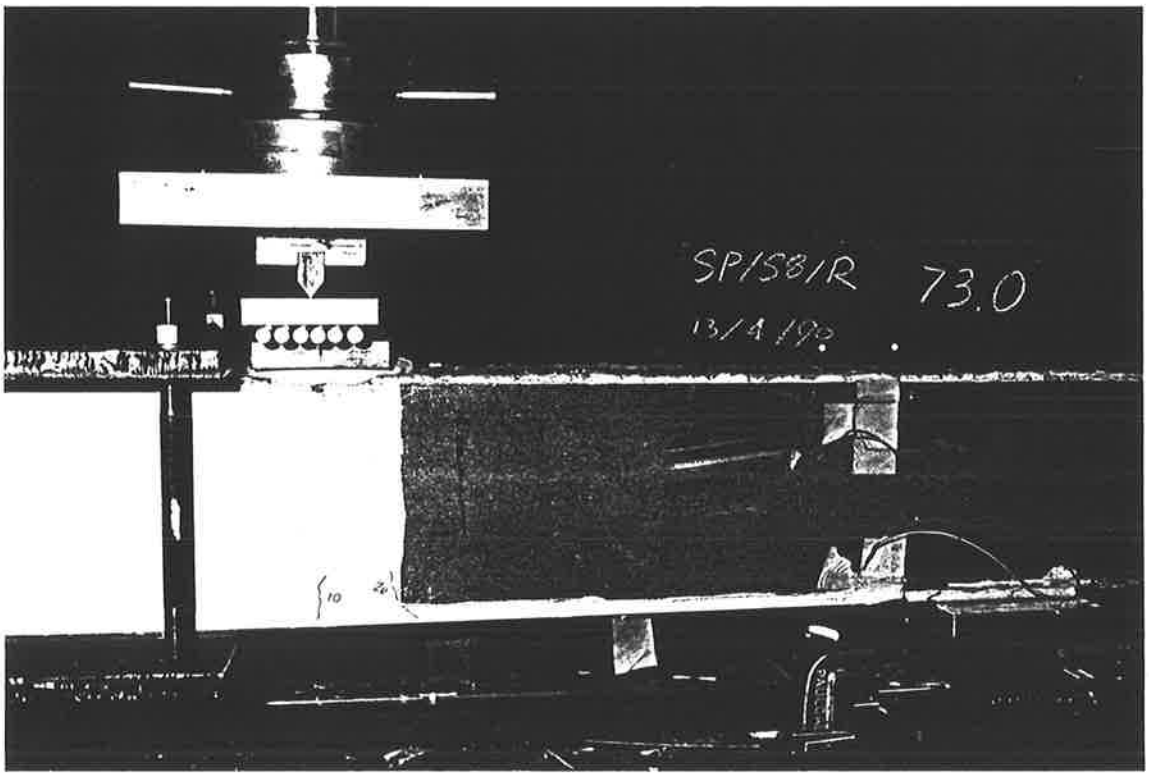

P3-58 The cracks formed along the edge of the side plate

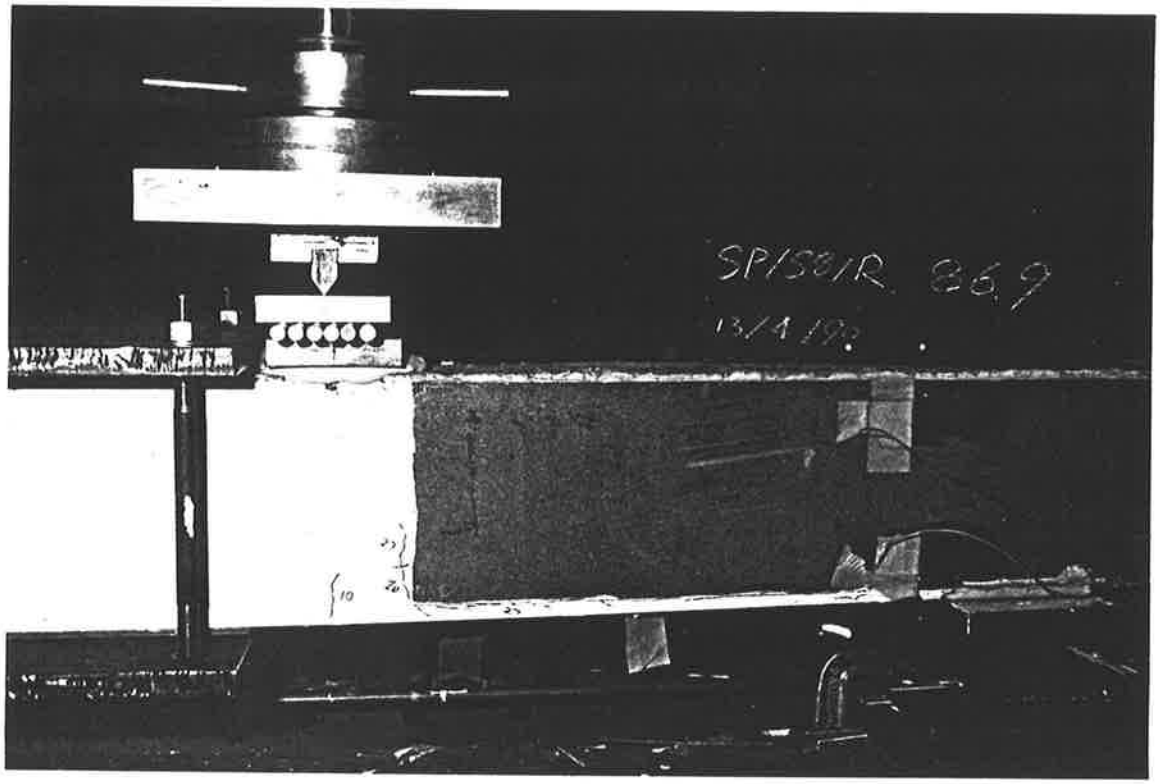

P3-59 The cracks developed along the edge of the plate

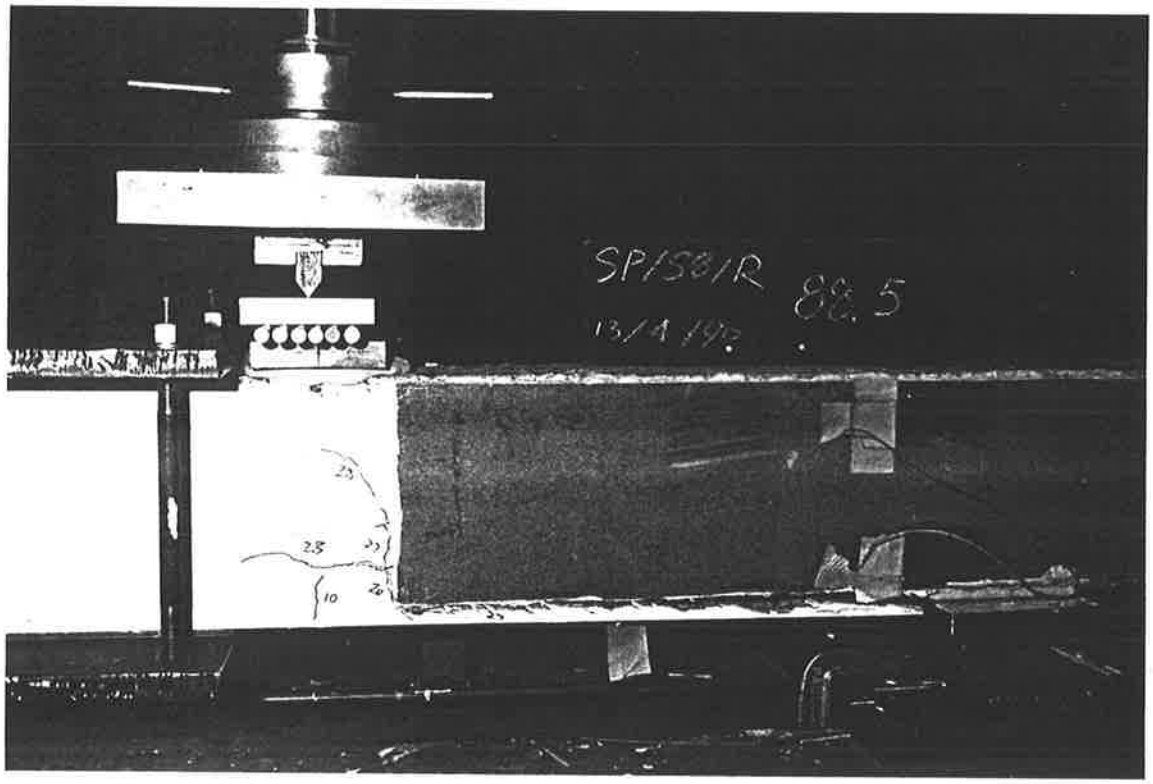

P3-60 Debonding of the soffit plate occurred

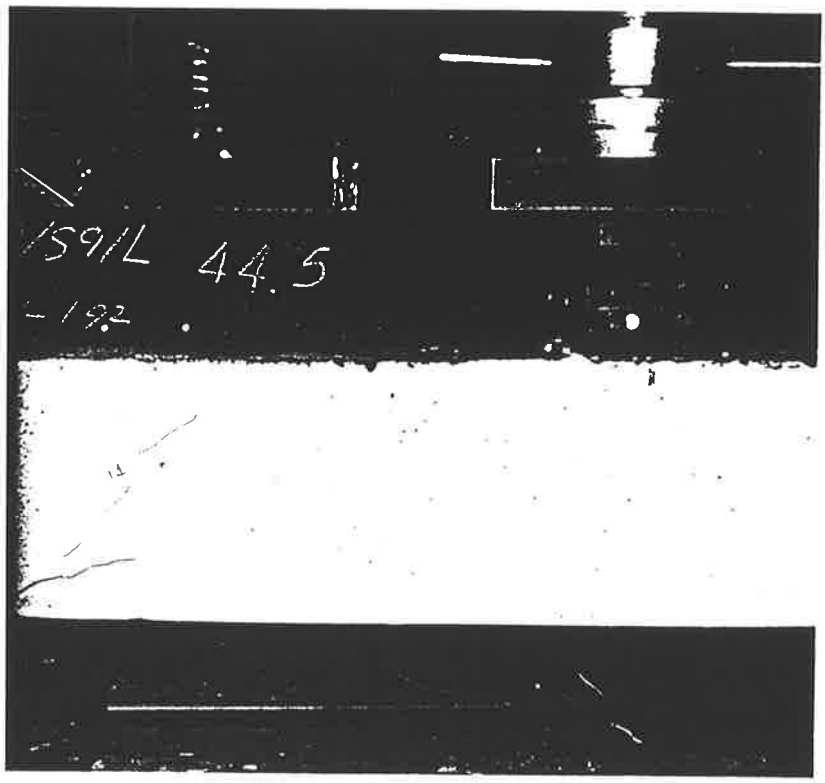

P3-61 The inclined and horizontal cracks formed

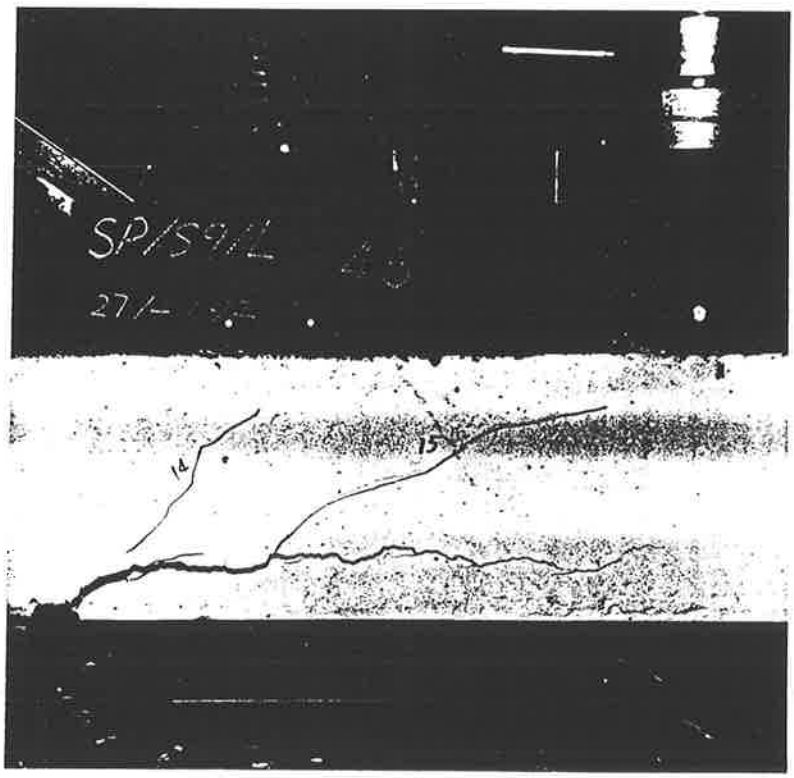

P3-62 The shear peeling and debonding of the soffit plate

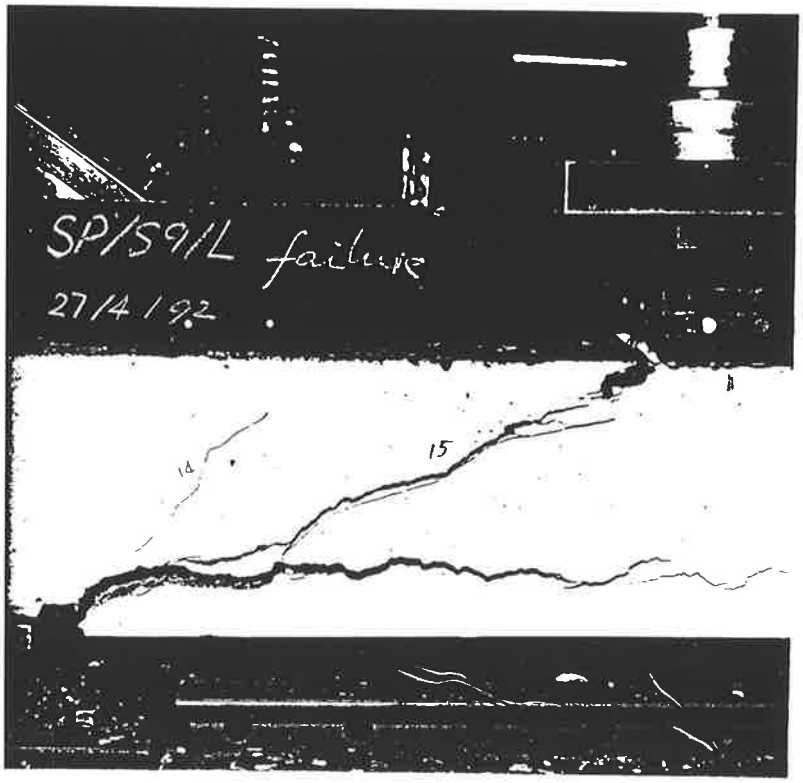

P3-63 The beam failed in shear

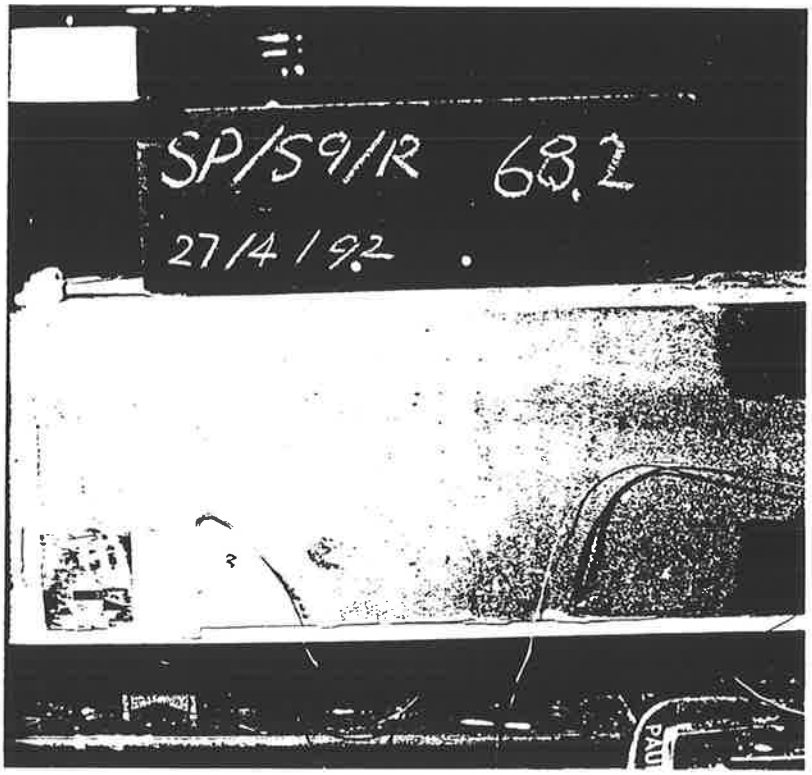

P3-64 The first visible crack occurred

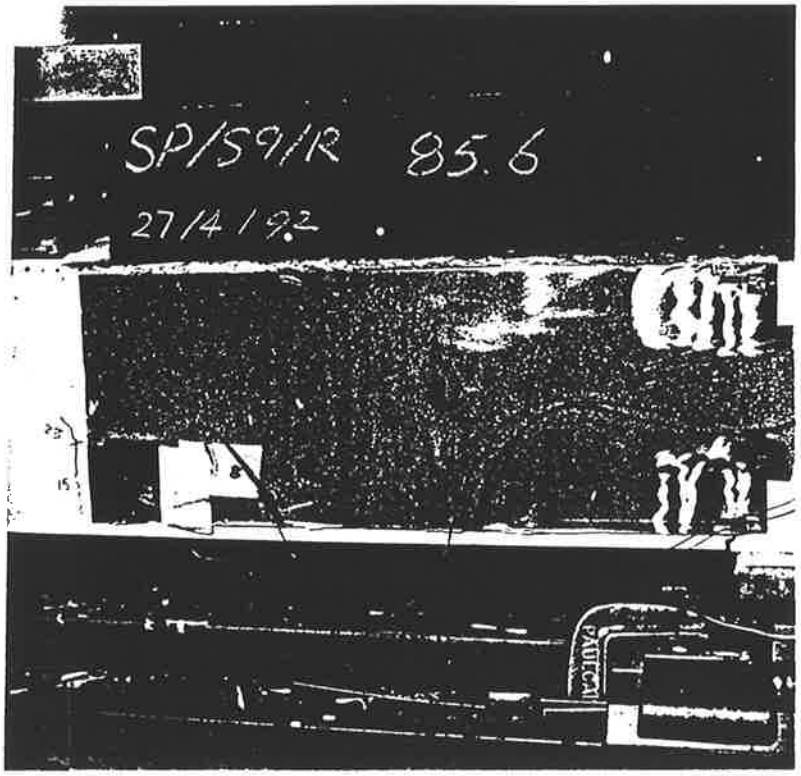

P3-65 The cracks developed along the side plates

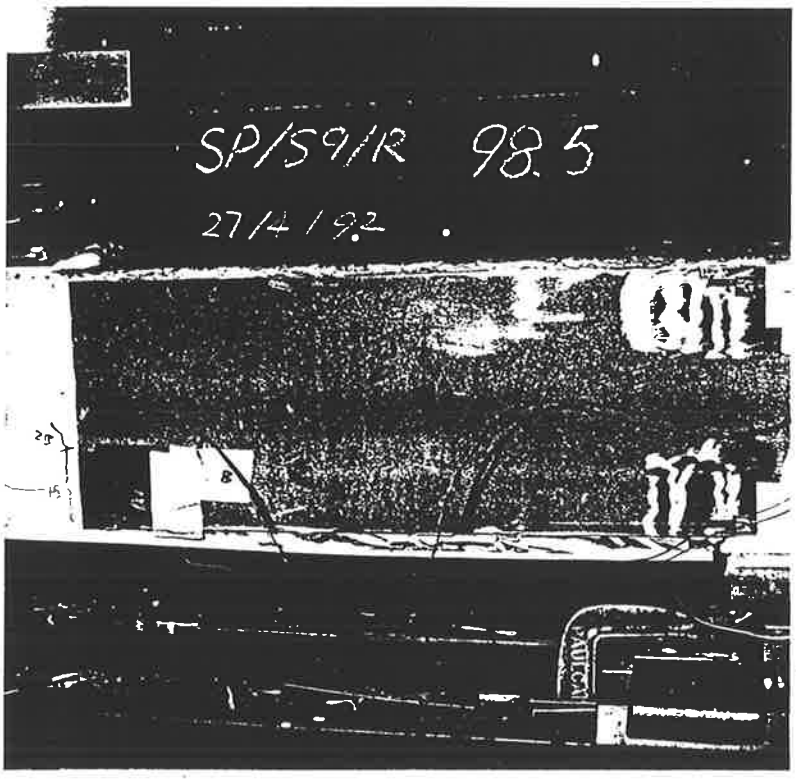

P3-66 Debonding of the soffit plate

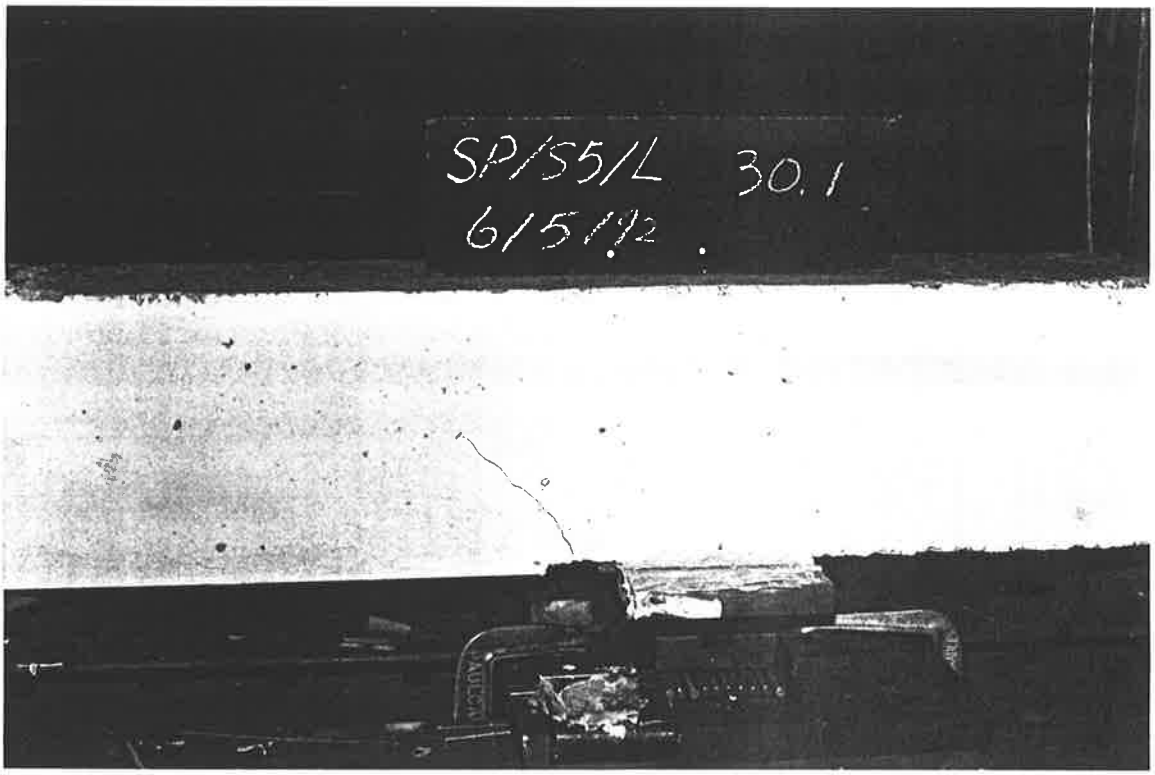

P3-67 The inclined crack occurred

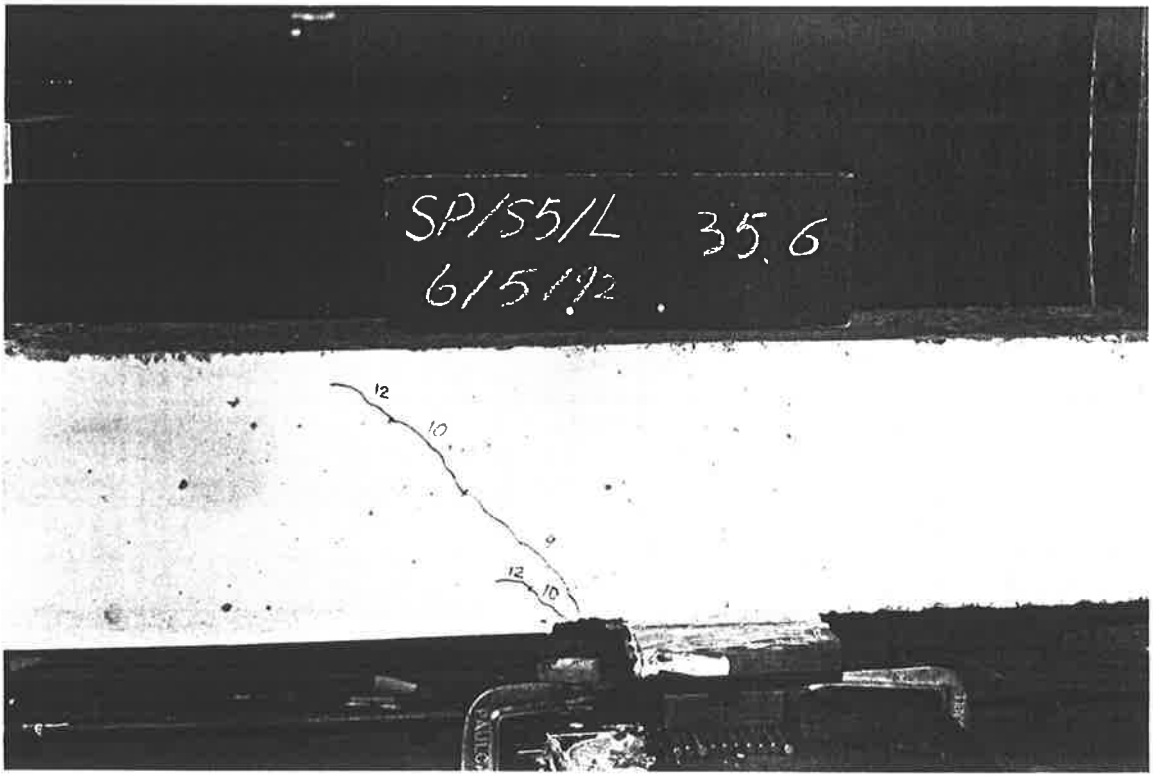

P3-68 The horizontal peeling cracks occurred along the level of the bottom reinforcement

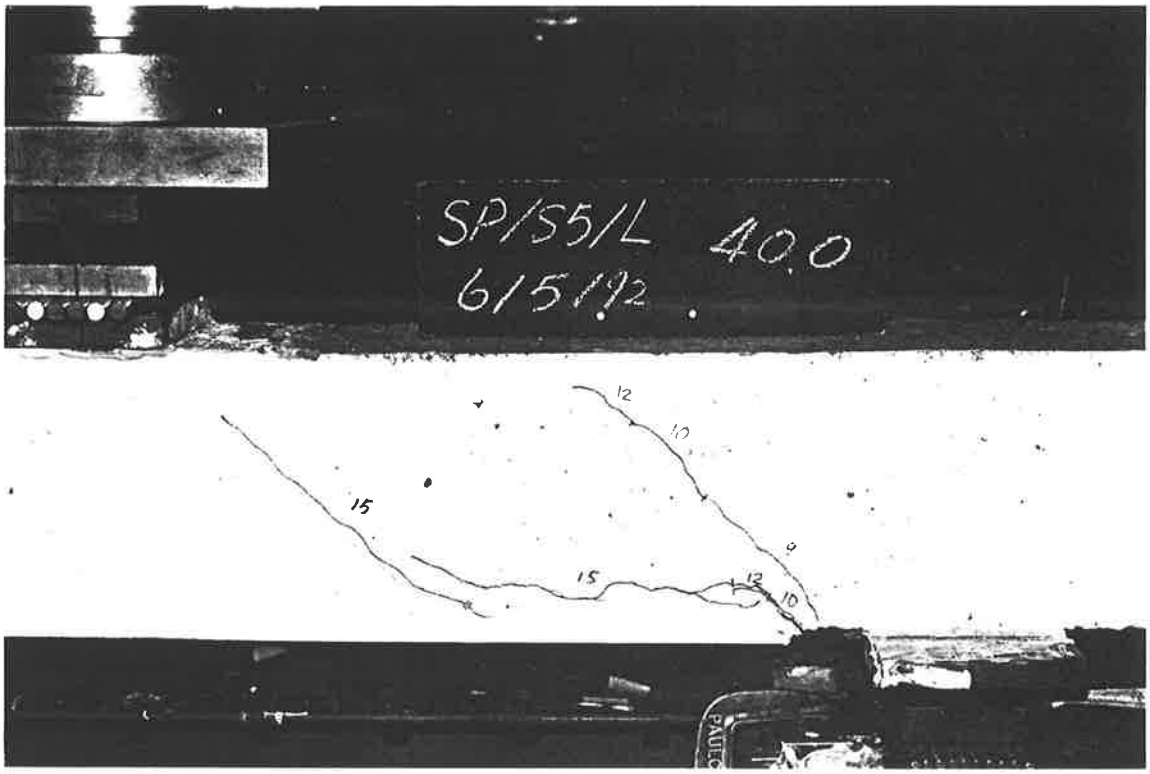

P3-69 The shear peeling and debonding of the soffit plate

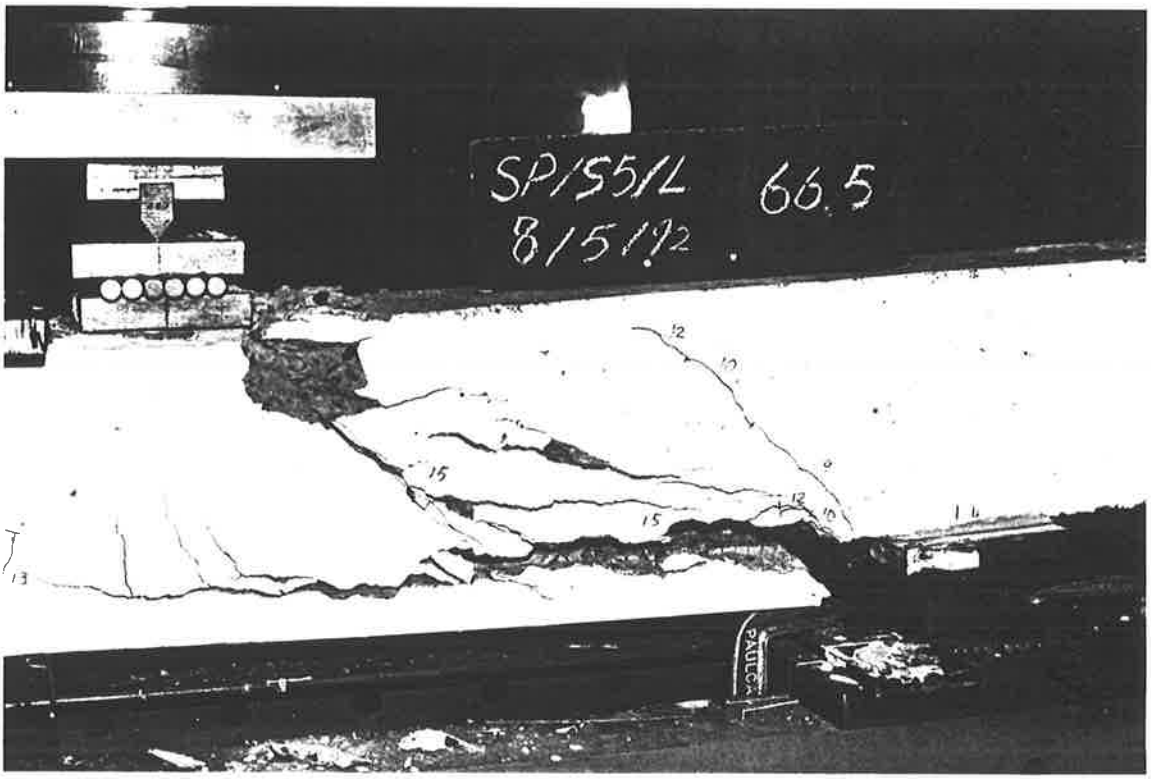

P3-70 The beam failed in shear

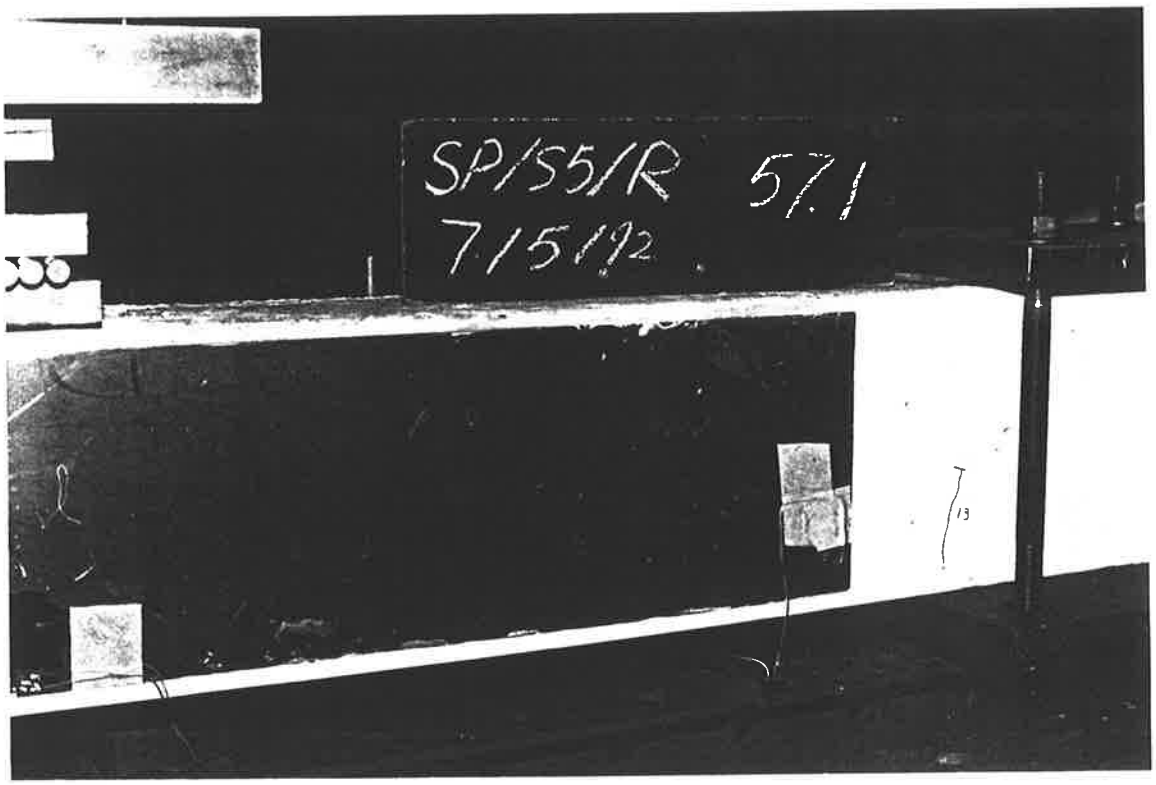

P3-71 The flexural crack formed

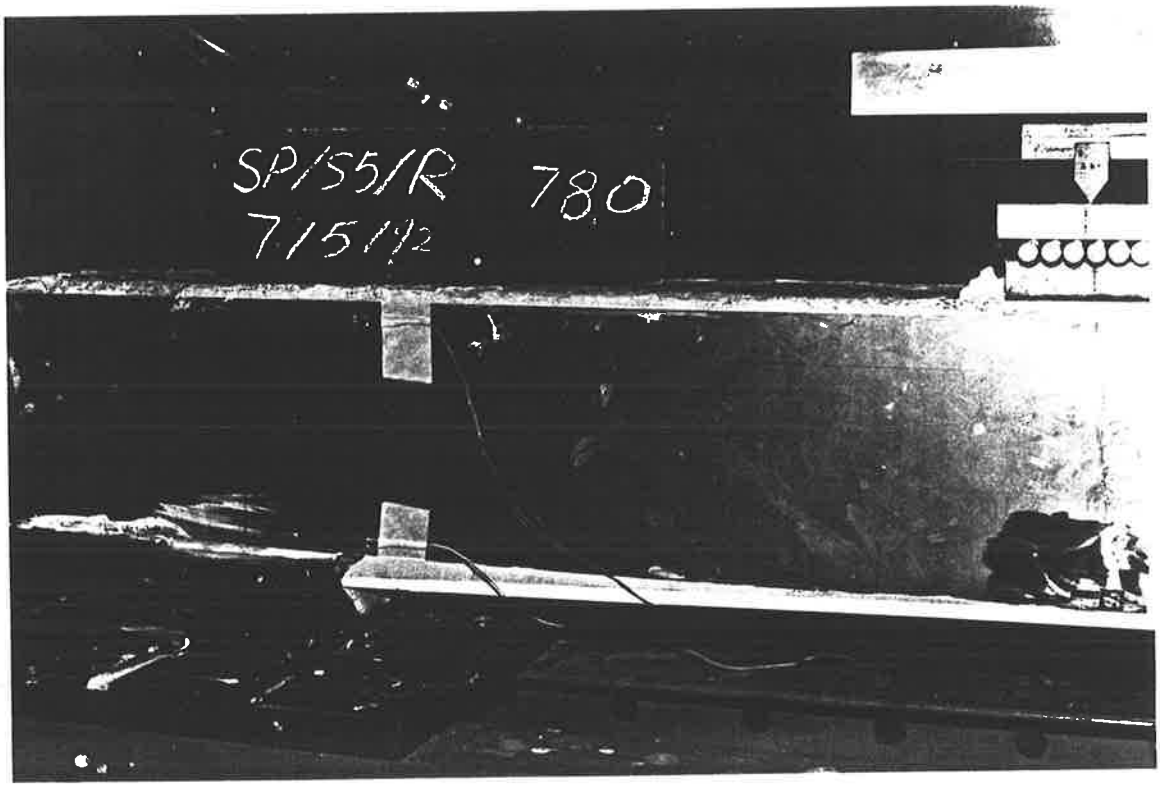

P3-72 Debonding of the soffit plate

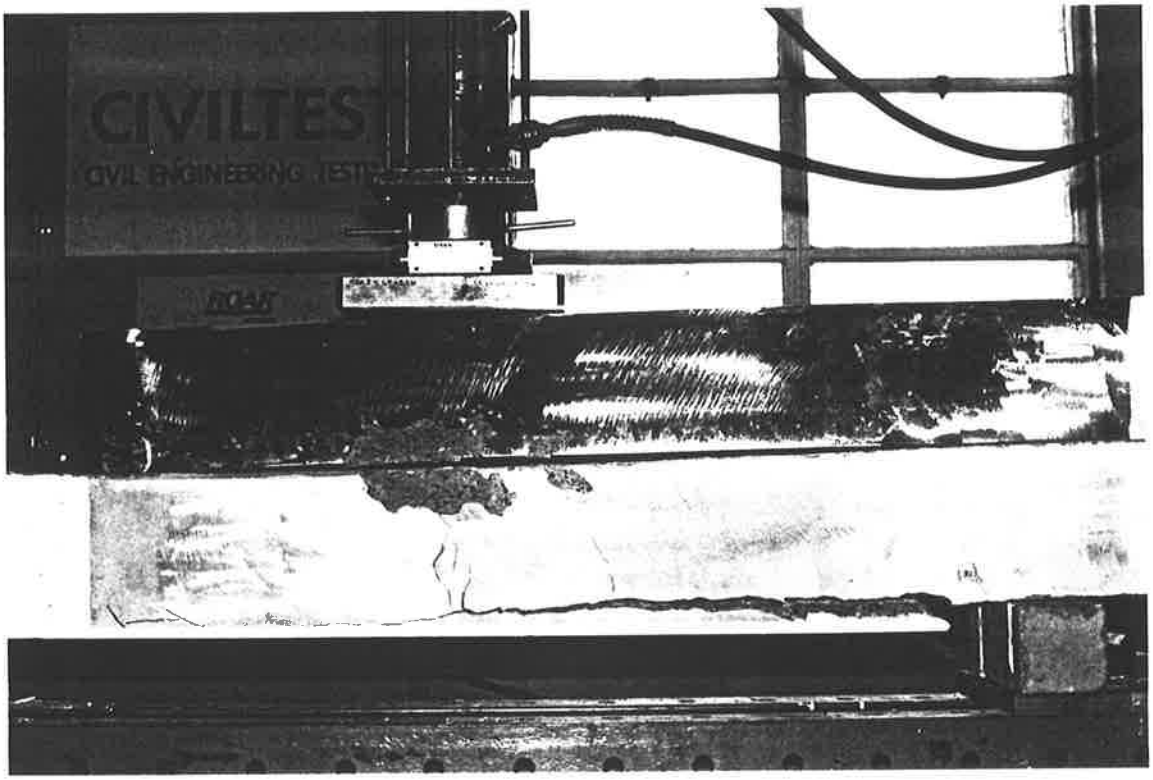

P3-73 The side plates were chopped off from a beam after the beam had been tested

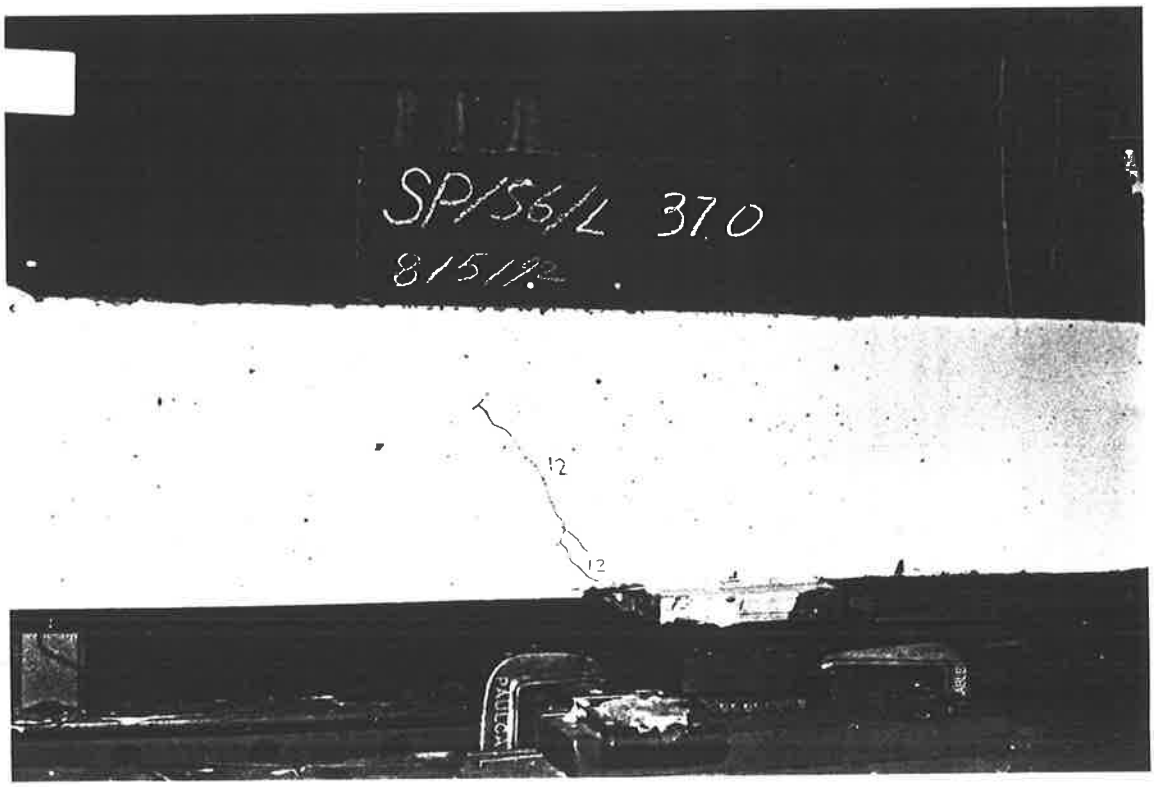

P3-74 The inclined cracks formed

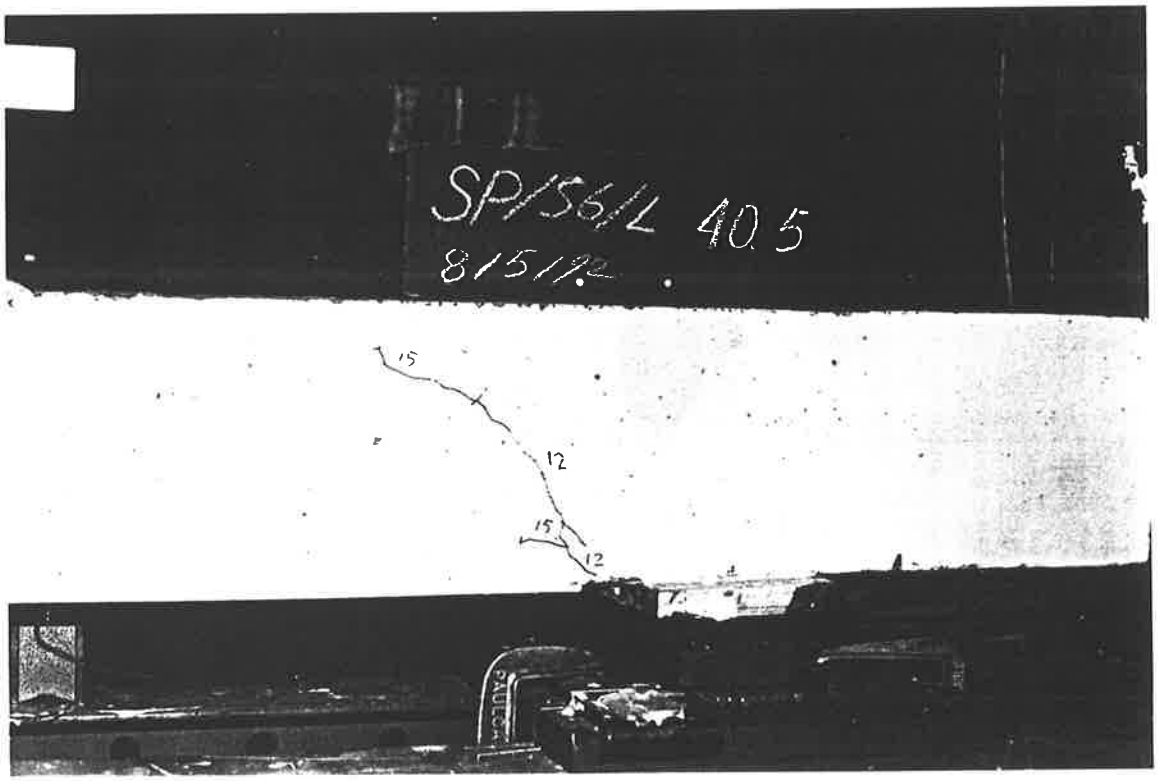

P3-75 The horizontal peeling crack had formed along the level of the bottom reinforcement

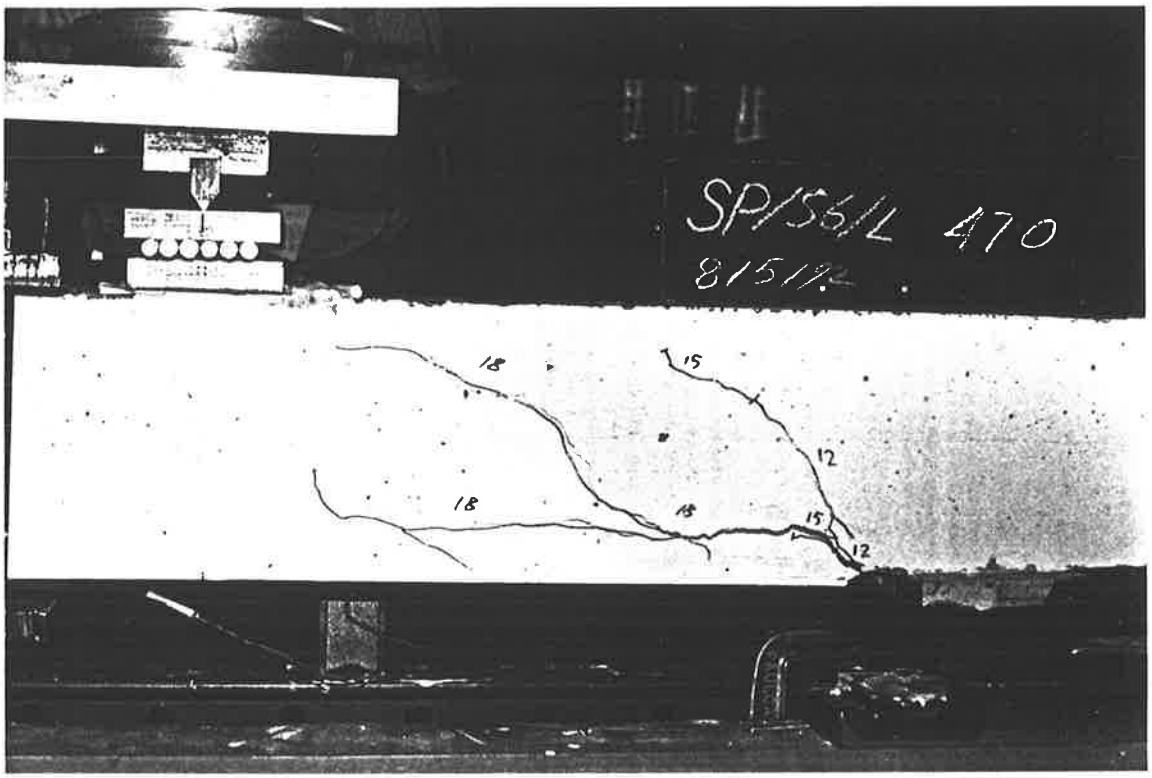

P3-76 The shear peeling and debonding of the soffit plate

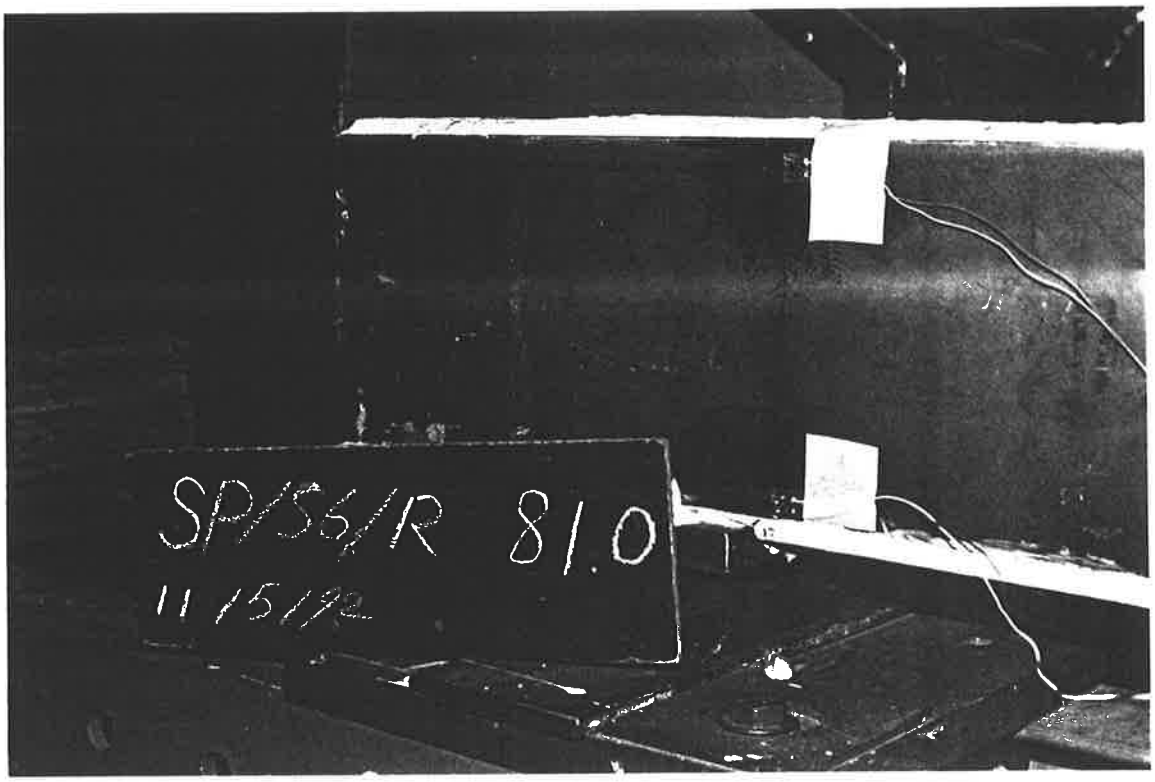

P3-77 The first visible crack occurred

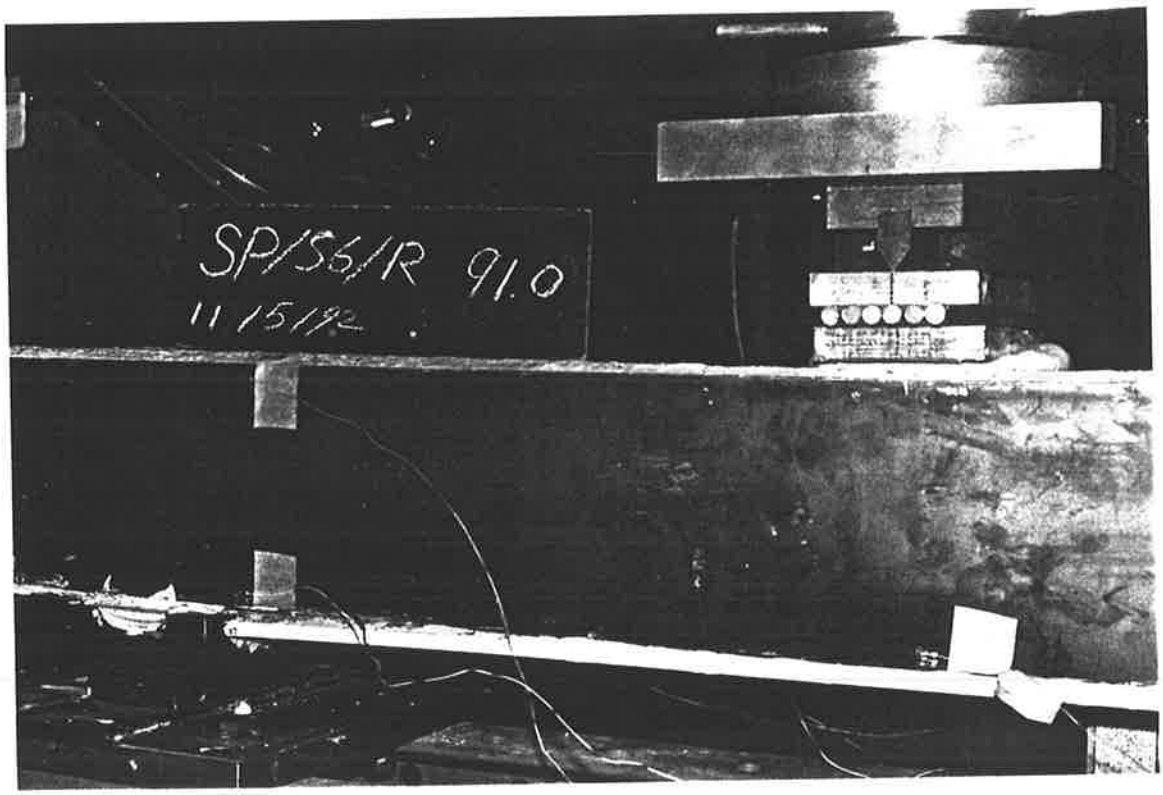

P3-78 Debonding of the soffit plate occurred

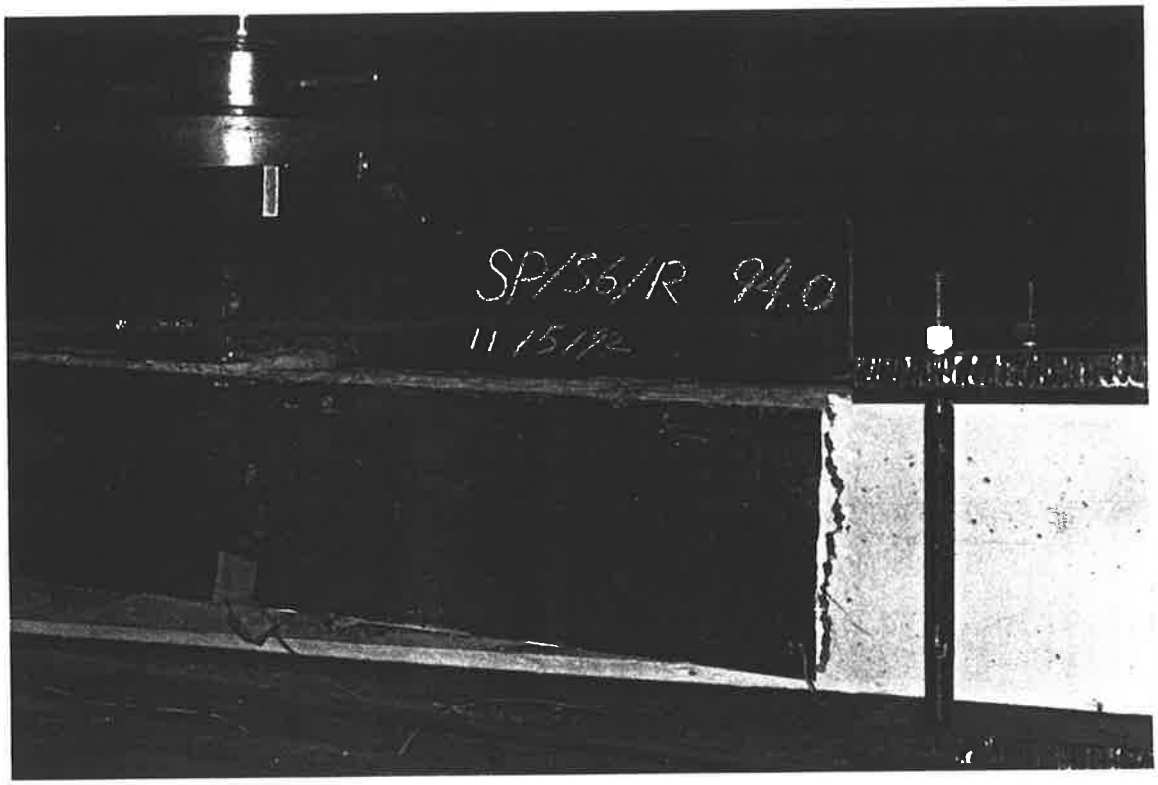

P3-79 The beam failed eventually in flexure

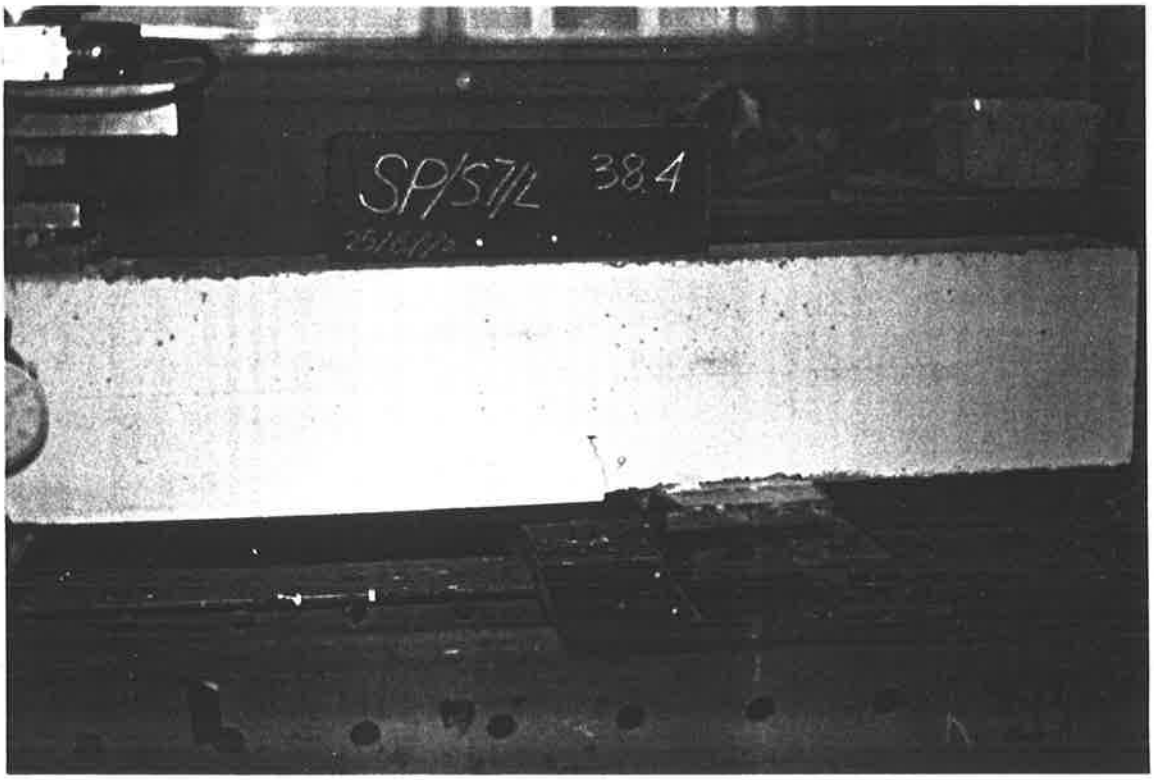

P3-80 The crack formed at the end of the soffit plate

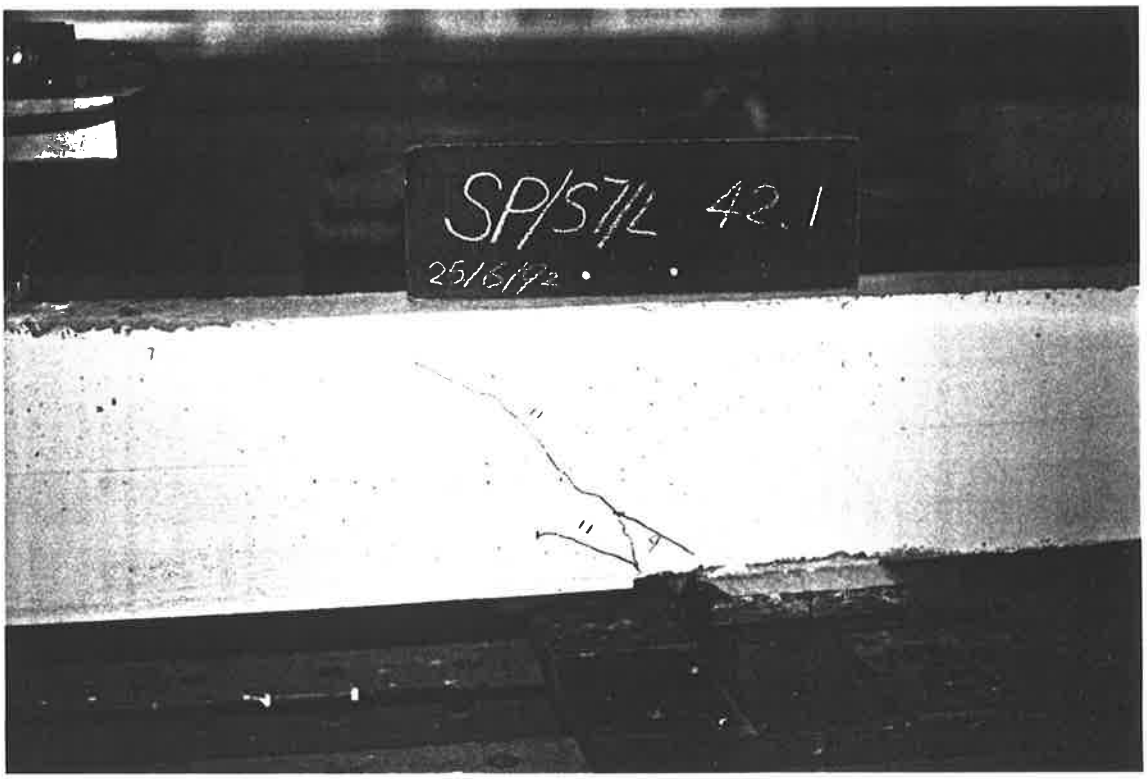

P3-81 The inclined cracks formed

P3-82 Debonding of the soffit plate occurred

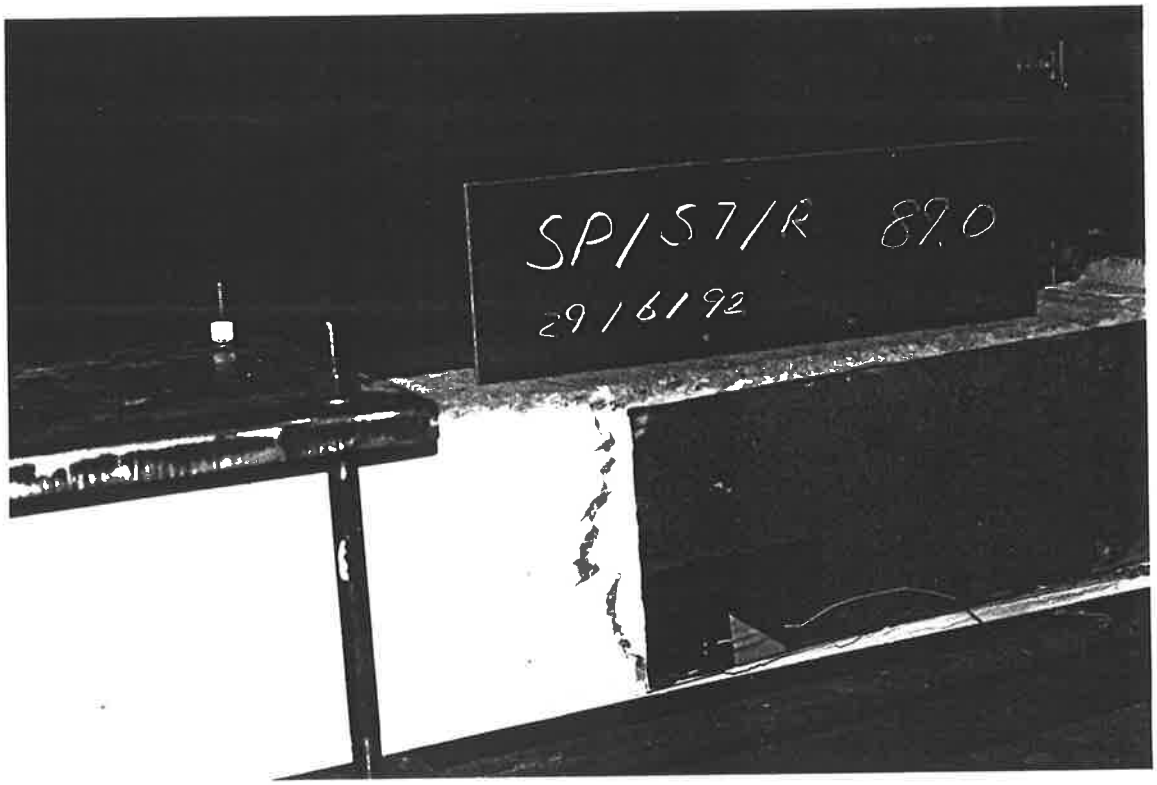

P3-83 The cracks formed along the edge of the side plate

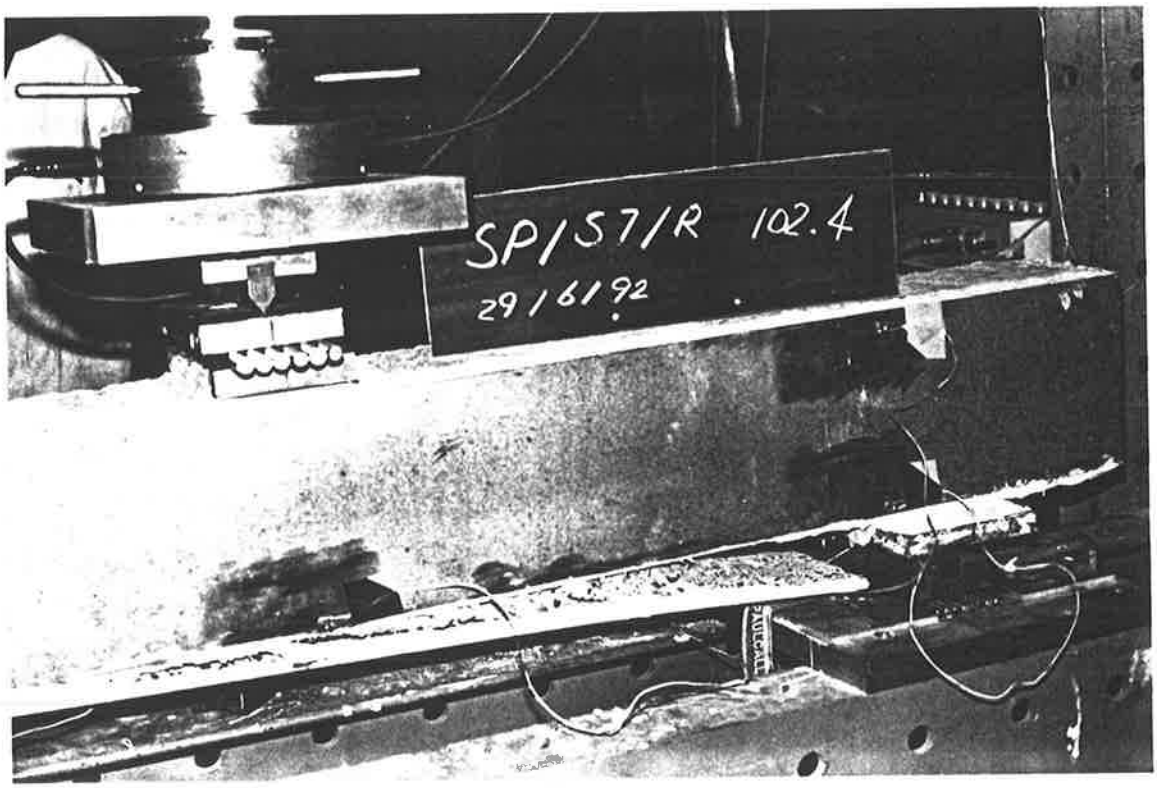

P3-84 Debonding of the soffit plate

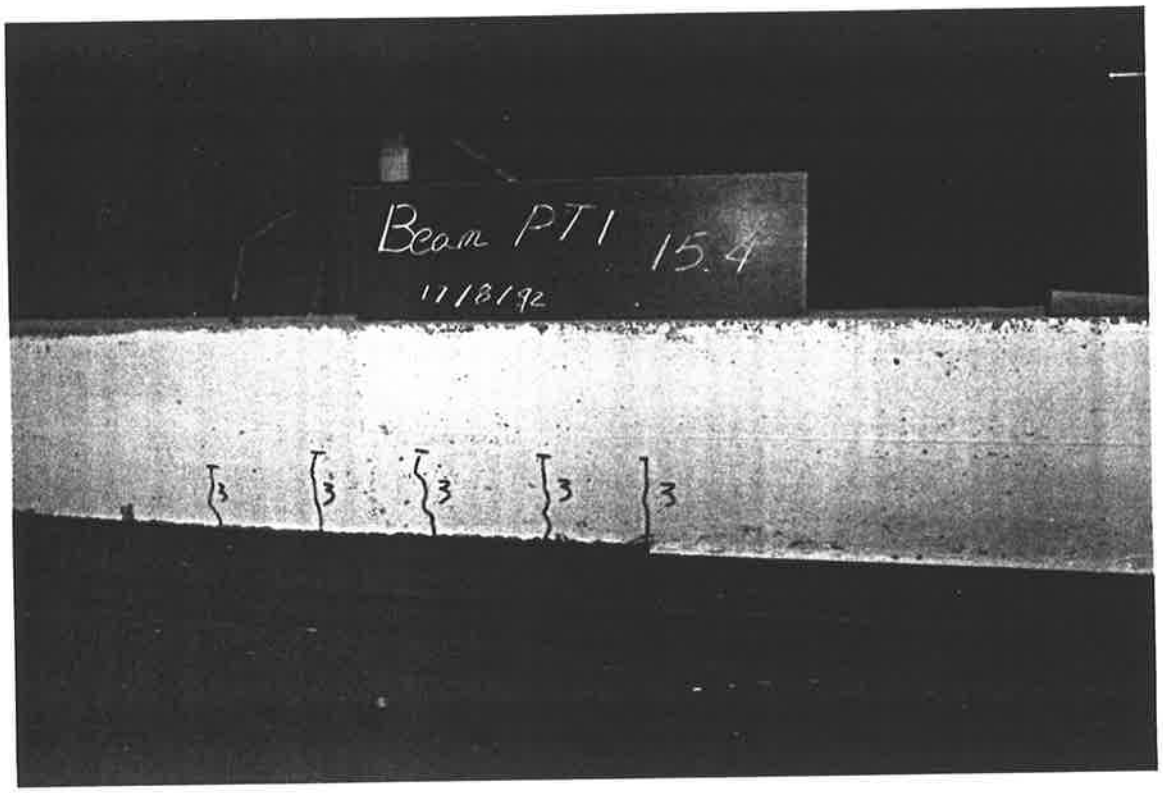

P3-85 The flexural crack formed

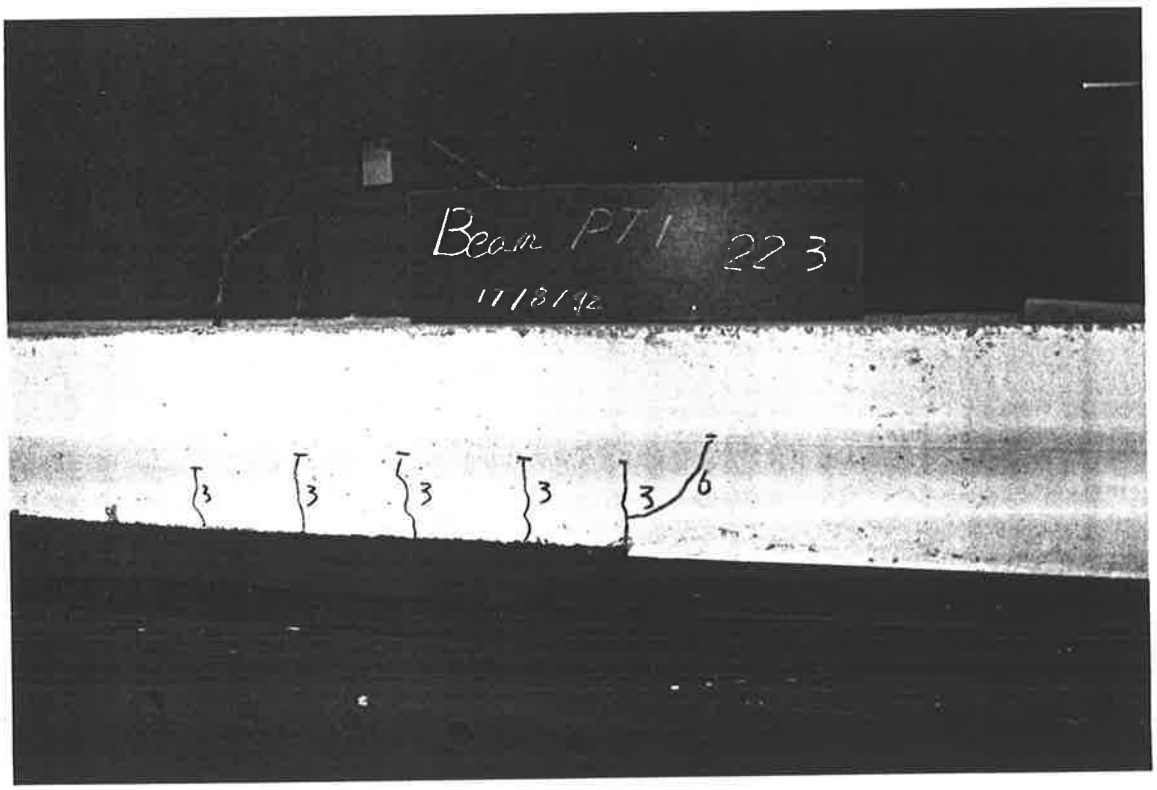

P3-86 The flexure-shear cracks occurred at the end of the soffit plate

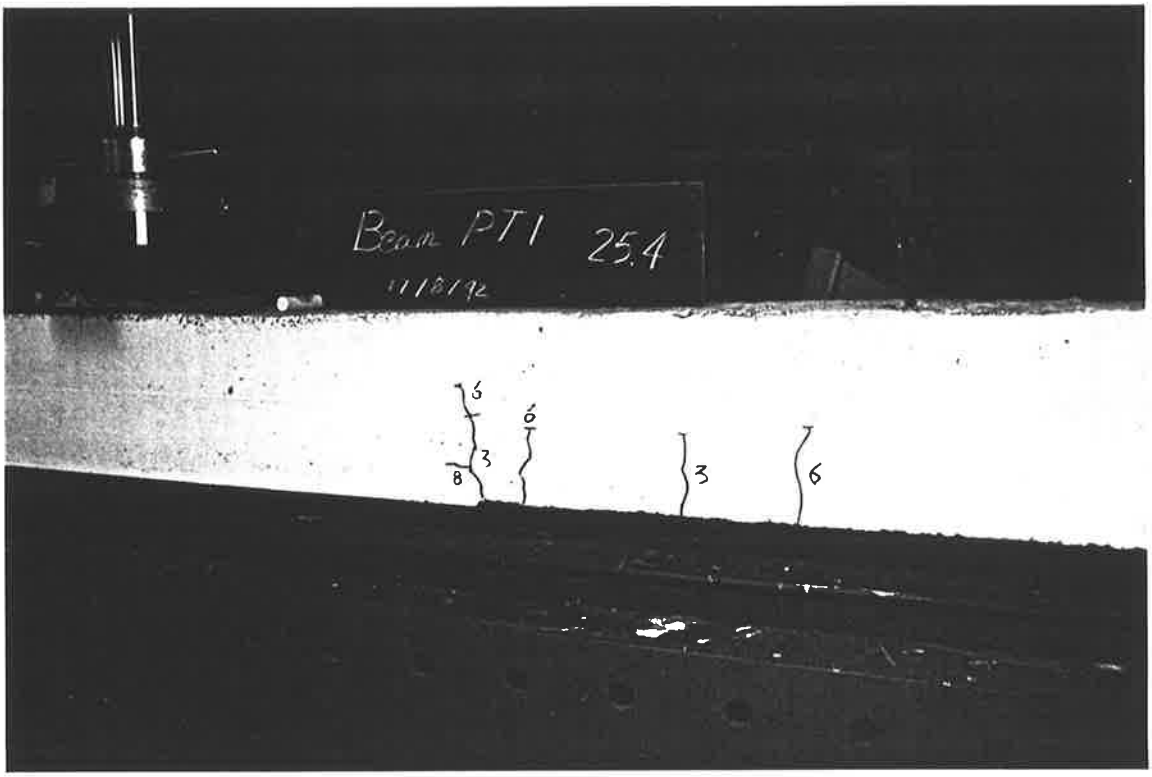

P3-87 The horizontal peeling cracks formed

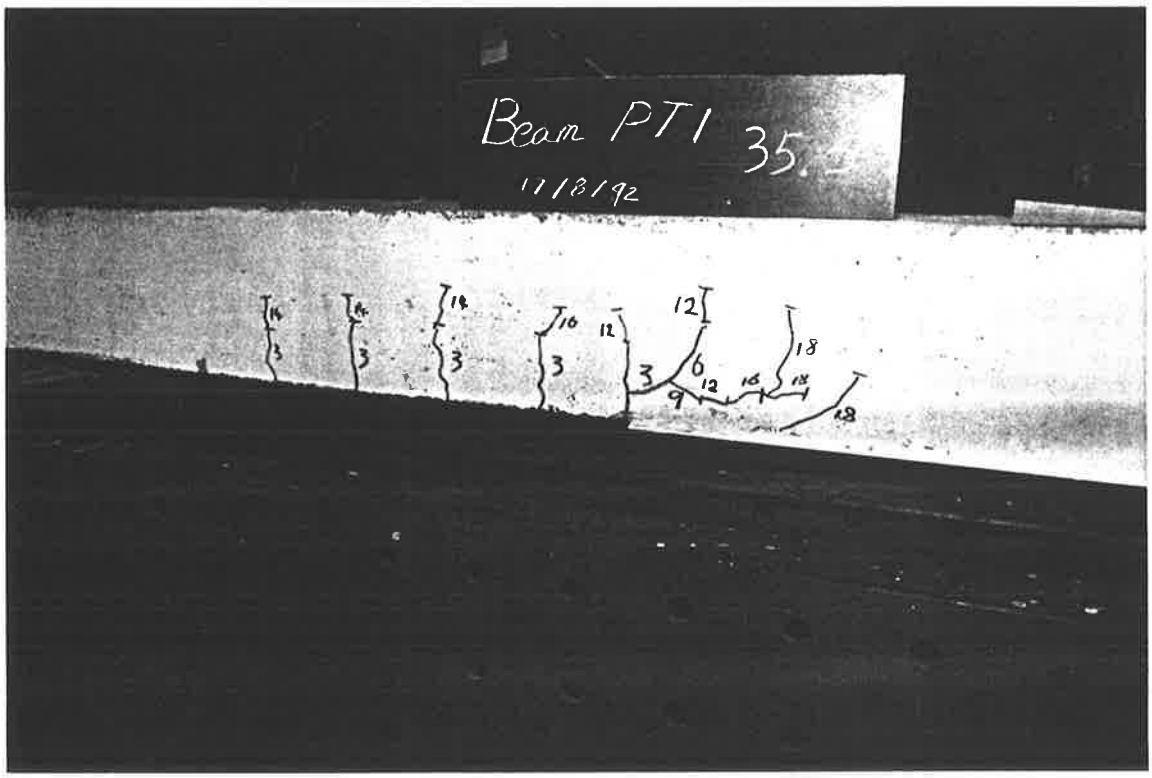

P3-88 The horizontal peeling cracks occurred

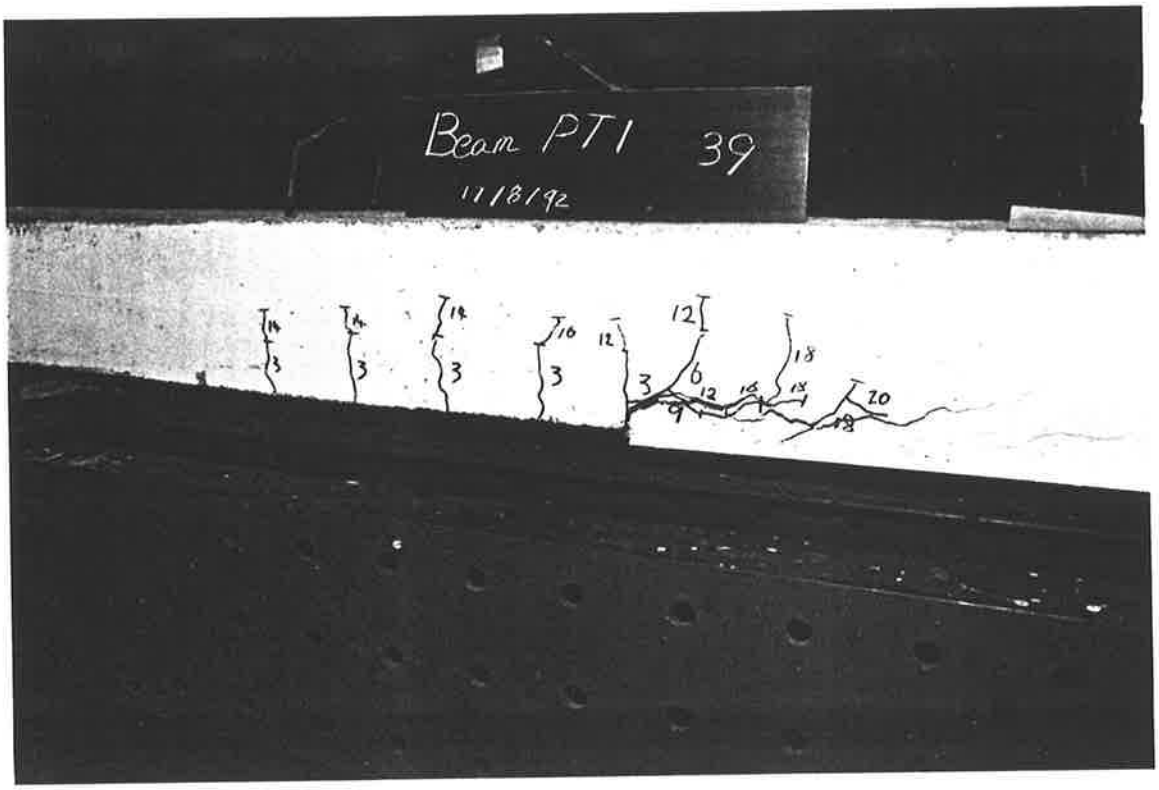

P3-89 Debonding of the soffit plate

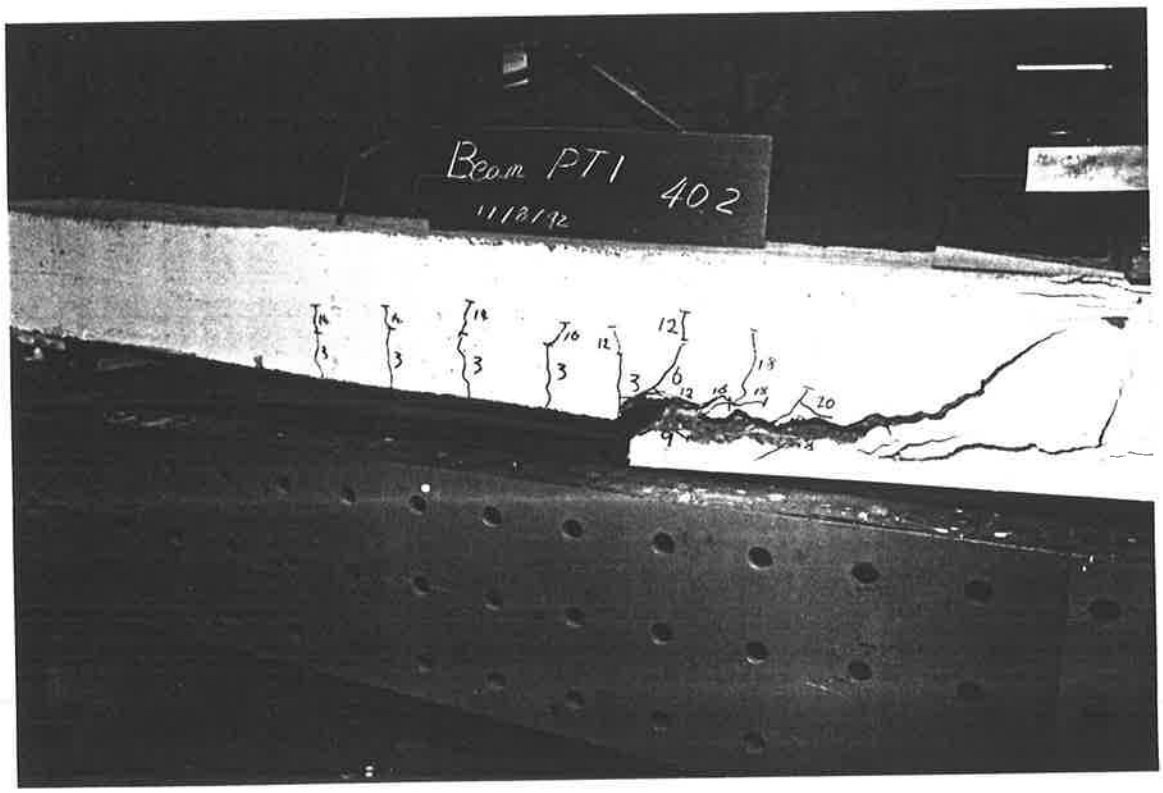

P3-90 The beam failed in flexure

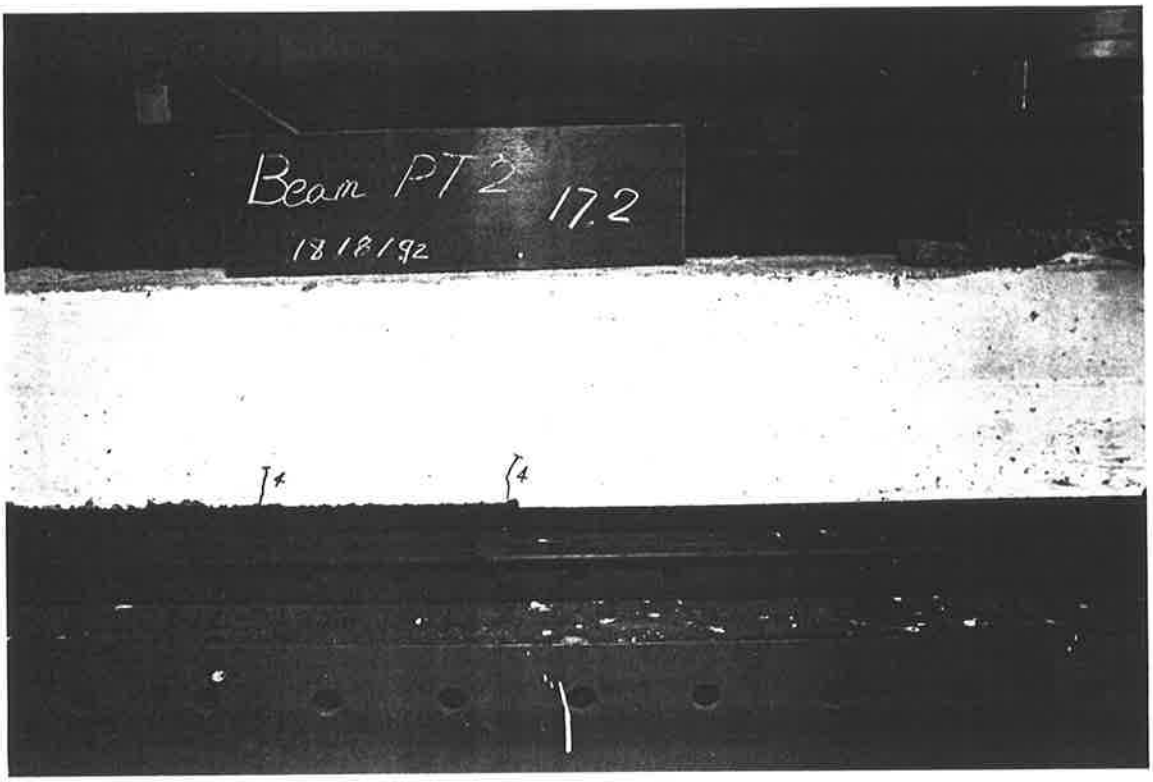

P3-91 The flexural crack occurred

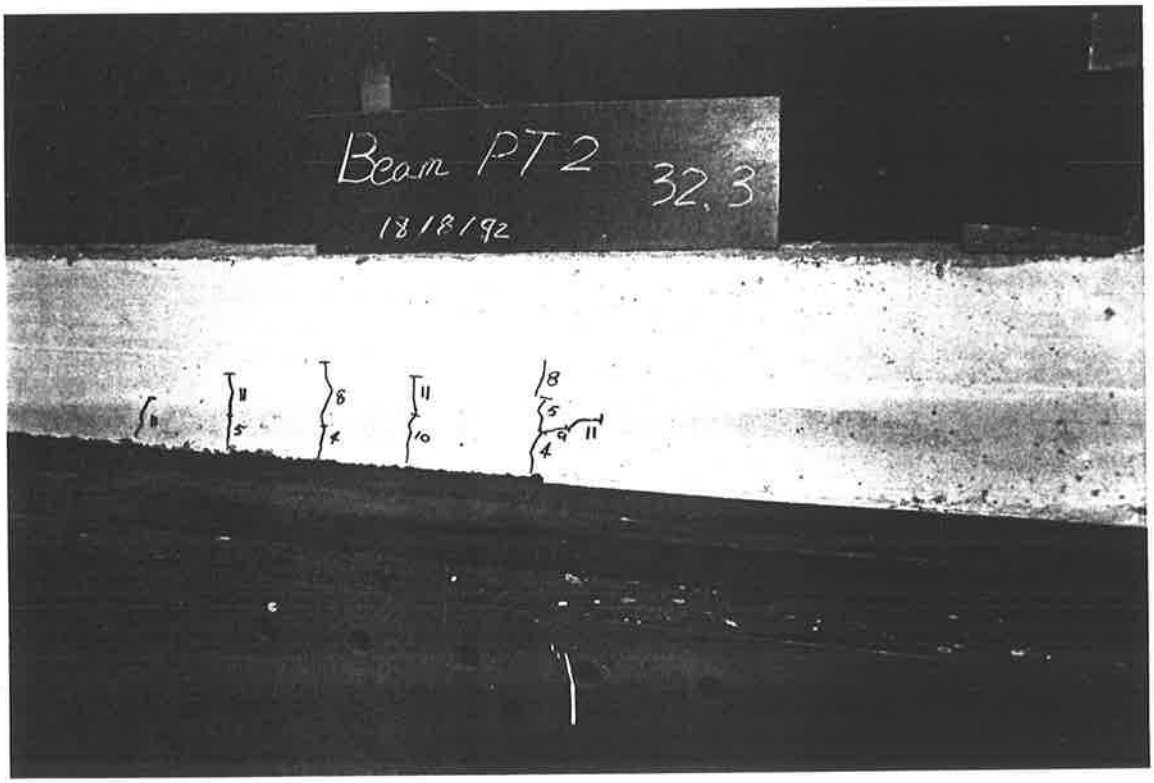

P3-92 The horizontal peeling cracks formed

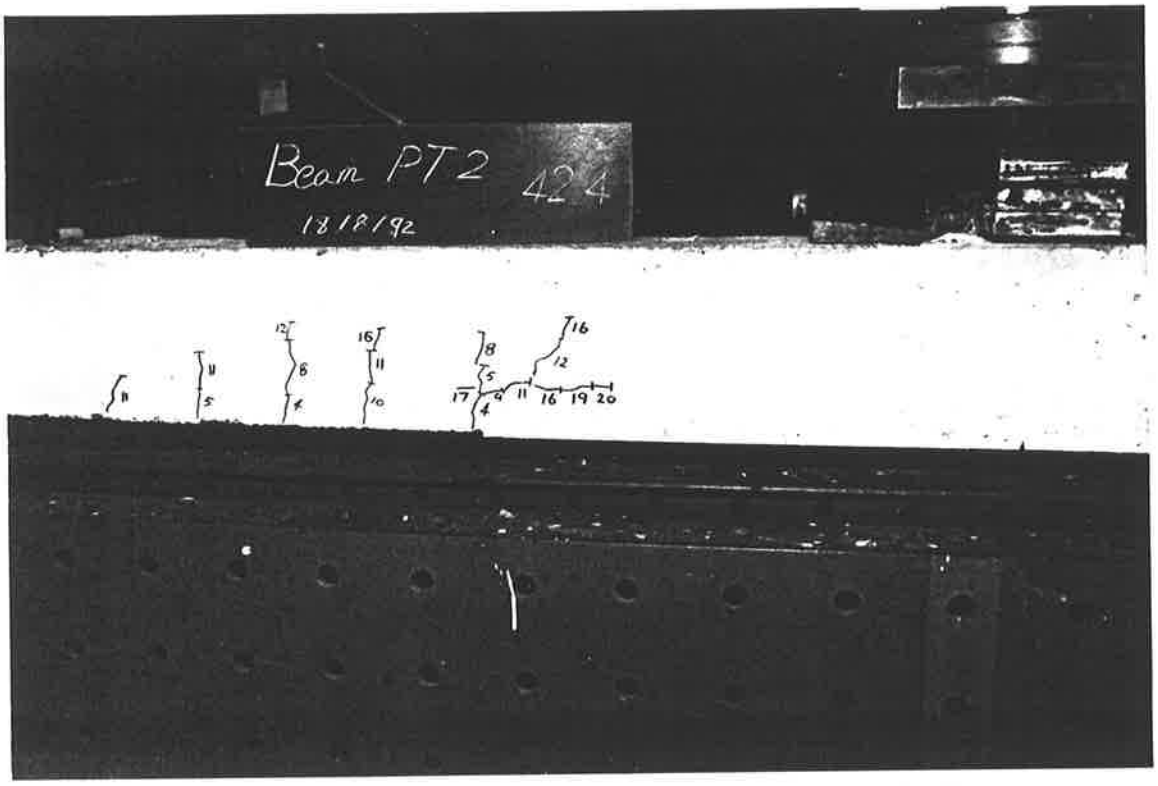

P3-93 The peeling cracks developed progressively along the level of the bottom reinforcement

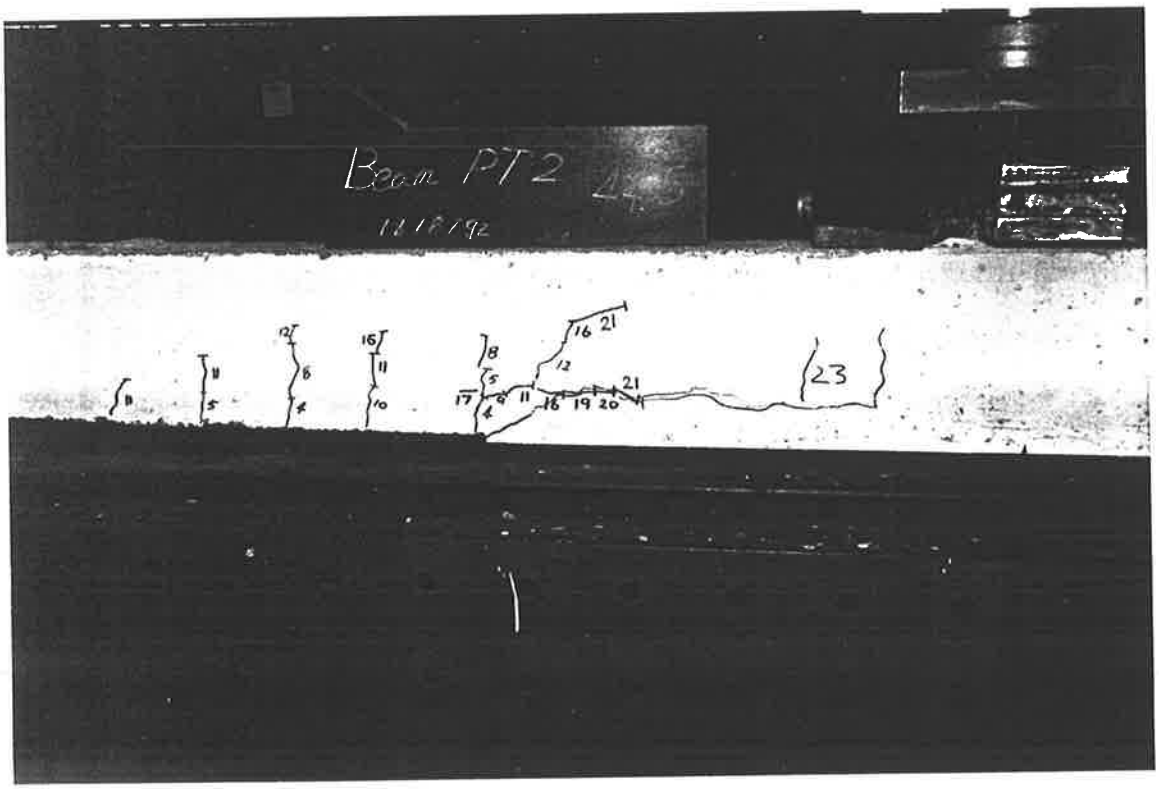

P3-94 Debonding of the soffit plate

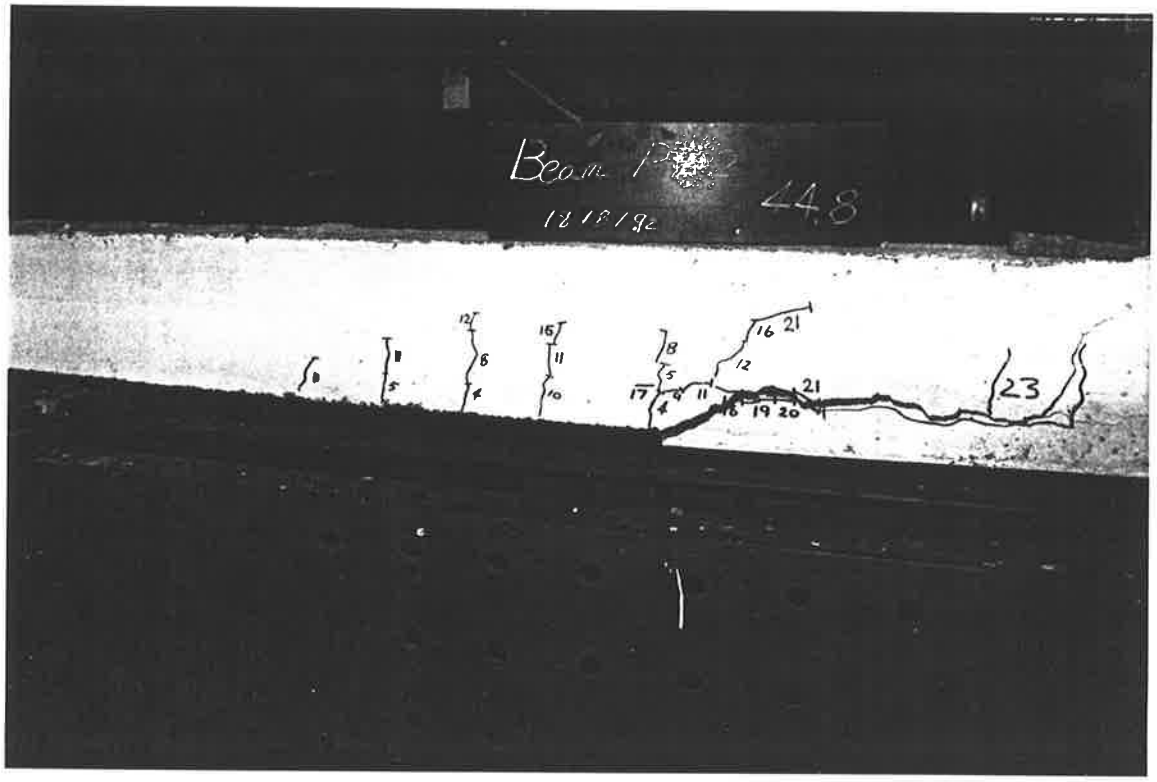

P3-95 Finally the beam failed in flexure

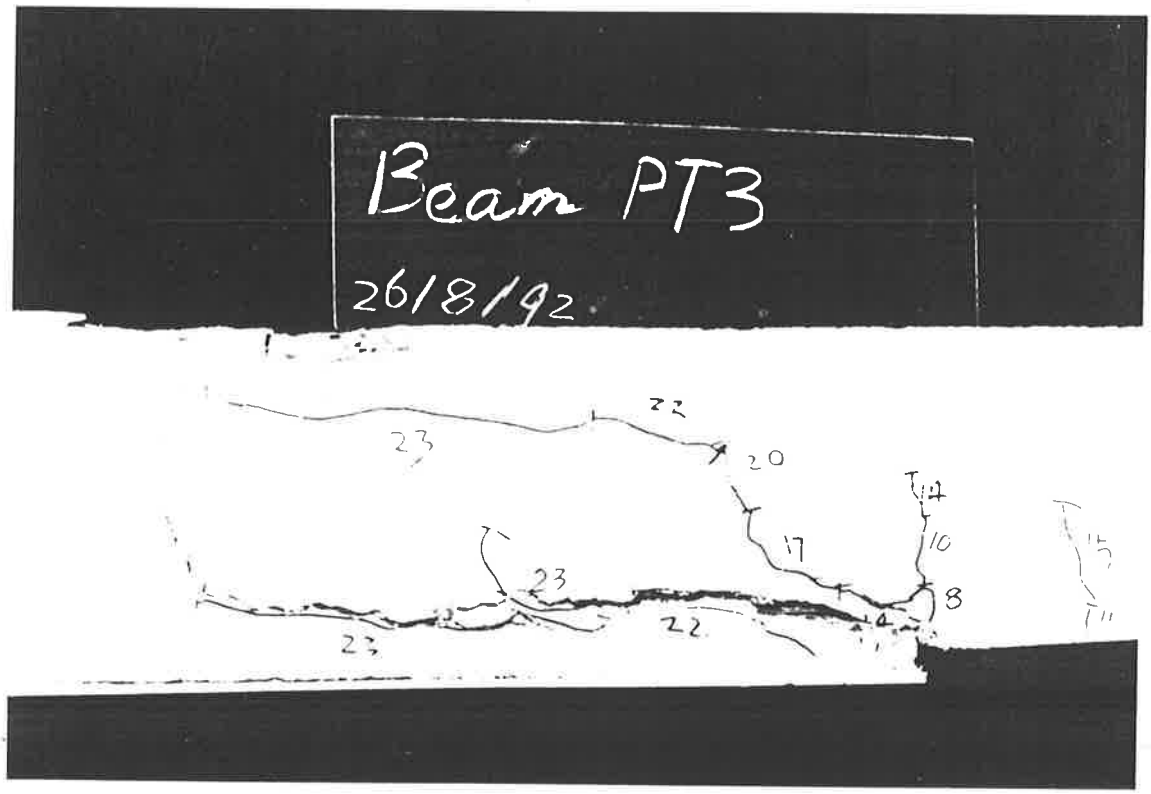

P3-96 The cracks formed and developed in a beam during the testing

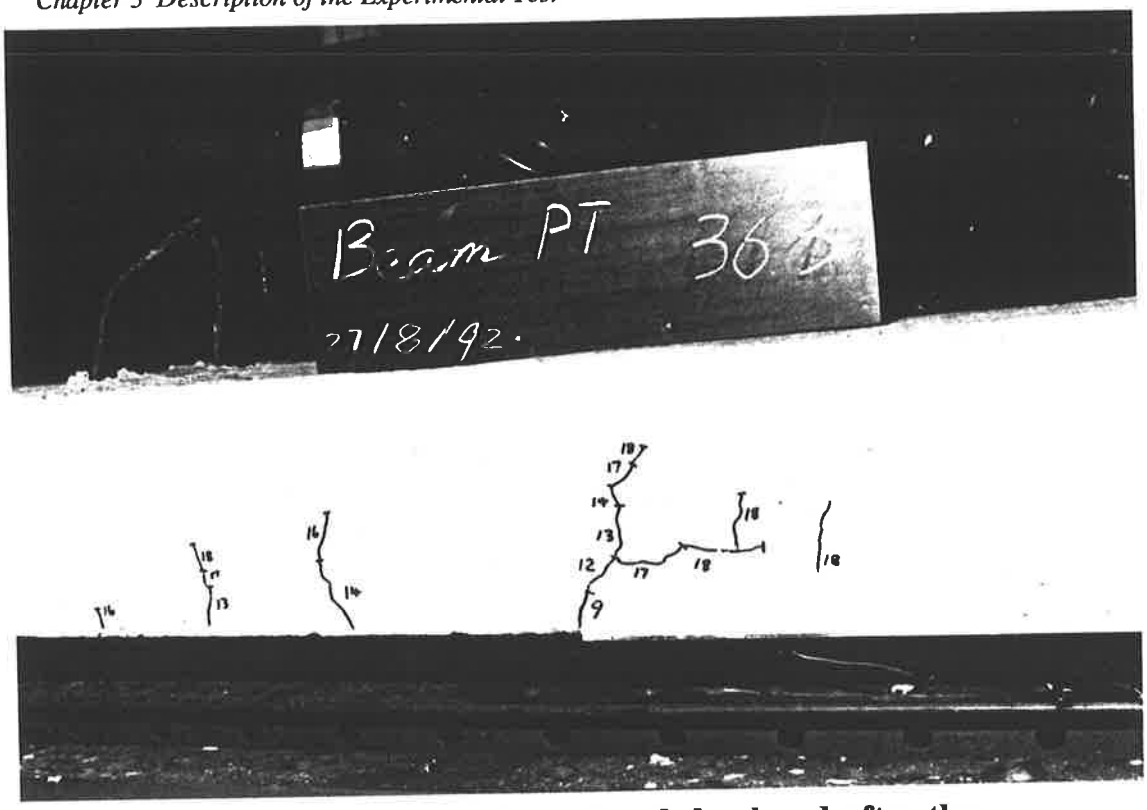

P3-97 the crack formed and developed after the horizontal peeling cracks had formed

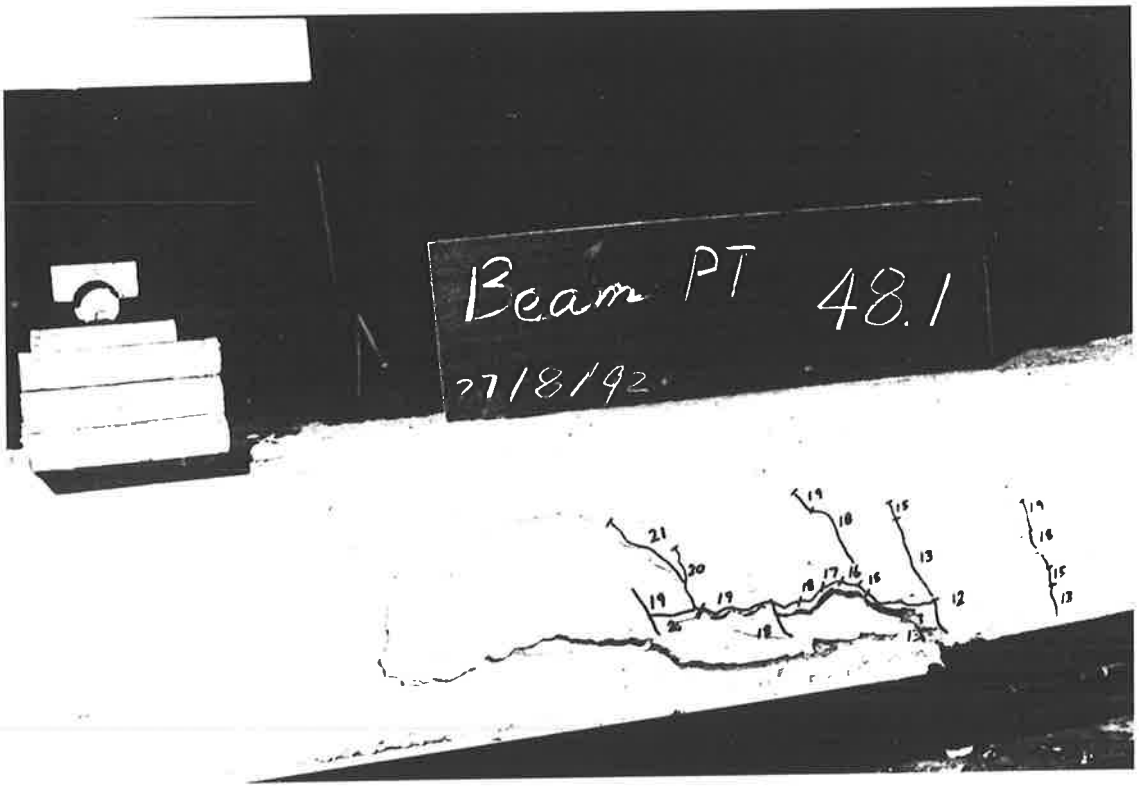

P3-98 The beam failed in flexure eventually

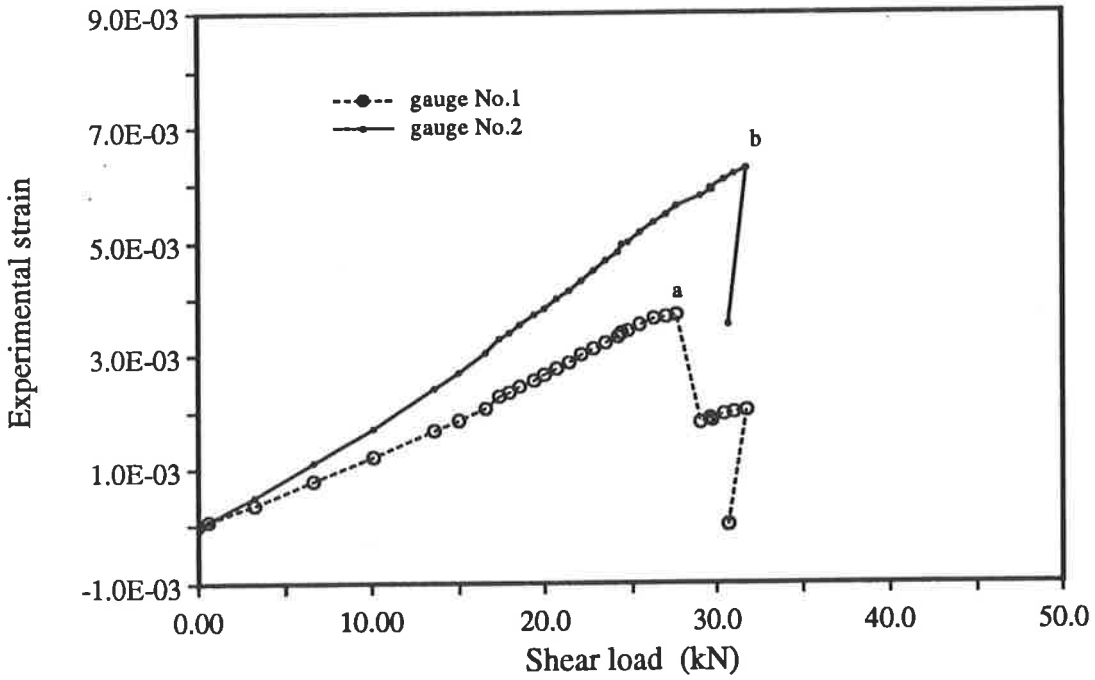

Fig.3-1 L_{sp} = 0.0 mm. Longitudinal strains in the soffit plate of Specimen SP/S1/L

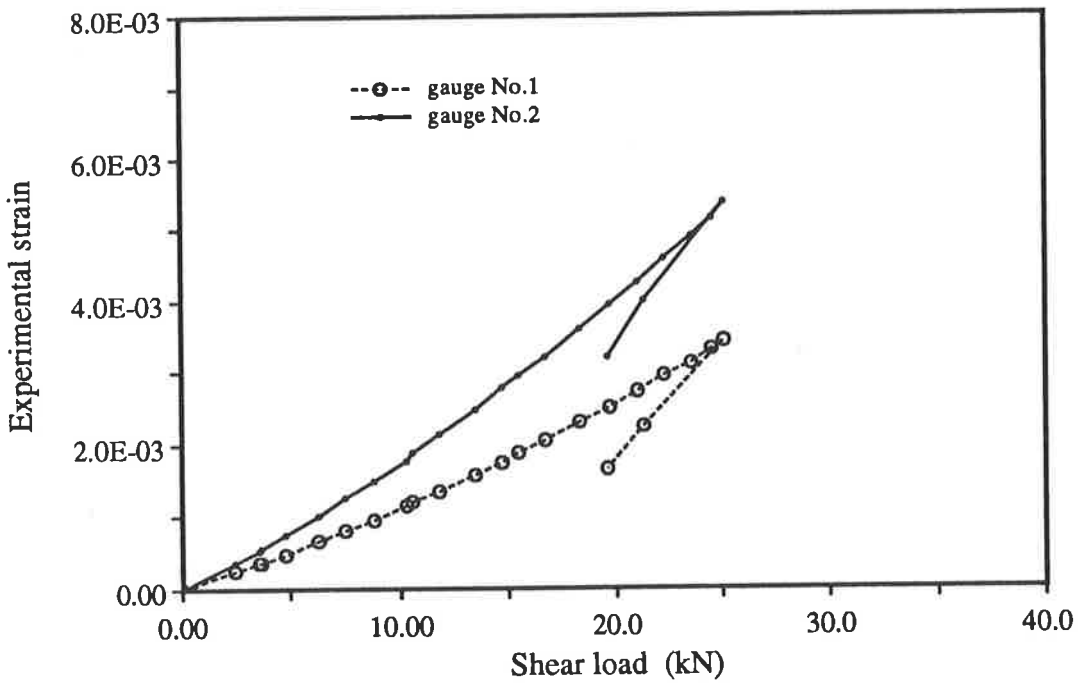

Fig.3-2 L_{sp} = 0.0 mm. Longitudinal strains in the soffit plate of Specimen SP/S2/L

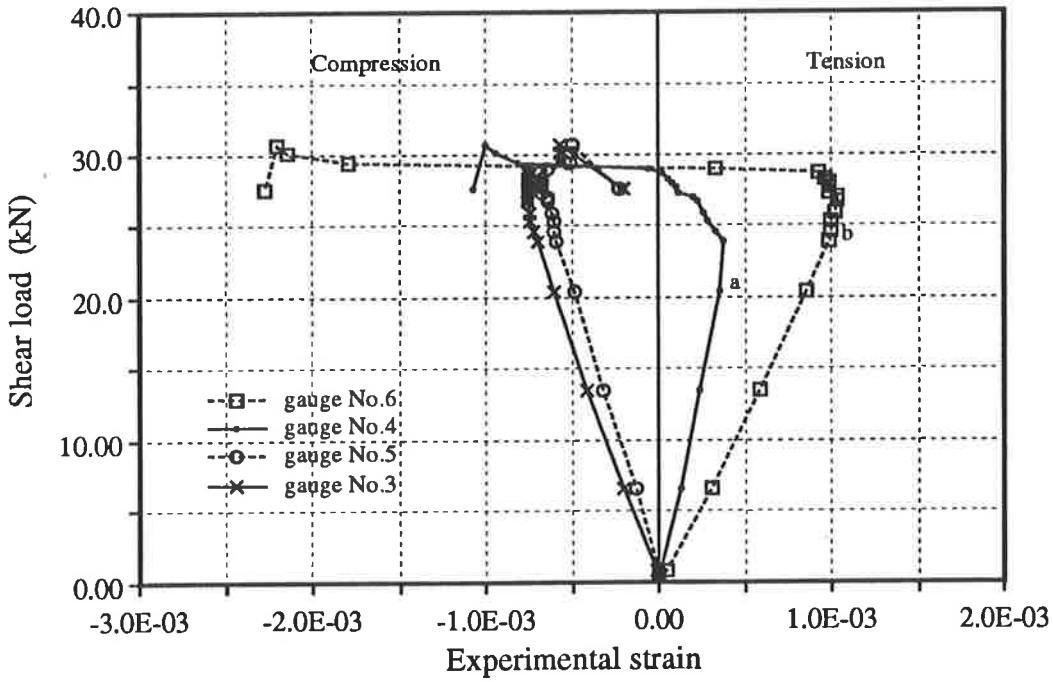

Fig.3-3 L_{sp} = 90.0 mm. Strains in the side plates of Specimen SP/S3/L

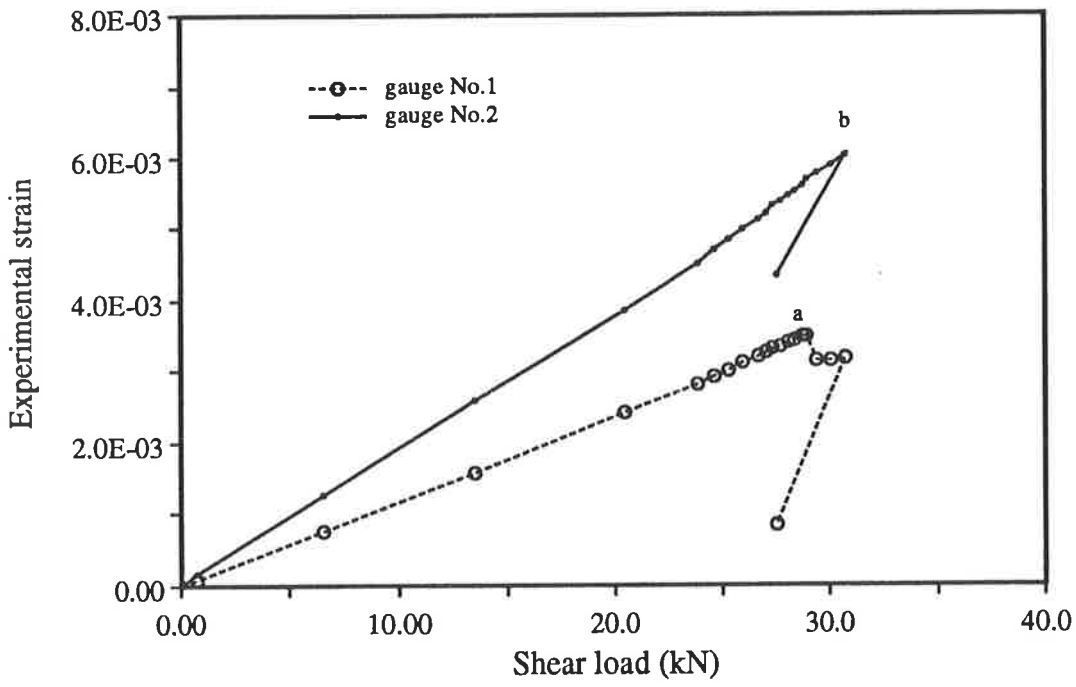

Fig.3-4 L_{sp} = 90.0 mm. Longitudinal strains in the soffit plate of Specimen SP/S3/L

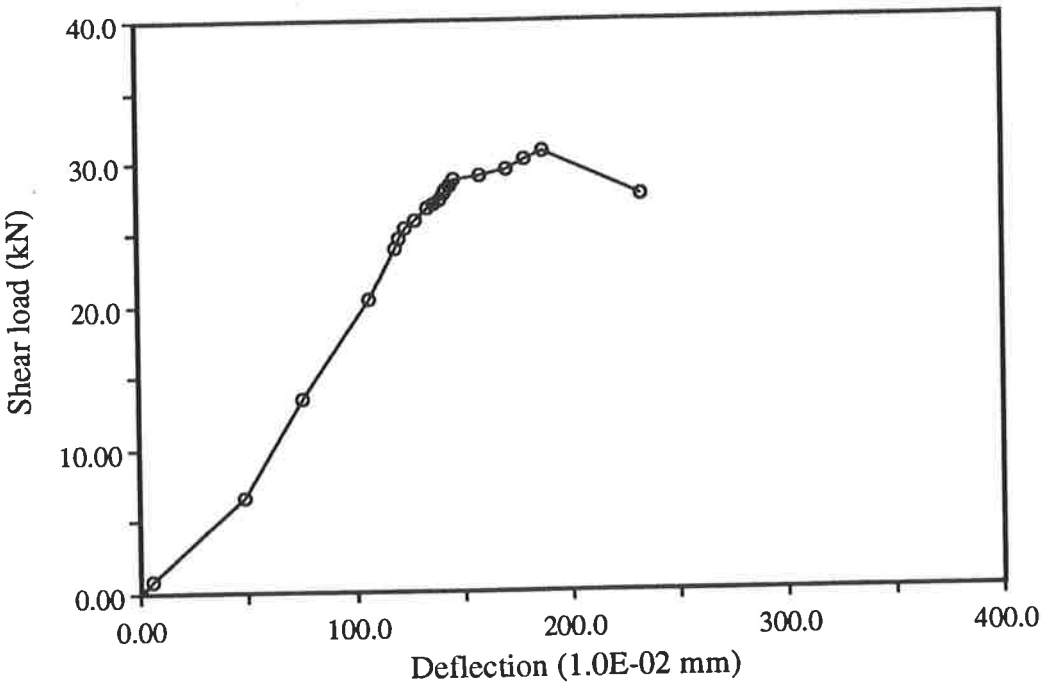

Fig.3-5 L_{sp} = 90.0 mm. The deflection of Specimen SP/S3/L

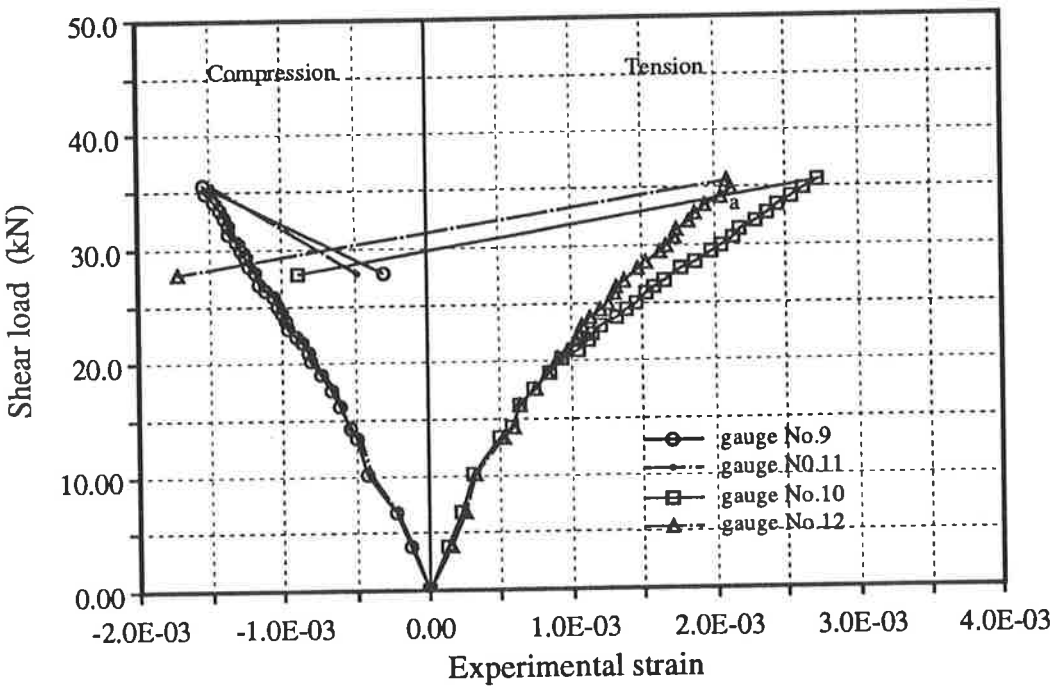

Fig.3-6 L_{sp} = 180.0 mm. Strains in the side plates of Specimen SP/S2/R

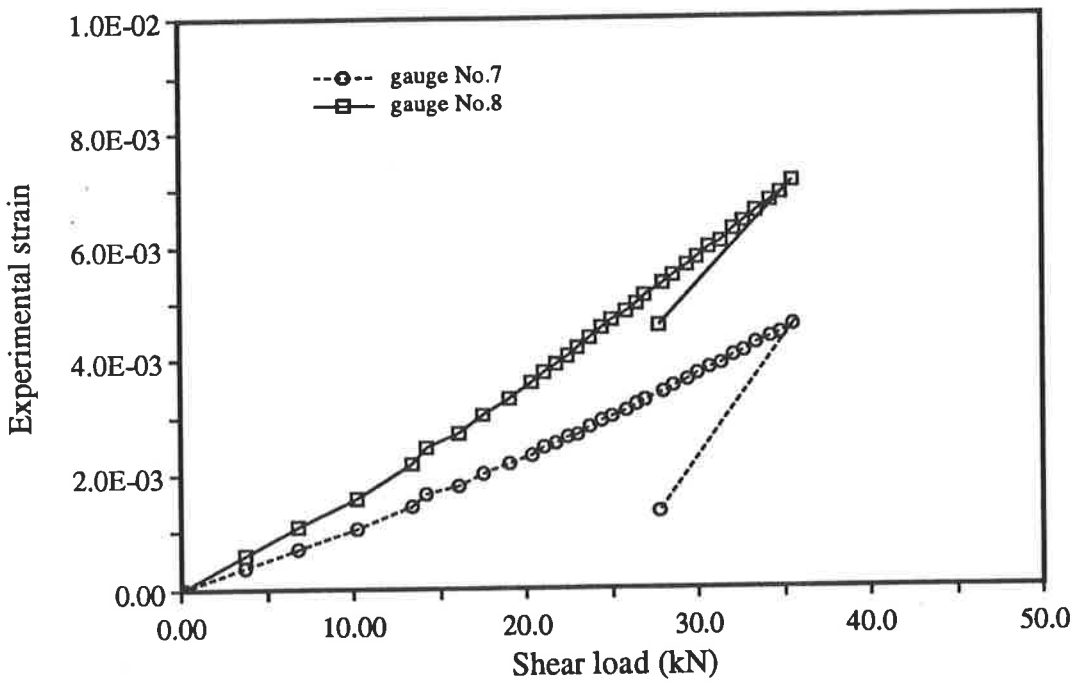

Fig.3-7 L_{sp} = 180.0 mm. Longitudinal strains in the soffit plate of Specimen SP/S2/R

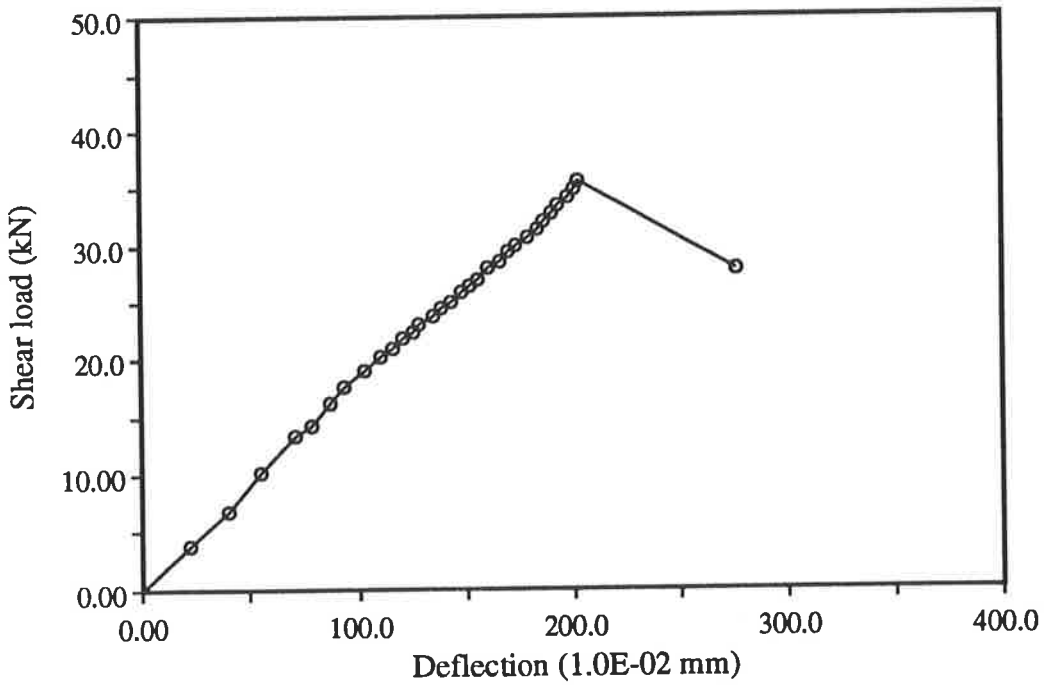

Fig.3-8 L_{sp} = 180.0 mm. The deflection of Specimen SP/S2/R

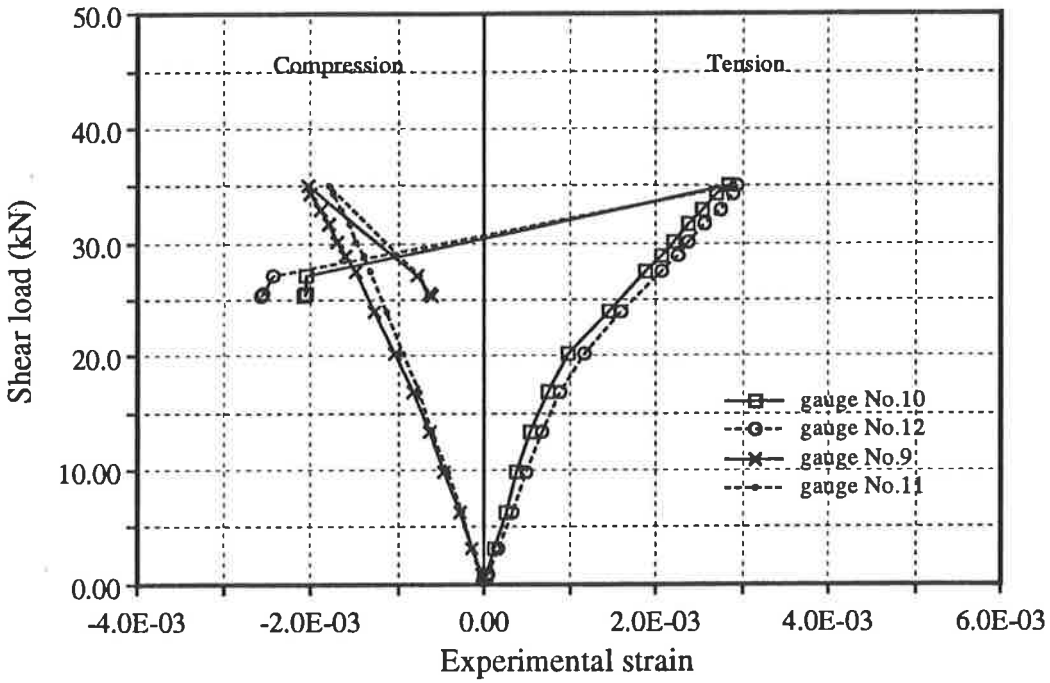

Fig.3-9 L_{sp} = 270.0 mm. Strains in the side plates of Specimen SP/S4/R

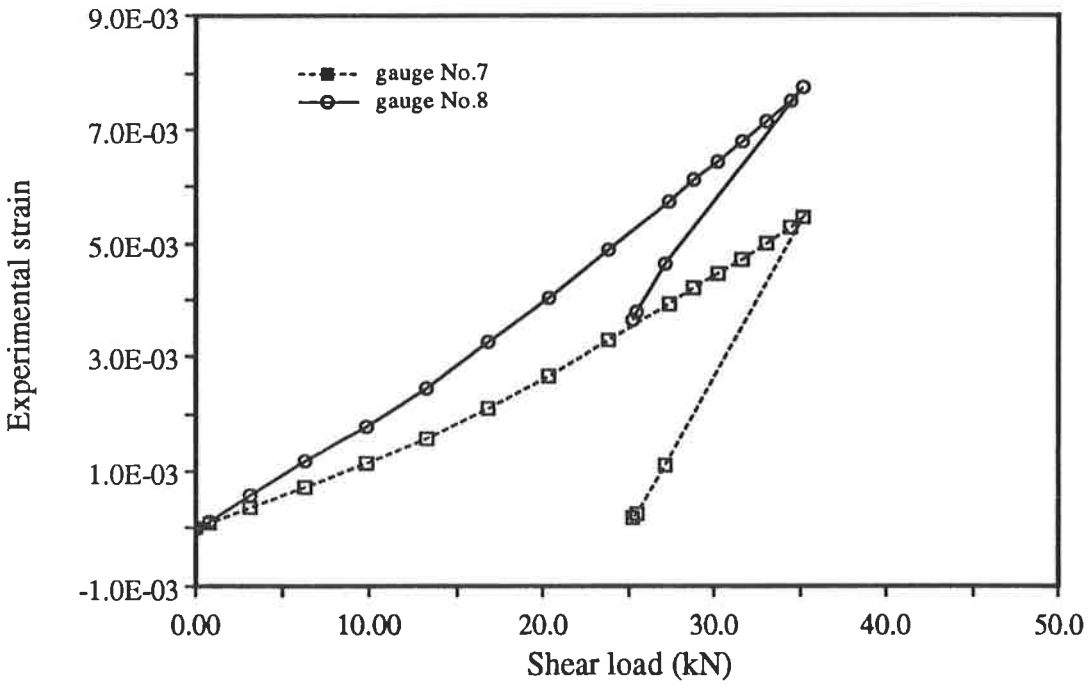

Fig.3-10 L_{sp} = 270.0 mm. Longitudinal strains in the soffit plate of Specimen SP/S4/R)

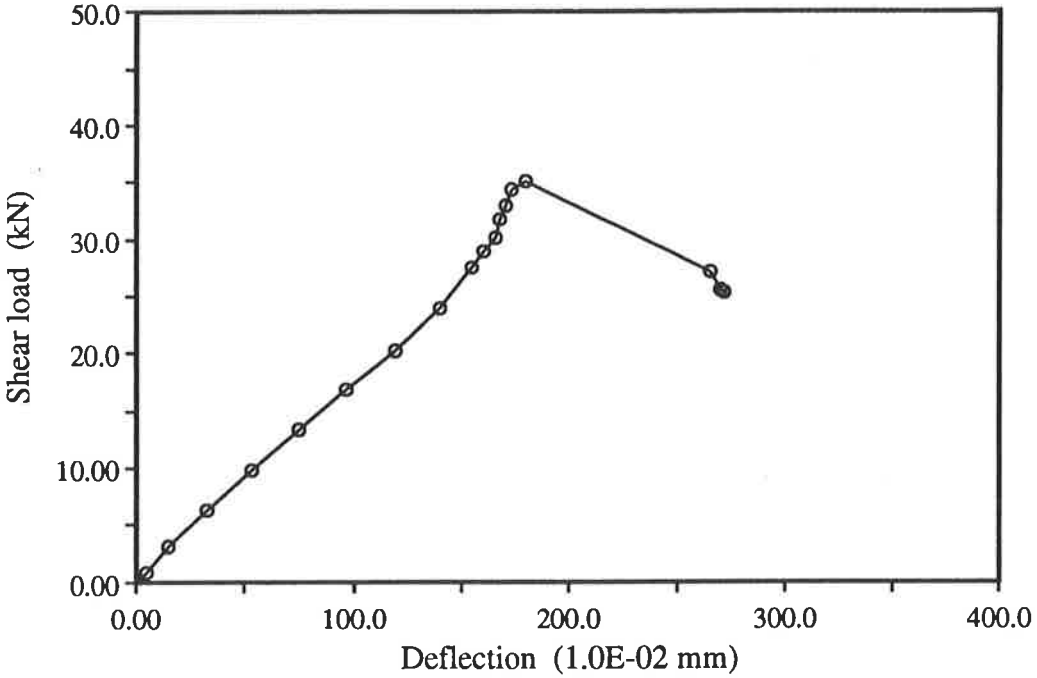

Fig.3-11 L_{sp} = 270.0 mm. The deflection of Specimen SP/S4/R

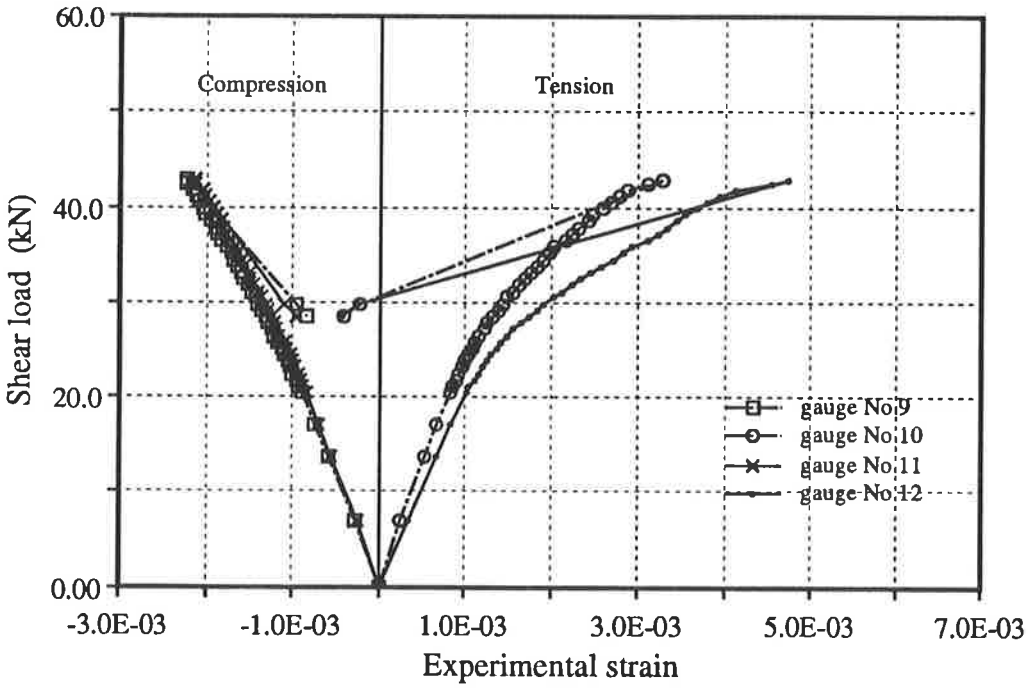

Fig.3-12 L_{sp} = 360.0 mm. Strains in the side plates of Specimen SP/S1/R

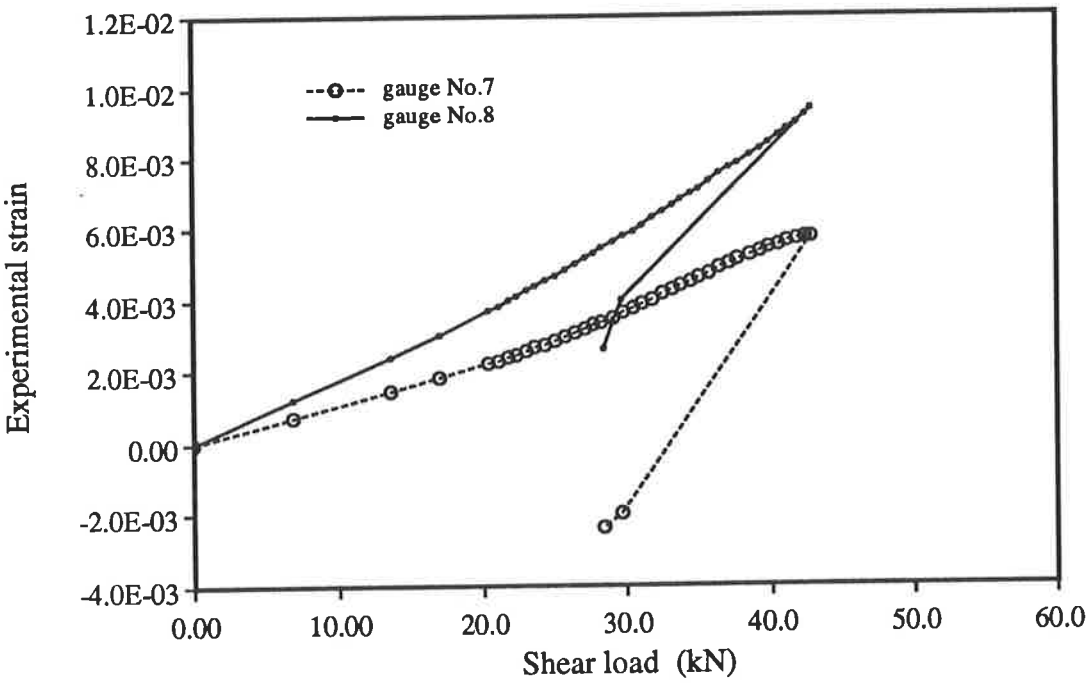

Fig.3-13 L_{sp} = 360.0 mm. Longitudinal strains in the soffit plate of Specimen SP/S1/R

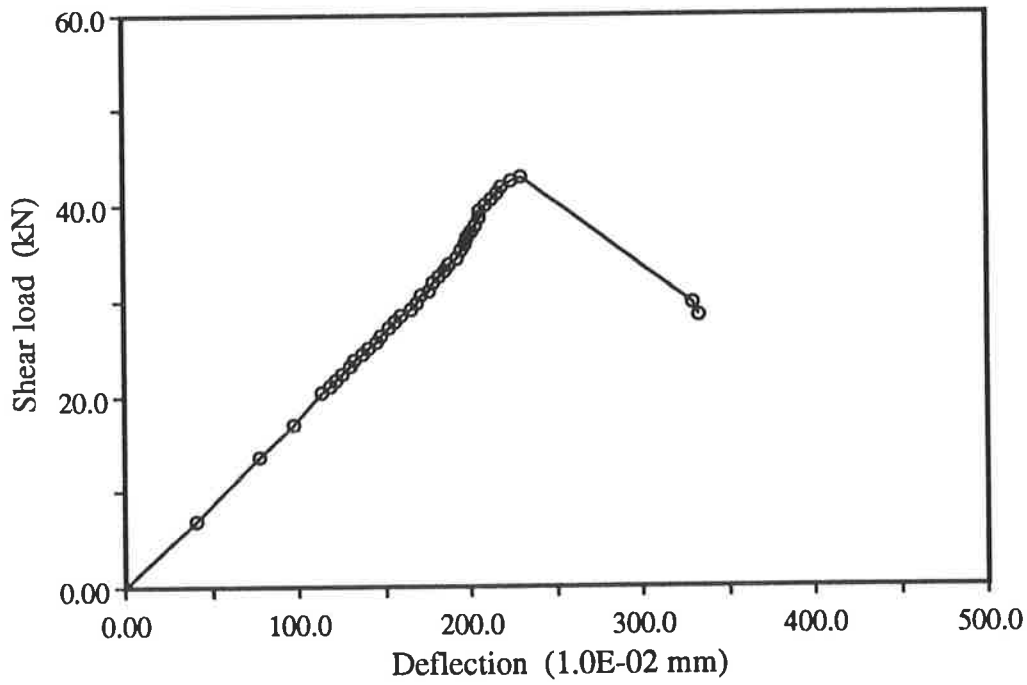

Fig.3-14 L_{sp} = 360.0 mm. The deflection of Specimen SP/S1/R

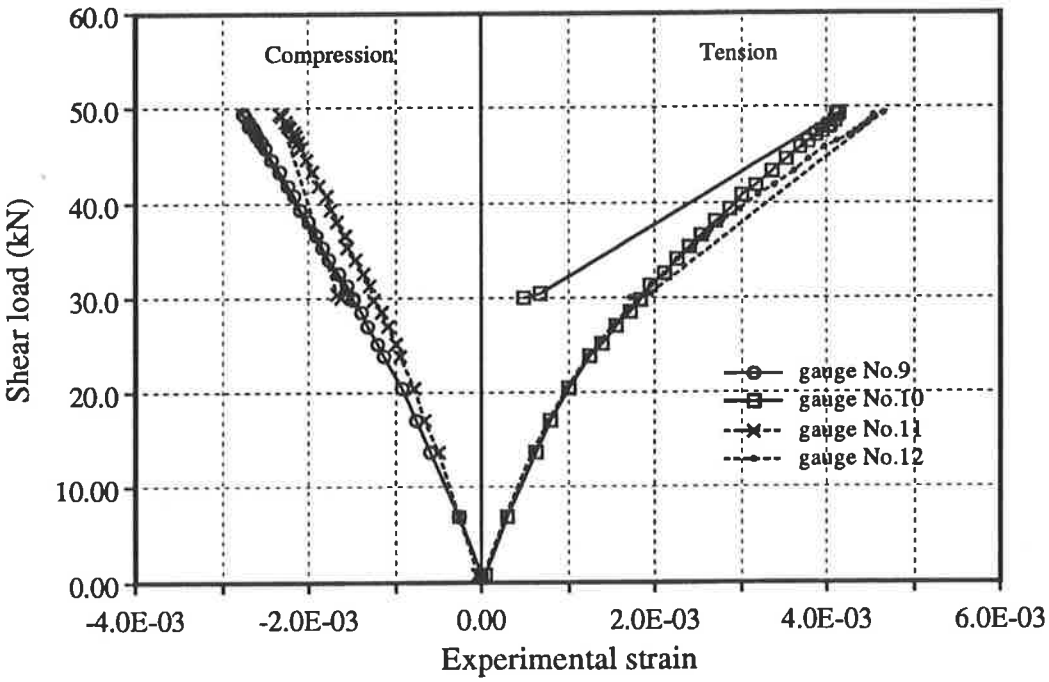

Fig.3-15 L_{sp} = 540.0 mm. Strains in the side plates of Specimen SP/S3/R

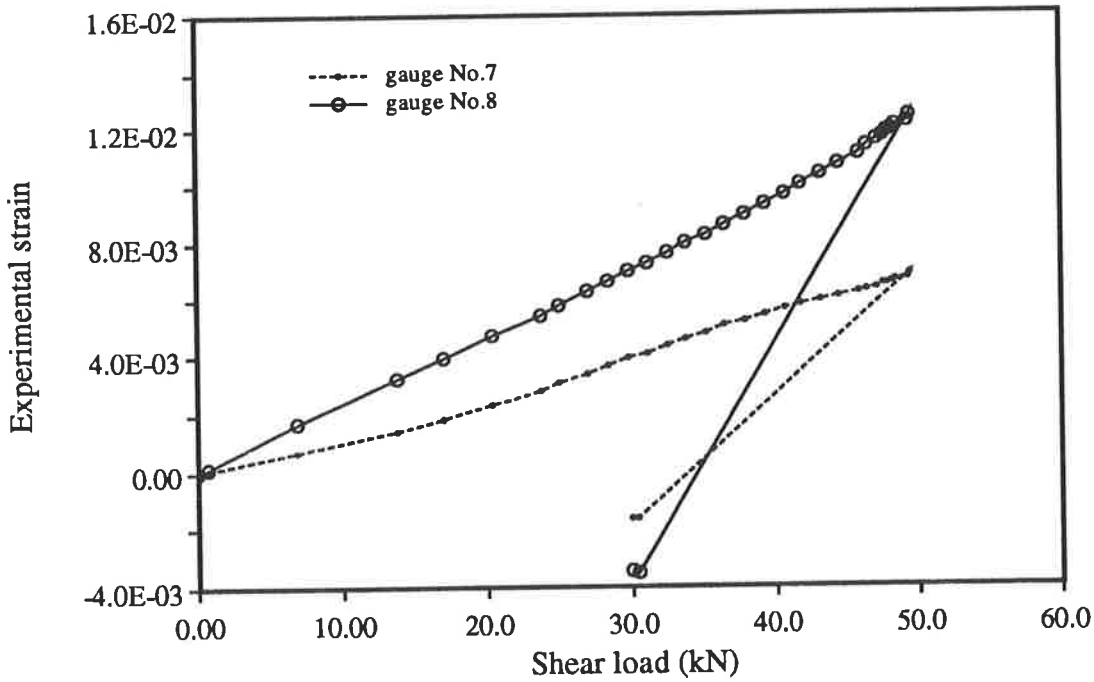

Fig.3-16 L_{sp} = 540.0 mm. Longitudinal strains in the soffit plate of Specimen SP/S3/R

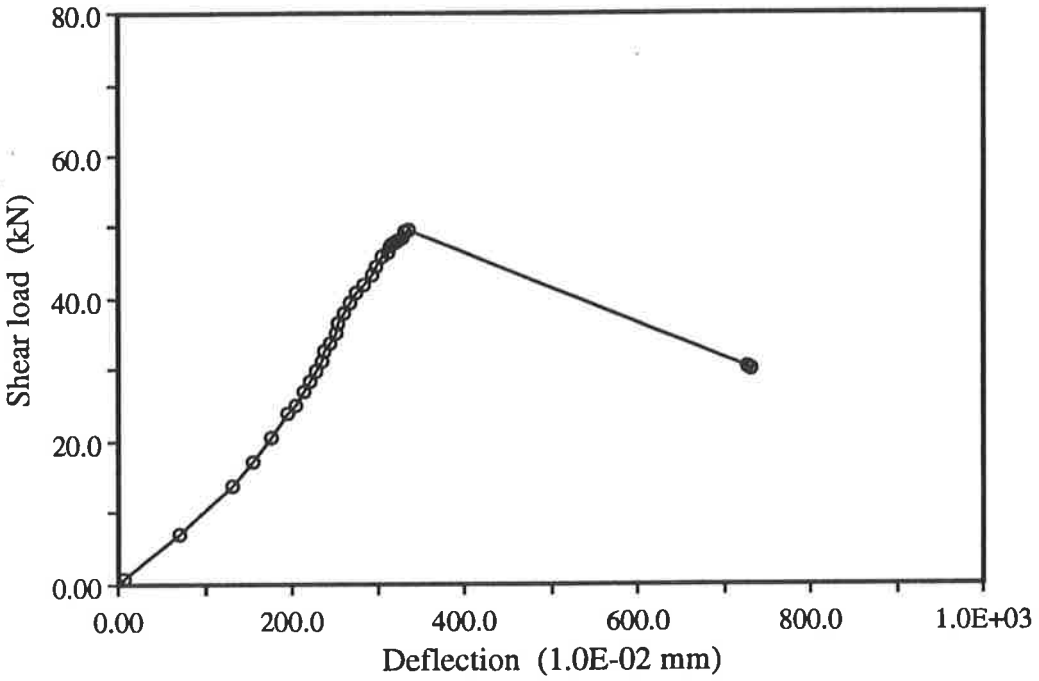

Fig.3-17 L_{sp} = 540.0 mm. The deflection of Specimen SP/S3/R

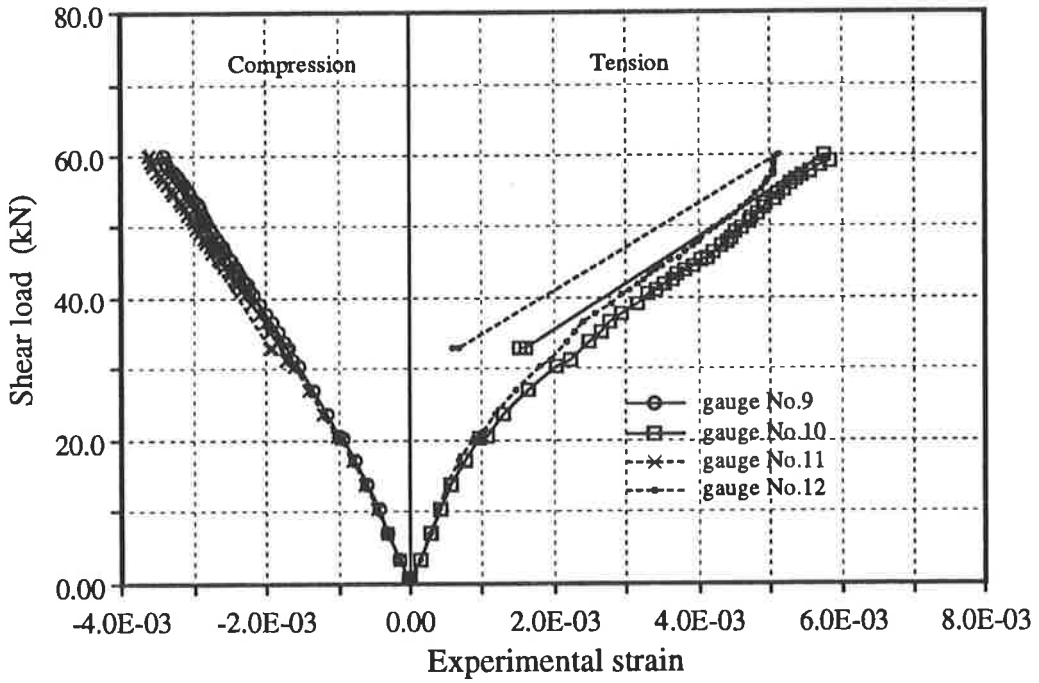

Fig.3-18 L_{sp} = 690.0 mm. Strains in the side plates of Specimen SP/S4/L

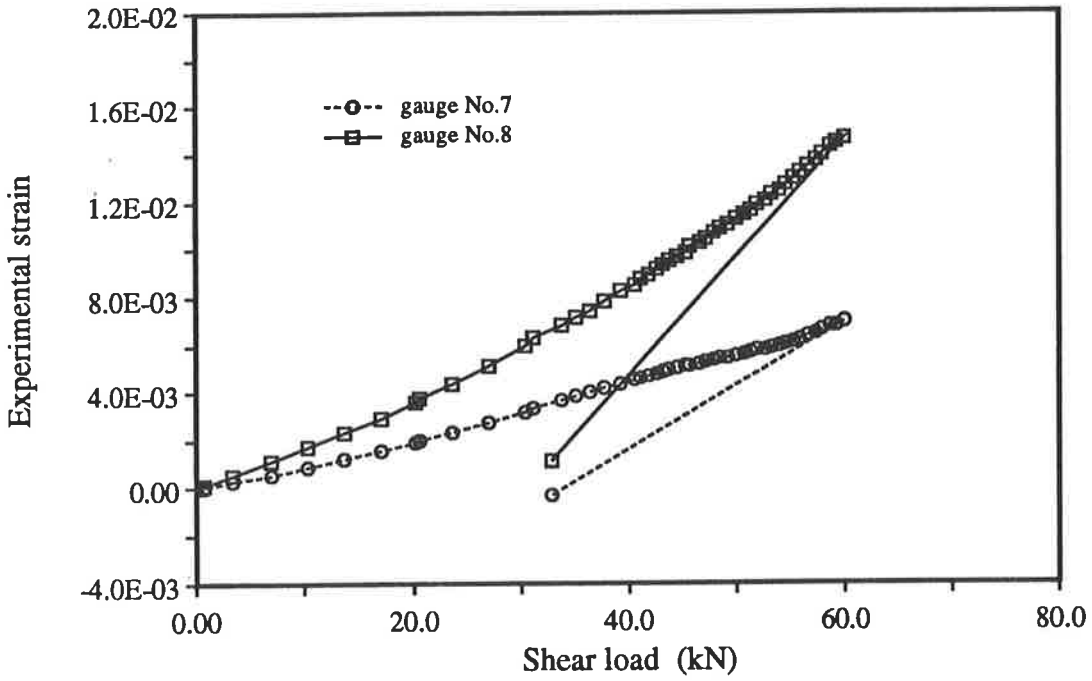

Fig.3-19 L_{sp} = 690.0 mm. Longitudinal strains in the soffit plate of Specimen SP/S4/L

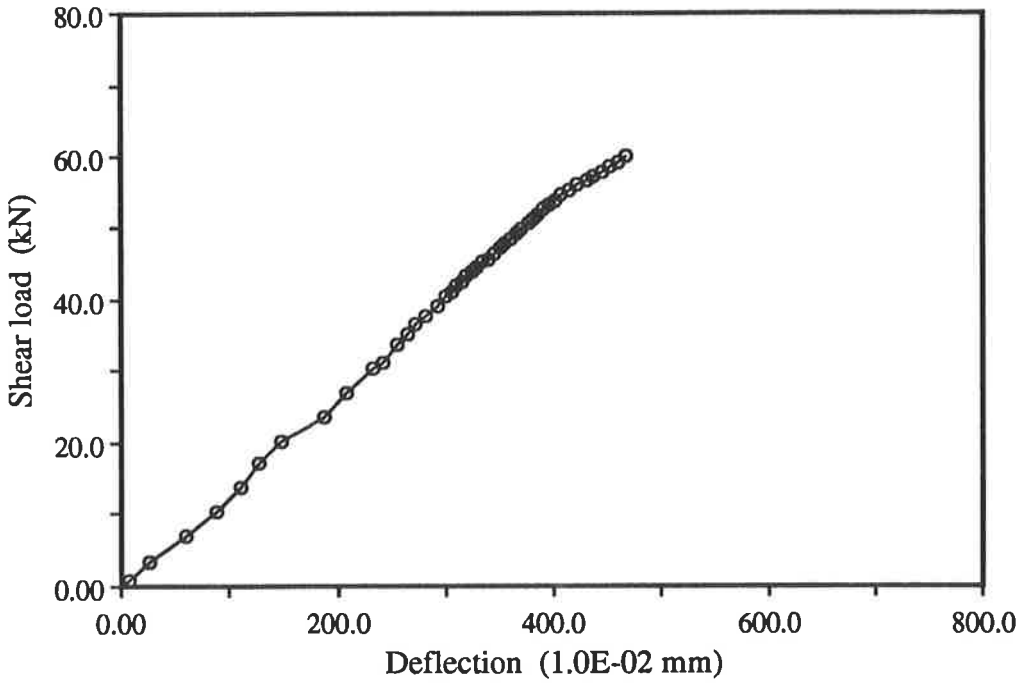

Fig.3-20 L_{sp} = 690.0 mm. The deflection of Specimen SP/S4/L

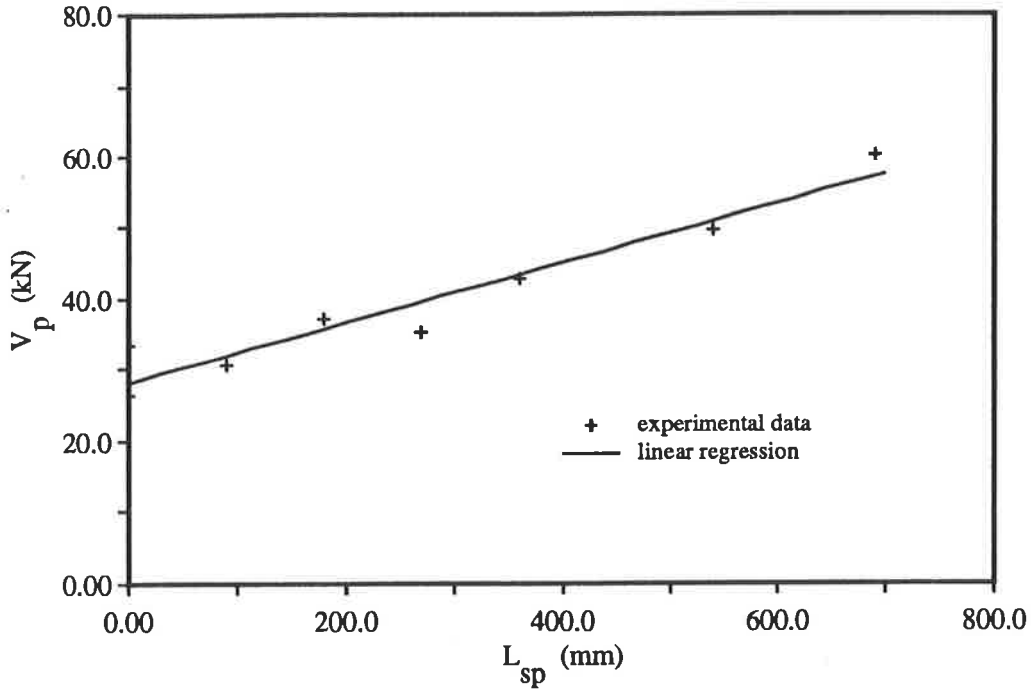

Fig.3-21 Experimental results of series 1

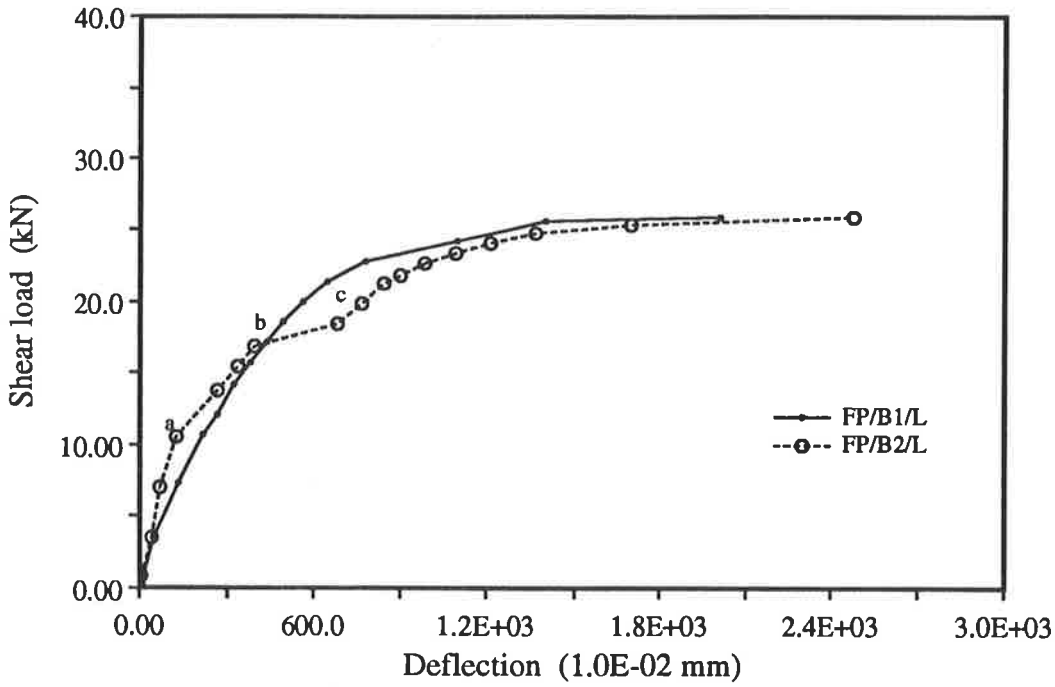

Fig.3-22 t_p = 0.0 mm. The deflection of Specimen FP/B1/L and Specimen FP/B1/R

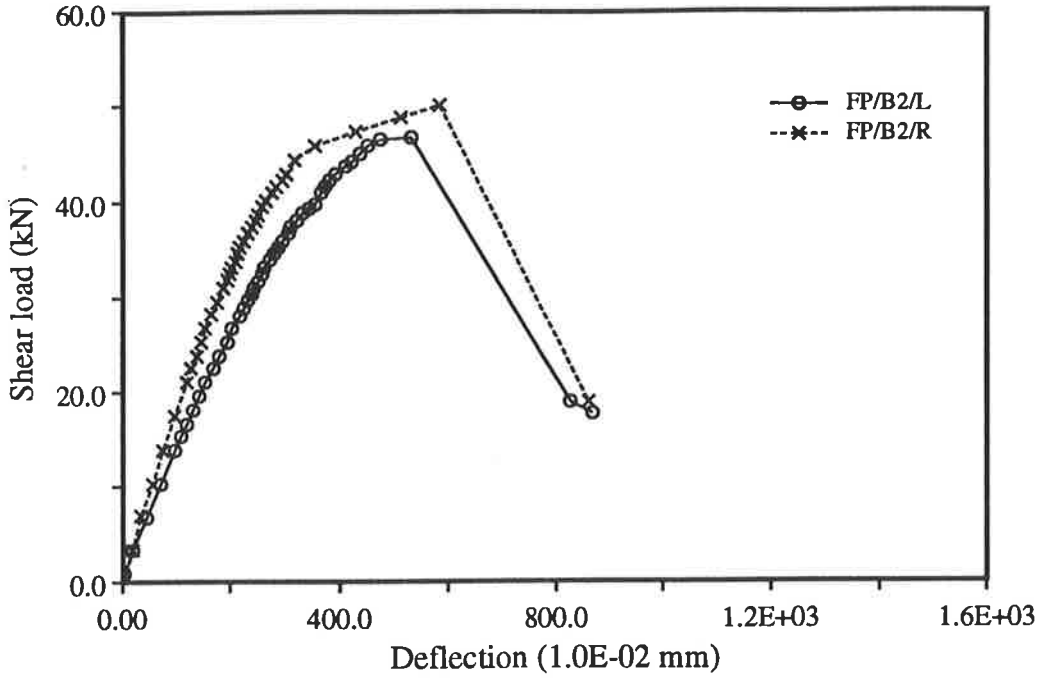

Fig.3-23 t_p = 3.0 mm. The deflection of Specimen FP/B2/L and Specimen FP/B2/R

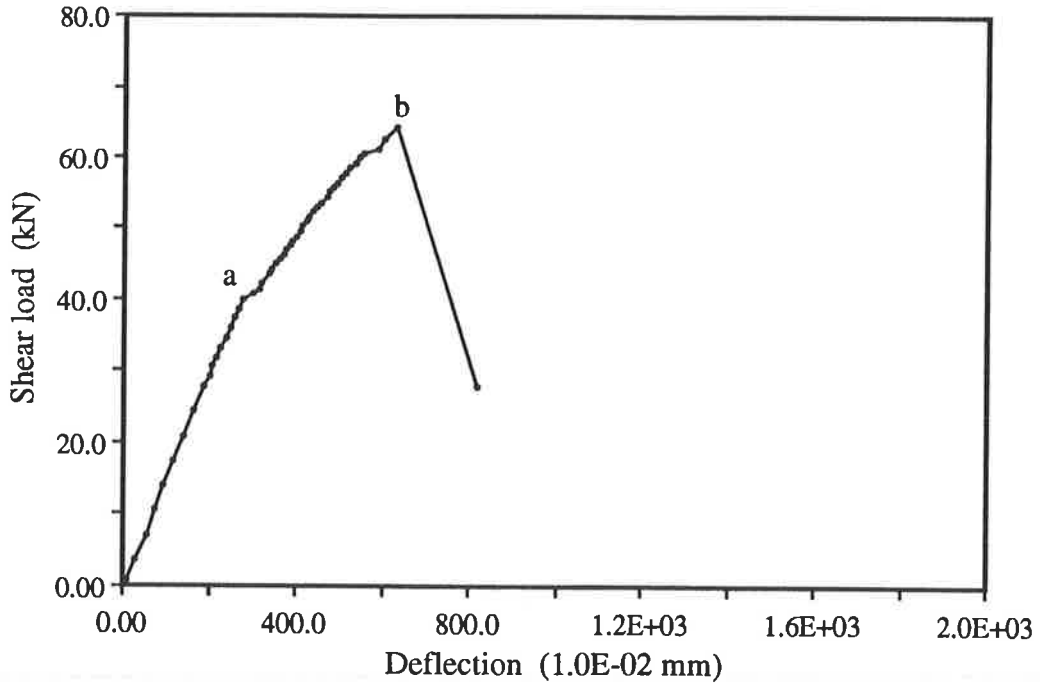

Fig.3-24 t_p = 5.0 mm. The deflection of Specimen FP/B3/L

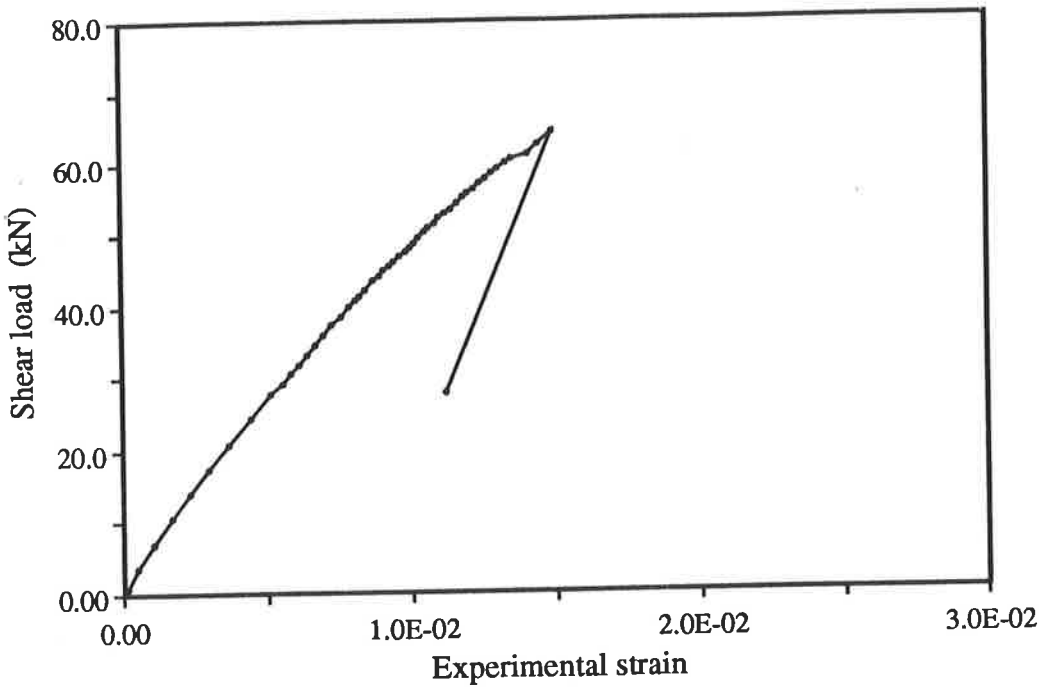

Fig.3-25 t_p = 5.0 mm. Longitudinal strain in the soffit plate of Specimen FP/B3/L

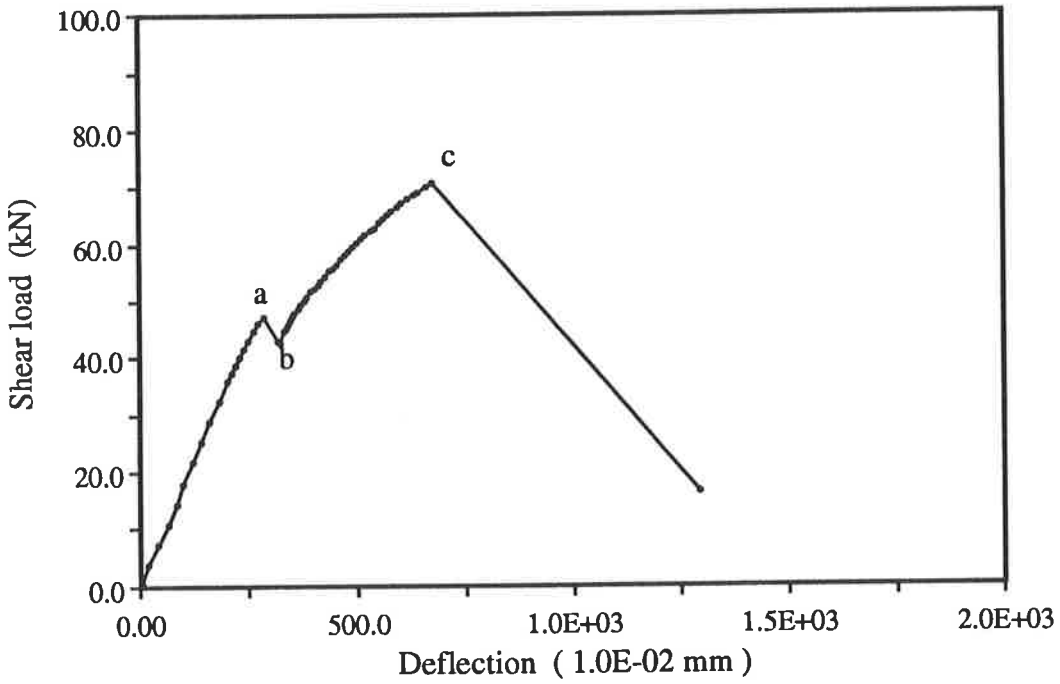

Fig.3-26 t_p = 5.0 mm. The deflection of Specimen FP/B3/R

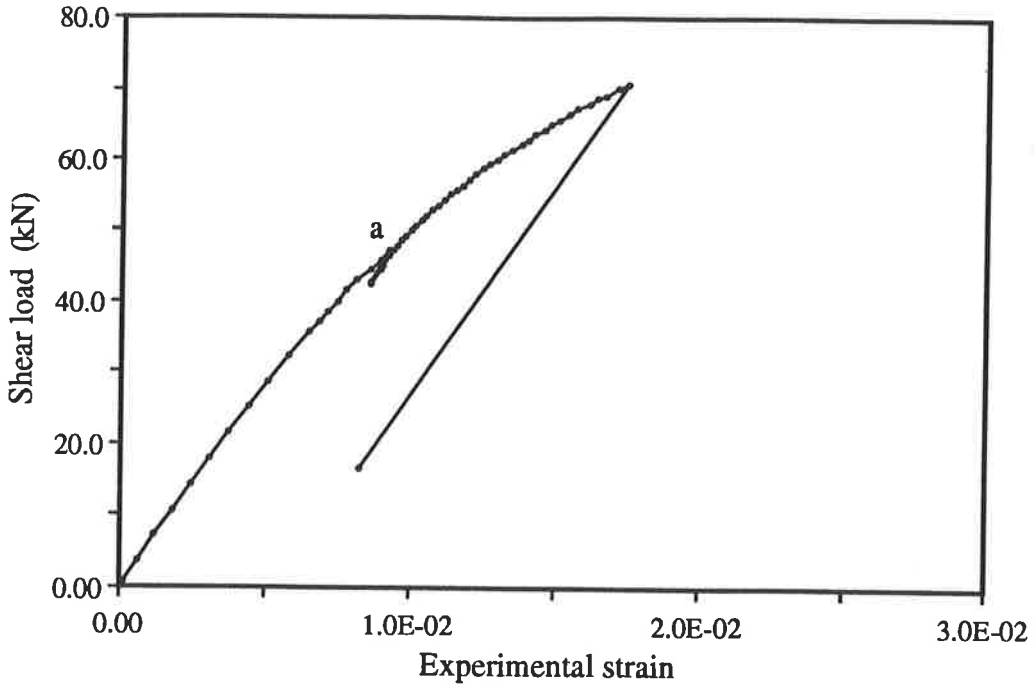

Fig.3-27 t_p = 5.0 mm. Longitudinal strain in the soffit plate of Specimen FP/B3/R

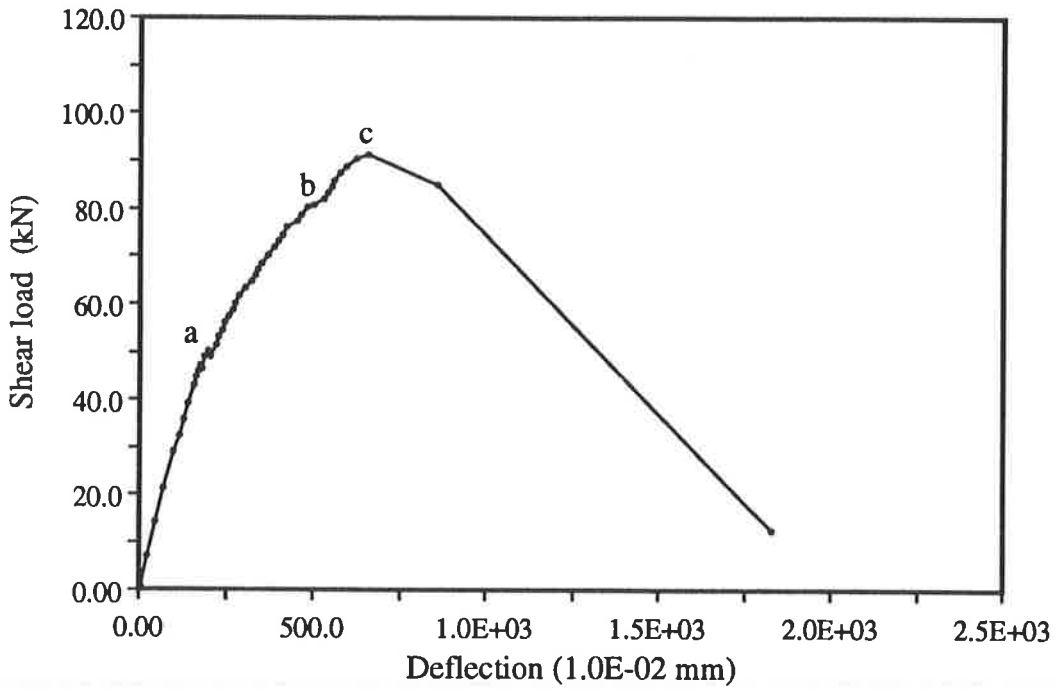

Fig.3-28 t_p = 10.0 mm. The deflection of Specimen FP/B4/L

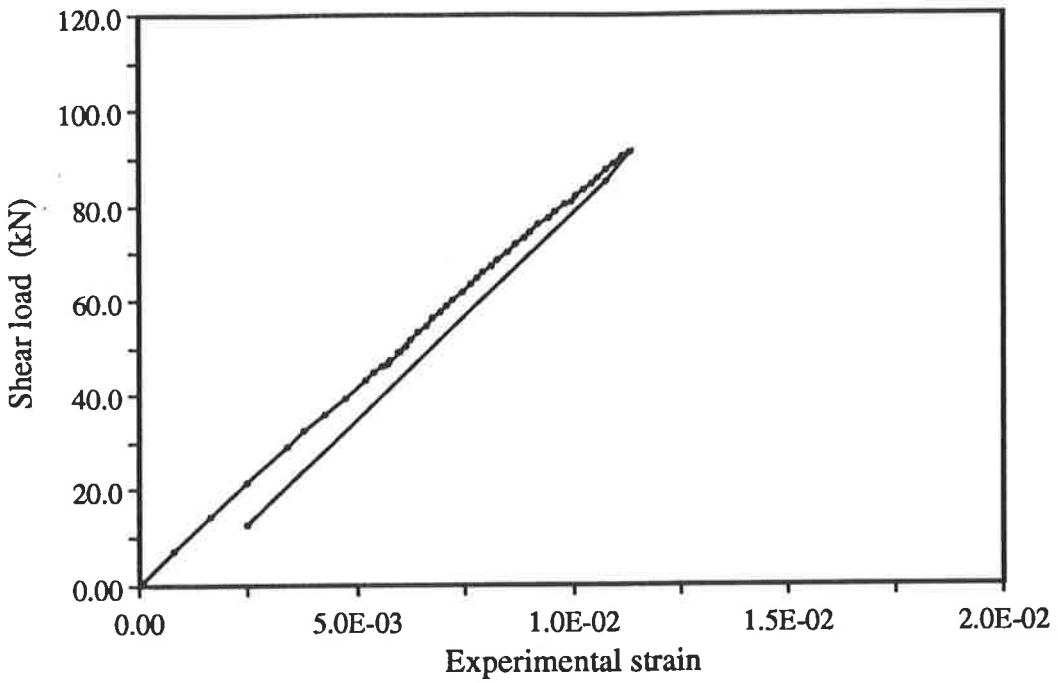

Fig.3-29 t_p = 10.0 mm. Longitudinal strain in the soffit plate of Specimen FP/B4/L

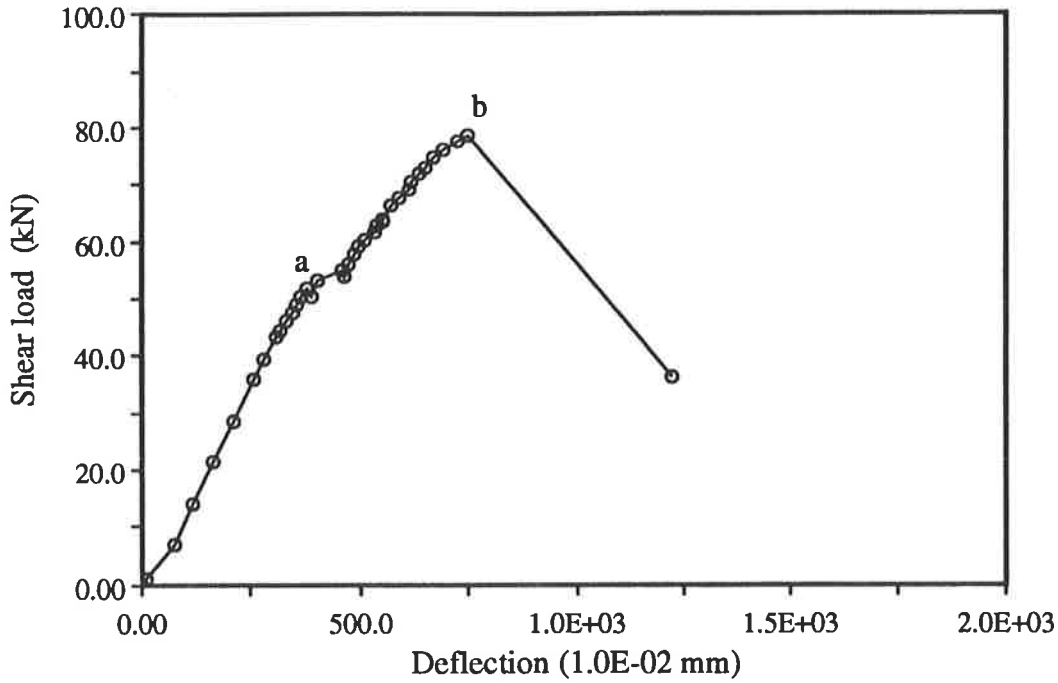

Fig.3-30 t_p = 10.0 mm. The deflection of Specimen FP/B4/R

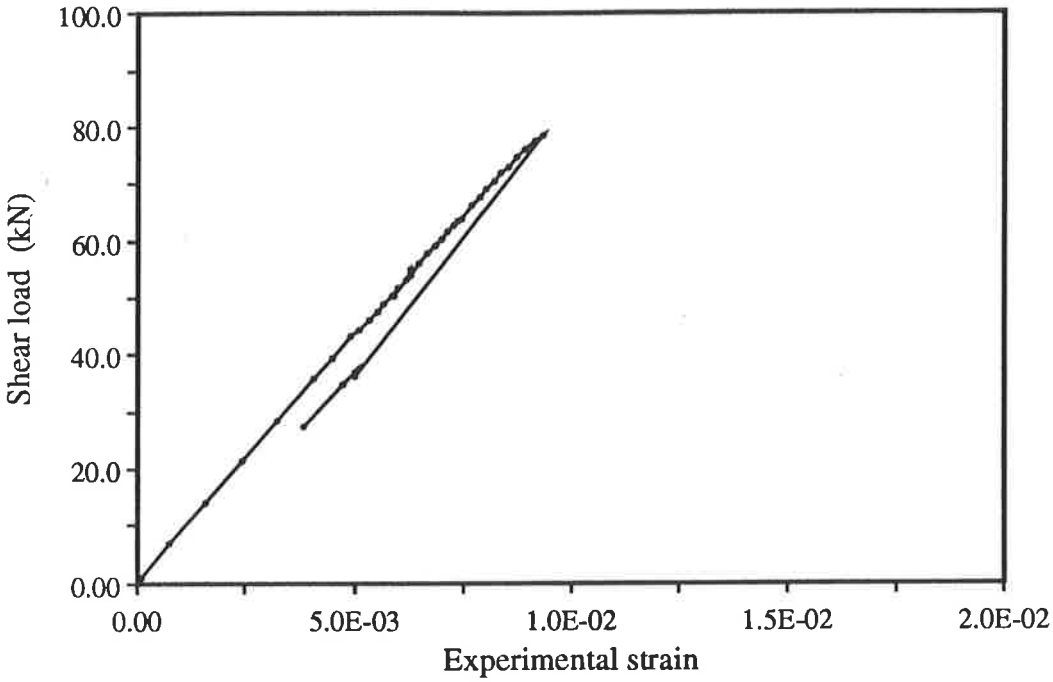

Fig.3-31 t_p = 10.0 mm. Longitudinal strain in the soffit plate of Specimen FP/B4/R

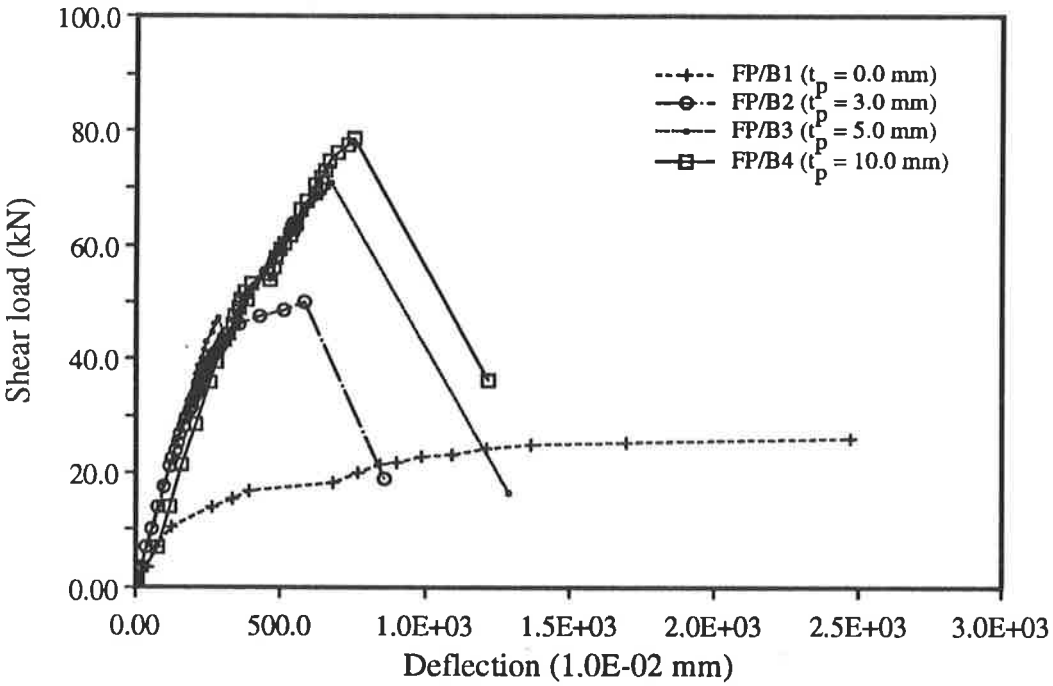

Fig.3-32 Experimental results of series 2

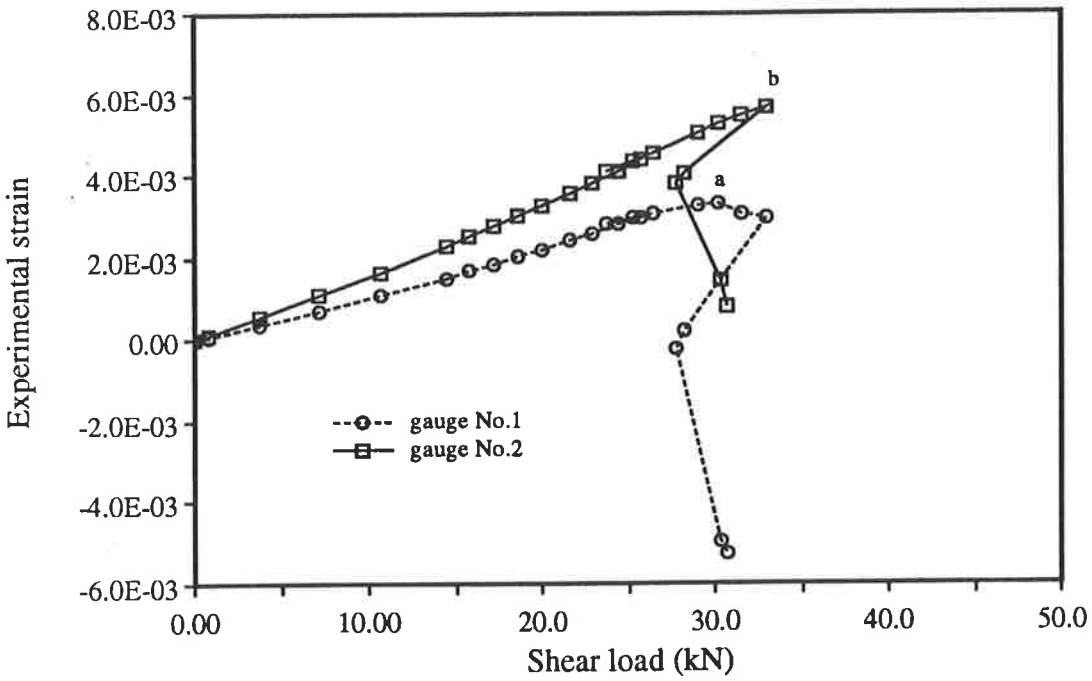

Fig.3-33 A_{st} = 157.0 mm², L_{sp} = 0.0 mm.

Longitudinal strains in the soffit plate of Specimen SP/S8/L

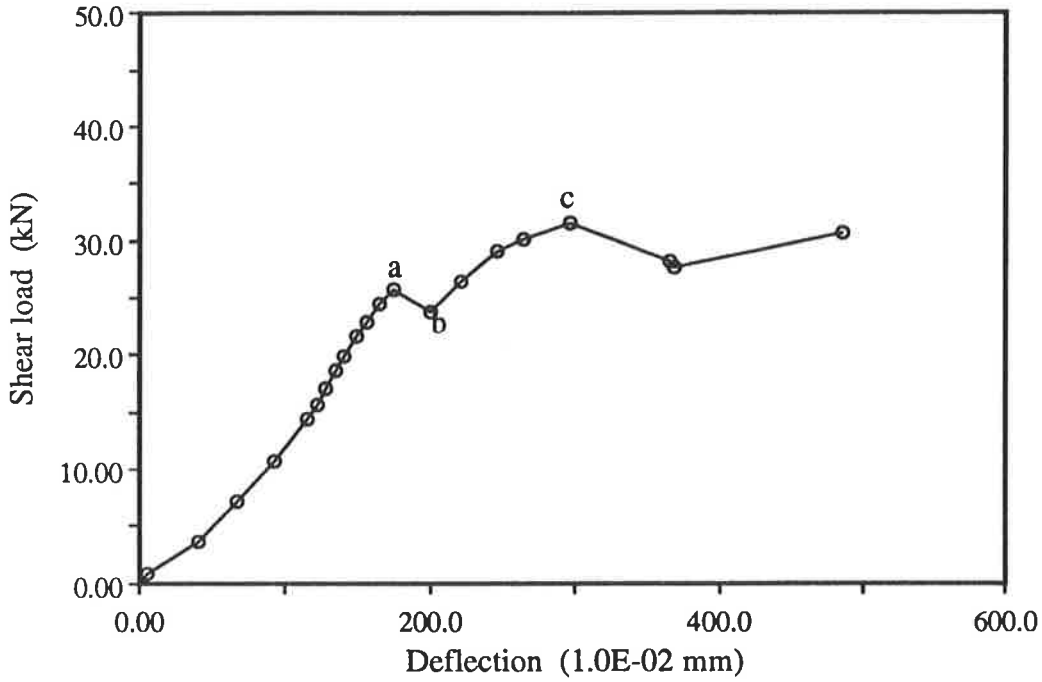

Fig.3-34 A_{st} = 157.0 mm², L_{sp} = 0.0 mm.

The deflection of Specimen SP/S8/L

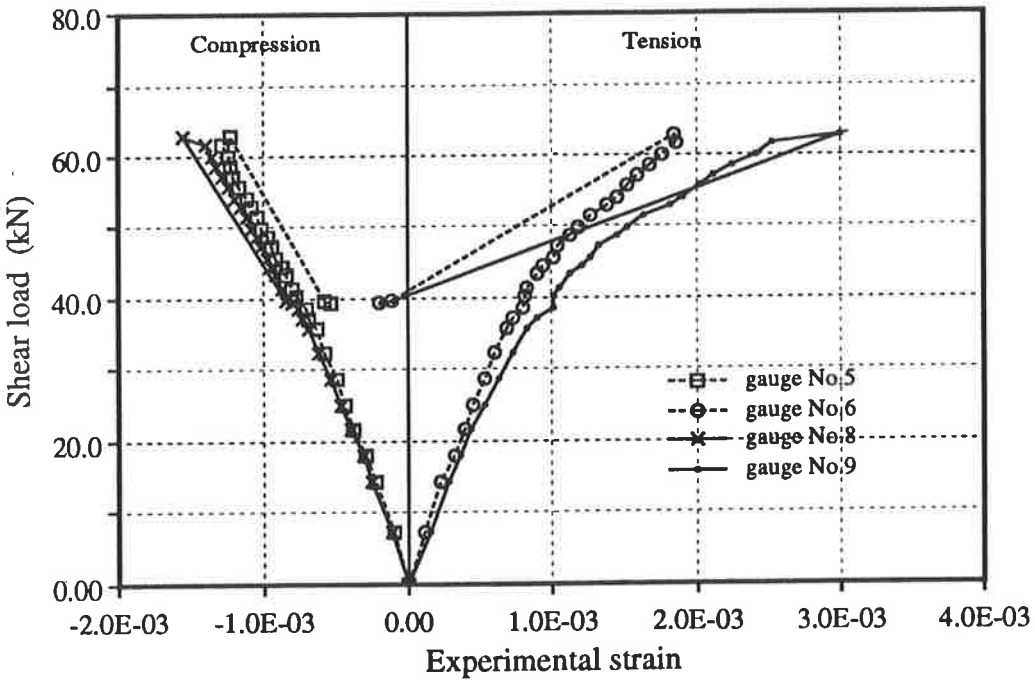

Fig.3-35 A_{st} = 157.0 mm², L_{sp} = 690.0 mm.

Strains in the side plates of Specimen SP/S8/R

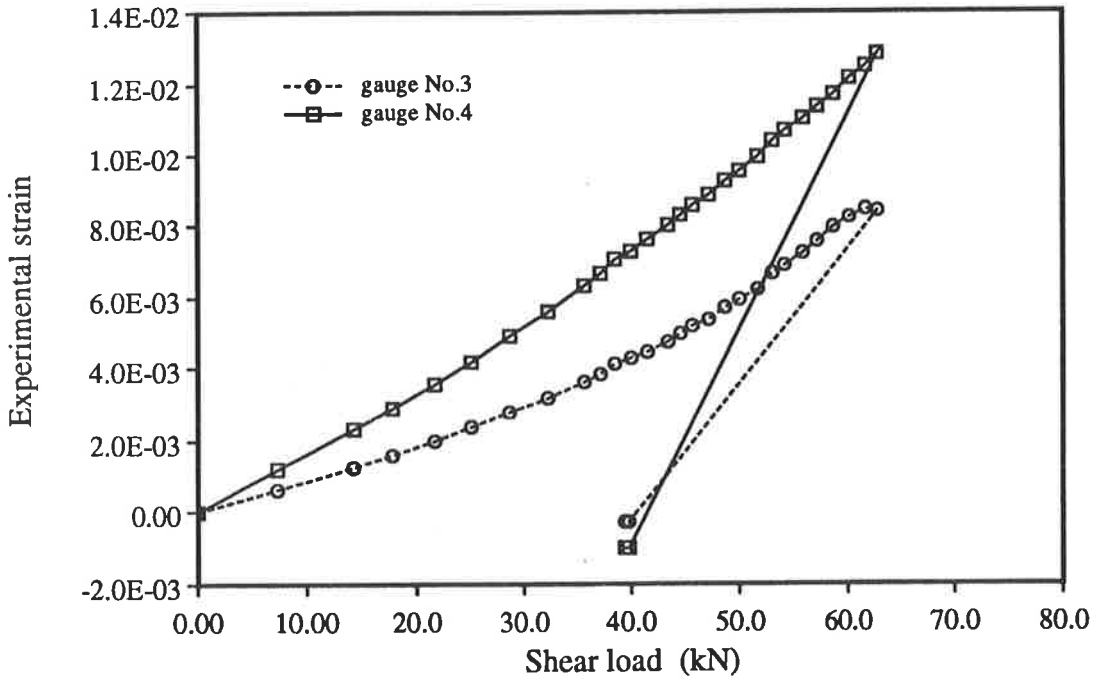

Fig.3-36 A_{st} = 157.0 mm², L_{sp} = 690.0 mm.

Longitudinal strains in the soffit plate of Specimen SP/S8/R

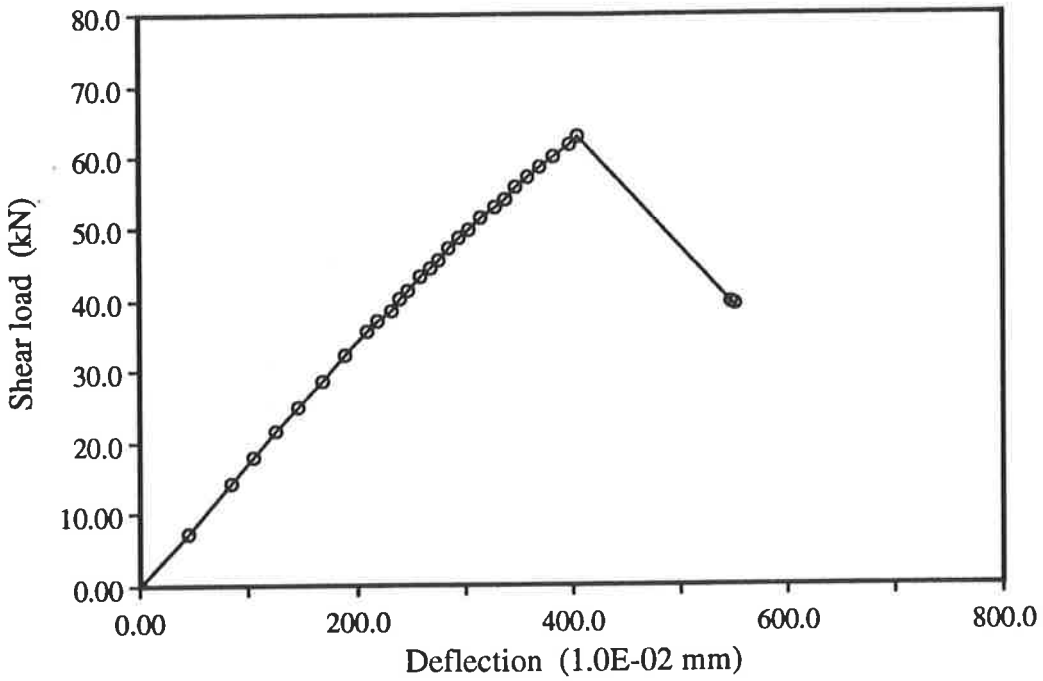

Fig.3-37 A_{st} = 157.0 mm², L_{sp} = 690.0 mm.

The deflection of Specimen SP/S8/R

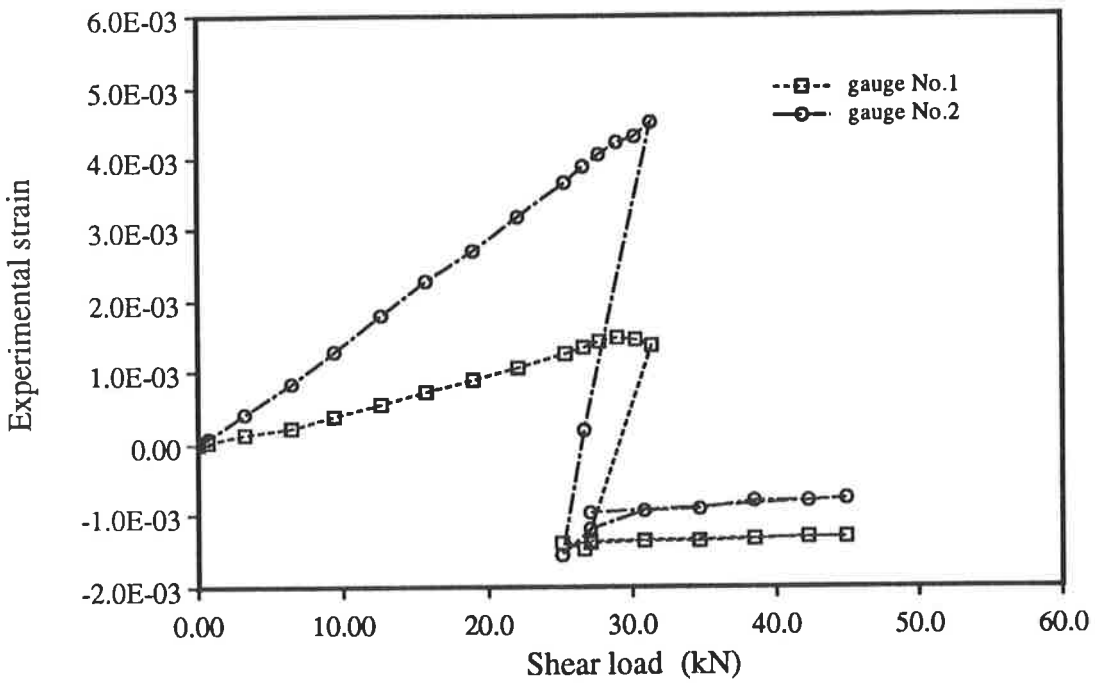

Fig.3-38 A_{st} = 628.0 mm², L_{sp} = 0.0 mm.

Longitudinal strains in the soffit plate of Specimen SP/S9/L

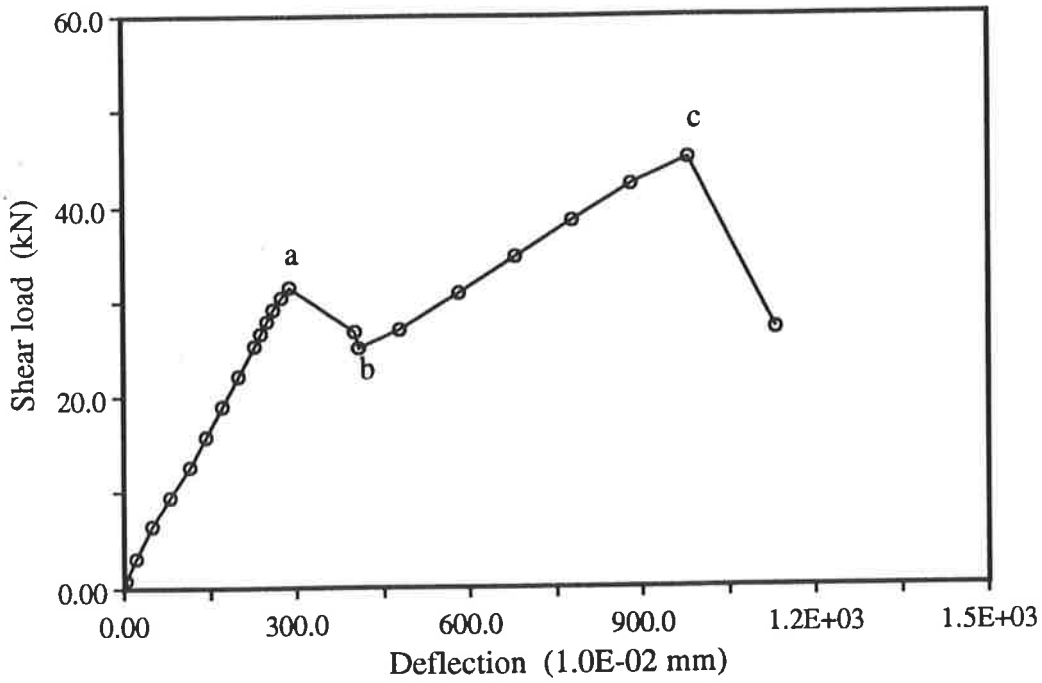

Fig.3-39 A_{st} = 628.0 mm², L_{sp} = 0.0 mm.

The deflection of Specimen SP/S9/L

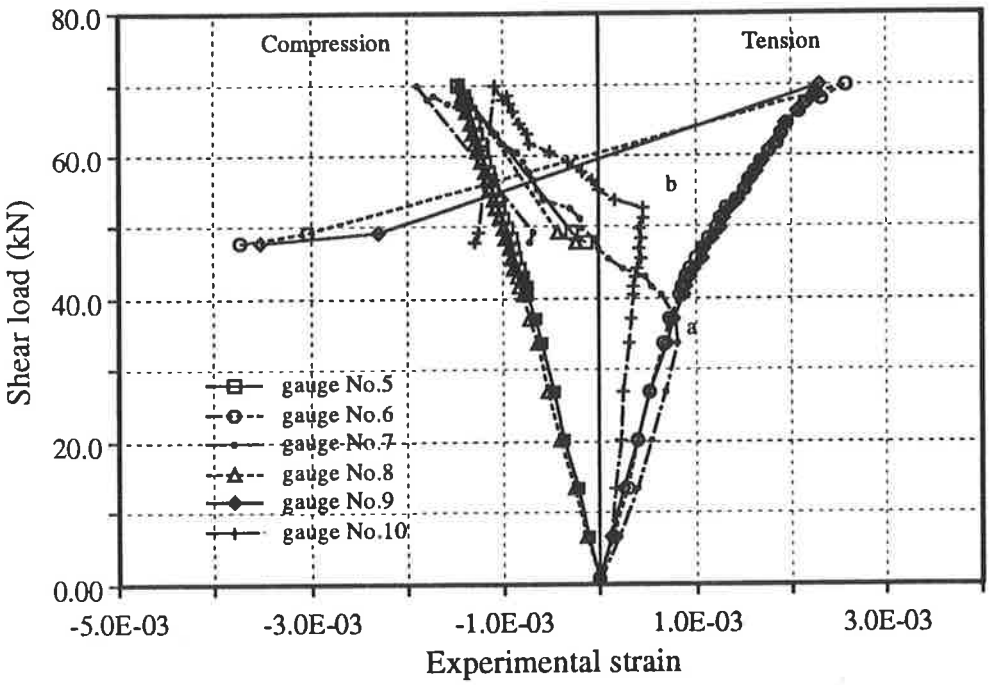

Fig.3-40 A_{st} = 628.0 mm², L_{sp} = 690.0 mm.

Strains in the side plates of Specimen SP/S9/R

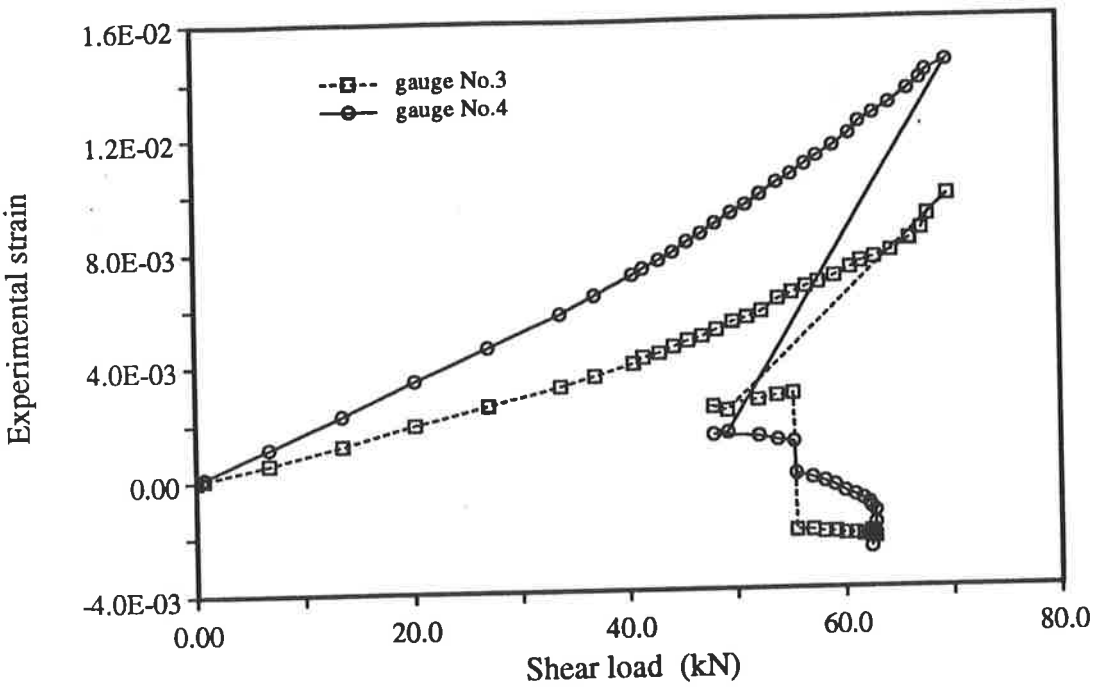

Fig.3-41 A_{st} = 628.0 mm², L_{sp} = 690.0 mm.

Longitudinal strains in the soffit plate of Specimen SP/S9/R

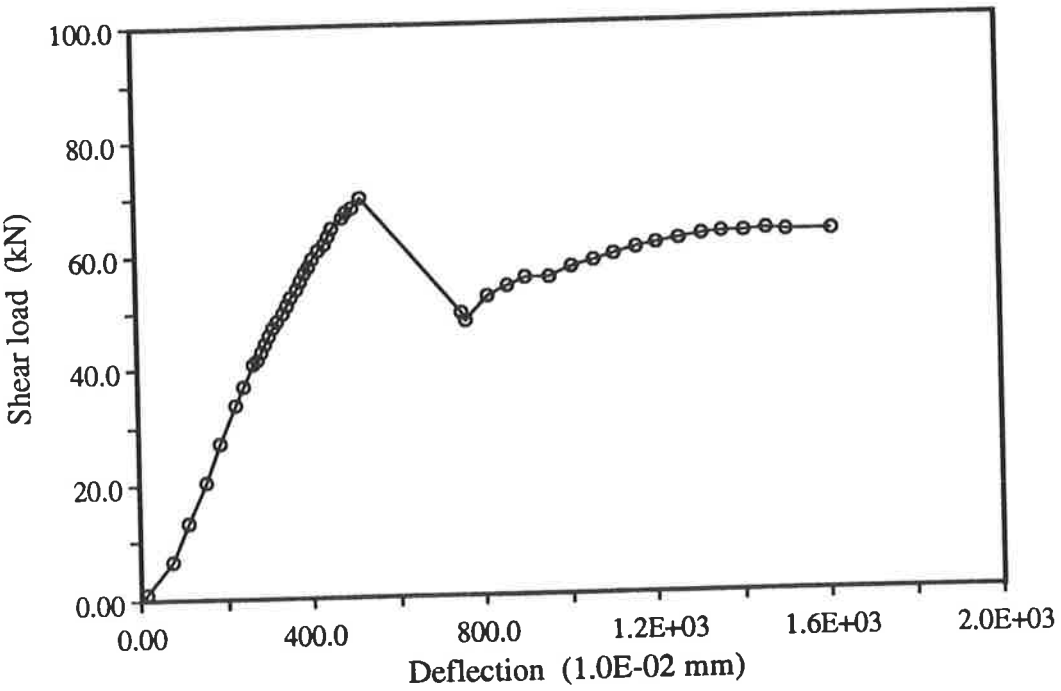

Fig.3-42 A_{st} = 628.0 mm², L_{sp} = 690.0 mm.

The deflection of Specimen SP/S9/R

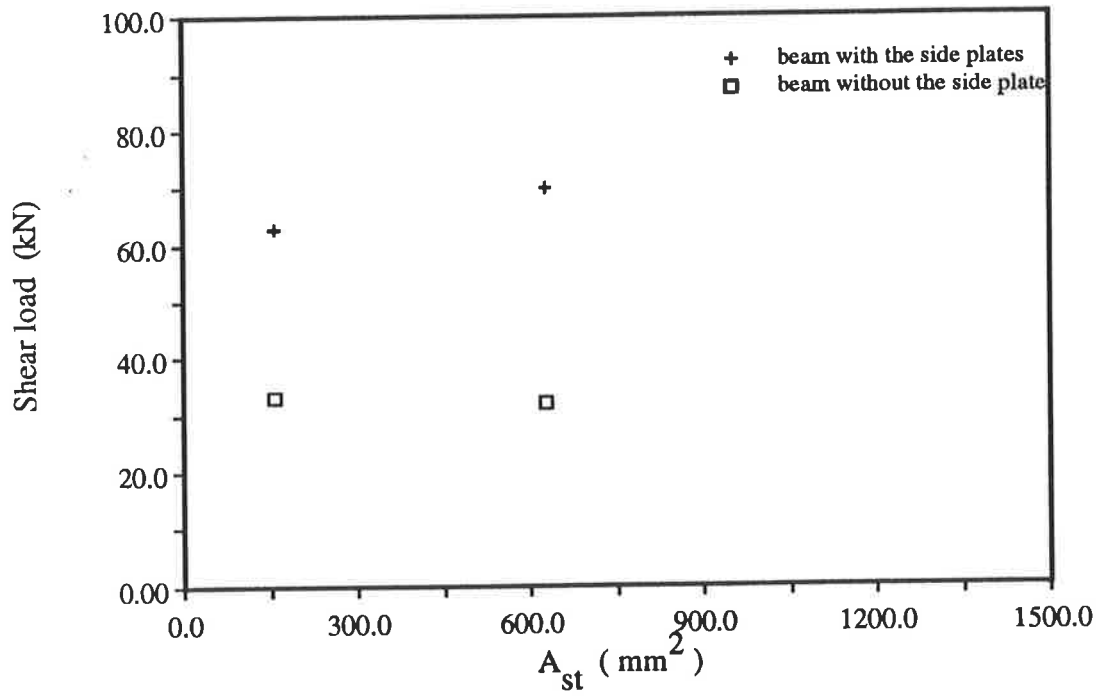

Fig.3-43 Experimental results of series 3

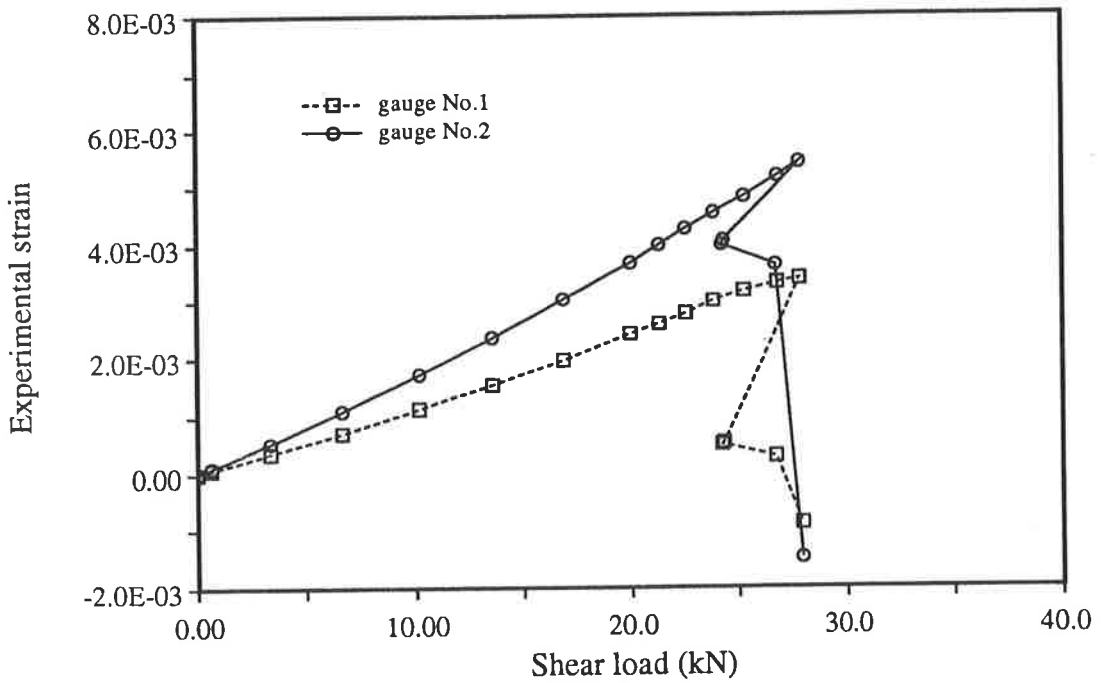

Fig.3-44 t_{sp} = 0.0 mm, L_{sp} = 0.0 mm.

Longitudinal strains in the soffit plate of Specimen SP/S5/L

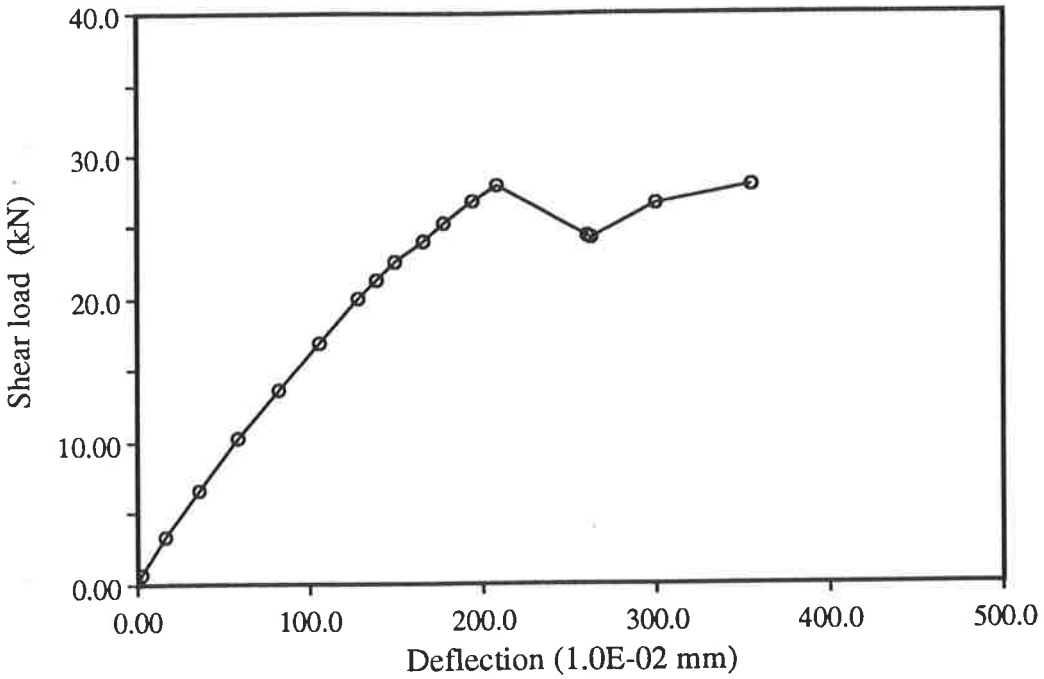

Fig.3-45 t_{sp} = 0.0 mm, L_{sp} = 0.0 mm.

The deflection of Specimen SP/S5/L

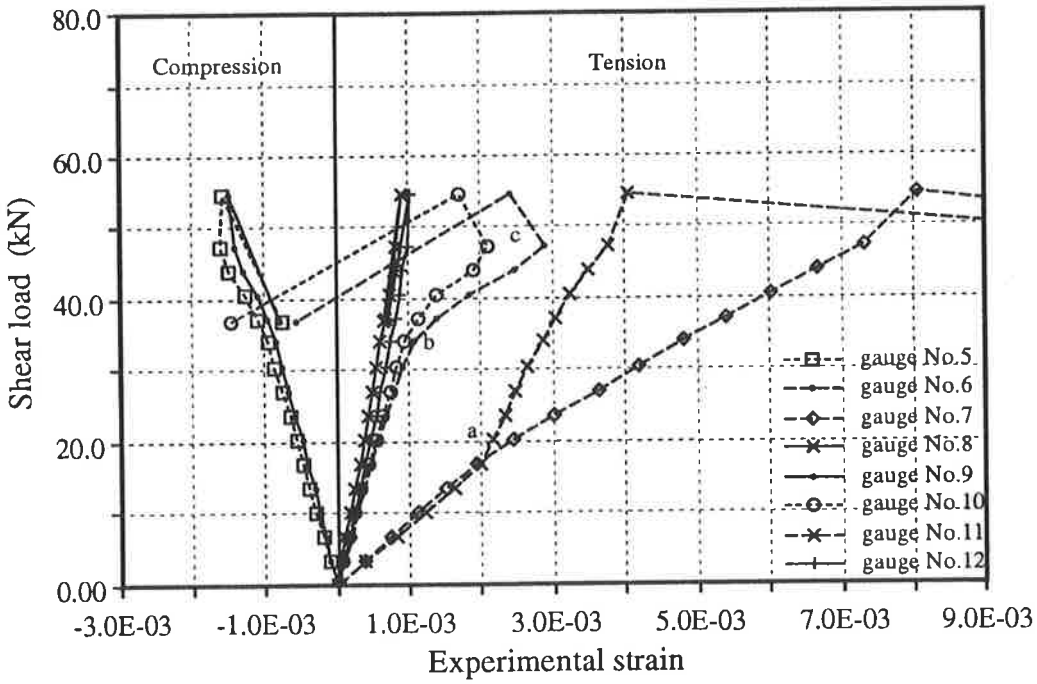

Fig.3-46 t_{sp} = 1.0 mm, L_{sp} = 1250.0 mm.

Strains in the side plates of Specimen SP/S5/R

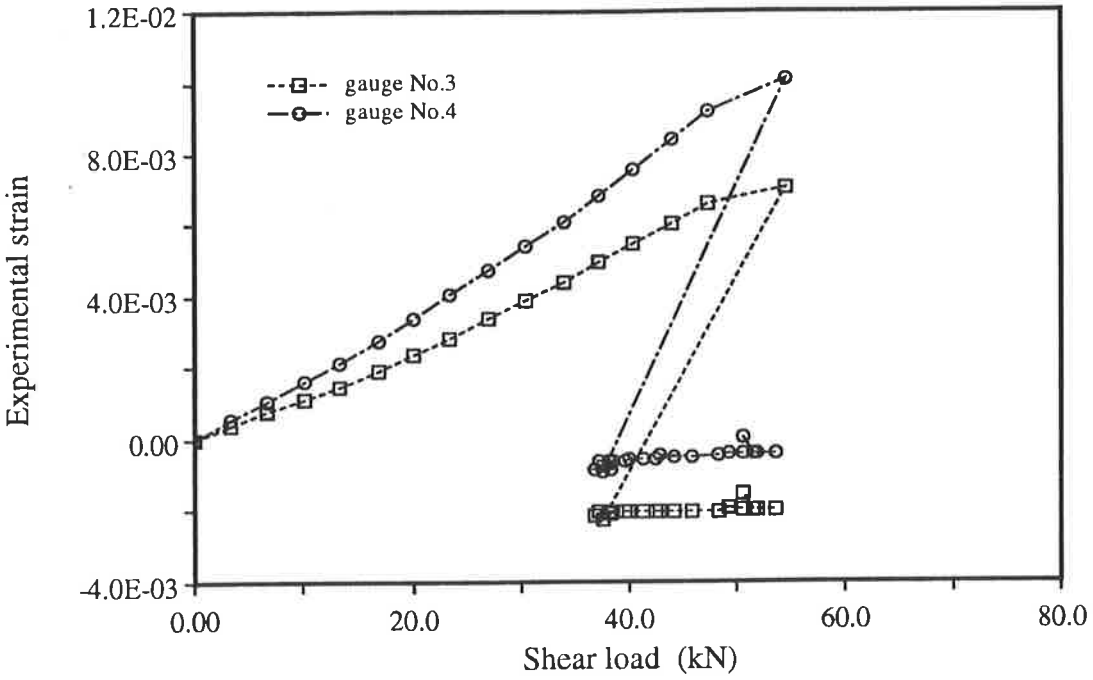

Fig.3-47 t_{sp} = 1.0 mm, L_{sp} = 1250.0 mm. Longitudinal strains in the soffit plate of Specimen SP/S5/R

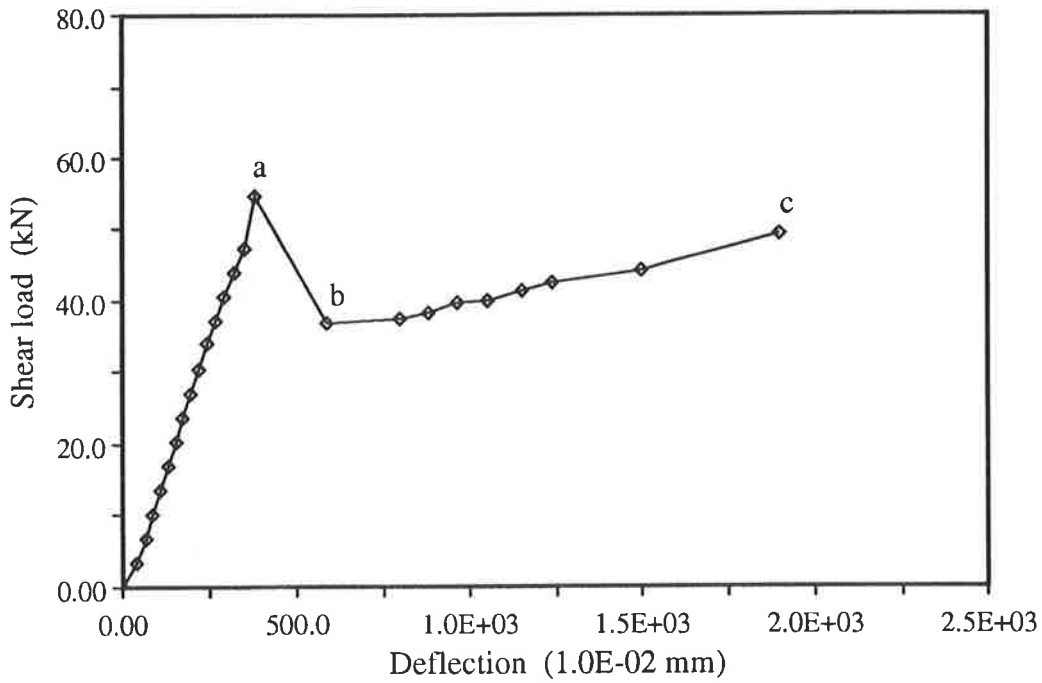

Fig.3-48 t_{sp} = 1.0 mm, L_{sp} = 1250.0 mm. The deflection of Specimen SP/S5/R

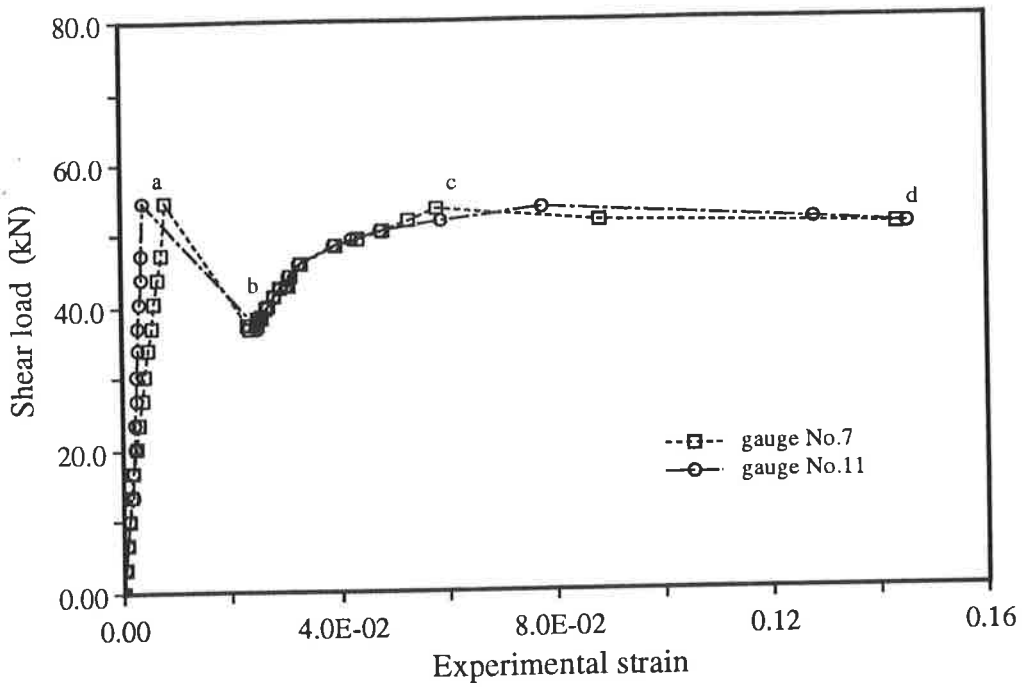

Fig.3-49 t_{sp} = 1.0 mm, L_{sp} = 1250.0 mm. Strains in strain gauges No.7,11 of Specimen SP/S5/R

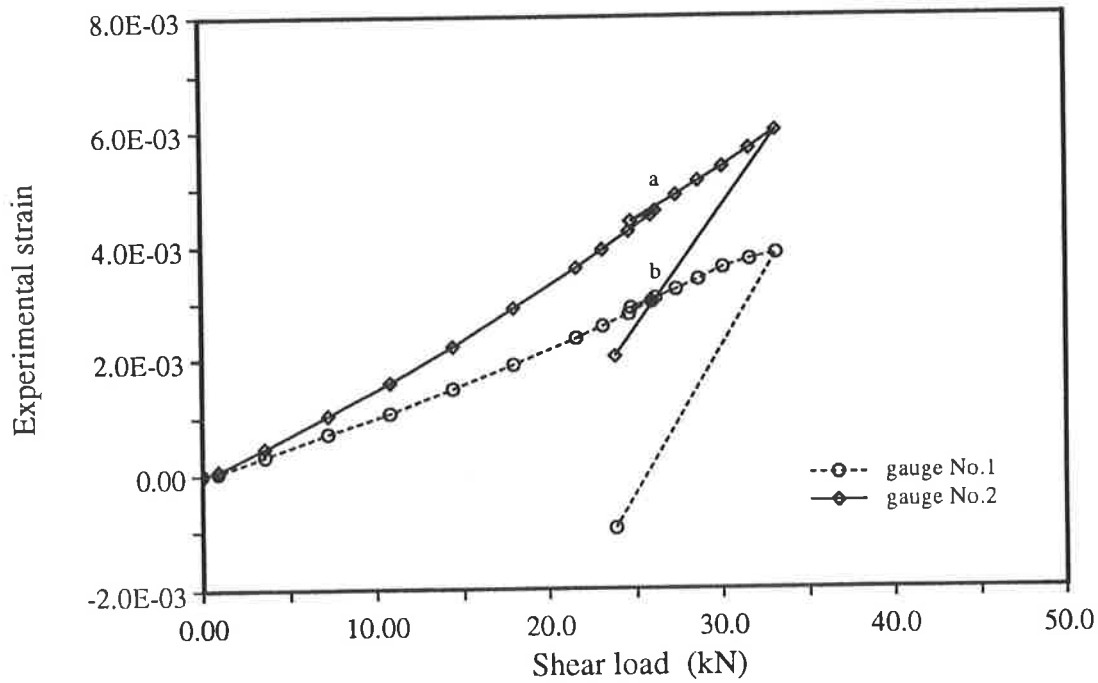

Fig.3-50 t_{sp} = 0.0 mm, L_{sp} = 0.0 mm. Longitudinal strains in the soffit plate of Specimen SP/S6/L

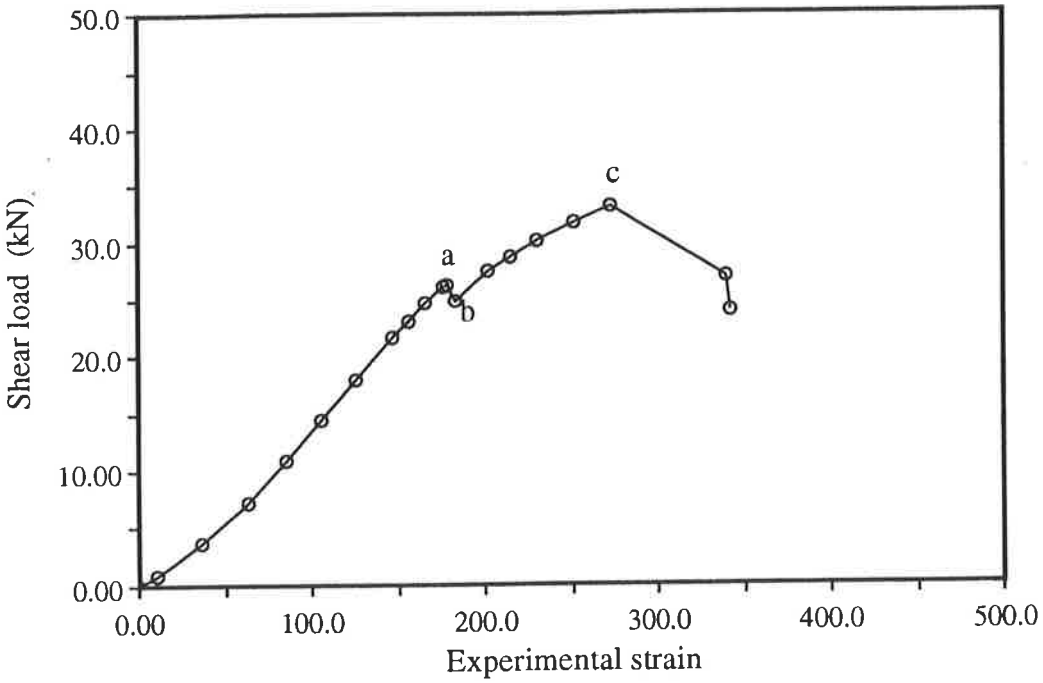

Fig.3-51 t_{sp} = 0.0 mm, L_{sp} = 0.0 mm.

The deflection of Specimen SP/S6/L

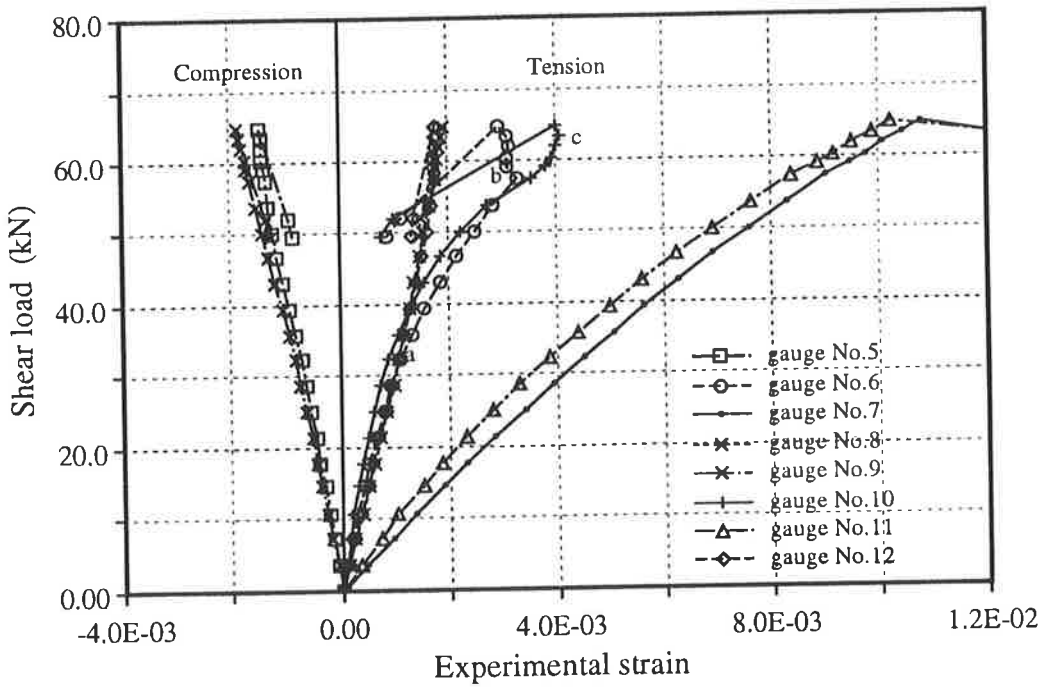

Fig.3-52 t_{sp} = 2.0 mm, L_{sp} = 1250.0 mm. Strains in the side plates of Specimen SP/S6/R

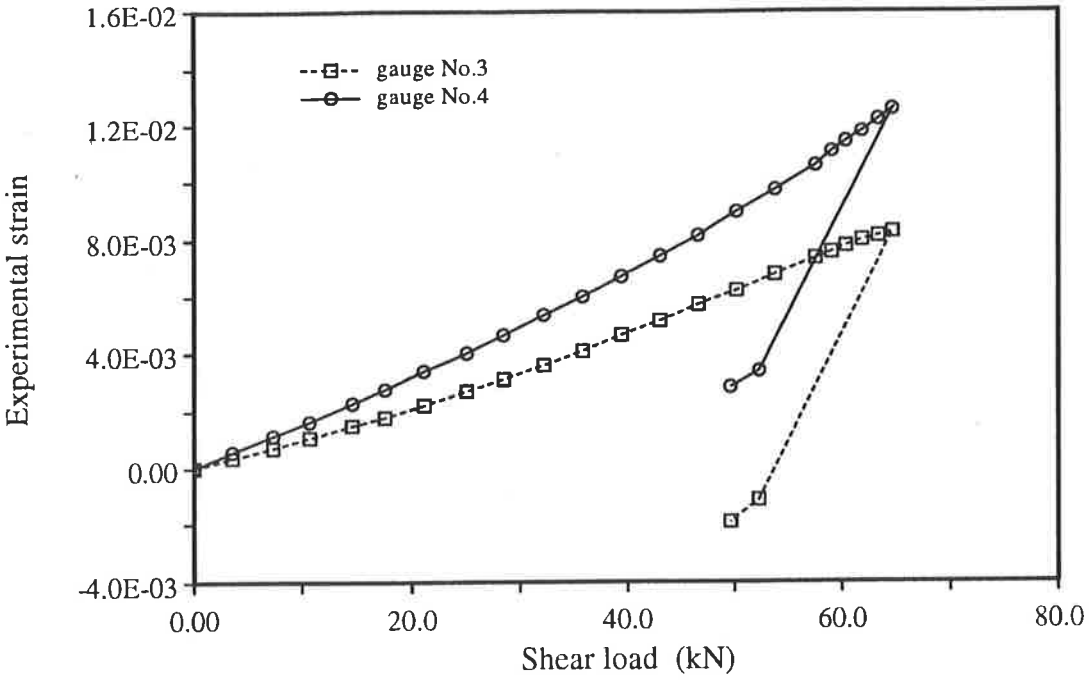

Fig.3-53 t_{sp} = 2.0 mm, L_{sp} = 1250.0 mm. Longitudinal strains in the soffit plate of Specimen SP/S6/R

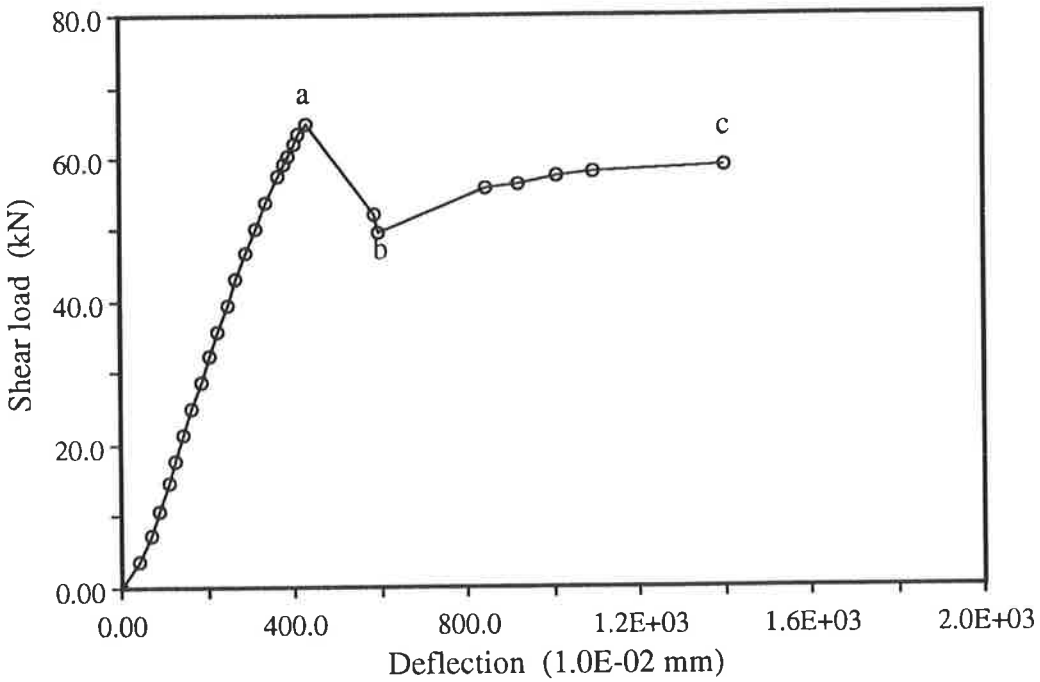

Fig.3-54 t_{sp} = 2.0 mm, L_{sp} = 1250.0 mm. The deflection of Specimen SP/S6/R

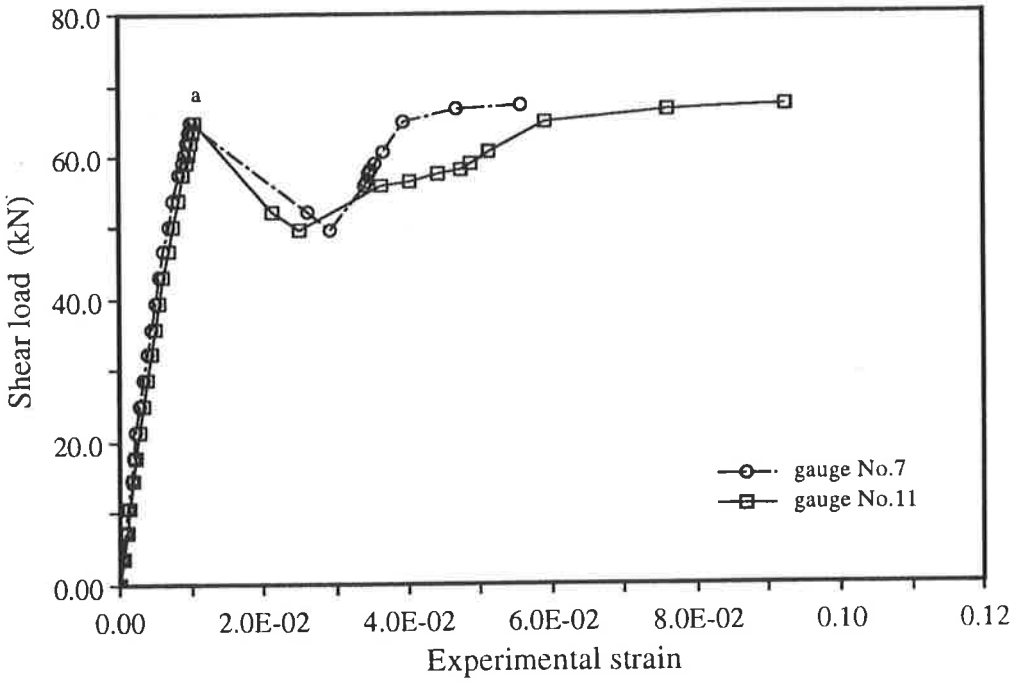

Fig.3-55 t_{sp} = 2.0 mm, L_{sp} = 1250.0 mm. Strains in the strain gauges No.7,11 in the side plates of Specimen SP/S6/R

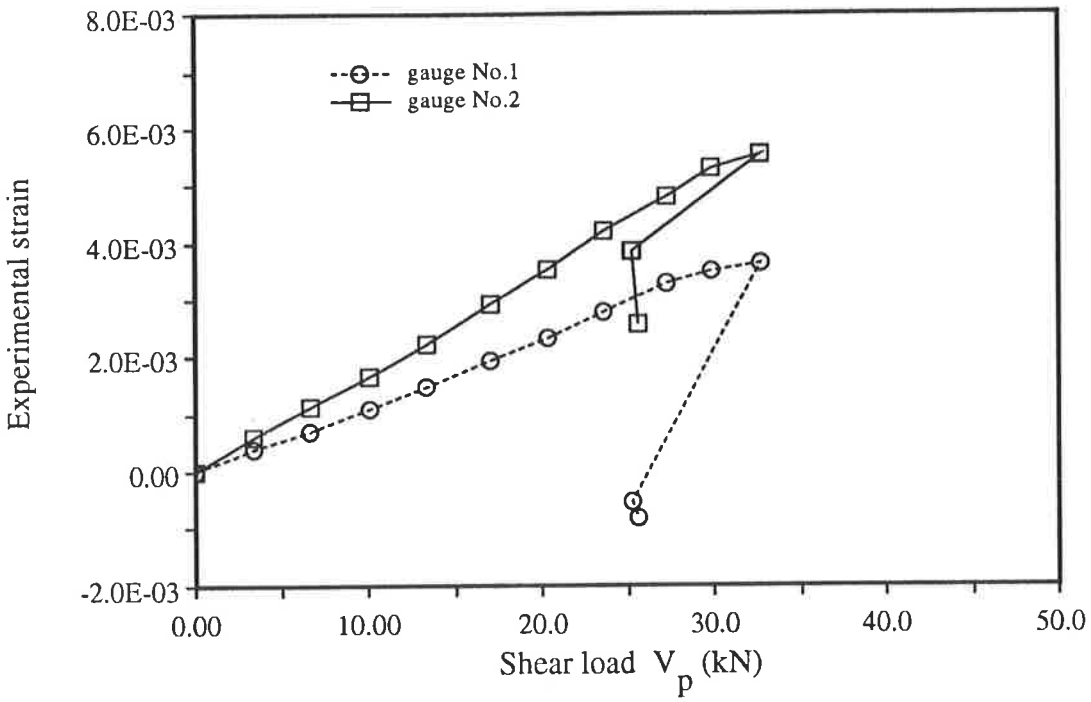

Fig.3-56 t_{sp} = 0.0 mm, L_{sp} = 0.0 mm. Longitudinal strains in the soffit plate of Specimen SP/S7/L

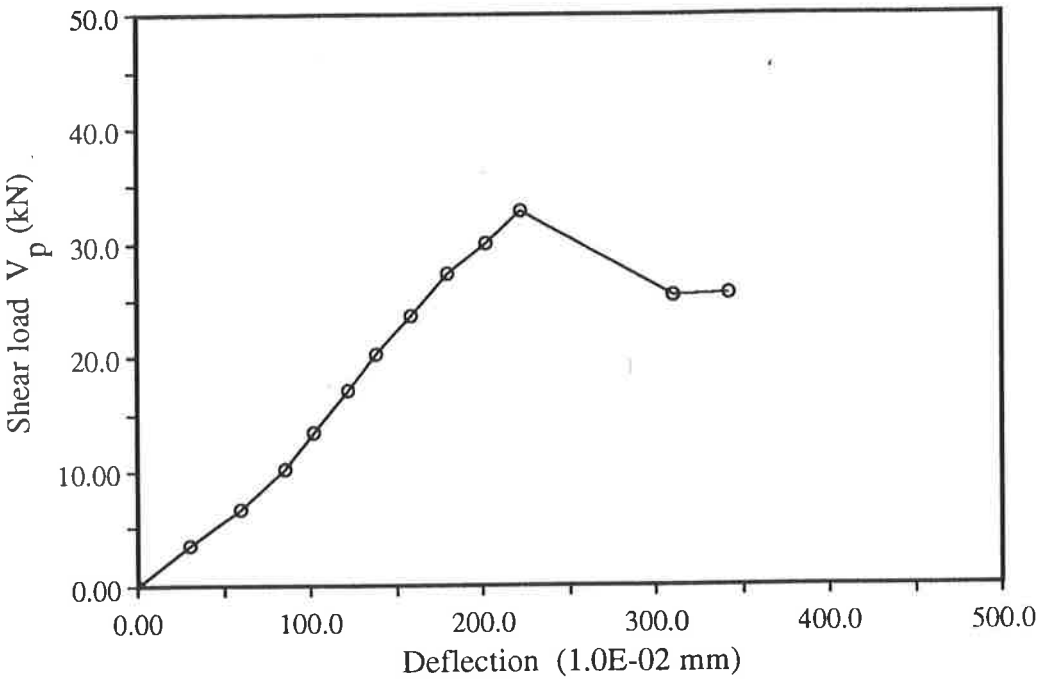

Fig.3-57 t_{sp} = 0.0 mm, L_{sp} = 0.0 mm.

The deflection of Specimen SP/S7/L

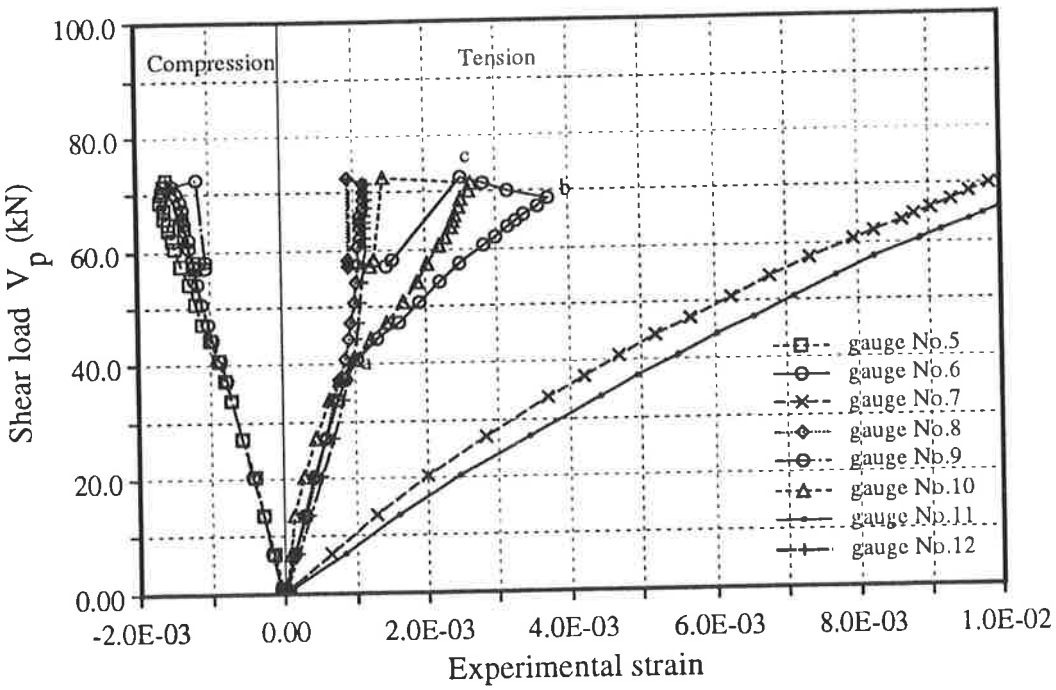

Fig.3-58 t_{sp} = 3.0 mm, L_{sp} = 1250.0 mm. Strains in the side plates of Specimen SP/S7/R

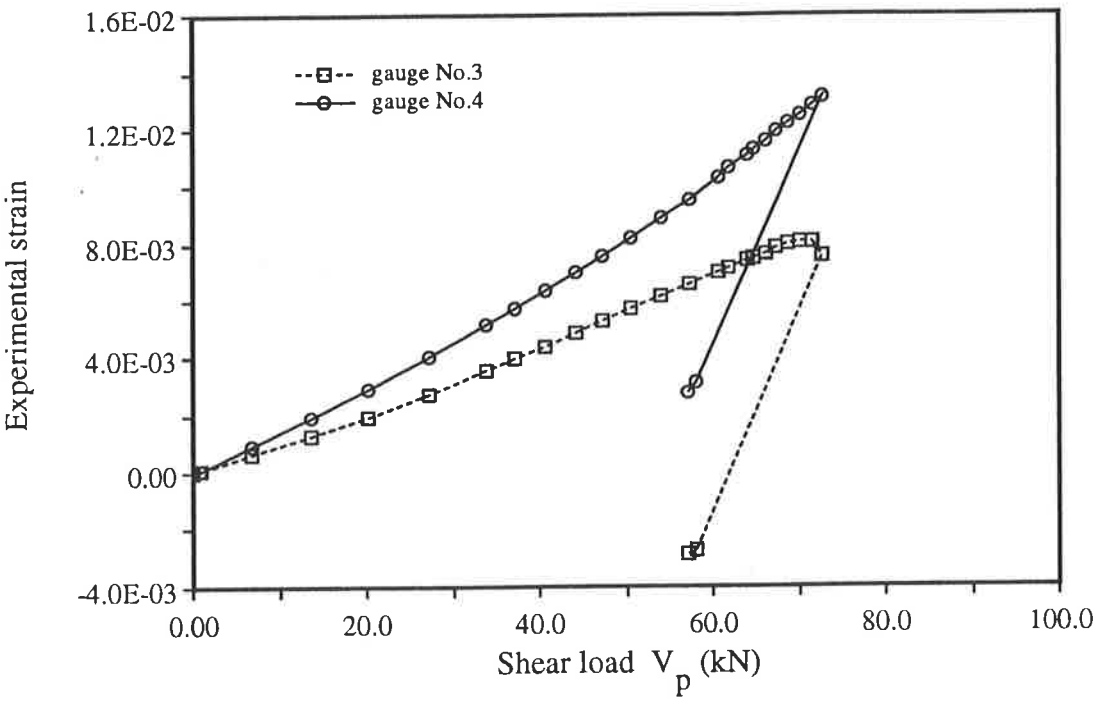

Fig.3-59 t_{sp} = 3.0 mm, L_{sp} = 1250.0 mm. Longitudinal strains in the soffit plate of Specimen SP/S7/R

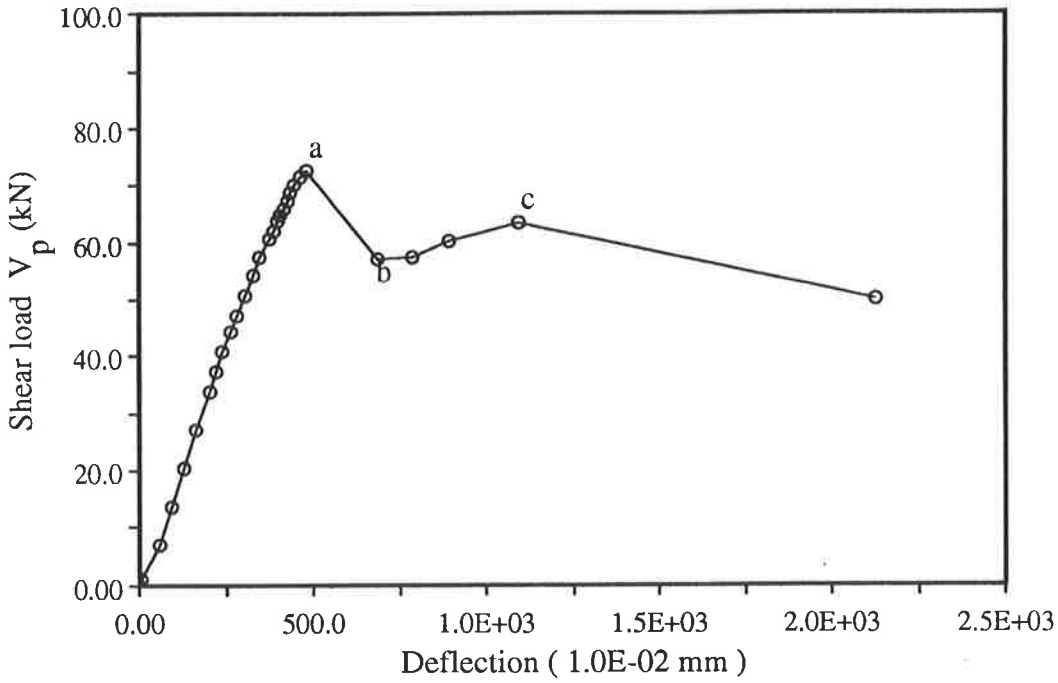

Fig.3-60 t_{sp} = 3.0 mm, L_{sp} = 1250.0 mm. The deflection of Specimen SP/S7/R

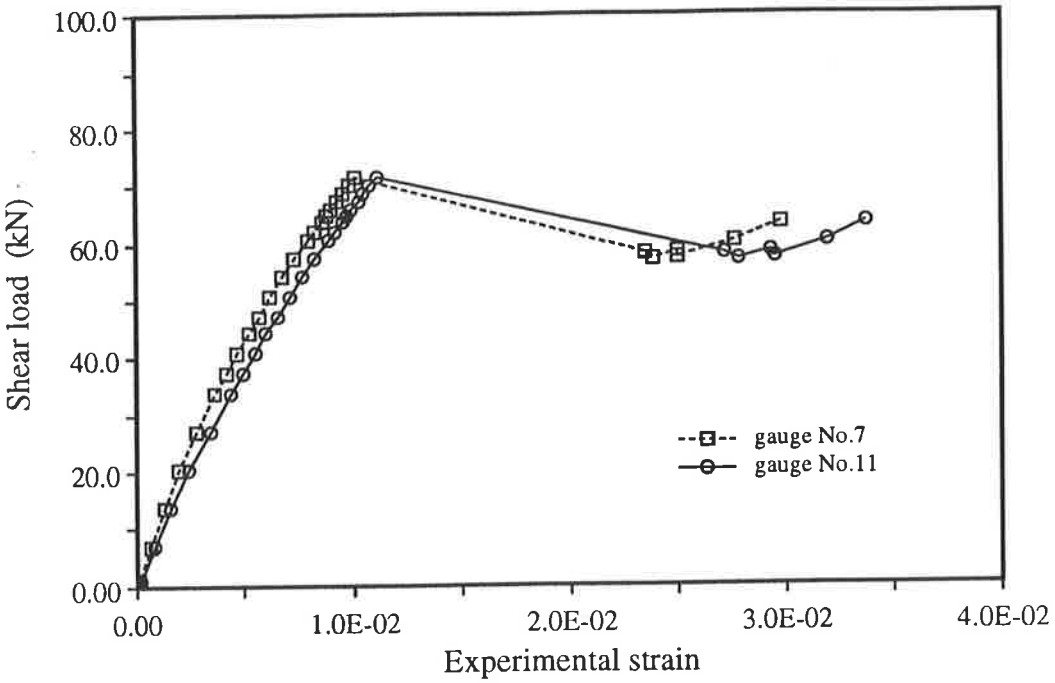

Fig.3-61 t_{sp} = 3.0 mm, L_{sp} = 1250.0 mm. Strains in the strain gauges No.7,11 in the side plates of Specimen SP/S7/R

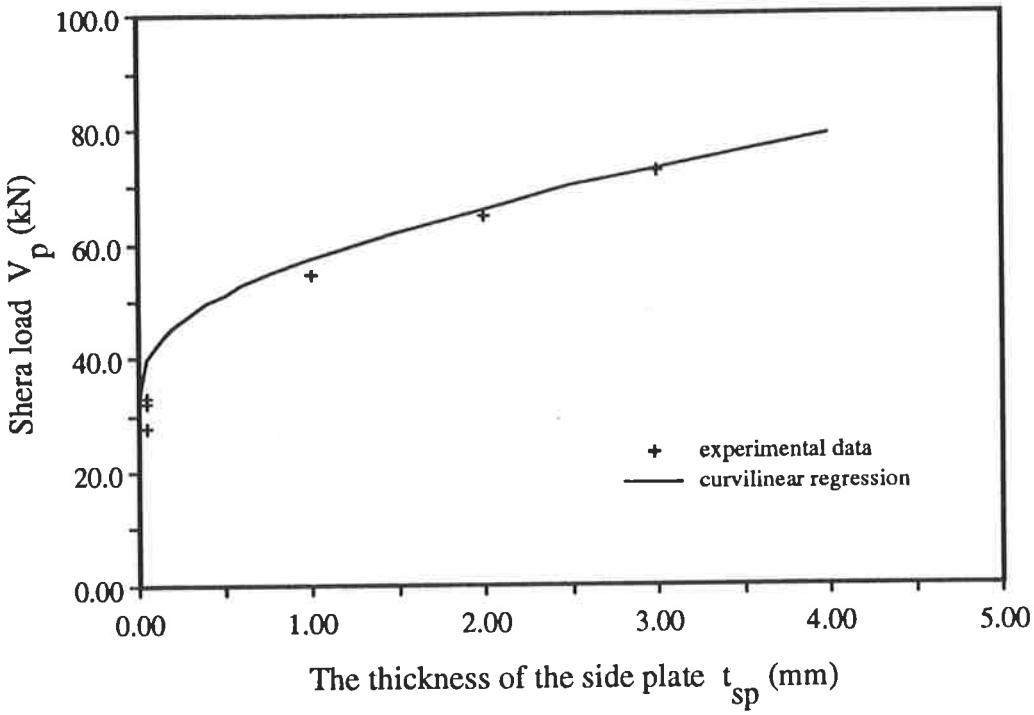

Fig.3-62 Experimental results of series 4

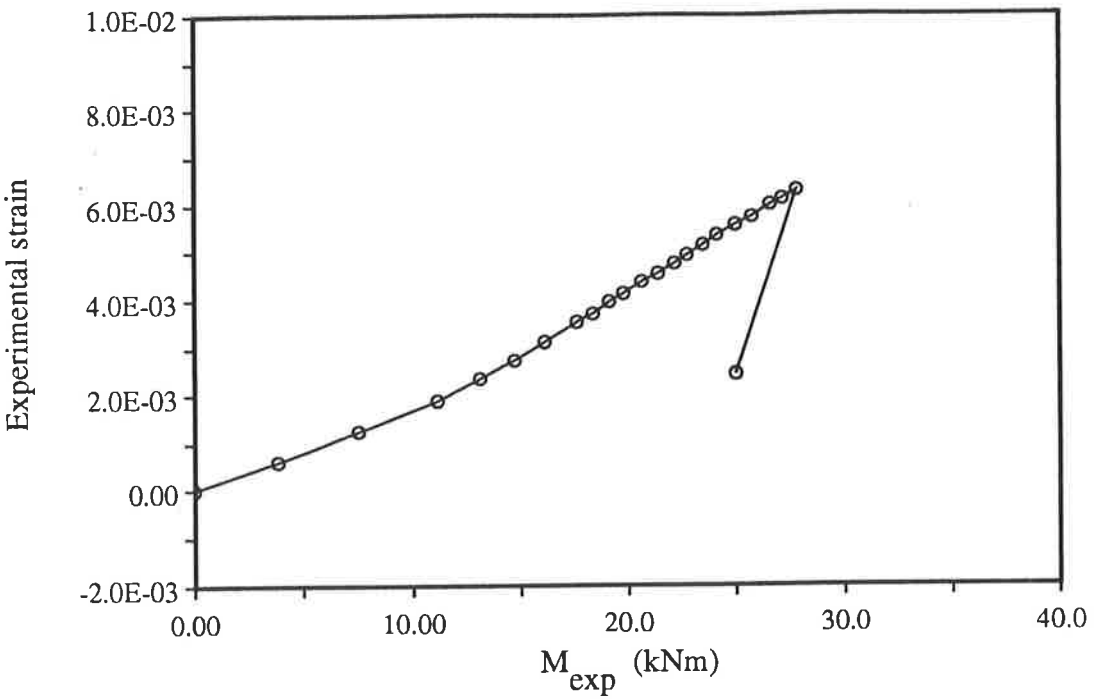

Fig.3-63 P_i = 3.0 kN. Longitudinal strain in the middle of the soffit plate of Beam PT1

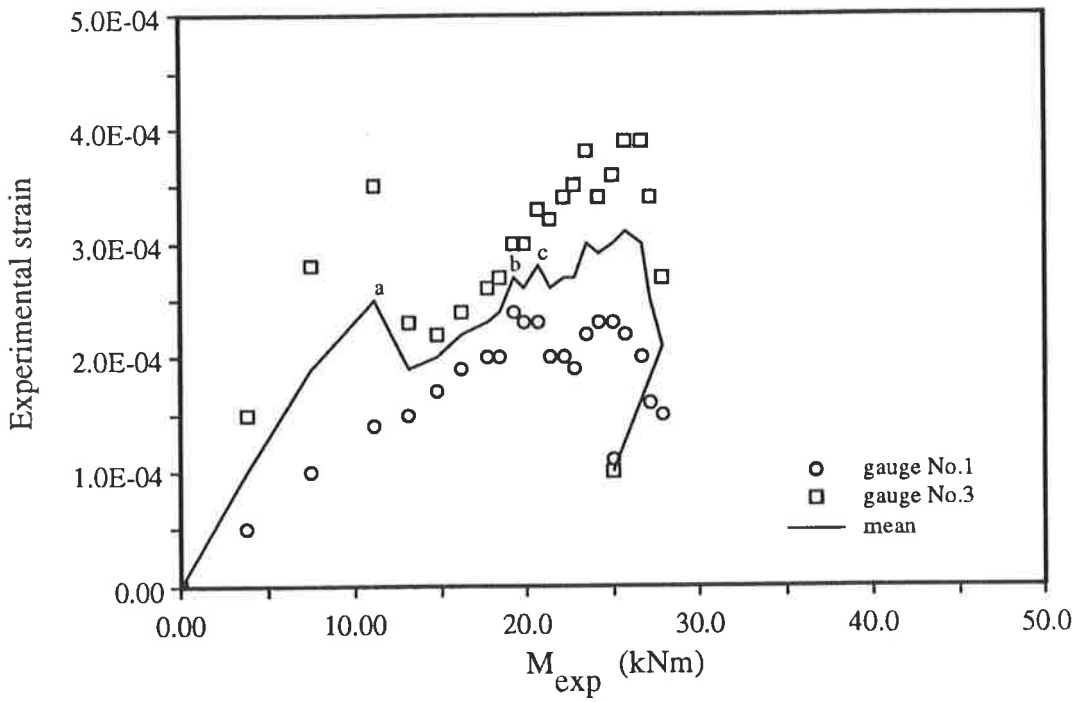

Fig.3-64 P_i = 3.0 kN. The average strains at the plate-end of Beam PT1

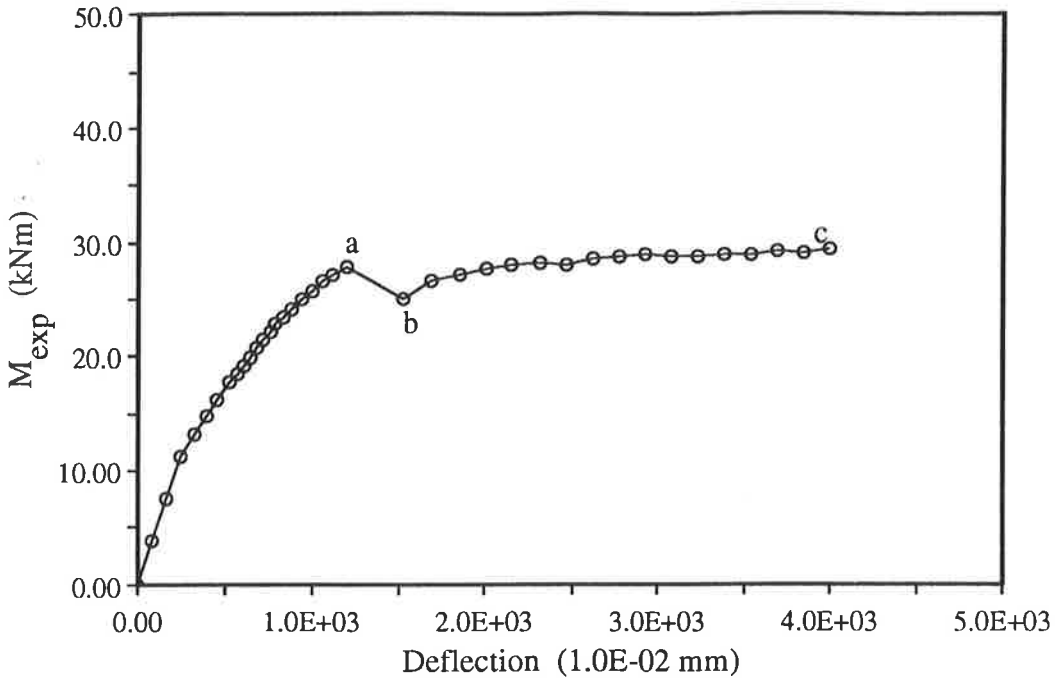

Fig.3-65 P_i = 3.0 kN. The deflection of Beam PT1

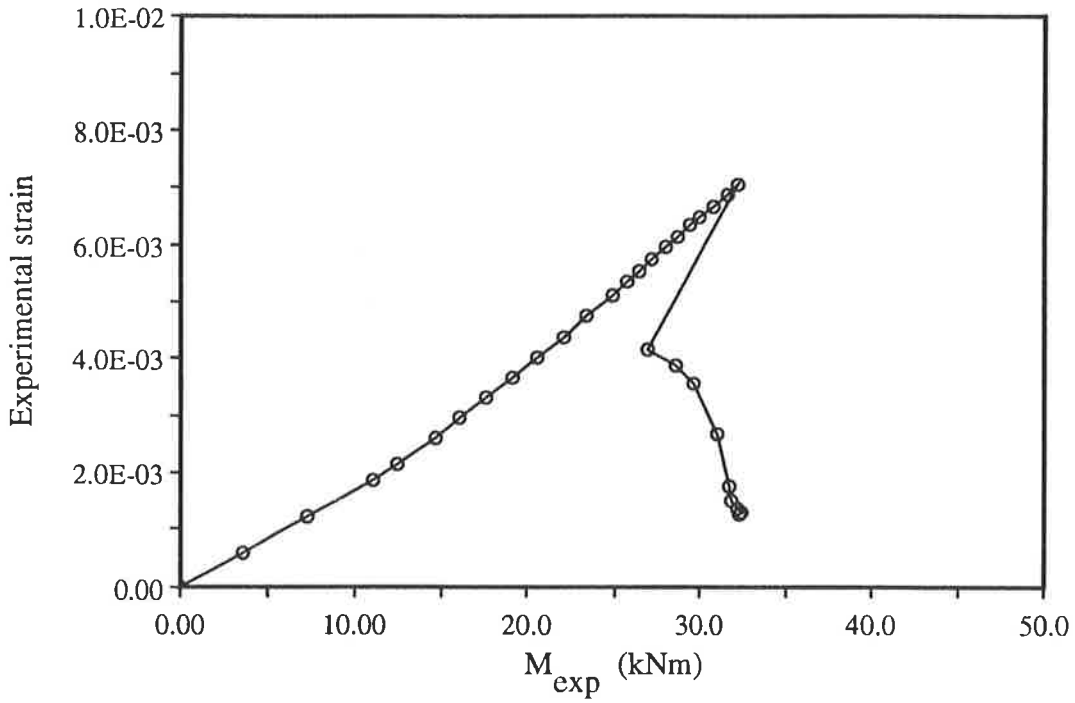

Fig.3-66 P_i = 30.0 kN. Longitudinal strain in the middle of the soffit plate of Beam PT2

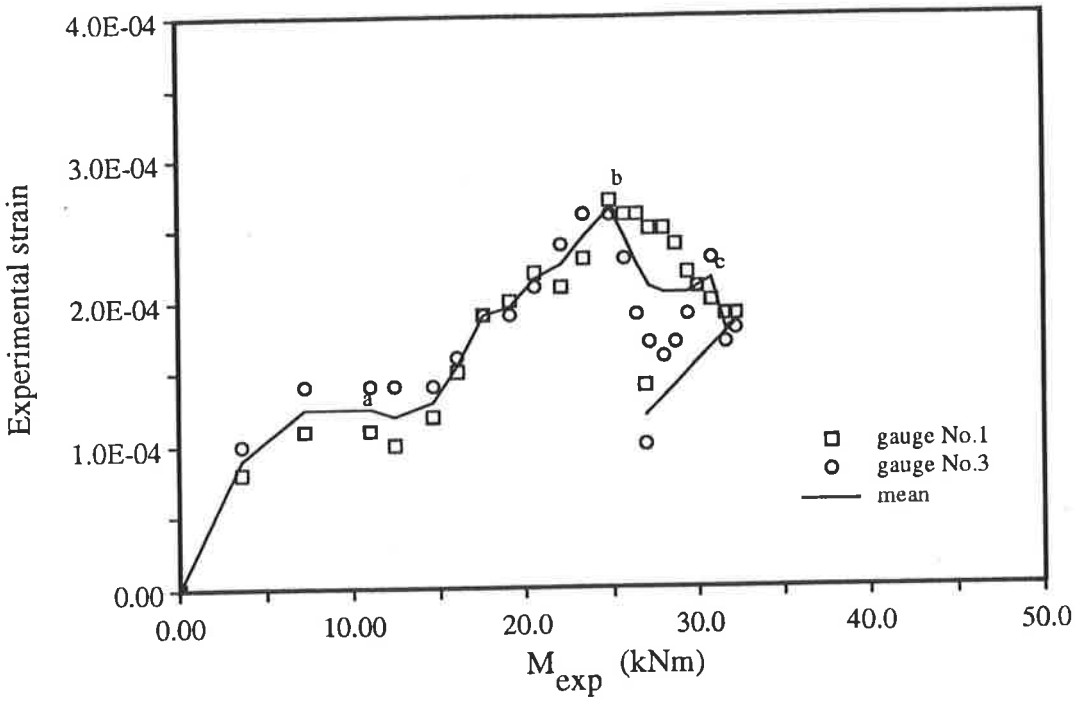

Fig.3-67 P_i = 30.0 kN. The average strains at the plate-end of Beam PT2

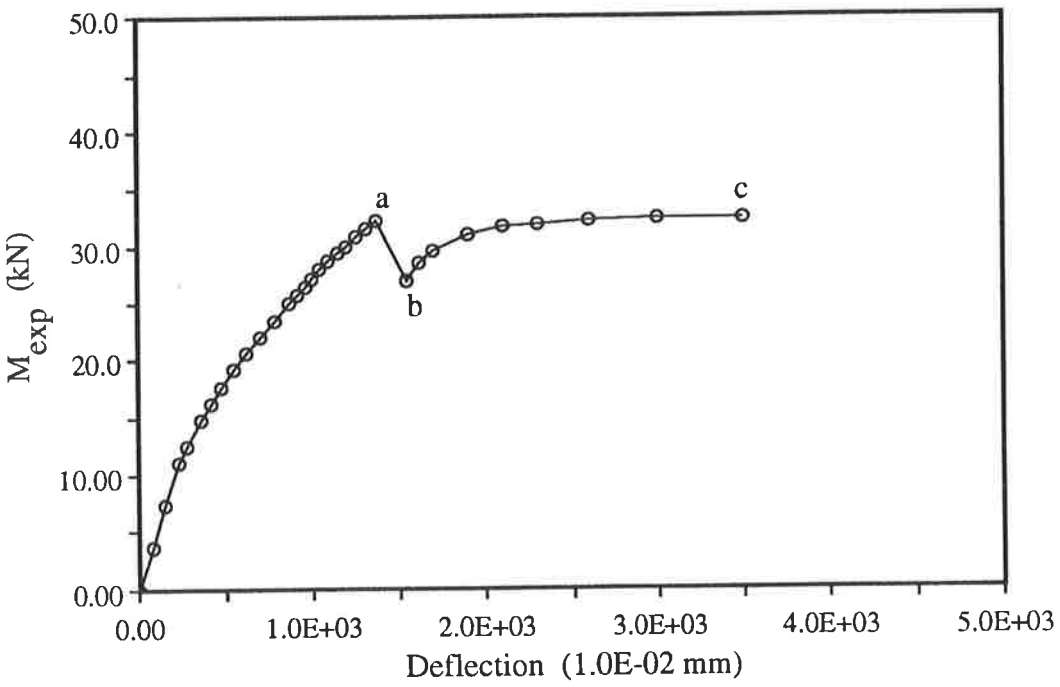

Fig.3-68 P_i = 30.0 kN. The deflection of Beam PT2

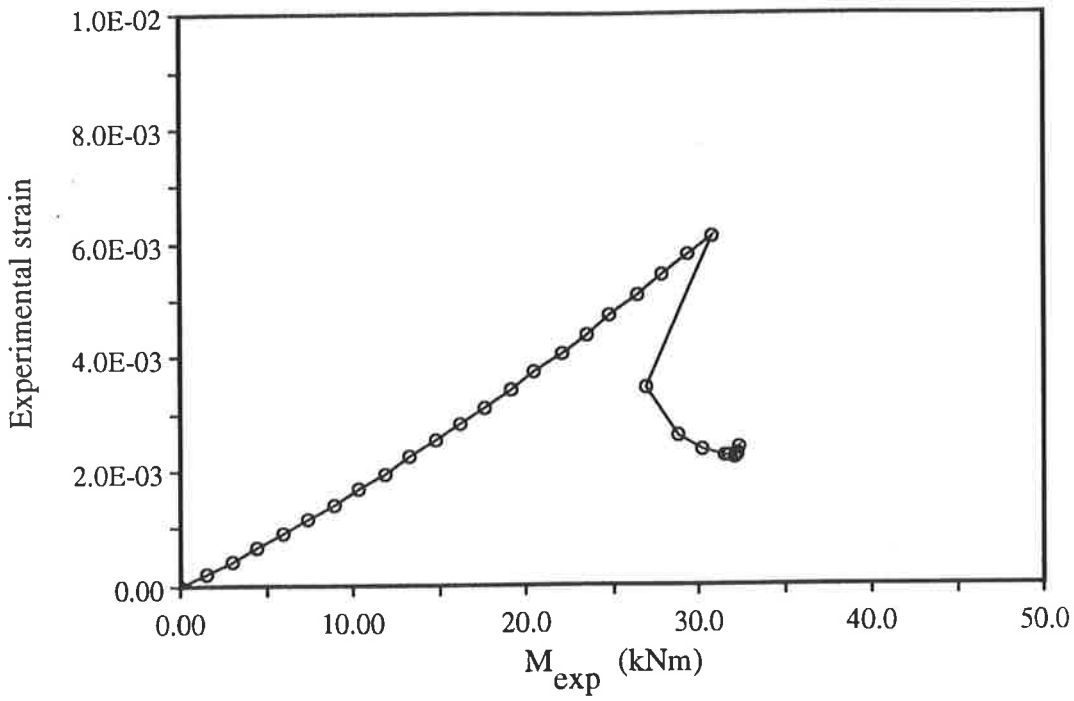

Fig.3-69 P_i = 18.0 kN. Longitudinal strain in the middle of the soffit plate varied of Beam PT3

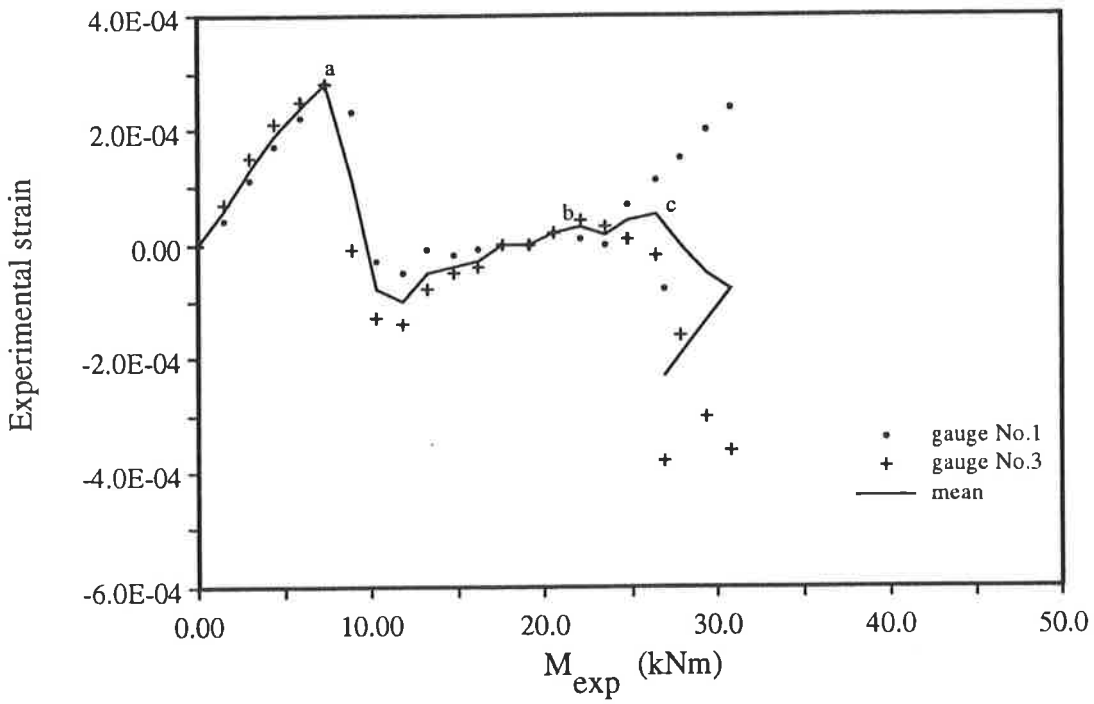

Fig.3-70 P_i = 18.0 kN. The average strains at the plate-end of Beam PT3

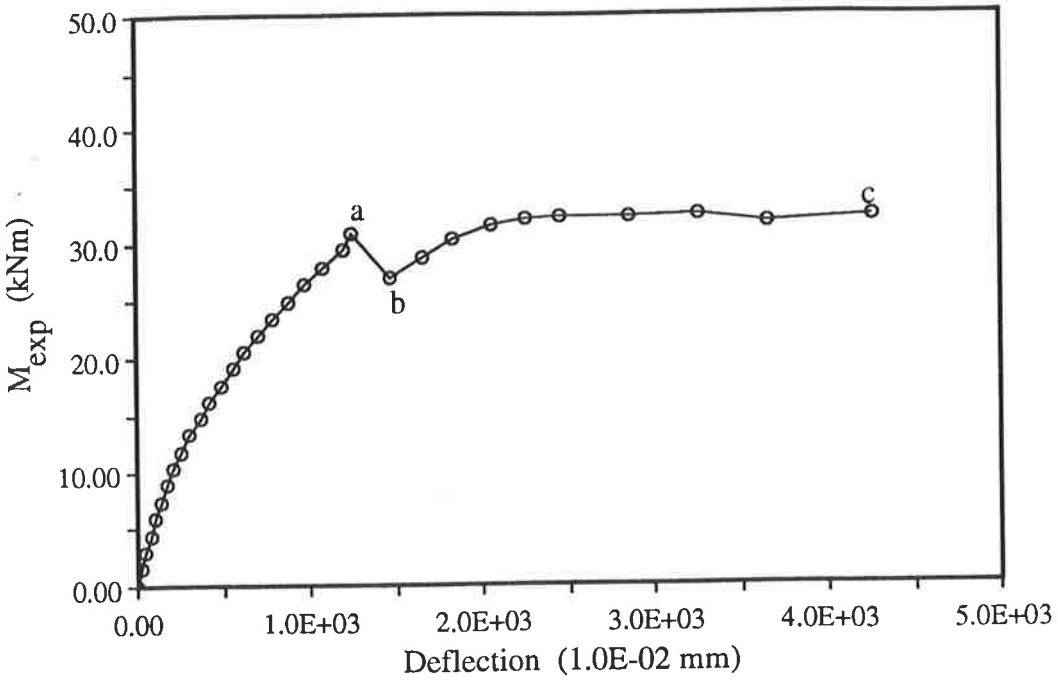

Fig.3-71 P_i = 18.0 kN. The deflection of Beam PT3

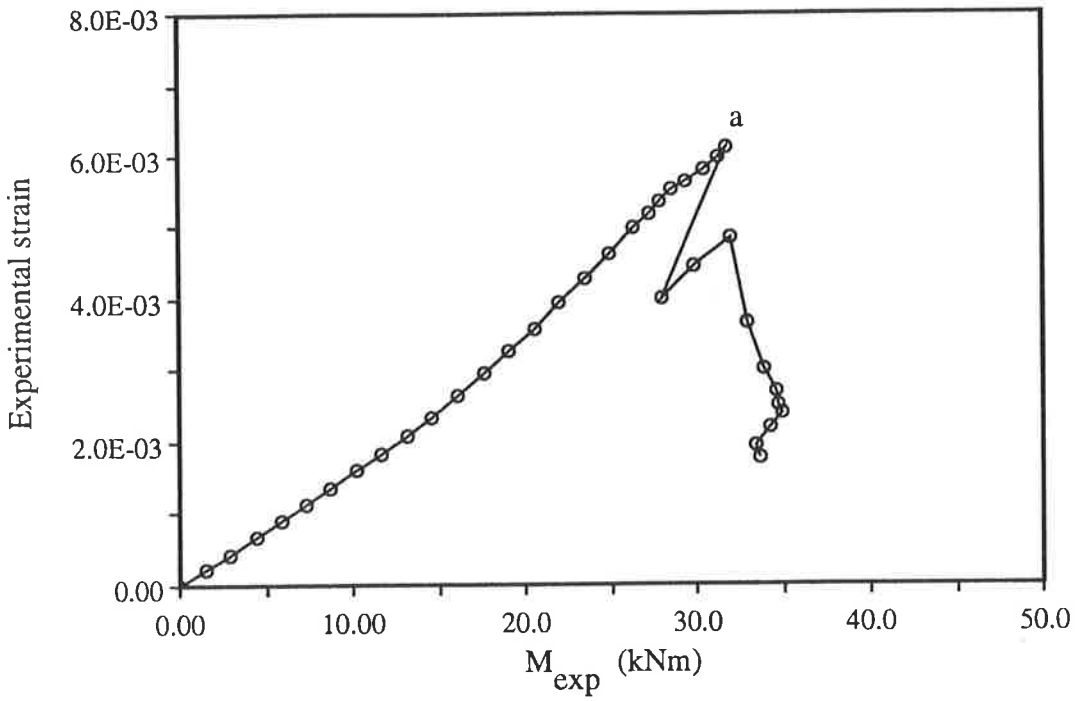

Fig.3-72 P_i = 42.0 kN. Longitudinal strain in the middle of the soffit plate of Beam PT4

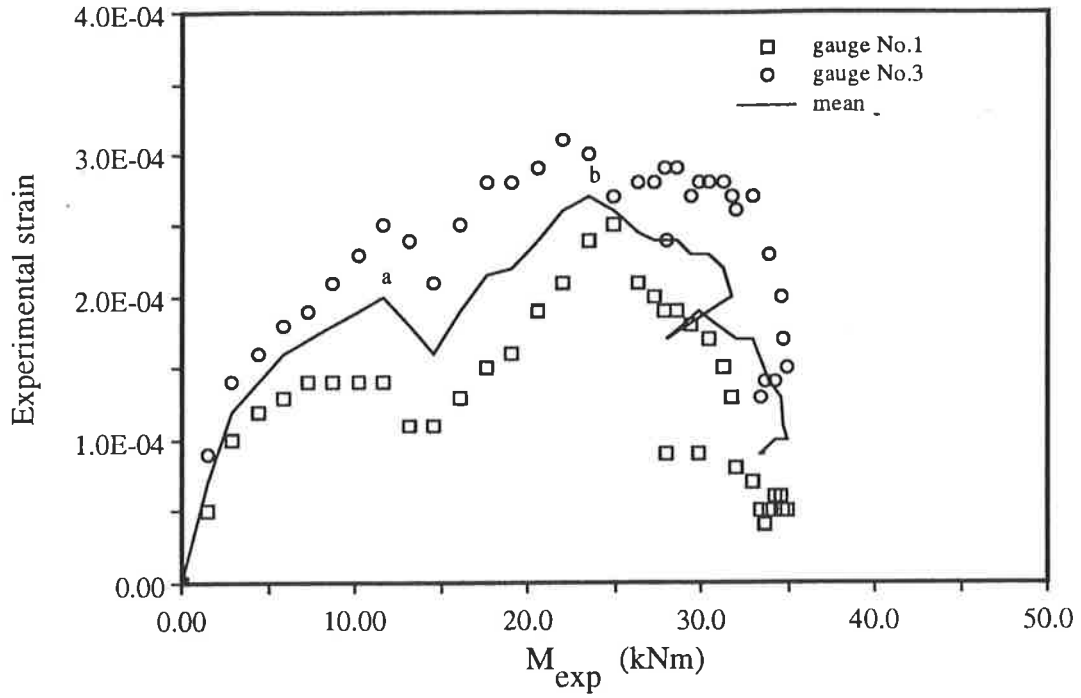

Fig.3-73 P_i = 42.0 kN. The average strains at the plate-end of Beam PT4

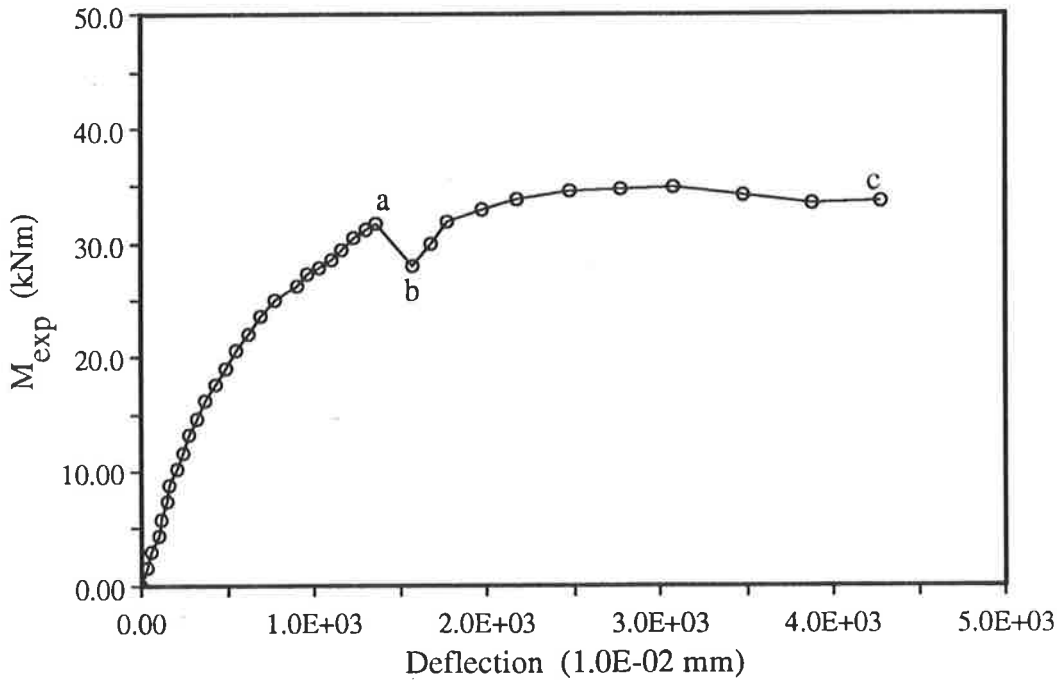

Fig.3-74 P_i = 42.0 kN. The Deflection of Beam PT4

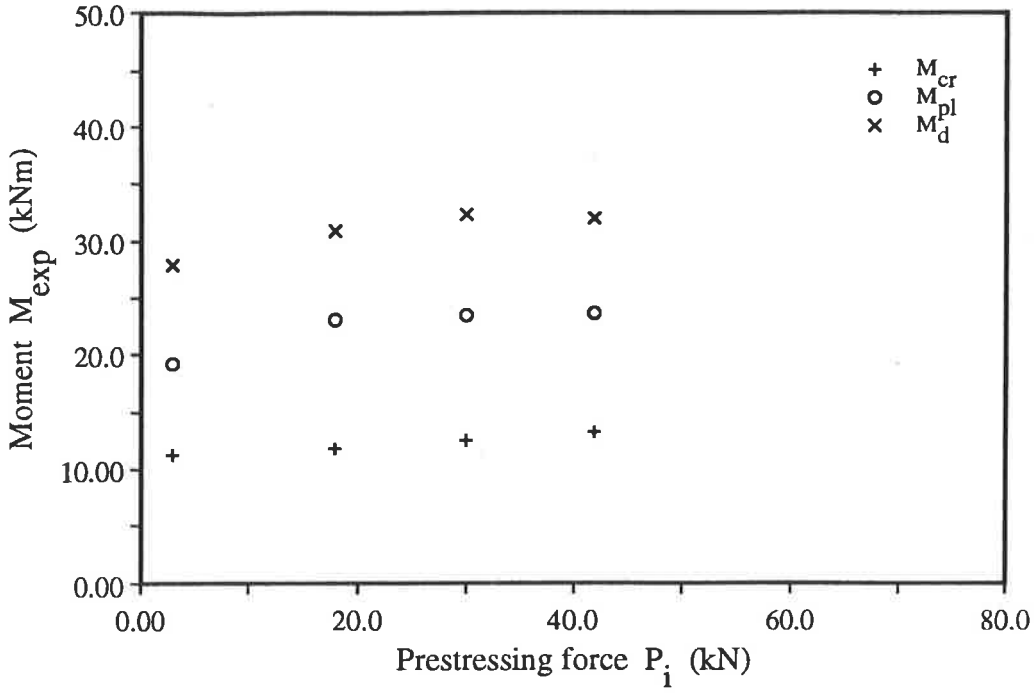

Fig.3-75 Experimental results of series 5

Chapter Four

Computer Model

4.1 Introduction

Previous research as described in Section 1.2.1 had shown that debonding due to flexural peeling forces depends on the flexural rigidity of the section. As the flexural rigidity changes with the degree of prestress [16] a computer model had been developed to predict the flexural rigidity of the plated reinforced concrete beam with varying degrees of the initial prestressing forces. The overall flexural rigidity depends on the applied load, the degree of the cracking, the plate thickness and the initial prestress. In order to determine the flexural rigidity of the plated reinforced concrete beam at each applied moment stage, a computer program is developed to carry out the numerical calculation. This can be achieved by determining the moment versus the curvature diagram in terms of the different stress-strain laws of the concrete some of which include the effect of tension stiffening.

Analytical models based on the compatibility of deformations and equilibrium of forces are presented to predict the flexural rigidity and hence the debonding moment of the plated reinforced concrete beam with varying degrees of the initial prestressing forces.

4.2 Assumptions

For any symmetrical plated prestressed or non-prestressed reinforced concrete section the theoretical flexural rigidity of the section is based on the following three major assumptions: the first, the Bernoulli theorem, assumes that plane sections that are plane before bending remain plane after bending (the deformation due to shear strains are neglected); the second assumption is that the stress-strain relationship of concrete, reinforcement and steel plate are known; and the final assumption is that the reinforcement is subjected to the same variation in strain as the adjacent concrete so that the bond at the interface has infinite stiffness. In the case of a post-tensioned beam, it is assumed that the duct is grouted just after transfer and there is no slip between concrete and reinforcement. However, the bonded tendons do not have the same strain as concrete at the same distance from the neutral axis of the section. It is also assumed that the effect of the adhesive layer is negligible in comparison to that of the reinforced concrete and steel plate because the thickness of the epoxy is very small.

In general, a rectangular cross section of the plated reinforced concrete member consists of three types of reinforcement as shown in Fig.4-1a: steel plate, non-prestressed and prestressed steel bars. The forces acting on each element of the cross section are illustrated in Fig.4-1b.

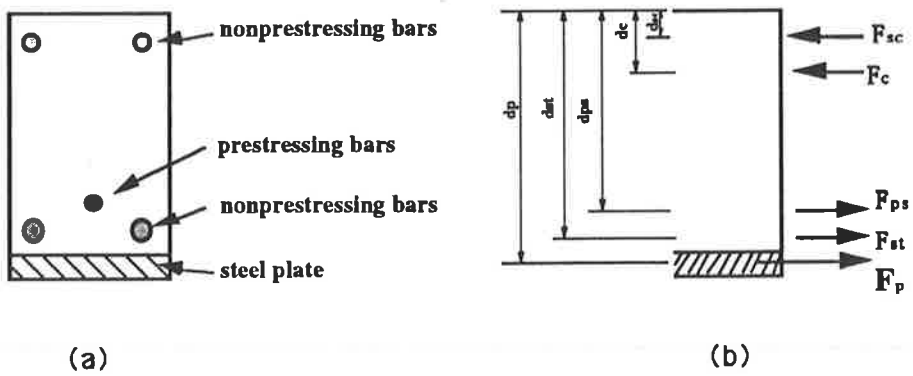

Fig.4-1 Analysis cross section

4.3 Material Properties

The materials are assumed to be in a state of uniaxial stress and have the following properties.

4.3.1 Stress-strain relationship of concrete in uniaxial compression

For concrete in uniaxial compression, two relationships between stress and strain are assumed: firstly the stress is proportional to the strain as shown in Fig.4-2(a); and secondly the short-term uniaxial stress-strain curve adopted for the concrete is based on the widely used relationship in compression suggested by Hognestad [17], as shown in Fig.4-2(b).

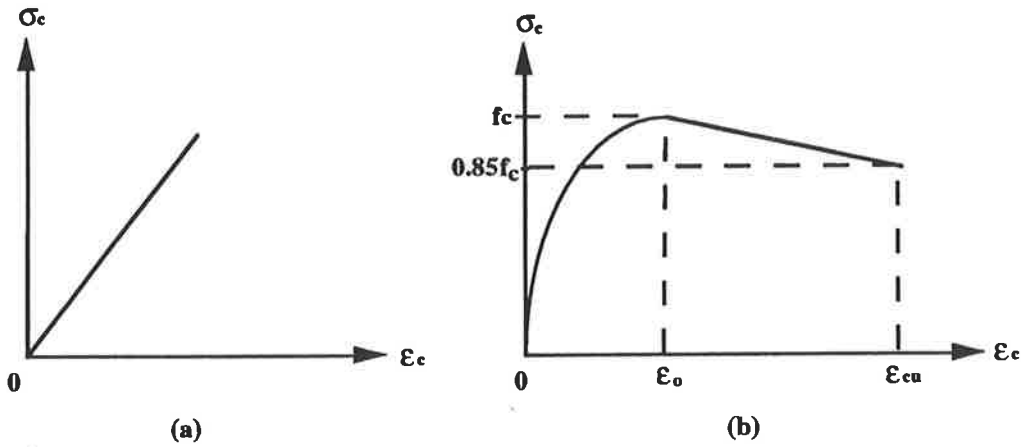

Fig. 4-2 Stress-strain relationship of the concrete in uniaxial compression

The concrete stress-strain relationship suggested by Hognestad is expressed as follows.

$$\sigma_c = f_c\left[2\left(\frac{\varepsilon_c}{\varepsilon_o}\right)-\left(\frac{\varepsilon_c}{\varepsilon_o}\right)^2\right] \qquad \text{for } 0 \le \varepsilon_c < \varepsilon_o \qquad (4\text{-}1)$$

and

$$\sigma_c = f_c\left[1-0.15\frac{\varepsilon_c-\varepsilon_o}{\varepsilon_{cu}-\varepsilon_c}\right] \qquad \text{for } \varepsilon_o \le \varepsilon_c \le \varepsilon_{cu} \qquad (4\text{-}2)$$

where

σ_c = compressive stress in concrete

f_c = peak stress on the stress-strain curve of concrete in compression

ε_c = compressive strain in concrete

$\varepsilon_o = 2\frac{f_c}{E_c}$

$\varepsilon_{cu} = 0.003$

E_c = modulus of elasticity of concrete

4.3.2 Stress-strain relationship of concrete in tension

The tension stiffness effect represents the capacity of the intact concrete to carry internal tensile forces between adjacent cracks. If this effect is disregarded in analysis of a plated reinforced concrete beam, especially at the level of service loads, the stiffness of a beam may be underestimated. Tension stiffening has therefore been included using the model shown in Fig.4-3.

Researches [18-23] have found that the effect of tension-stiffness mostly depends upon the value of $m\rho$ in the member. The term m and ρ are commonly called the modulus ratio and the steel ratio, respectively. Tension-stiffness is most predominant when $m\rho$ is relatively small and diminishes as $m\rho$ increases, as shown in Fig.4-3. In a plated reinforced concrete beam, the value of $m\rho$ is much higher than that of reinforced concrete beam since the external soffit steel plate acts as a

part of tensile reinforcement.

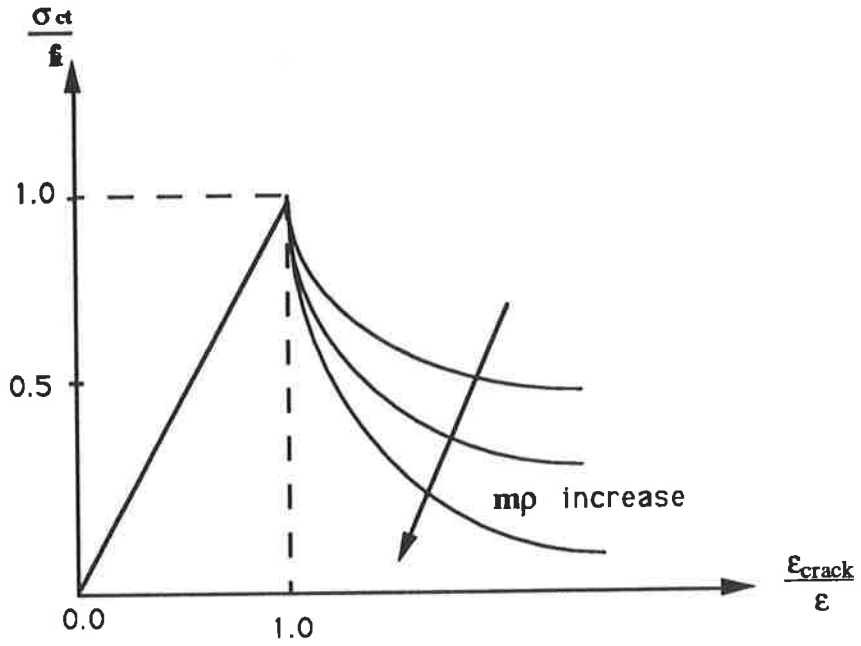

Fig.4-3 Concrete tensile stress-strain curves

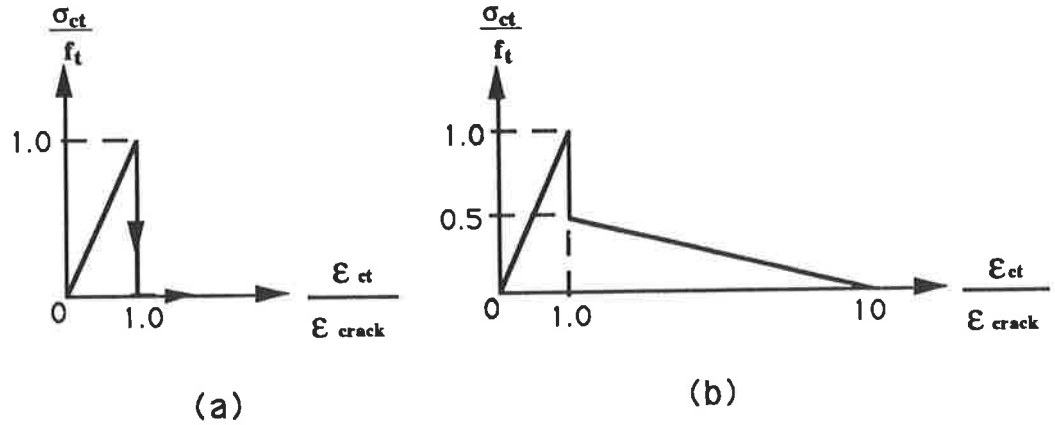

Fig.4-4 Concrete tensile stress-strain curves used in analysis

In the present study, it is assumed that the bond stress is constant. Three models for tension are employed in this study. In the first model the concrete is assumed not to

be able to have tension. In the second model, the concrete is allowed to retain finite tensile capacity, as shown in Fig.4-4(a). The tensile stress-strain relationship of concrete shown in Fig.4-4(b) is used in the third model to investigate the effect of tension stiffness on the flexural rigidity of a plated reinforced concrete beam. The relationship shown in Fig.4-4(b) is expressed as follows:

$$\sigma_{ct} = f_t \frac{\varepsilon_{ct}}{\varepsilon_{crack}} \qquad \text{for } \varepsilon_{ct} \le \varepsilon_{crack} \qquad (4\text{-}3)$$

$$\sigma_{ct} = f_t \left[1 - 0.5 \frac{\varepsilon_{ct} - \varepsilon_{crack}}{9\varepsilon_{crack}} \right] \qquad \text{for } \varepsilon_{crack} < \varepsilon_{ct} \le 10\,\varepsilon_{crack} \qquad (4\text{-}4)$$

$$\sigma_{ct} = 0 \qquad \text{for } \varepsilon_{ct} > 10\,\varepsilon_{crack} \qquad (4\text{-}5)$$

where

σ_{ct} = tensile stress in concrete

f_t = peak stress on the stress-strain curve for concrete in tension

ε_{ct} = tensile strain in concrete

ε_{crack} = strain of concrete corresponding to the maximum tensile stress

4.3.3 Stress-strain relationship of steel

For the non-prestressed steel bars, prestressed steel and the steel plate, a bilinear stress-strain relationship is assumed in the analysis, as shown in Fig.4-5. The relationship is expressed as follows:

$$f_s = E_s \varepsilon_s \qquad \text{for } \varepsilon_s \le \varepsilon_y \qquad (4\text{-}6)$$

and

$$f_s = f_y \qquad \text{for } \varepsilon_s > \varepsilon_y \qquad (4\text{-}7)$$

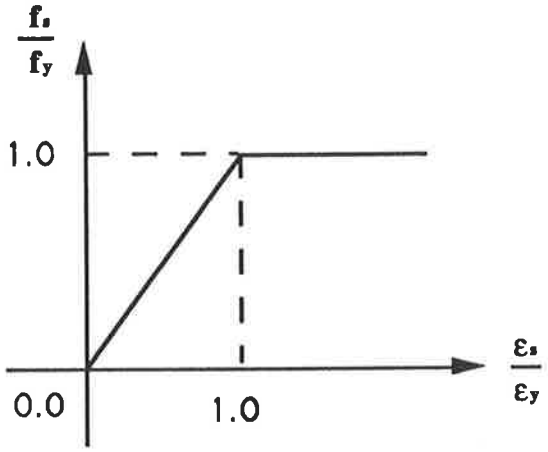

Fig.4-5 Stress-strain curves of steel

The prestressed plated reinforced concrete beams considered here are assumed to be simple-support beams with rectangular sections. Furthermore the ends of the plates are assumed to be terminate far away from the maximum moment region and close to the supports, hence the steel is considered to be linear elastic in the following analyses.

4.4 Method of Analysis

The segmental method is used in this analysis. The cross-section is divided into segments, as shown in Fig.4-6. The behaviour of each segment is defined by the moment versus the curvature relationship obtained for the whole section as described as following. The analysis of the section is carried out by selecting a value of the extreme fibre strain ε_t in section and then finding, by the method of iteration, the curvature θ and hence the location of neutral axis d_{ni} which simultaneously satisfies compatibility and equilibrium. The process is then repeated for increasing values of the extreme fibre strain. By calculating at every step the internal moment and the curvature, the corresponding flexural rigidity of the plated reinforced beam with varying degrees of prestress can be determined and in particular the flexural rigidity at the debonding moment.

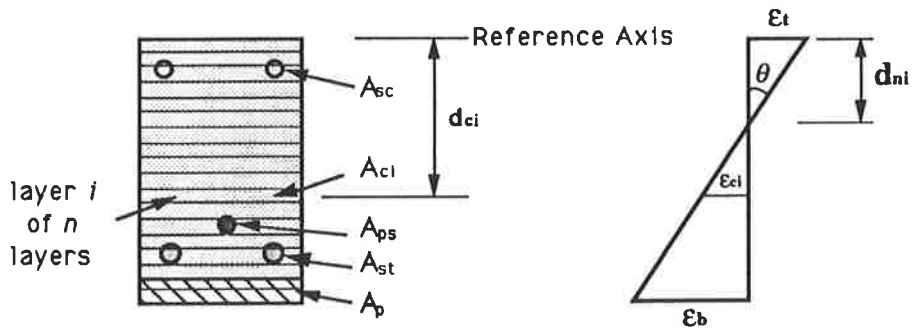

Fig.4-6 Layers in cross section and strain distribution

The prestressed plated reinforced concrete beam is assumed to have a curved cable profile as shown in Fig.4-7, and also to have tensile and compressive reinforcing bars. The analysis procedure has two stages: the reinforced concrete beam without the external soffit plate is first prestressed and this is referred to as at Stage One; and the steel plate is then assumed to be bonded to the prestressed member, so that Stage

Two consists of the analysis of the externally loaded prestressed plated beam.

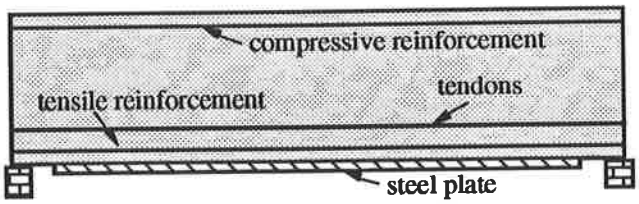

Fig.4-7 Plated reinforced concrete beam profile

It is assumed that the duct is grouted just after transfer and there is no slip between concrete and reinforcement. However, it should be noted that the bonded tendons do not have the same strain as the concrete at the same distance from the neutral axis of the beam.

4.4.1 Stage One

Here we are considering a post-tensioned reinforced concrete beam without an external soffit plate. The post-tensioned reinforced concrete beam consists of tendons at a depth d_{ps}, as shown in Fig.4-8, and tensile and compressive reinforcing steel at the depths d_{sc} and d_{st}.

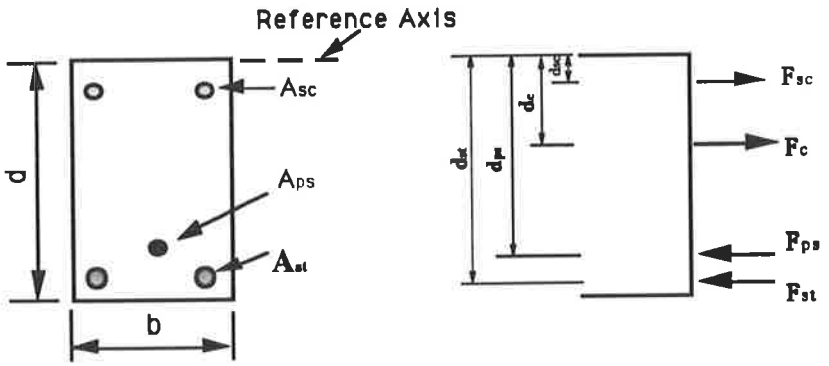

Fig.4-8 Analysis cross-section at Stage One

The section is represented as n number of thin layers as in Fig.4-6. With a predetermined strain ε_t and a trial value for the curvature θ as shown in Fig.4-6, the linear strain distribution in the section is specified. The location of neutral axis, d_{ni}, in the section and the strain ε_{ci} at layer i can be determined by the following:

$$d_{ni} = \varepsilon_t \theta \tag{4-8}$$

$$\varepsilon_{ci} = \varepsilon_t \frac{d_{ni} - d_{ci}}{d_{ni}} \tag{4-9}$$

where

d_{ci} = depth of element to the top fibre section

The stress, σ_{ci}, and hence force, F_{ci}, in each layer of concrete can be determined by means of the stress-strain relationships of concrete, as given by the following equations:

$$\sigma_{ci} = f(\varepsilon_{ci}) \tag{4-10}$$

$$F_{ci} = \sigma_{ci} A_{ci} \tag{4-11}$$

where the stress-strain relationships are described in *Sect. 4.3* and

A_{ci} = $\frac{bd}{n}$, ie., the area of a concrete layer

b = width of the cross-section

d = depth of the cross-section

Therefore, the resultant force in the concrete layers, F_c, can be determined by:

$$F_c = \sum_{i=1}^{n} \sigma_{ci} A_{ci} = \sum_{i=1}^{n} f(\varepsilon_{ci}) \frac{bd}{n} \qquad (4\text{-}12)$$

The forces in the reinforcement and tendons, as shown in Fig.4-8, are determined by:

$$F_{sc} = \varepsilon_{sc} E_s A_{sc} = \varepsilon_t \frac{d_{ni} - d_{sc}}{d_{ni}} E_s A_{sc} \qquad (4\text{-}13)$$

$$F_{st} = \varepsilon_{st} E_s A_{st} = \varepsilon_t \frac{d_{ni} - d_{st}}{d_{ni}} E_s A_{st} \qquad (4\text{-}14)$$

$$F_{ps} = \varepsilon_{pi} E_{ps} A_{ps} \qquad (4\text{-}15)$$

where

A_{sc} = area of reinforcement in the top section

A_{st} = area of reinforcement in the bottom section

A_{ps} = area of tendons

E_s = modulus of elasticity of reinforcement

E_{ps} = modulus of elasticity of tendon

F_{sc} = force in reinforcement in the top section

F_{st} = force in reinforcement in the bottom section

F_{ps} = force in tendons

ε_{sc} = strain in reinforcement of the top section

ε_{st} = strain in reinforcement of the bottom section

ε_{pi} = Strain in tendon due to initial prestress

It is convenient to treat the total forces in the reinforcement and concrete layers as being a resultant force, F_{sec}, as shown in Fig.4-9.

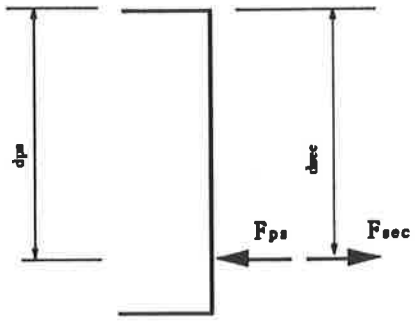

Fig.4-9 Forces equilibrium at Stage One

For a simply supported post-tensioned beam, the resultant force, F_{sec}, must be equal to the force acting in the cables as shown in Fig.4-9, hence for equilibrium:

$$F_{sec} = F_{ps} \tag{4-16}$$

where

$$F_{sec} = F_{sc} + F_{st} + F_c \tag{4-17}$$

The external bending moment in the section is zero at Stage One. Therefore the depth d_c of the resultant forces in the concrete layers can be determined as:

$$d_c = \frac{\sum_{i=1}^{n} \sigma_{ci} A_{ci} d_{ci}}{\sum_{i=1}^{n} \sigma_{ci} A_{ci}} \tag{4-18}$$

Taking moments about the reference axis, as shown in Fig.4-8, the depth d_{sec} of the resultant forces in the reinforcement and concrete layers can then be determined as:

$$d_{sec} = \frac{F_{sc} d_{sc} + F_{st} d_{st} + F_c d_c}{F_{sec}} \tag{4-19}$$

The depth of resultant force in the reinforcement and concrete layers must equal the

depth of the cable during this prestressing stage, ie. Stage One, hence:

$$d_{sec} = d_{ps} \qquad (4\text{-}20)$$

The following iterative procedure is used to ensure that Eq.(4-20) is complied with. With a fixed value of strain say ε_x, the total force F_{sec} in the reinforcement and concrete layers can be calculated by selecting trial values of curvature θ_x, θ_y and so on, as shown in Fig.4-10(a), until the equilibrium of Eq.(4-16) is satisfied in terms of Eqs.(4-8) to (4-15), ie. $F_{sec}/F_{ps} = 1$ in Fig.4-10(a). The initial curvature θ_i for a strain ε_x, at the top fibre in the section is then determined. Furthermore, the depth of resultant forces d_{sec} can be determined by Eq.(4-19). If Eq.(4-20) is not satisfied to within a required error tolerance, ie. $d_{sec}/d_{ps} \neq 1$ in Fig.4-10(b), then an improved value of strain say ε_y is chosen and the procedure illustrated in Fig.4-10(a) is repeated. By selecting different values of strain ε_x, ε_y and so on, in the top section as shown in Fig.4-10(b) and repeating the above process shown in Fig.4-10(a), the Eqs.(4-16) and (4-20) can be satisfied simultaneously, as shown in a flow-chart in Fig.4-11. Finally, we can work out the initial curvature, θ_i, and extreme fibre strains, ε_i, in the section due to the initial prestressing force P_i acting alone as shown in Fig.4-12. Hence, for a specific reinforced concrete section, the variation of initial curvature, θ_i, in the reinforced concrete beams with the varying degrees of initial prestressing forces P_i can be determined in this way for Stage One.

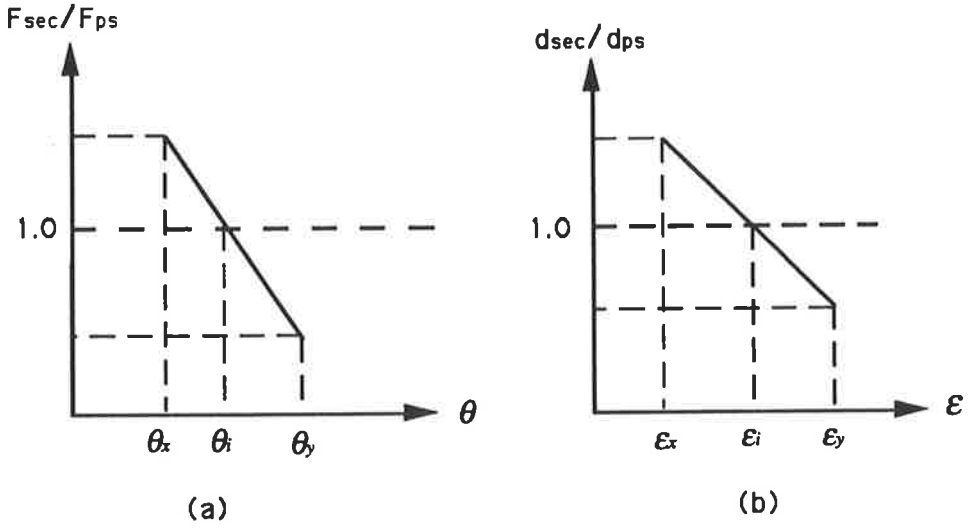

Fig.4-10

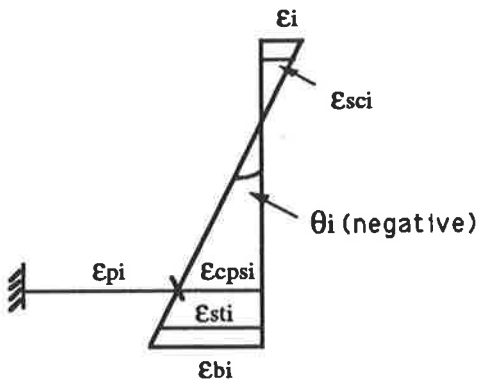

Fig.4-12 Strain distribution in the section at Stage One

where,

ε_{bi} = strain in the bottom fibre of concrete due to initial prestressing forces

ε_{cpsi} = concrete strain at tendon level due to the initial prestressing forces

ε_i = strain in the top fibre of concrete due to the initial prestressing forces

ε_{pi} = strain in prestressing steel due to initial prestress

ε_{sci} = concrete strain at the level of reinforcement in the top section due to

initial prestress

ε_{sti} = concrete strain at the level of reinforcement in the bottom section due to initial prestress

θ_i = initial curvature of section due to initial prestress

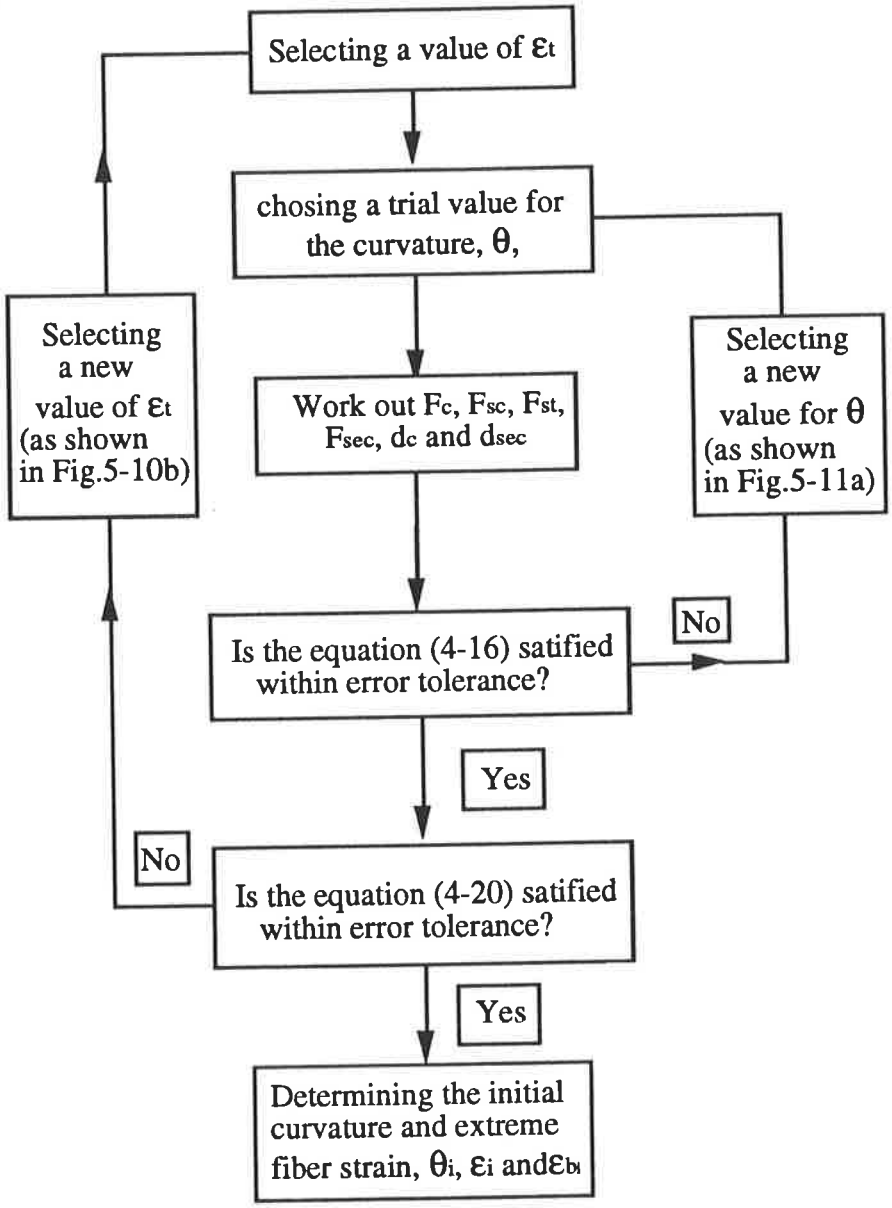

Fig.4-11 Flow-chart at stage one

4.4.2 Stage Two

At the second stage, the post-tensioned concrete beam is strengthened by bonding the external soffit steel plate as shown in Fig.4-7 and it is then subjected to an applied load. The ends of the plate are terminated far away from the maximum moment region and close to the supports. The post-tensioned beam consists of the prestressed tendons, the non-prestressed bars and the steel plate. It is necessary to determine the relationship between the moment and curvature in the prestressed plated section in terms of the different stress-strain laws of the concrete, described in Sect.4.3 in order to determine the variation in the flexural rigidity. This is because the peeling forces have been shown in Sect.1.2.1 depend on the change in the curvature of the section. In order to determine the change in the curvature of the section, the applied-moment/curvature relationship for the plated post-tensioned beam is determined. This is achieved in the following analysis by determined the moment and curvature for a fixed extreme fibre strain ε_t and fixed prestressing forces. In this way the complete diagram of the moment-curvature is constructed point-by-point through a succession of analysis in which ε_t is gradually increased. The flexural rigidity of beam can then be found at each point of moment-curvature diagram.

The section is represented by a number of thin layers, as shown in Fig.4-6. The strain distribution and forces acting on the section is given in Fig.4-13, where, θ = total curvature in the section, $\Delta\theta$ = the change in curvature, d_p = depth of steel plate to the top section, F_p = force in steel plate, ε_p = concrete strain at the level of steel plate, ε_{cps} = concrete strain at tendon level.

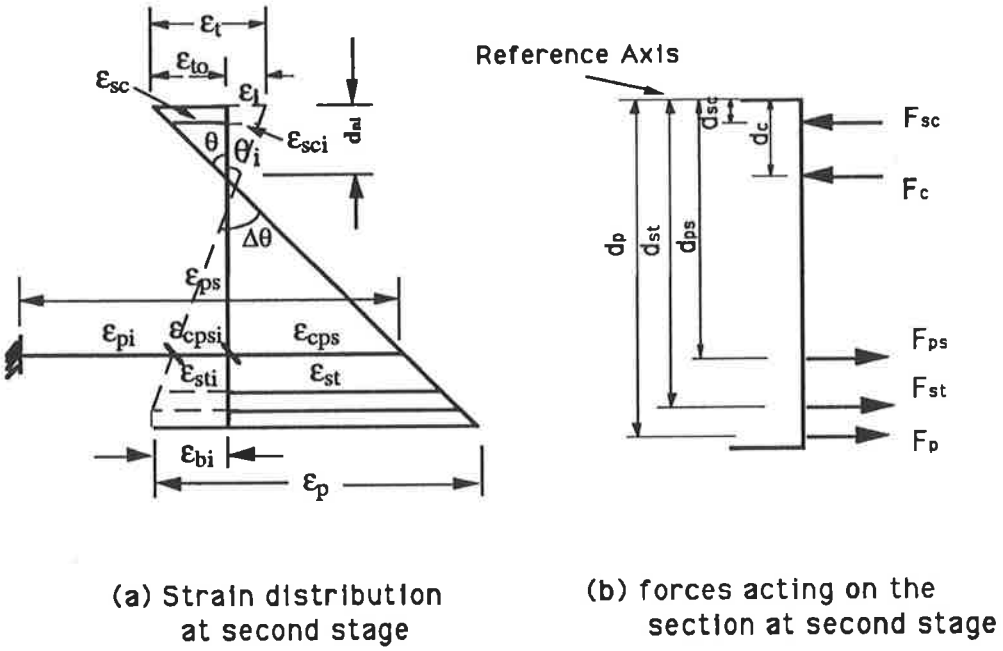

Fig.4-13 Strain distribution in the section at second stage

We assume that the strain in the section is linearly distributed as shown in Fig.4-13(a), with a predetermined value ε_{to} at the extreme top fibre of section. A trial value of curvature θ is chosen. The neutral axis d_{ni} can be determined in terms of Eq.(4-8). The strain in each concrete layer can be calculated from Eq.(4-9). The strains in the concrete at the levels of tensile reinforcement, prestressing tendon, compressive reinforcement and steel plate are thus

$$\varepsilon_{sc} = \varepsilon_{to}\frac{d_{ni} - d_{sc}}{d_{ni}} \tag{4-21}$$

$$\varepsilon_{cps} = \varepsilon_{to}\frac{d_{ps} - d_{ni}}{d_{ni}} \tag{4-22}$$

$$\varepsilon_{st} = \varepsilon_{to}\frac{d_{st} - d_{ni}}{d_{ni}} \tag{4-23}$$

$$\varepsilon_{p} = \varepsilon_{to}\frac{d_{p} - d_{ni}}{d_{ni}} + \varepsilon_{bi} \tag{4-24}$$

The strain in the tendon is

$$\varepsilon_{ps} = \varepsilon_{pi} + \varepsilon_{cpsi} + \varepsilon_{cps} \quad (4\text{-}25)$$

As it is being assumed that the steel remains linear elastic, the forces in tensile reinforcement, prestressing tendon, compressive reinforcement and steel plate are

$$F_{sc} = (\varepsilon_{sc} + \varepsilon_{sci})E_sA_{sc} - \sigma_{sc}A_{sc} \quad (4\text{-}26)$$

$$F_{ps} = \varepsilon_{ps}E_{ps}A_{ps} - \sigma_{ps}A_{ps} \quad (4\text{-}27)$$

$$F_{st} = (\varepsilon_{st} + \varepsilon_{sti})E_sA_{st} - \sigma_{st}A_{st} \quad (4\text{-}28)$$

$$F_p = \varepsilon_pE_pA_p \quad (4\text{-}29)$$

in which, $\sigma_{sc} = f(\varepsilon_{sc} + \varepsilon_{sci})$, $\sigma_{ps} = f(\varepsilon_{cps} + \varepsilon_{cpsi})$, $\sigma_{st} = f(\varepsilon_{st} + \varepsilon_{sti})$, ie., the stress in the concrete at the same level of the reinforcement.

The stress and force in each concrete layer and the resultant forces in the concrete layers can be determined by the following equations:

$$\sigma_{ci} = f(\varepsilon_{ci}) \quad (4\text{-}30)$$

$$F_{ci} = \sigma_{ci}A_{ci} \quad (4\text{-}31)$$

$$F_c = \sum_{i=1}^{n}\sigma_{ci}A_{ci} = \sum_{i=1}^{n}f(\varepsilon_{ci})\frac{bd}{n} \quad (4\text{-}32)$$

where, $\varepsilon_{ci} = f(\varepsilon_i, \varepsilon_{to})$. The depth of resultant forces of concrete layers is then determined by the following equation:

$$d_c = \frac{\sum_{i=1}^{n}\sigma_{ci}A_{ci}d_{ci}}{\sum_{i=1}^{n}\sigma_{ci}A_{ci}} \quad (4\text{-}33)$$

For the forces equilibrium in the section, we have

$$F_c + F_{sc} + F_{ps} + F_{st} + F_p = 0 \qquad (4\text{-}34)$$

Equation (4-34) can be solved by selecting trial values of curvature in the section for the predetermined extreme fibre strain. Then by taking moments about the reference axis of section, as shown in Fig.4-13, the bending moment M in the section is given by:

$$M = F_c d_c + F_{sc} d_{sc} + F_{ps} d_{ps} + F_{st} d_{st} + F_p d_p \qquad (4\text{-}35)$$

The procedure is then repeated for different values of ε_t to form the moment-curvature relationship for the prestressed plated beam from which the flexural rigidity can be obtained at the debonding moment as described in Chapter 5. The procedure can be repeated for varying degrees of prestressing force. A flow chart summarising this calculation procedure is shown in Fig.4-14.

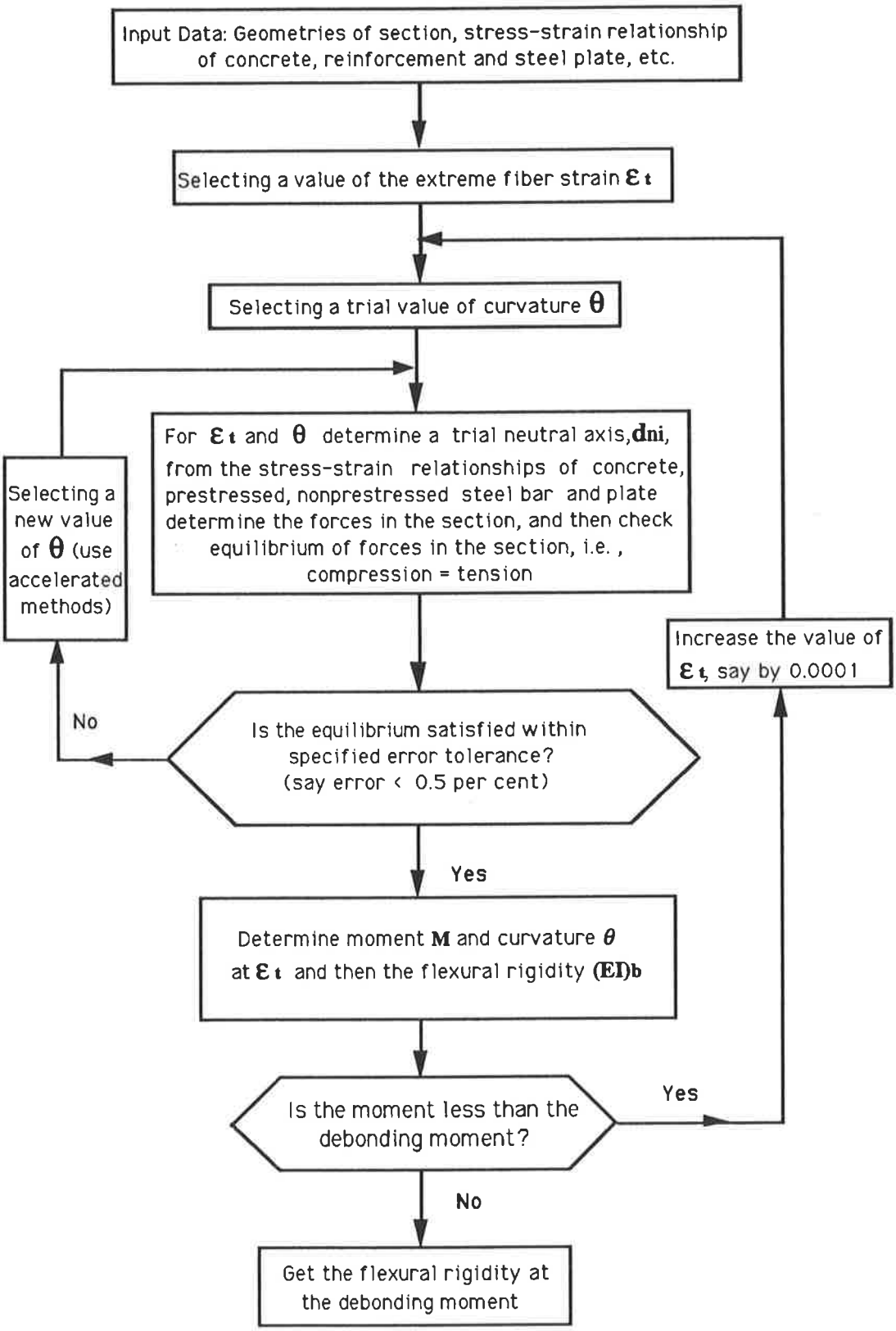

Fig.4-14 Flow-chart for stage two

Chapter Five

Parametric Study

5.1 Introduction

A parametric study was conducted, using the computer program described in Chapter 4, to investigate the effects of varying the degree of the initial prestressing forces on debonding of plated reinforce concrete beams. The results of the analytical models will be compared with results of the experimental beams later in Chapter 6.

5.2 Criteria of debonding moment

Debonding of plated reinforced concrete beams results from the forces at the interface of the steel-plate/concrete-beam as shown in Fig.5-1 and as described in Sect.1.2.1 & 1.2.2. The interface is subjected to a shear flow that reduces to zero at the end of the plate and also to the peeling forces normal to the interface that are induced by the discontinuity of the plate and that are concentrated in the region in the vicinity of the end of the plate. From previous research[4] as described in Sect.1.2.2, it was shown that debonding due to the peeling action of shear forces and flexural forces can be prevented by using the following equation:

$$\frac{M_e}{M_{up}} + \frac{V_e}{V_{uc}} \leq C_1 \qquad (5\text{-}1)$$

in which

V_e is shear force at the end of steel plate,

V_{uc} is shear strength of reinforced concrete beam without stirrups,

M_e is the moment at the end of plate,

M_{up} is the ultimate peeling moment at the end of steel plate,

C_1 is an empirical coefficient, ie., $C_1 = 1.17$.

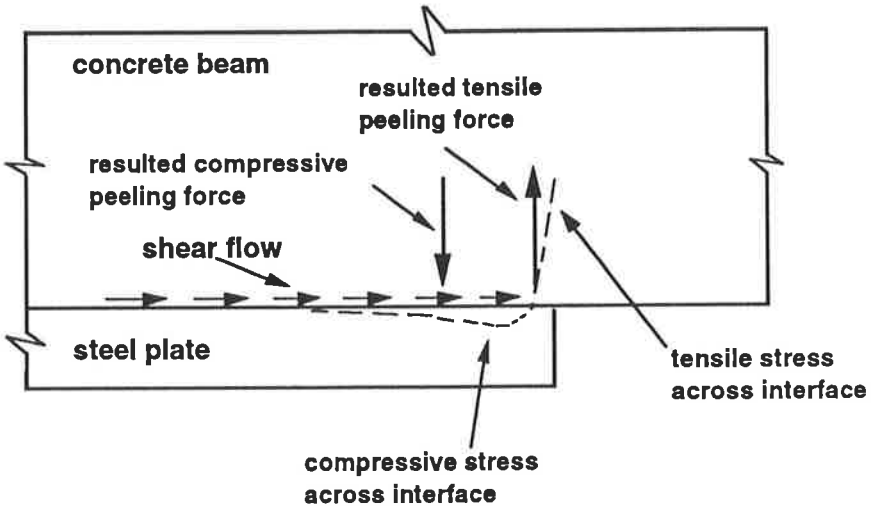

Fig.5-1 Debonding forces

In order to apply Eq.(5-1), the properties M_{up} and V_{uc} are needed and their derivation is determined below.

5.2.1 Shear strength of a reinforced concrete beam without stirrups

Debonding due to peeling of the plated reinforced concrete beams due to the shear forces has been found to depend only upon the shear strength, V_{uc}, of the reinforced concrete beam without stirrups, since it is the formation of the diagonal shear crack in the unplated region adjacent to the plate-end that induces shear peeling. Therefore, this form of debonding is not controlled by the shear flow along the steel-plate/concrete-beam interface and also not prevented by the inclusion of stirrups. The ultimate shear strength V_{uc} of the reinforced concrete beam with varying degrees of prestressing forces and excluding the contribution of shear reinforcement, can be determined from AS 3600 [24] where it is given by the following equation:

$$V_{uc} = \beta_1\beta_2\beta_3 b_v d_o \left[\frac{(A_{st} + A_{ps})f_c}{b_v d_o}\right]^{\frac{1}{3}} + V_o + P_v \qquad (5\text{-}2)$$

where

$\beta_1 = 1.4 - (d_o/2000) \geq 1.1$

$\beta_2 = 1.0$ or

$= 1.0 - (N^*/3.5A_g) \geq 0$ for members subject to significant tension; or

$= 1.0 + (N^*/14A_g)$ for members subject to significant axial compression

A_g = the gross cross-sectional area of a beam

N^* = the axial compressive or tensile force on a cross-section

$\beta_3 = 1.0$

A_{st} = area of longitudinal tensile reinforcement

A_{ps} = area of the tendons

P_v = the vertical component of the prestressing force

V_o = the shear force which would occur at the section when the bending moment at that section was equal to the decompression moment, M_o, which is the moment that causes the concrete stress in the bottom fibre to reduce to zero.

For simply-supported conditions,

$V_o = M_o/(M^*/V^*)$

where M^* and V^* are the bending moment and shear force respectively, at the section under consideration.

5.2.2 Peeling moment M_{up}

The moment, M_{up}, at which pure flexural peeling occurs has been quantified in Sect.1.2.1 and is given by the following equation:

$$M_{up} = \frac{(EI)_{cp} f_t}{0.474 E_p t_p} \tag{5-3}$$

in which

$(EI)_{cp}$ = flexural rigidity of cracked plated section,

E_p = Young's modulus of plate,

f_t = indirect tensile strength of concrete,

t_p = the thickness of the soffit steel plate.

In determining the above equation (5-3), the flexural rigidity of the cracked plated section was based on a idealise linear elastic analysis in which it was assumed that the tensile strength of concrete was zero. Hence the bending stiffness of the cracked plated section was assumed as to be constant. Therefore the curvature of the cracked plated section, θ_{up}, at which flexural peeling M_{up} occurs can be derived from Eq.(5-3) and is given by the following equation:

$$\theta_{up} = \frac{f_t}{0.474 E_p t_p} \tag{5-4}$$

However, the flexural rigidity of plated prestressed reinforced concrete beams varies with the degree of the initial prestressing forces and also varies with the applied moment [16]. Hence, θ_{up} in Eq.(5-4) is the change in curvature required for pure flexural peeling, which can not be determined from Eq.(5-4) for prestressed beam.

The computer program described in Chapter 4 was developed to simulate the actual flexural behaviour of the plated prestressed reinforced concrete beams using different stress-strain laws for the concrete. The flexural rigidity, $(EI)_b$, of the plated reinforced concrete beam can be determined from the moment versus curvature plots for varying degrees of the initial prestressing forces; example of which are shown in Fig.5-2.

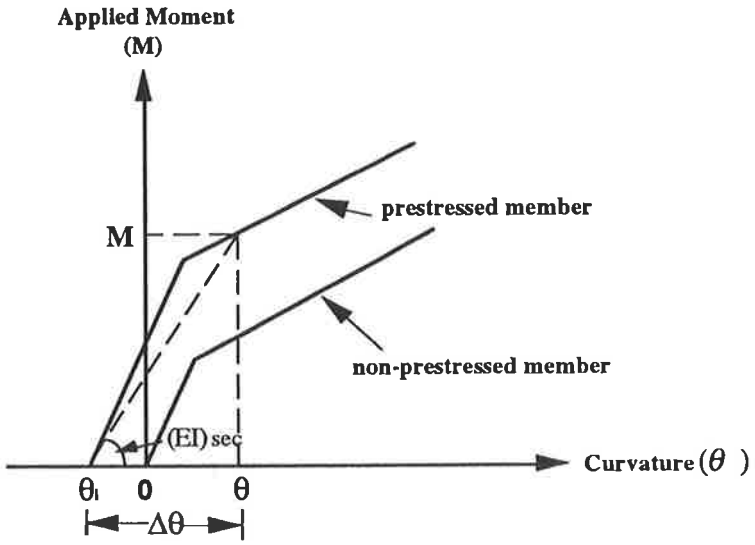

Fig.5-2 Moment-curvature plots

For the applied moment M and curvature θ in the section as shown in Fig.5-2, the 'secant' bending stiffness $(EI)_{sec}$, is the required flexural rigidity needed to determine the debonding moment of the prestressed plated reinforced concrete beam and is given by the following equation:

$$(EI)_{sec} = \frac{M}{\Delta\theta} \qquad (5\text{–}5)$$

in which

$\Delta\theta$ = $(\theta - \theta_i)$, ie., the change in curvature after the external soffit plate has been bonded to the prestressed beam

θ = total curvature in the section

θ_i = initial curvature in the section due to the prestressing forces

The initial curvature θ_i, the total curvature θ, and the change in curvature $\Delta\theta$ in the section after the beams are plated are illustrated in Fig.5-3.

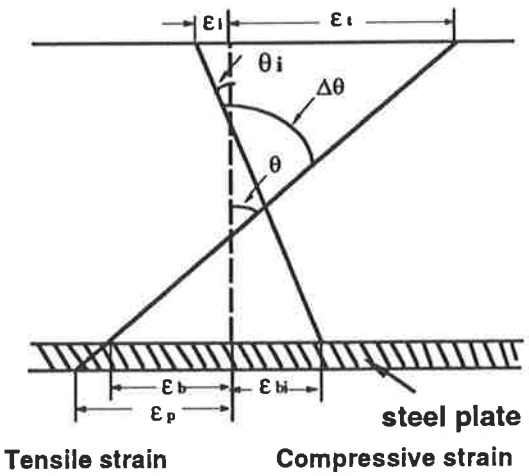

Fig.5-3 Curvature in the section

where

ε_i = strain in the top section due to the initial prestress

ε_{bi} = strain in the bottom section due to prestress

$\varepsilon_i + \varepsilon_t$ = strain in the top section due to applied moment

$\varepsilon_{bi} + \varepsilon_b$ = strain in the bottom section due to applied moment

ε_p = strain at the level of plate due to applied moment

Therefore the relationship between the bending stiffness of the section $(EI)_{sec}$ and the moment at plate-end M_e can be determined at each applied load stage, as shown in Fig.5-4.

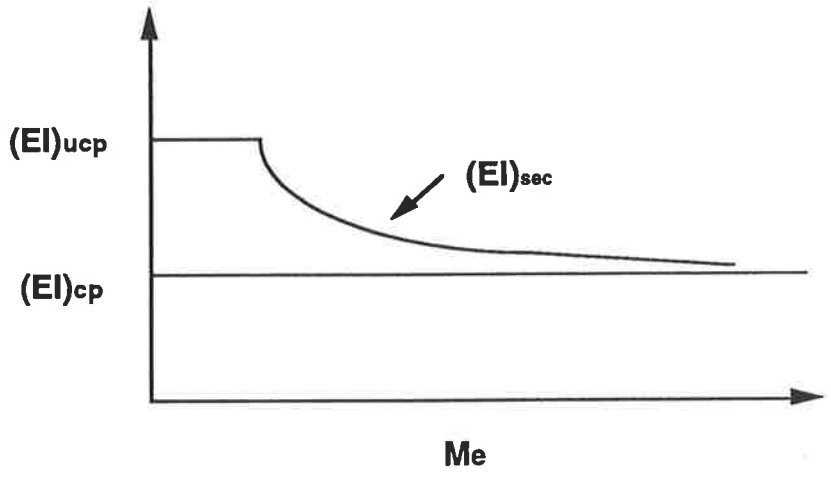

Fig.5-4 Variation of bending stiffness with moment at plate-end

where

$(EI)_{ucp}$ = flexural rigidity of uncracked plated section

$(EI)_{cp}$ = flexural rigidity of cracked plated section

The ultimate peeling moment, ie., the debonding moment due to pure flexure, can then be determined by the following equation:

$$M_{up} = \frac{(EI)_{sec} f_t}{0.474 E_p t_p} \tag{5-6}$$

5.2.3 Debonding load

The load to cause debonding can be determined by calculating the parameter C_1 in Eq.(5-7) at each applied load stage as shown in Fig.5-5.

$$\frac{M_e}{M_{up}} + \frac{V_e}{V_{uc}} = C_1 \tag{5-7}$$

Debonding occurs when C_1 equals to 1.17, as shown in Eq.(5-1).

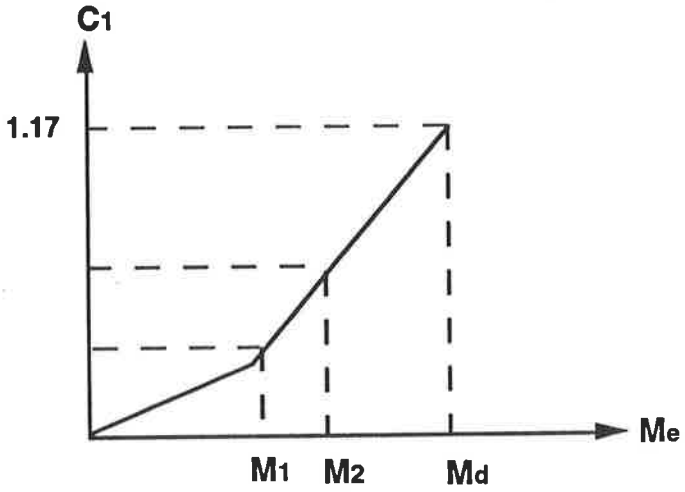

Fig.5-5 Variation of C_1 with moment at plate-end

5.2.4 The parameters used in the calculations

The material and geometric properties of the experimental beams in Chapter 2 were used in this parametric study. The initial prestressing forces applied in the tendons were varied from 0 to 67 % of the yield stress of the tendon. The properties of concrete, reinforced steel bars, tendons and steel plates were the same as experimental tests and are given by: f_c = 37.1 N/mm^2, f_t = 4.0 N/mm^2, E_c = 34.2 kN/mm^2, t_p = 4.0 mm, f_{sty} = 460 N/mm^2, f_{psy} = 1527.0 N/mm^2, f_{py} = 243.0 N/mm^2, E_s = 210.0 kN/mm^2, E_p = 210.0 kN/mm^2, M^*/V^* = 0.95. The geometric properties of reinforced concrete cross-section are given in Table 2.5.

5.3 Analysis of the plated reinforced concrete beam with varying degrees of the prestressing forces

Analytical models are presented to predict the flexural rigidity and debonding moment of plated reinforced concrete beams with varying degrees of the initial prestressing forces. The models are given for beams having rectangular section. The moment versus curvature diagrams for various degrees of prestressing forces in the plated reinforced concrete beams are plotted and compared. The moment-curvature plots are terminated when the debonding moment has been reached. A plated reinforced concrete beam without prestressing forces is regarded as a reference beam with which to compare the prestressed beam. Therefore, the debonding moment of this beam is a reference moment, which is compared the debonding moment of the prestressed beam; the result of comparison is referred to as a moment ratio C_2.

5.3.1 Model One

The stress-strain law of concrete employed in the analysis of the Model One is shown in Fig.5-6. The tensile strength of concrete is zero. The concrete is assumed to be an idealised linear elastic material.

A family of the moment versus curvature diagrams of the beams with different degrees of the initial prestressing forces are shown in Fig.5-7. A family of the change in curvature of the section versus applied moment at the plate-end are plotted in Fig.5-8. The relationship between the flexural rigidities $(EI)_{sec}$ of the sections and applied moments M_e at the plate-end are plotted in Fig.5-9. The relationship between the coefficient C_1 in Eq.(5-7) and moments M_e at the end of the plate diagrams are shown in Fig.5-10.

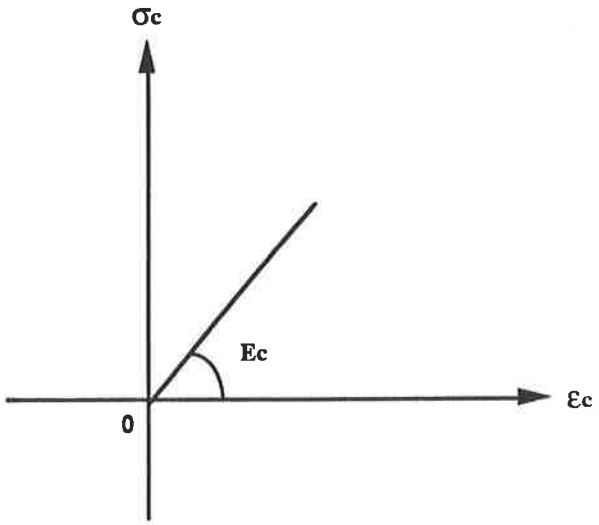

Fig.5-6 The stress-strain law of concrete used in the Model One

5.3.1.1 Example of an Analysis

As an example of the analysis procedure, we take a beam with a prestressing forces P_i = 30.0 kN. The results of the calculations are given in Table 5.1. The variation of the strain and stress profiles in the section with the applied moment are shown in Fig.5-11a and Fig.5-11b, respectively. It can be seen in Fig.5-11a that initially the strain in the top fibre of section is tensile and the strain in the bottom section is compressive due to the prestressing forces applied to the section. The stress profile in the section indicates that the concrete section only has compressive stress because the tensile stress of the concrete is ignored in this model, as shown in Fig.5-11b. When the strain in the bottom concrete section is tensile, the section changes from a plated uncracked section to a plated cracked section. It is also shown in Fig.5-9 that the peeling flexural rigidity $(EI)_{sec}$ is decreasing with the increase in moment.

Table 5.1

θ 1.0E-06 (mm^{-1})	$\Delta\theta$ 1.0E-06 (mm^{-1})	d_{ni} (mm)	ε_t 1.0E-06	ε_b 1.0E-06	M (kNm)	M_e (kNm)	$(EI)_{sec}$ 1.0E+12 (N mm^2)
-0.4676	0.0000	55.0	26	-58	0.0	0.0	5.43062
0.1585	0.6261	180	-29	0.00	3.0	2.2	5.43062
1.1377	1.6053	105	-120	85	7.8	5.1	4.8678
2.1477	2.6150	95.0	-204	183	11.6	7.6	4.4510
3.1497	3.6173	90.0	-284	283	15.4	10.1	4.2613
4.1477	4.6153	87.0	-361	386	19.2	12.6	4.1549
5.1447	5.6123	86.0	-442	484	22.9	15.0	4.0855
6.1407	6.6083	85.5	-525	580	26.7	17.5	4.0373
7.1367	7.6039	84.2	-601	684	30.4	20.0	4.0012

where

d_{ni} = depth of the neutral axial

ε_t = strain in the top section

ε_b = strain in the bottom section

M = moment in the middle of the beam

M_e = moment at the plate-end

5.3.1.2 Results of analysis

The variation of the applied moment with total curvature for the beams with six different degrees of the initial prestressing forces applied to the section are shown in Fig.5-7. For the prestressed beams, it can be seen that a kink occurs, which implies

that the strain in the bottom fibre concrete section is equal to zero at this moment. As the moment increases, the flexural rigidity of the section changes from the plated uncracked section to the plated cracked section. Also, it is indicated explicitly in Fig.5-8 that for the beam without a prestressing force the slope of the plot is a constant, and for those beams with prestressing forces the slope of plots are the same at the uncracked stages and that the change in slope changes at different moments. The change in slope is delayed as the prestressing force is increased. Therefore, it can be expected that the debonding moment will increase with the increase in the prestressing forces. Figure 5-9 shows the results of the variation of the flexural rigidity $(EI)_{sec}$ with the moment M_e at the plate-end. It can be seen that, for those beams with prestressing forces, the flexural rigidity of the section is initially equal to that of the plated uncracked section $(EI)_{ucp}$. The stiffness of beam then reduces gradually with increased moment and tends to approach the flexural rigidity of the plated cracked section $(EI)_{cp}$. The change in stiffness from plated uncracked section to plated cracked section is postponed due to the greater prestressing forces applied to the section.

Figure 5-10 illustrates the relationship between moment M_e at the end of the plate and the coefficient C_1 described in section 5.2.3. As the debonding moment occurs when C_1 equals to 1.17, it can be seen that the moment M_e at the plate-end at which debonding occurs progressively increases due to the result of increase in the initial prestressing forces applied to the section.

5.3.1.3 Summary of results

A comparison of the results is given in Table 5.2 and illustrated in Fig.5-12. Table 5.2 contains the flexural rigidity $(EI)_{sec}$ of the section when debonding occurs. The moment at the plate-end $(M_e)_o$ represents a beam without prestress and the moment at the plate-end $(M_e)_{pi}$ represents a beam with prestress when debonding occurs. It can

be seen in Fig.5-12 that the moment ratio, $C_2 = (M_e)_{pi}/(M_e)_o$, is proportional to the initial prestressing forces, P_i, applied to the section. The increase in the debonding moment is from 1 per cent to 17 per cent.

Table 5.2 Calculated data in Model One

P_i (kN)	V_{uc} (kN)	V_e (kN)	M_e (kNm)	M_{up} (kNm)	$(EI)_{sec}$ 1.0E+12 (N mm^2)	$C_2 = \frac{(M_e)_{pi}}{(M_e)_o}$
0.00	35.9	22.1	21.0	37.8	3.7626	1.00
3.00	36.3	22.4	21.3	38.4	3.8233	1.01
18.0	38.6	23.4	22.2	39.3	3.9140	1.06
30.0	40.3	24.0	22.8	39.9	3.9736	1.09
42.0	42.1	24.7	23.5	40.4	4.0245	1.12
60.0	44.8	25.9	24.6	41.6	4.1144	1.17

5.3.2 Model Two

The stress-strain law of concrete employed in the analysis of Model Two is shown in Fig.5-13. The tensile strength of concrete is not zero. The concrete is assumed to be a linear elastic material.

A family of applied-moment versus total curvature diagrams for beams with six different degrees of the initial prestressing force are shown in Fig.5-14 and a family of the change in curvature of the section $\Delta\theta$ versus moment at the plate-end M_e are illustrated in Fig.5-15. The relationship between the flexural rigidity $(EI)_{sec}$ of the section and moment at the plate-end M_e are plotted in Fig.5-16. The relationship between the coefficient C_1 and the moment M_e diagrams are given in Fig.5-17.

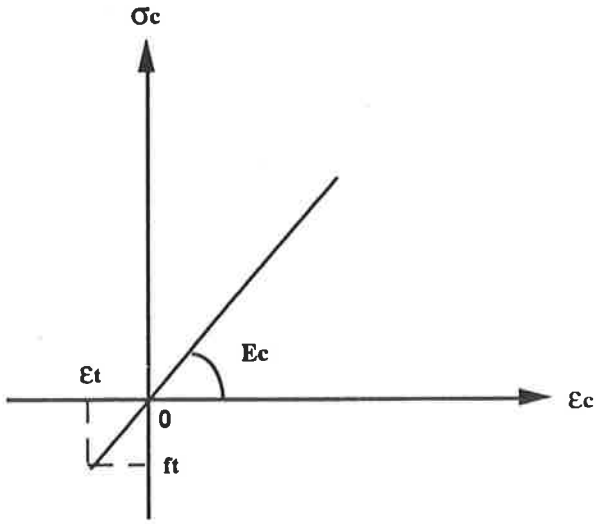

Fig.5-13 The stress-strain law of concrete used in model two

5.3.2.1 Example of an Analysis

The results from an analysis with a beam with a prestressing forces, P_i = 30.0 kN, are given in Table 5.3.

The variation of the strain and stress profiles in the section with the applied moment are illustrated in Fig.5-18a and Fig.5-18b, respectively. It can be seen in Fig.5-18a that initially the strain in the top fibre of the section is tensile and the strain in the bottom section is compressive due to the prestressing forces. The stress profiles shown in Fig.5-18b indicate that the concrete section has a tensile stress because the tensile strength of concrete is taken into account in this model. Table 5.3 shows that the strain in the bottom section is zero and the depth of neutral axis equals to the depth of concrete section when the applied moment was 3.4 kNm. At applied moments up to 10.4 kNm, the bottom strain in the concrete section is less than the tensile strain of concrete and hence the section is uncracked. High moments will cause the section to crack hence the stiffness of the section will changeover from a plated uncracked

section to a plated cracked section. Further increase in the moment cause the depth of the neutral axis to reduce gradually until debonding of the soffit plate takes place.

Table 5.3

θ 1.0E-06 (mm^{-1})	$\Delta\theta$ 1.0E-06 (mm^{-1})	d_{ni} (mm)	ε_t 1.0E-06	ε_b 1.0E-06	M (kNm)	M_e (kNm)	$(EI)_{sec}$ 1.0E+12 (N mm^2)
-0.3587	0.0000	34.0	12	-52	0.0	0.0	5.43062
0.2611	0.6198	180	-54	0.00	3.4	2.2	5.43062
0.9066	1.2653	127	-118	50	6.9	4.5	5.43062
1.5503	1.9090	117	-184	100	10.4	6.8	5.43062
2.8029	3.1616	99.7	-280	225	14.0	9.2	4.43715
4.0412	4.3999	91.7	-371	360	19.0	12.4	4.31832
5.4395	5.7973	88.2	-480	500	24.4	16.0	4.20886
6.8217	7.1795	86.2	-588	640	29.8	19.5	4.15073
8.2533	8.6120	84.8	-700	785	35.3	23.2	4.09891
8.9269	9.2856	84.5	-754	850	37.2	24.4	4.00620

5.3.2.2 Results of analysis

The results of applied-moment versus total-curvature diagrams are shown in Fig.5-14. The curvature varies linearly with the moment in the uncracked stages, and then the slope of the moment-curvature relationship changes when cracking has formed in the section considered. It is also illustrated explicitly in Fig.5-15 that during the uncracked stages the change in curvature of the section varies linearly with the moment in all the beams and hence the slope of moment-curvature is constant. For the beam without the initial prestressing force cracking causes a very sudden change in

curvature and for those beams with the prestressing forces there is a slower progressive change in the moment-curvature relationship.

The variation of the flexural rigidity $(EI)_{sec}$ is shown in Fig.5-16. During the uncracked stages the flexural rigidity of all the beams is constant at $(EI)_{ucp}$ as would be expected. For a beam without or with a small prestressing forces there is a sudden drop in stiffness due to the cracking and the stiffness becomes asymptotic with $(EI)_{cp}$. For those beams with prestressing forces, the flexural rigidity of the section drops off gradually as the moment increases. The greater the prestressing force that is applied to the section, the higher the cracking moment as would be expected. As the moment further increase, the flexural rigidity of a beam with prestressing forces reduces gradually and tends to approach that of a beam without prestressing forces $(EI)_{cp}$.

The results of the variation of the coefficient C_1 with moment at the plate-end M_e are shown in Fig.5-17. Where kink occurs the section changes from a plated uncracked to a plated cracked section. The debonding moments, indicated in Fig.5-17 ie. when the line cross $C_1 = 1.17$, increase with increasing initial prestressing forces.

5.3.2.3 Summary of results

A comparison of the results are given in Table 5.4 and shown in Fig.5-19. It can be seen in Fig.5-19 that the increase in the debonding moment given by ratio C_2 is proportional to the initial prestressing forces P_i applied in the section. The increase in the debonding moment ranges is from 1 per cent to 18 per cent when the prestressing force varies from 3 per cent to 67 per cent of yield stress of the tendons.

Table 5.4 Calculated data in model two

P_i (kN)	V_{uc} (kN)	V_e (kN)	M_{cr} (kNm)	M_e (kNm)	M_{up} (kNm)	$(EI)_{sec}$ 1.0E+12 (N mm^2)	$C_2 = \frac{(M_e)_{pi}}{(M_e)_o}$
0.00	35.9	22.1	8.2	21.0	37.9	3.7700	1.00
3.00	36.3	22.4	8.5	21.3	38.8	3.8608	1.01
18.0	38.6	23.6	9.2	22.4	40.0	3.9780	1.07
30.0	40.3	24.4	10.4	23.2	41.2	4.0989	1.10
42.0	42.1	25.1	11.7	23.9	41.6	4.1409	1.14
60.0	44.8	26.1	13.7	24.8	42.3	4.2153	1.18

5.3.3 Model Three

The stress-strain law of concrete used in the analysis in Model Three is Hognestad's parabola for the stress-strain curve in uniaxial compression, as shown in Fig.5-20 and discussed in Sect.4.3.1. The tensile stress of concrete is assumed to be zero.

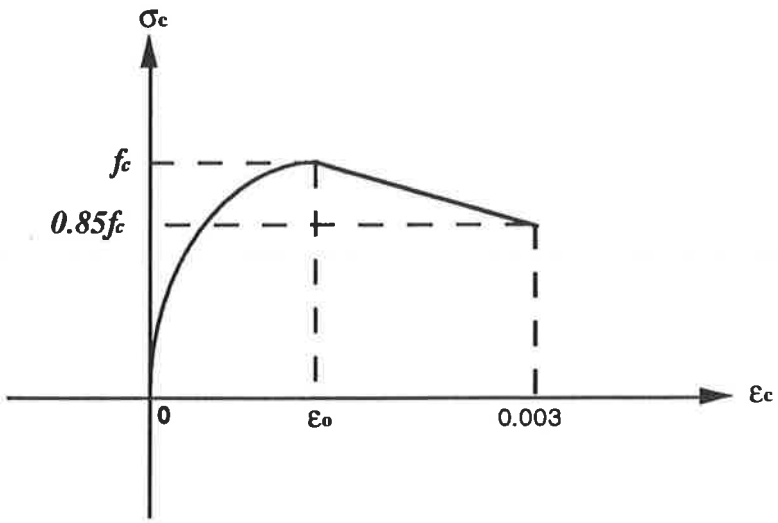

Fig.5-20 The stress-strain law of concrete used in Model Three

A family of the applied-moment versus total-curvature diagrams for the beams with the initial prestressing forces are shown in Fig.5-21. A family of the change in curvature $\Delta\theta$ of the section versus moment at the plate-end M_e are illustrated in Fig.5-22. The relationship between the flexural rigidity $(EI)_{sec}$ of the section and the moment M_e are plotted in Fig.5-23 and the variation of the coefficient C_1 with moment M_e diagrams are given in Fig.5-24.

5.3.3.1 Example of an Analysis

The results of a calculation of a beam with a prestressing force P_i = 30.0 kN are given in Table 5.5. The variations of strain and stress profiles in the section with the applied moment are shown in Fig.5-25a and Fig.5-25b, respectively.

Table 5.5

θ 1.0E-06 (mm^{-1})	$\Delta\theta$ 1.0E-06 (mm^{-1})	d_{ni} (mm)	ε_t 1.0E-06	ε_b 1.0E-06	M (kNm)	M_e (kNm)	$(EI)_{sec}$ 1.0E+12 (N mm^2)
-0.2487	0.0000	55.3	14	-31	0.0	0.0	7.41741
0.14906	0.3977	180	-27	0.00	3.0	1.9	7.41739
0.62034	0.8690	99.4	-62	50	5.6	3.7	6.48751
1.93733	2.1860	76.8	-150	200	11.7	7.6	5.33509
3.25032	3.4990	72.3	-235	350	17.5	11.5	5.00487
4.57730	4.8260	70.8	-324	500	23.3	15.3	4.82793
5.92229	6.1709	70.4	-416	650	29.0	19.0	4.70514
7.28928	7.5379	70.3	-512	800	34.7	22.7	4.60533
8.21553	8.4642	70.2	-580	900	38.5	25.2	4.54420

In this model the tensile strength of the concrete was assumed to be zero. Therefore, as soon as the strain in concrete section is greater than zero, in which the negative value of strain represents the compressive strain, the corresponding stress is equal to zero as shown in Fig.5-25b. It can be seen in Fig.5-25a that the strain in the section varies linear with the applied moment. The stress profiles shown in Fig.5-25b illustrate that the variations of stress in the section with the applied moment are linear at the lower applied moment stages. However, at the higher applied moment stages the stress in the section varies non-linearly with the moment as shown in Fig.5-25b. The calculated results in Table 5.5 show that the bottom strain in the concrete section is zero when the applied moment is 3.0 kNm. As soon as the applied moment is greater than 3.0 kNm the section changes from plated uncracked to plated cracked.

5.3.3.2 Results of analysis

The results of the applied-moment versus total-curvature are shown in Fig.5-21. For those beams with the initial prestressing forces, the kink occurs when the strain in the bottom fibre concrete section is equal to zero. As the moment is increased the flexural rigidity of the section changes from plated uncracked to plated cracked. Figure.5-22 indicates that for those beams with prestressing forces the slope of the plots are the same during the uncracked stages and the change in the slope depend upon the prestressing forces applied in the section. The change in slope is delayed as the result of the greater prestressing force.

The variation of the flexural rigidity with the moment at the plate-end are shown in Fig.5-23. It can be seen that for the beam without prestressing forces, the stiffness of the section reduces progressively with increasing moment due to the non-linear behaviour of the concrete. Furthermore, for those beams with prestressing forces, the flexural rigidity of the section is a constant and is equal to the flexural rigidity of the plated uncracked section. After cracking the stiffness of the beam reduces gradually

as the moment increases and the stiffness tends to approach the flexural rigidity of the plated cracked section. The prestressing forces postpone the change in stiffness from the plated uncracked section to the plated cracked section.

Figure 5-24 illustrates the relationship between moment M_e at the plate-end and the coefficient C_1. It can be seen in Fig.5-24 that there is a slight kink in the curves which indicates that the section changes from plated uncracked to plated cracked. The debonding moment, ie. when C_1 equals to 1.17 in Fig.5-24 increases due to the increase in the initial prestressing force.

5.3.3.3 Summary of results

A comparison of all the results are given in Table 5.6 and shown in Fig.5-26. The increase in the debonding moment ranges from 1 per cent to 16 per cent.

Table 5.6 Calculated data in Model Three

P_i (kN)	V_{uc} (kN)	V_e (kN)	M_e (kNm)	M_{up} (kNm)	$(EI)_{sec}$ 1.0E+12 (N mm^2)	$C_2 = \frac{(M_e)_{pi}}{(M_e)_o}$
0.00	35.9	23.7	22.5	44.1	4.38971	1.00
3.00	36.3	23.9	22.7	44.4	4.41958	1.01
18.0	38.6	24.9	23.7	45.2	4.49921	1.05
30.0	40.3	25.7	24.4	45.9	4.56889	1.08
42.0	42.1	26.5	25.2	46.6	4.63856	1.12
60.0	44.8	27.6	26.2	47.2	4.69829	1.16

5.3.4 Model Four

The stress-strain law of concrete used in this analysis is Hognestad's parabola of idealised stress-strain curve in uniaxial compression as used in Model Three. However in this case the tensile strength of concrete is taken into account as shown in Fig.5-27.

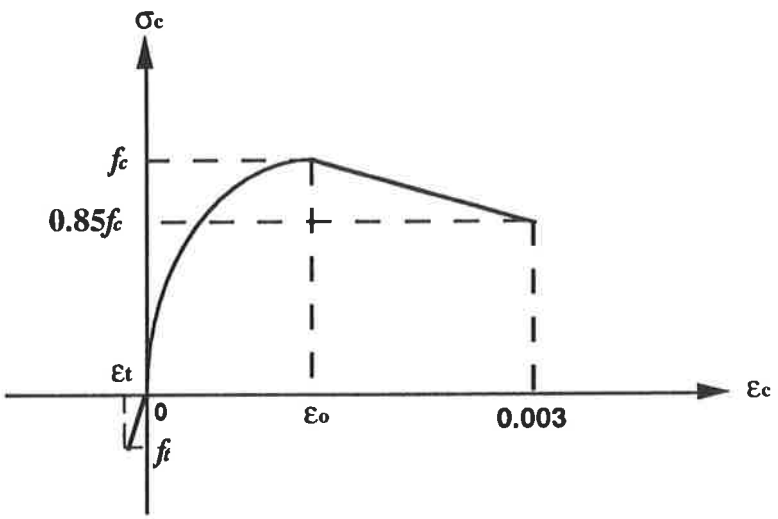

Fig.5-27 The stress-strain law of concrete used in model four

The family of the applied-moment versus total-curvature diagrams of beams with the six different degrees of the initial prestressing forces are shown in Fig.5-28. A family of the change in curvature $\Delta\theta$ of the section versus moment M_e at the end of the plate are plotted in Fig.5-29. The relationship between the flexural rigidity $(EI)_{sec}$ of the section and moment M_e at the plate-end are illustrated in Fig.5-30 and the relationship between the coefficient C_1 and moment M_e diagrams are given in Fig.5-31.

5.3.4.1 Example of an Analysis

The results of the calculations for a beam with a prestressing forces Pi = 30.0 kN are given in Table 5.7. The strain and stress profiles in the section vary with the applied moment are illustrated in Fig.5-32a and Fig.5-32b, respectively.

Table 5.7

θ 1.0E-06 (mm^{-1})	$\Delta\theta$ 1.0E-06 (mm^{-1})	d_{ni} (mm)	ε_t 1.0E-06	ε_b 1.0E-06	M (kNm)	M_e (kNm)	$(EI)_{sec}$ 1.0E+12 (N mm^2)
-0.2148	0.00000	42.6	9	-30	0.0	0.0	7.41731
0.18162	0.39637	180	-33	0.00	3.0	1.9	7.41731
0.74516	0.95991	107	-80	55	7.1	4.7	7.39653
1.26825	1.48700	98.7	-125	100	11.0	7.2	7.39744
2.50500	2.71975	80.2	-201	250	15.1	9.9	5.55630
3.78499	3.99974	74.3	-281	400	20.2	13.2	5.05752
5.09998	5.31473	72.2	-368	550	25.7	16.9	4.84082
6.43596	6.65037	71.2	-458	700	31.3	20.5	4.70202
7.34795	7.56270	71.1	-523	800	35.0	22.9	4.63025
8.26923	8.48398	71.0	-588	900	38.7	25.4	4.56362

Comparing with the stress profiles as shown in Fig.5-25b, it can be seen in Fig.5-32b that the section has tensile stress due to the tensile strength of concrete. Also the compressive stress profiles in the section at the high applied moment vary non-linearly with the moment as expected. Table 5.7 indicates that the depth of neutral axis reduces gradually with the increase in the applied moment until debonding of the soffit plate takes place.

5.3.4.2 Results of Analysis

The curvature varies linearly with the moment during the uncracked stage, and then the slope changes as shown in Fig.5-28 and Fig.5-29 respectively. The results of the flexural rigidity $(EI)_{sec}$ versus moment M_e shown in Fig.5-30 indicate that at

uncracked stages the flexural rigidity of all the beams is constant. The stiffness reduces gradually until debonding has taken place. It can be seen in Fig.5-31 that the increase in moment, M_e, at the end of soffit steel plate is the results of the greater initial prestressing forces applied to the section.

5.3.4.3 Summary of results

The results of comparison are given in Table 5.8 and shown in Fig.5-33. The increase in the debonding moment of the plated reinforced concrete beams is from 1 per cent to 17 per cent.

Table 5.8 Calculated data in model four

P_i (kN)	V_{uc} (kN)	V_e (kN)	M_{cr} (kNm)	M_e (kNm)	M_{up} (kNm)	$(EI)_{sec}$ 1.0E+12 (N mm^2)	$C_2 = \frac{(M_e)_{pi}}{(M_e)_o}$
0.00	35.9	23.8	9.2	22.6	44.2	4.40166	1.00
3.00	36.3	23.9	9.4	22.8	44.5	4.42953	1.01
18.0	38.6	25.0	10.3	23.8	45.4	4.51912	1.05
30.0	40.3	25.8	11.2	24.5	46.1	4.58879	1.08
42.0	42.1	26.6	12.3	25.3	46.8	4.65847	1.12
60.0	44.8	27.7	14.2	26.4	47.7	4.74806	1.17

5.3.5 Model Five

The stress-strain law of concrete used in this analysis is shown in Fig.5-34. The concrete compression part is Hognestad's parabola and the tension part allows for tension stiffness as described in Section 4.3.2.

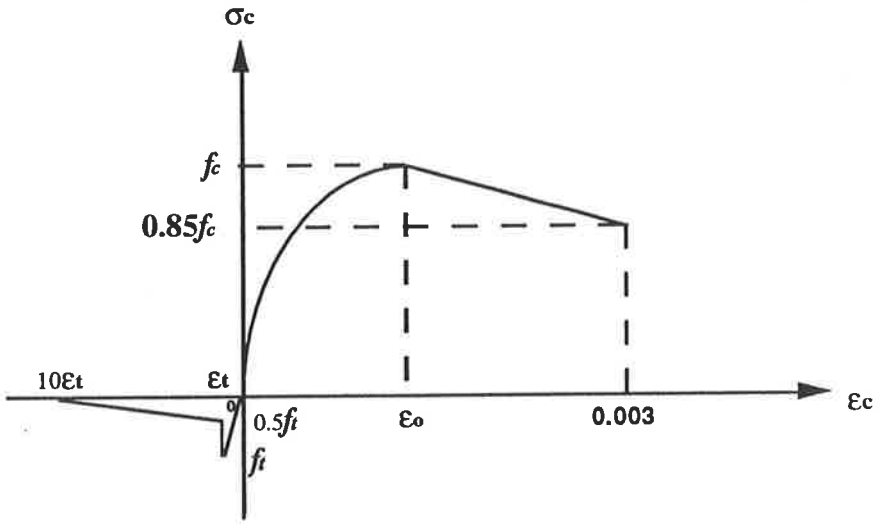

Fig.5-34 The stress-strain law of concrete used in model five

5.3.5.1 Example of an Analysis

The variation of strain and stress profiles in the section with the applied moment are illustrated in Fig.5-39a and Fig.5-39b, respectively. The results of the calculations for a beam with prestressing forces P_i = 30.0 kN are given in Table 5.9.

It can be seen in Fig.5-39a that the strain profiles in the section are the same as the previous models. However the stress profiles are different as shown in Fig.5-39b. The variations of the stress in the section with the applied moment are almost linear prior to cracking. After cracking and at the moment up to debonding moment, the compressive stresses in the section vary non-linearly with the moment and the tensile stresses are proportional to the strains.

Table 5.9

θ 1.0E-06 (mm^{-1})	$\Delta\theta$ 1.0E-06 (mm^{-1})	d_{ni} (mm)	ε_t 1.0E-06	ε_b 1.0E-06	M (kNm)	M_e (kNm)	$(EI)_{sec}$ 1.0E+12 (N mm^2)
-0.2148	0.00000	42.6	9	-30	0.0	0.0	7.41741
0.18157	0.39632	180	-33	0.00	3.0	1.9	7.41718
1.27457	1.81992	99.7	-126	115	13.5	7.2	7.41763
2.17853	2.39329	88.2	-192	200	15.6	10.2	6.51689
4.11510	4.62626	78.0	-344	450	24.9	16.3	5.37795
7.10848	7.32323	74.5	-530	750	35.6	23.3	4.86438
8.02165	8.23640	74.0	-594	850	39.1	25.6	4.75075

5.3.5.2 Results of analysis

A family of the applied-moment versus total-curvature diagrams of beams with varying degrees of the initial prestressing forces are shown in Fig.5-35 and a family of the change in curvature $\Delta\theta$ with moment M_e at the end of plate are given in Fig.5-36. The relationship between the flexural rigidity $(EI)_{sec}$ and moment M_e are plotted in Fig.5-37. The variation of the coefficient C_1 with moment M_e are shown in Fig.5-38. Comparing with Model Four, the change in slope at the kink is less in Model Five than that in Model Four, as illustrated in Fig.5-35 and Fig.5-36, respectively.

5.3.5.3 Summary of results

A comparison of the results is given in Table 5.10 and shown in Fig.5-40. It can be seen in Fig.5-40 that the increase in the debonding moment given by ratio C_2 is proportional to the initial prestressing forces P_i applied to the section.

Table 5.10 Calculated data in model five

P_i (kN)	V_{uc} (kN)	V_e (kN)	M_{cr} (kNm)	M_e (kNm)	M_{up} (kNm)	$(EI)_{sec}$ 1.0E+12 (N mm^2)	$C_2 = \frac{(M_e)_{pi}}{(M_e)_o}$
0.00	35.9	24.2	10.0	23.0	46.2	4.59875	1.00
3.00	36.3	24.4	10.5	23.2	46.4	4.61866	1.01
18.0	38.6	25.4	12.3	24.2	47.2	4.69829	1.05
30.0	40.3	26.3	13.5	25.0	48.0	4.77792	1.09
42.0	42.1	26.9	14.9	25.7	48.7	4.84760	1.12
60.0	44.8	28.3	17.0	26.9	49.9	4.96705	1.17

5.4 Comparison of analysis models

To predict the debonding forces, M_e and V_e, and the flexural rigidity, $(EI)_{sec}$, of the prestressed plated beams, five different models were used in the analysis as described above. The results of the five models are compared in Fig.5-41 and Fig.5-42.

It can be seen in Fig.5-41 that the slope of the moment-curvature relationship in Model One is the same as that in Model Two during uncracked stages as would be expected. After cracking, the slope of Model Two is parallel to that in Model One. Also, before cracking, the slope of Model Three is the same as that in Model Four and Five. As the moment further increases the slope of Model Four and Five tend to be close to that in Model Three. It can be seen in Fig.5-42 that the debonding moment calculated from Model Three, Four and Five are greater than that from Model One and Two, but the difference is not significant.

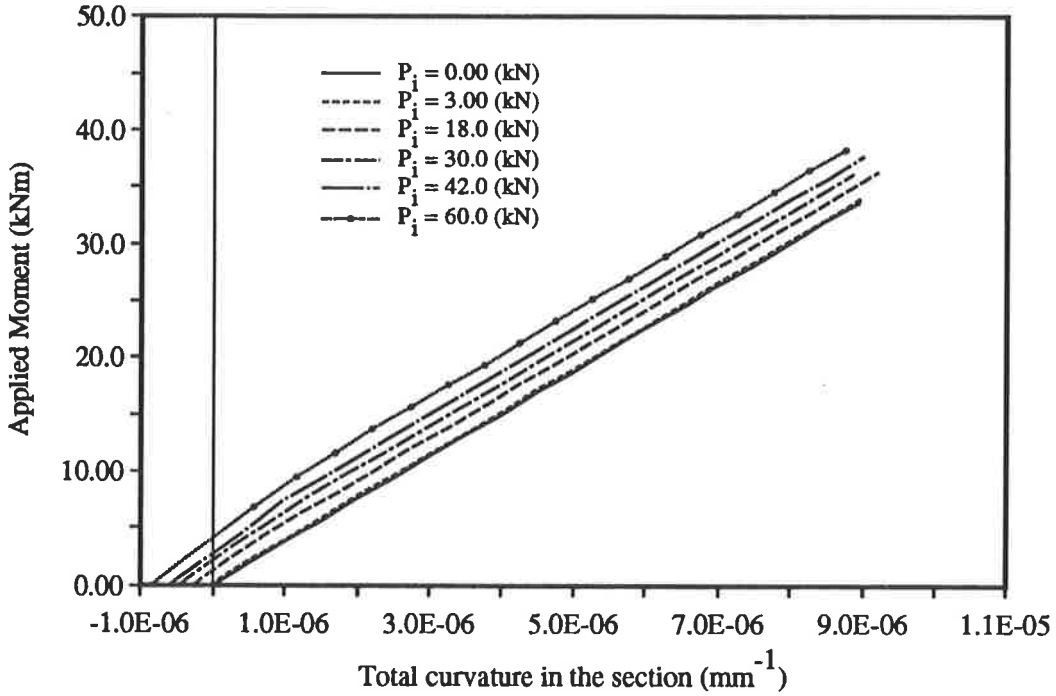

Fig.5-7 Moment versus curvature for Model One

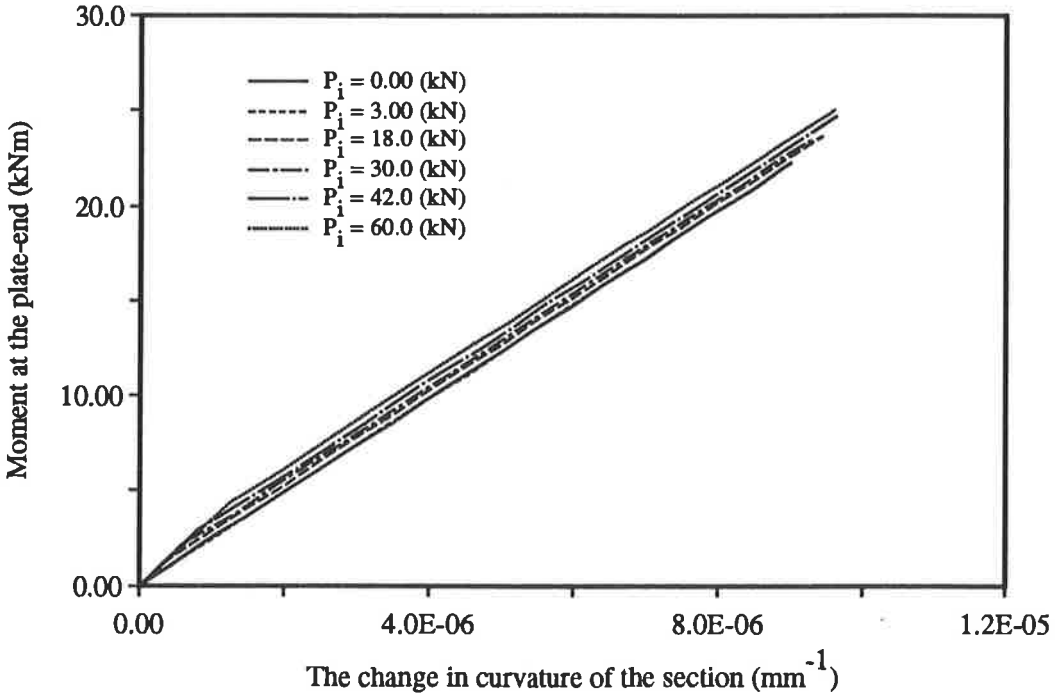

Fig.5-8 Moment versus the change in curvature for Model One

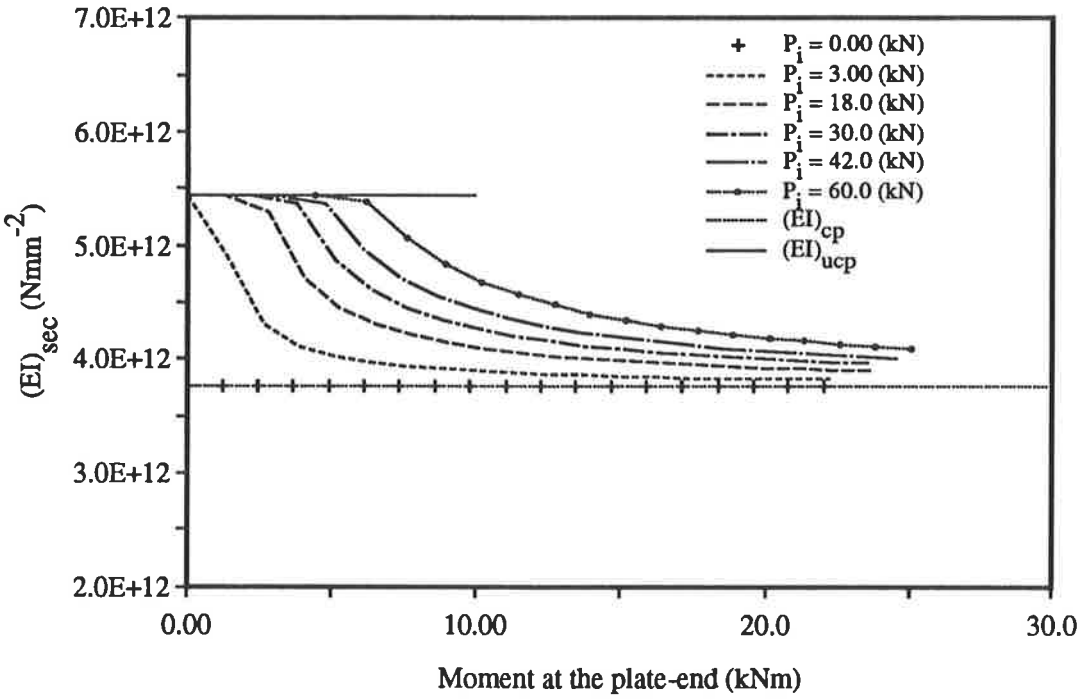

Fig.5-9 The variation of peeling flexural rigidity with moment for Model One

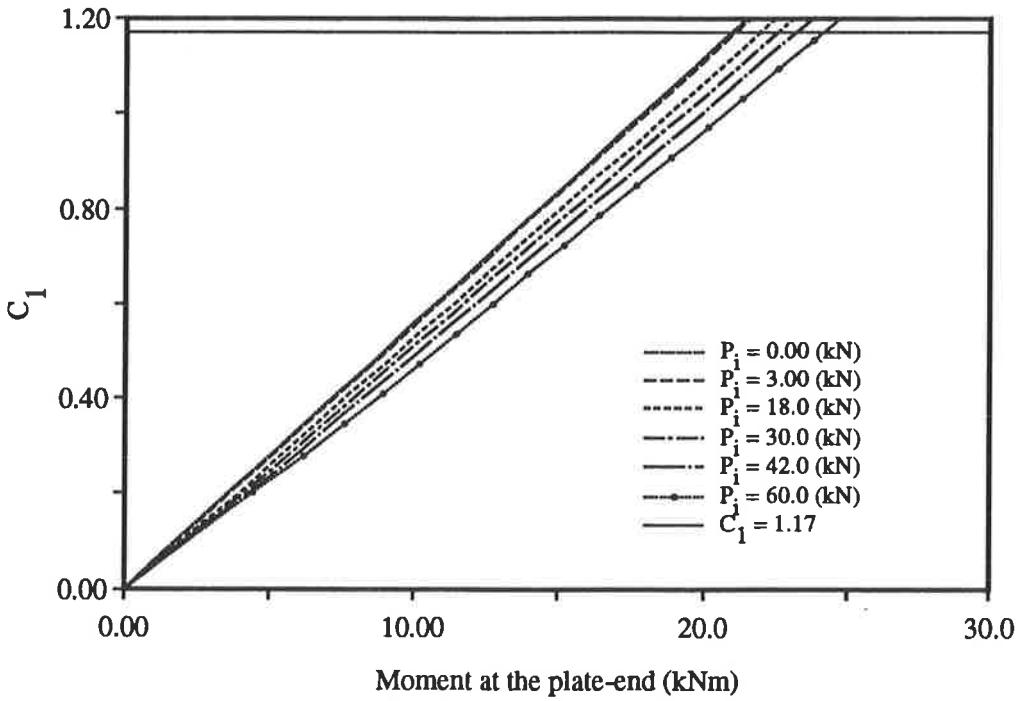

Fig.5-10 The relationship between C_1 and moment at the plate-end for Model One

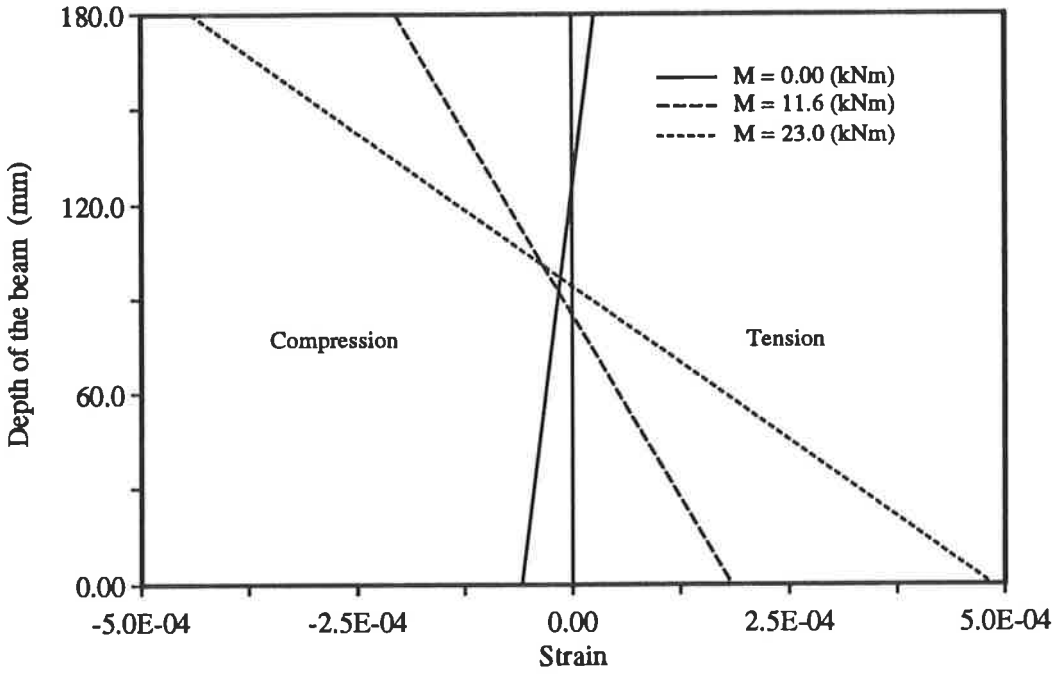

Fig.5-11a The variation of strain profile with the applied moment for Model One

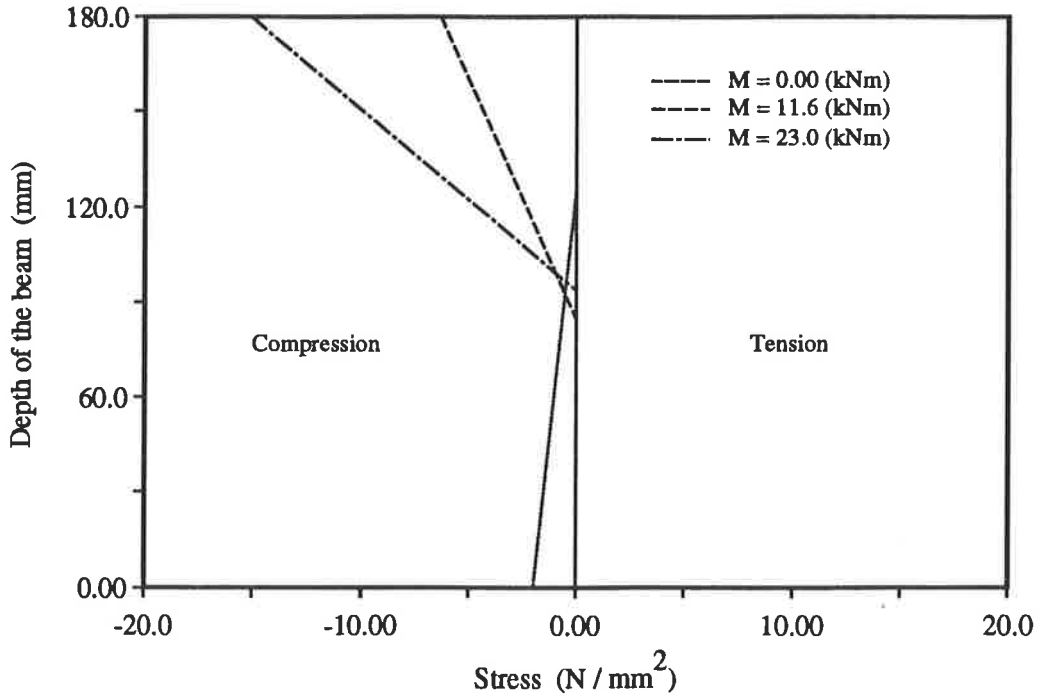

Fig.5-11b The variation of stress profile with the applied moment for Model One

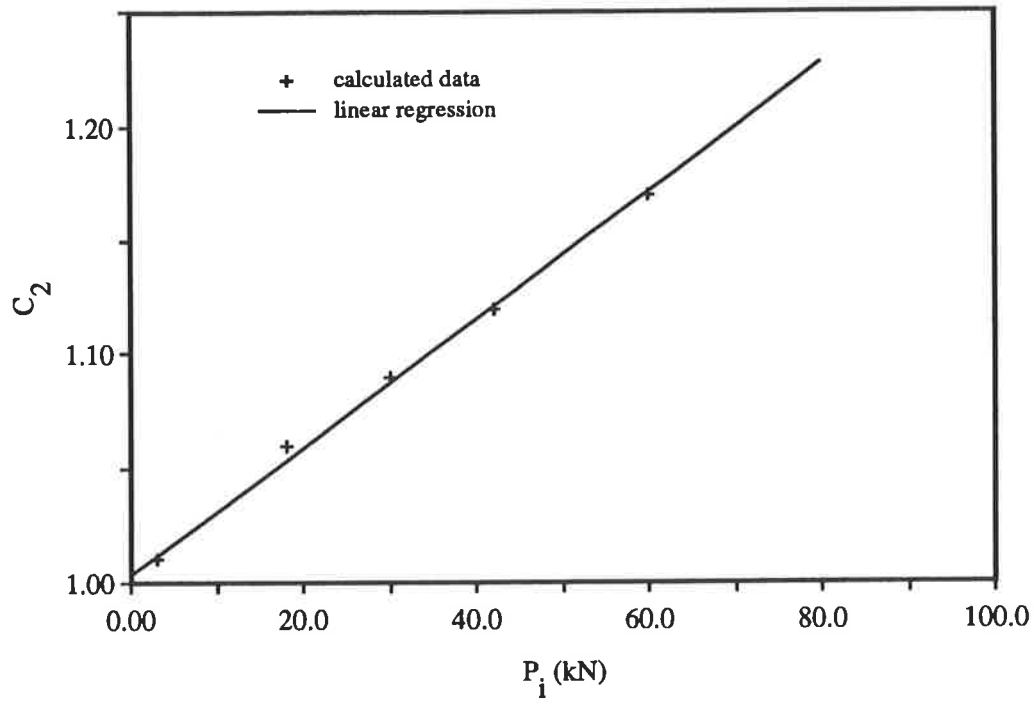

Fig.5-12 The relationship between C_2 and the prestressing forces P_i for Model One

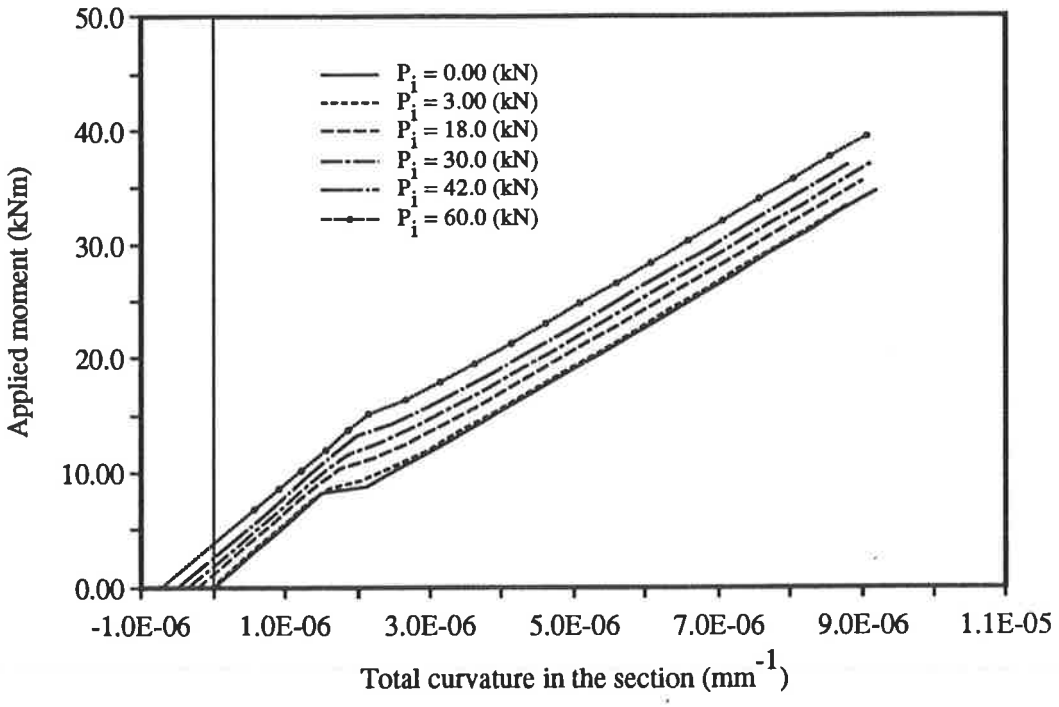

Fig.5-14 Moment versus curvature for Model Two

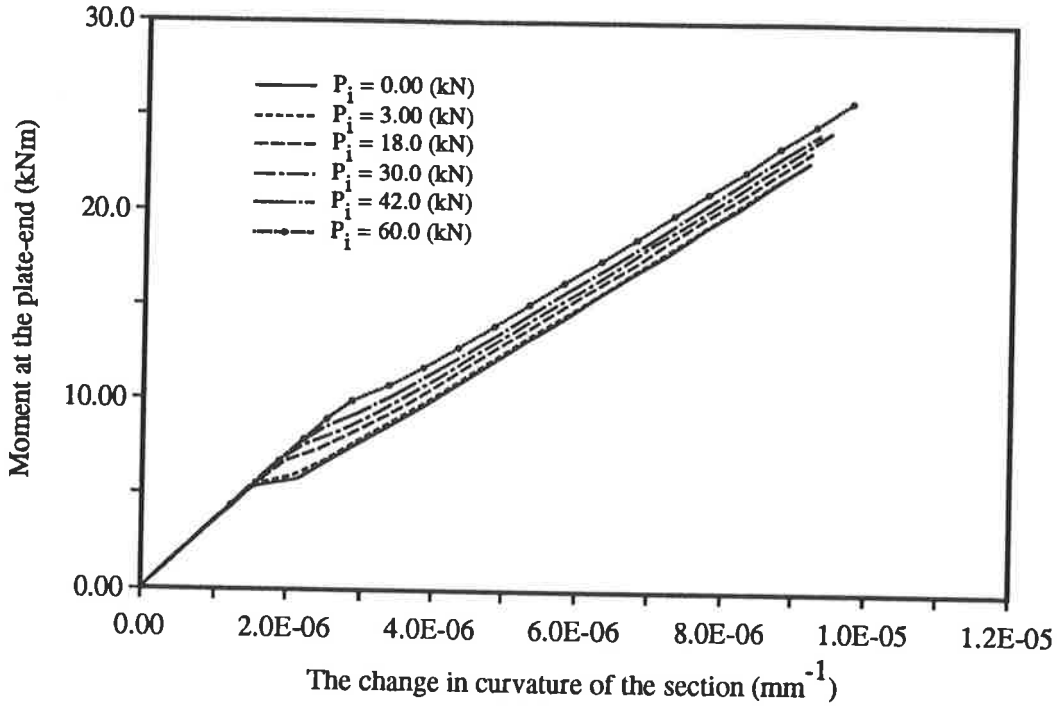

Fig.5-15 Moment versus the change in curvature for Model Two

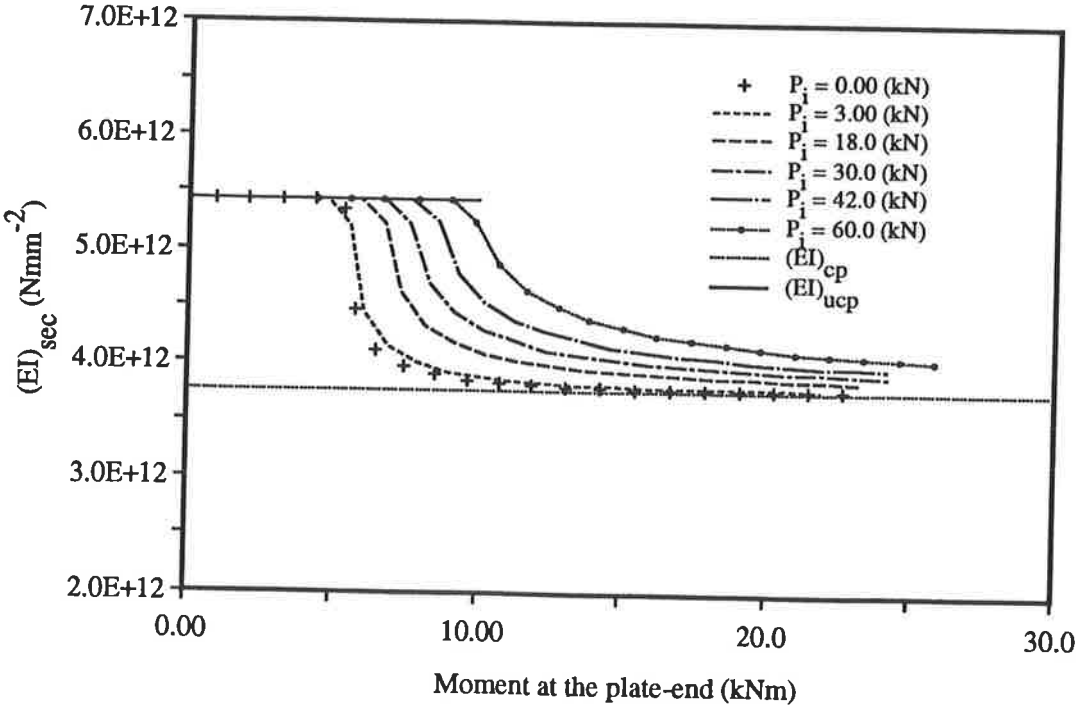

Fig.5-16 The variation of peeling flexural rigidity with moment for Model Two

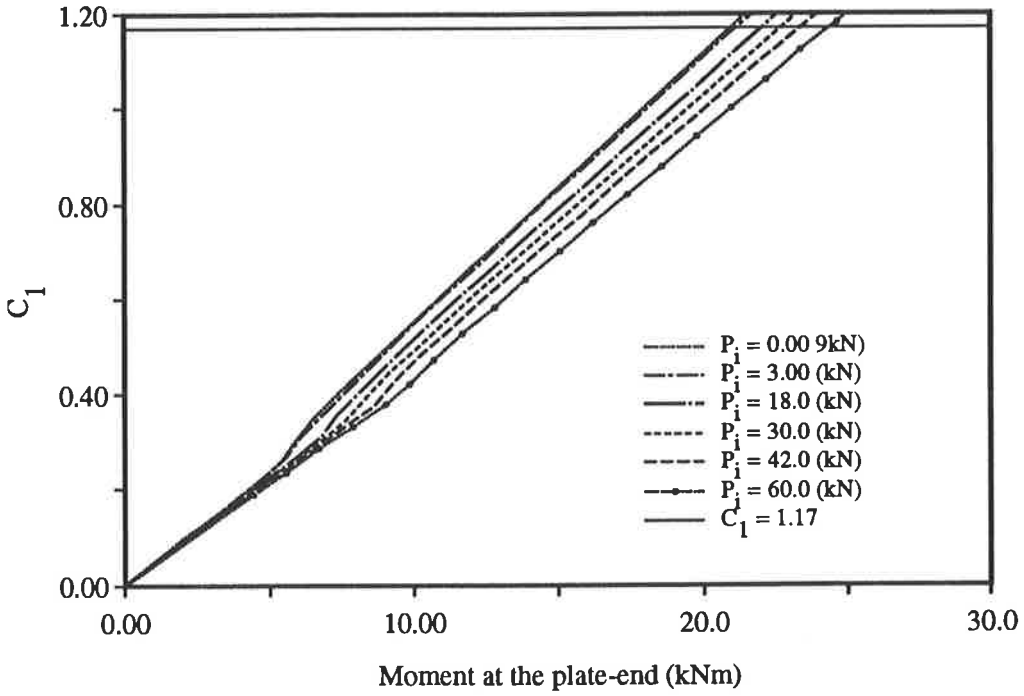

Fig.5-17 The relationship between C_1 and moment at the plate-end M_e for Model Two

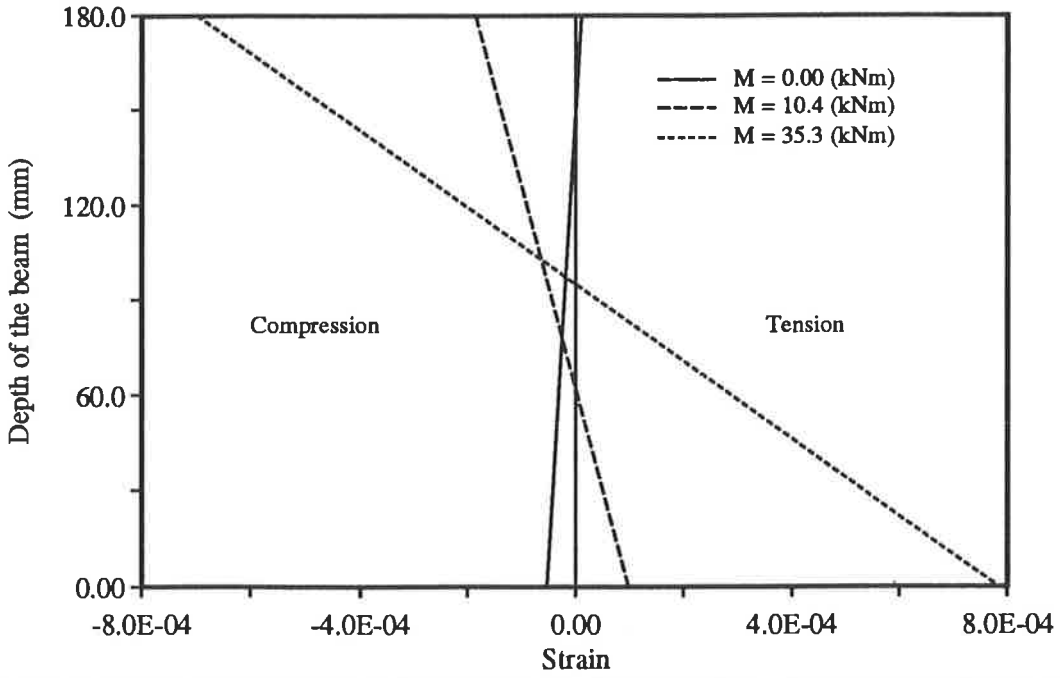

Fig.5-18a The variation of strain profile with the applied moment for Model Two

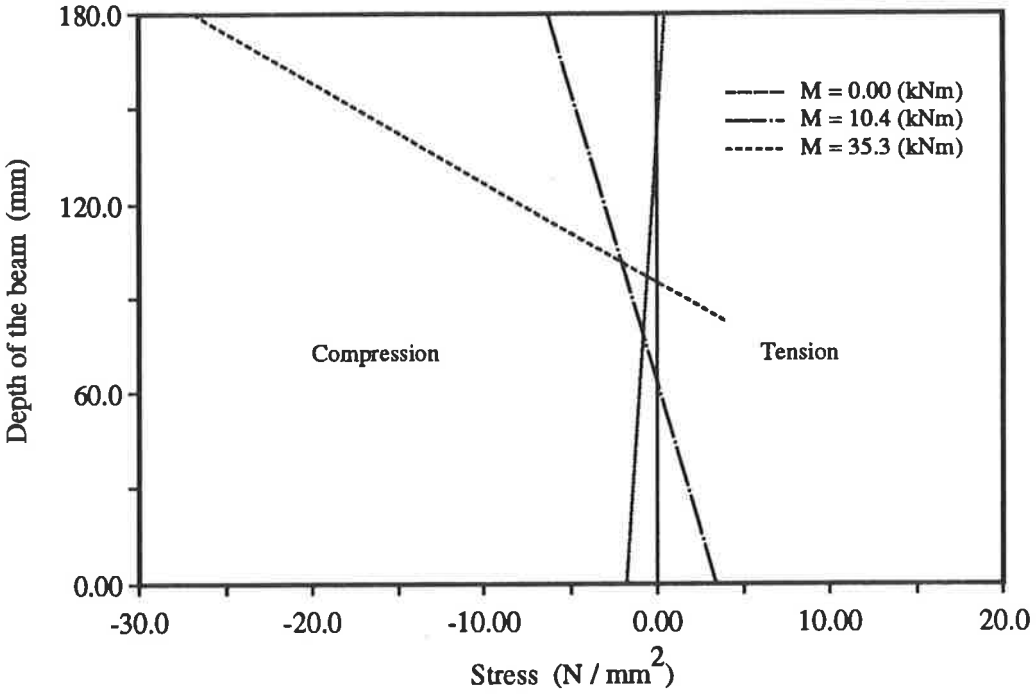

Fig.5-18b The variation of stress profile with the applied moment for Model Two

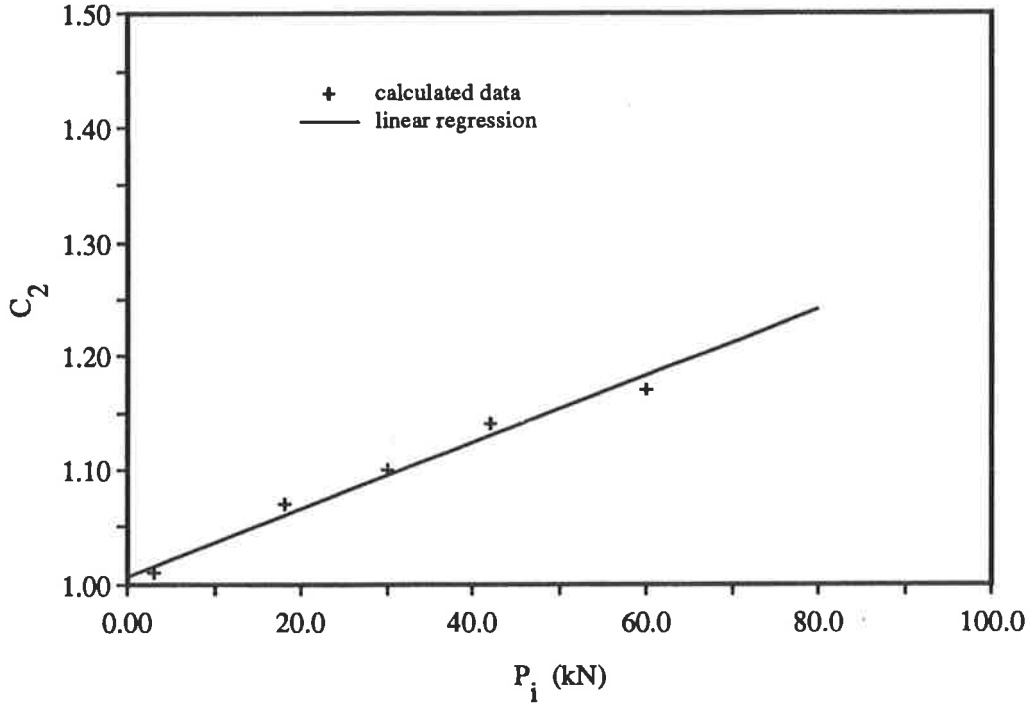

Fig.5-19 The relationship between C_2 and the prestressing forces P_i for Model Two

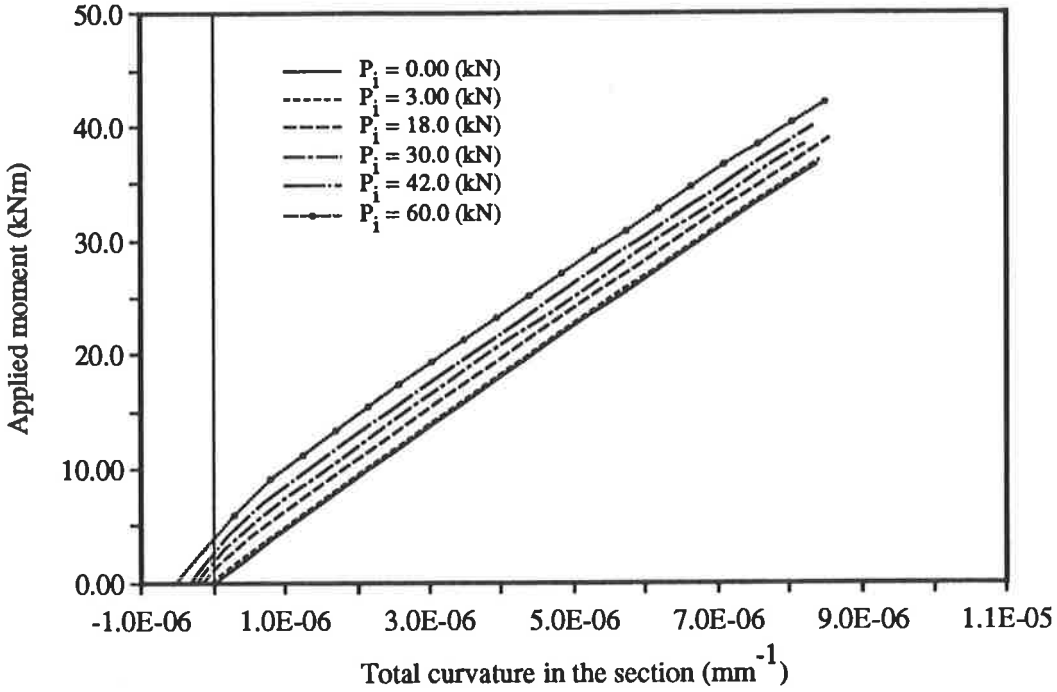

Fig.5-21 Moment versus curvature for Model Three

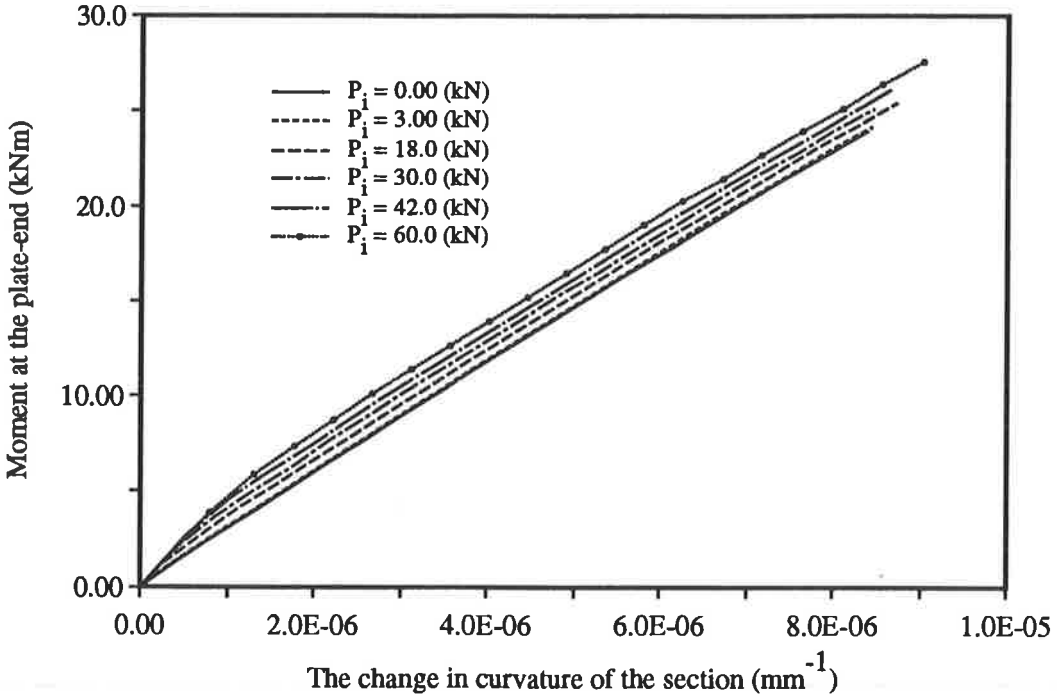

Fig.5-22 Moment versus the change in curvature for Model Three

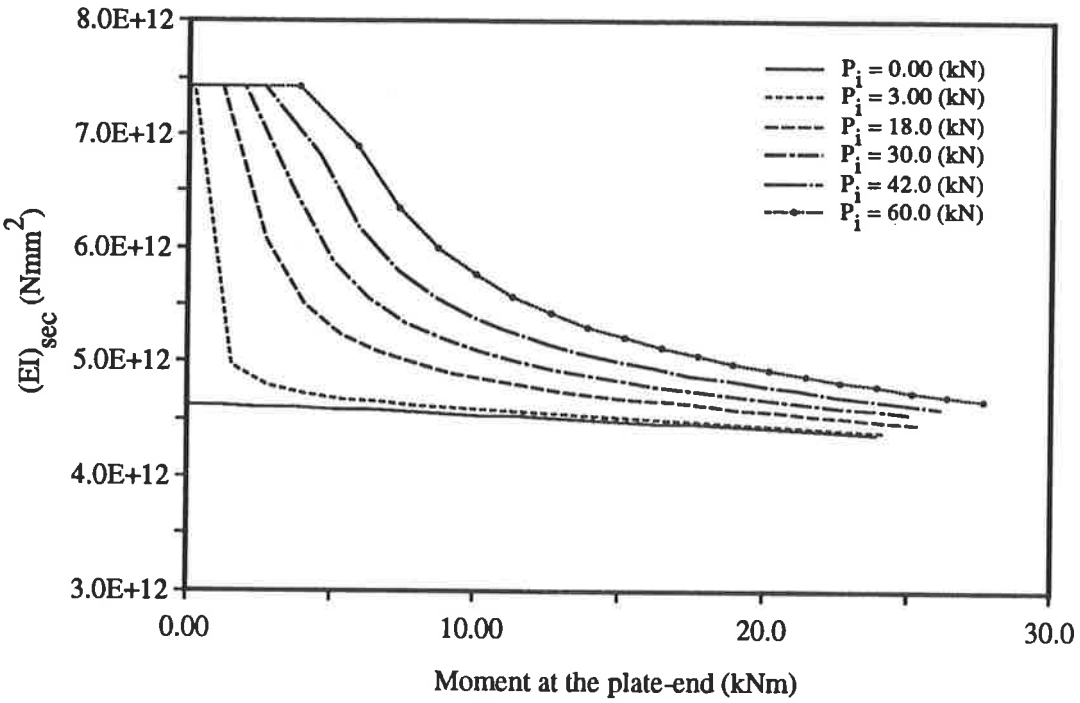

Fig.5-23 The variation of peeling flexural rigidity with moment for Model Three

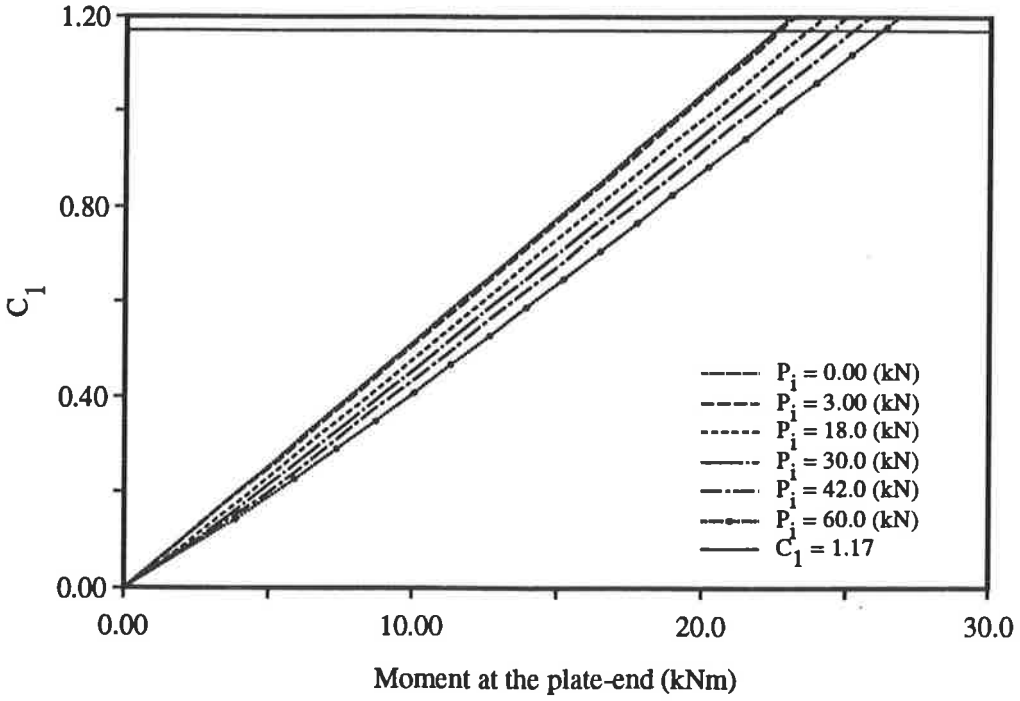

Fig.5-24 The relationship between C_1 and moment at the plate-end M_e for Model Three

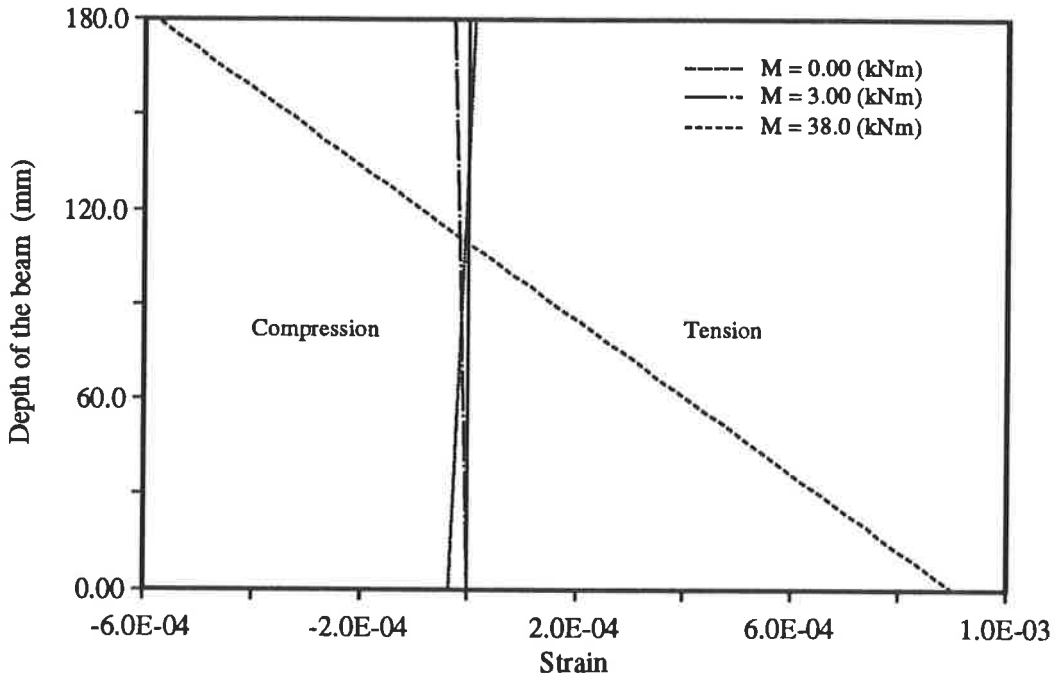

Fig.5-25a Variation of strain profile with the applied moment for Model Three

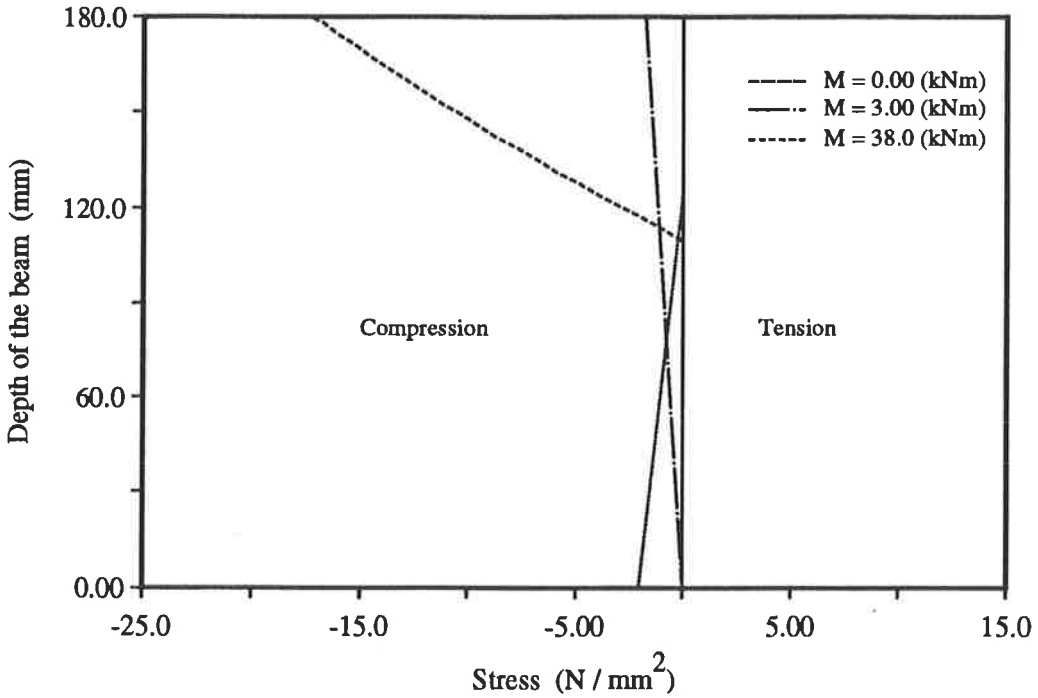

Fig.5-25b Variation of stress profile with the applied moment for Model Three

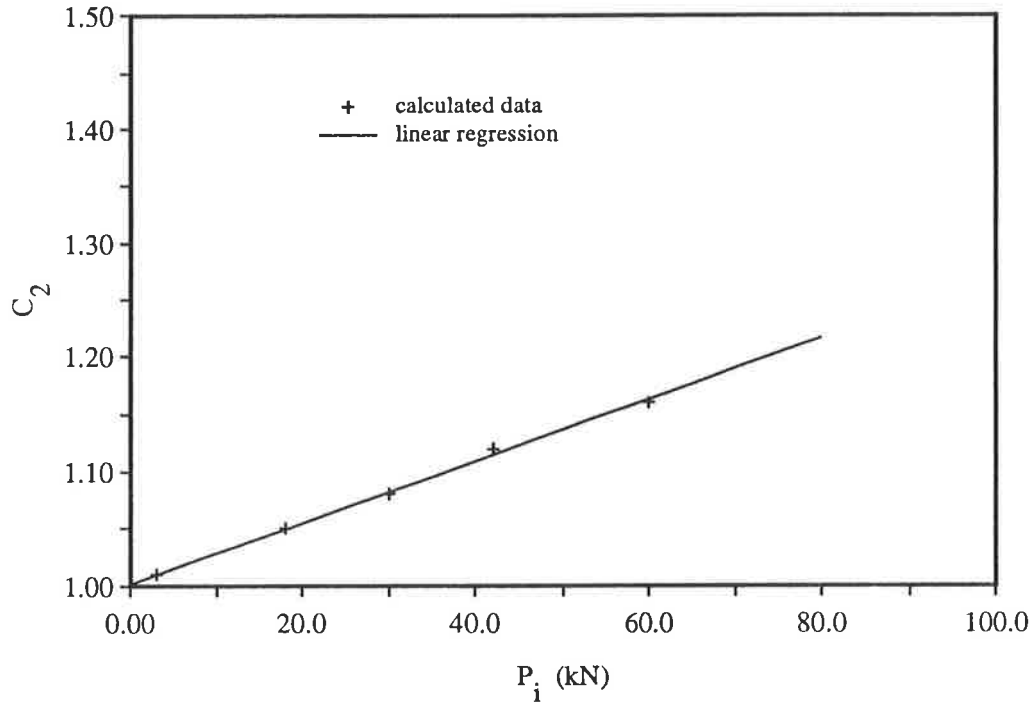

Fig.5-26 The relationship between C_2 and the prestressing forces P_i for Model Three

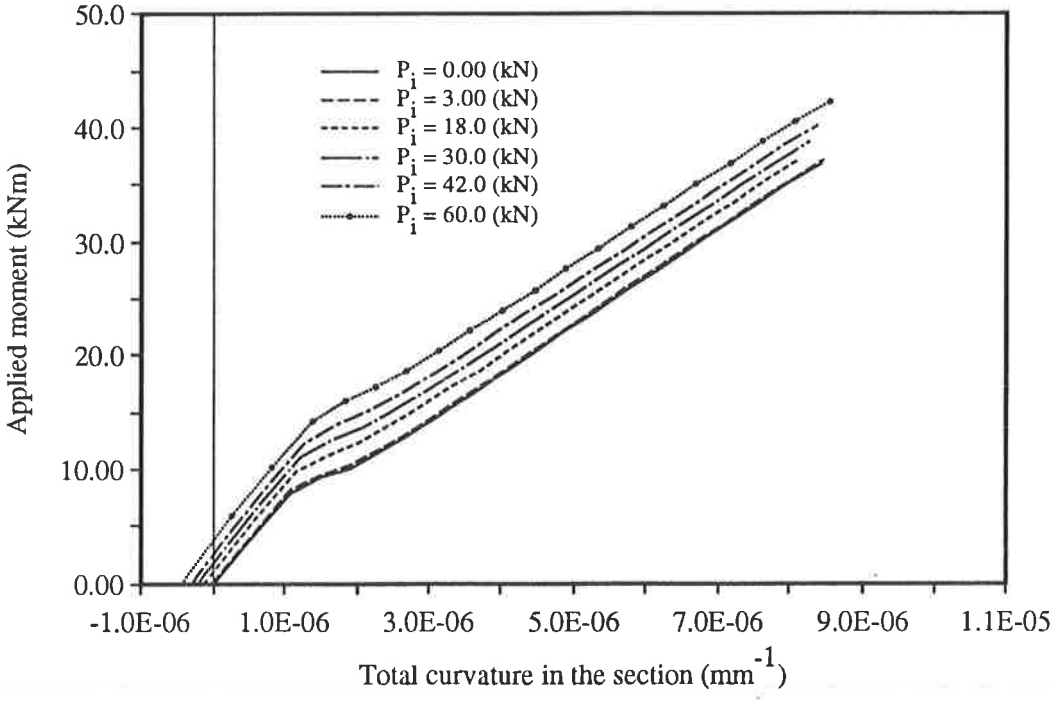

Fig.5-28 Moment versus curvature for Model Four

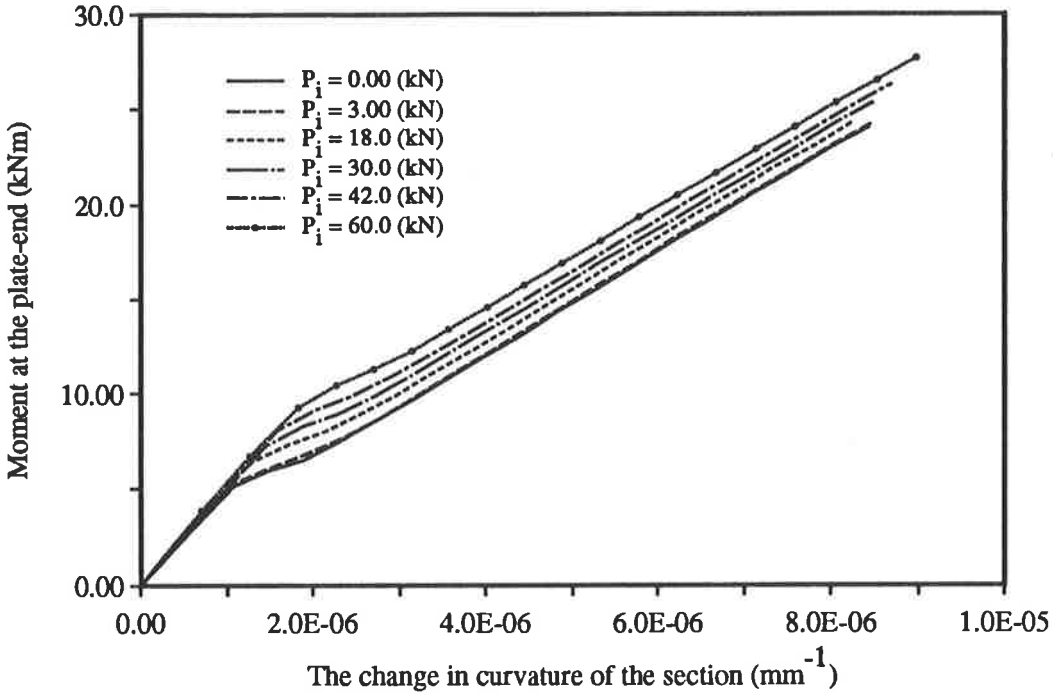

Fig.5-29 Moment versus the change in curvature for Model Four

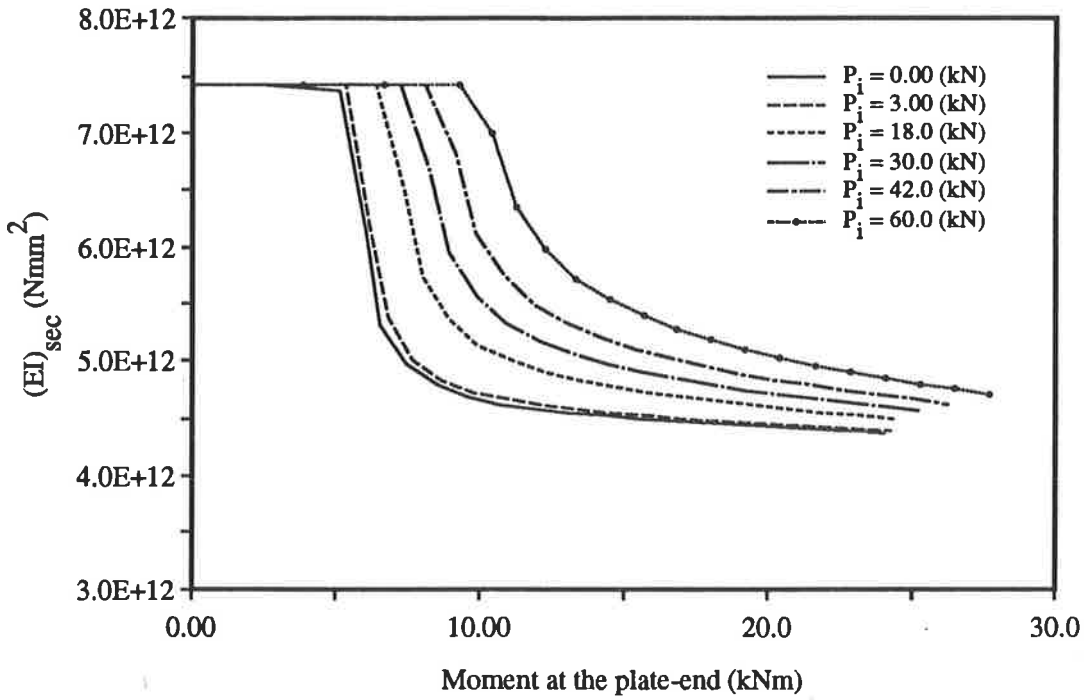

Fig.5-30 The variation of peeling flexural rigidity with moment for Model Four

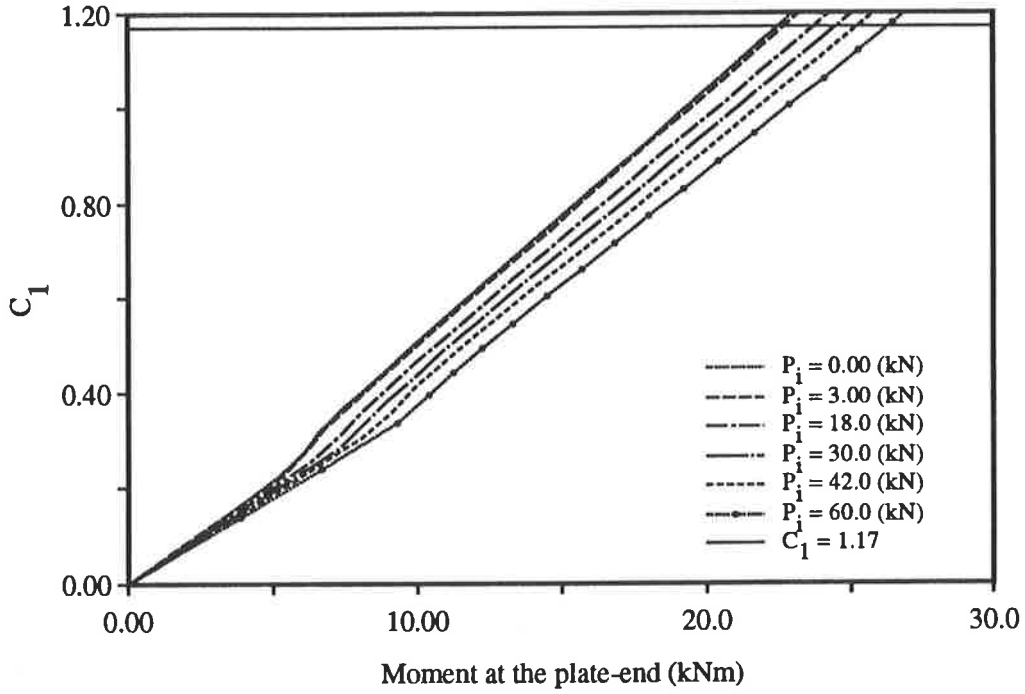

Fig.5-31 The relationship between C_1 and moment at the plate-end M_e for Model Four

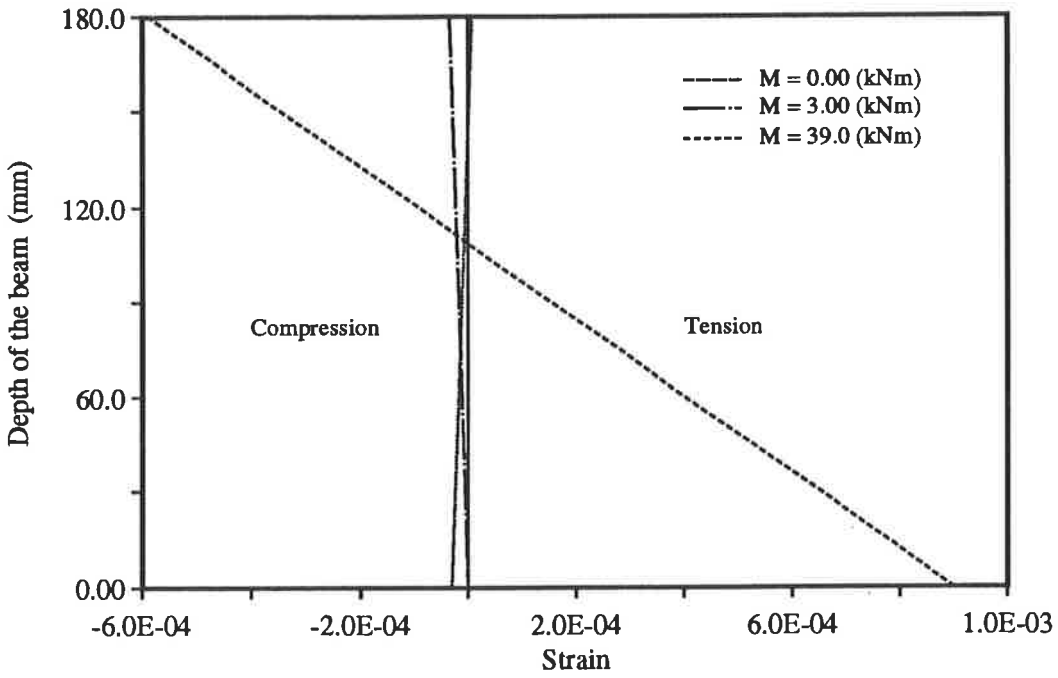

Fig.5-32a The variation of strain profile with the applied moment for Model Four

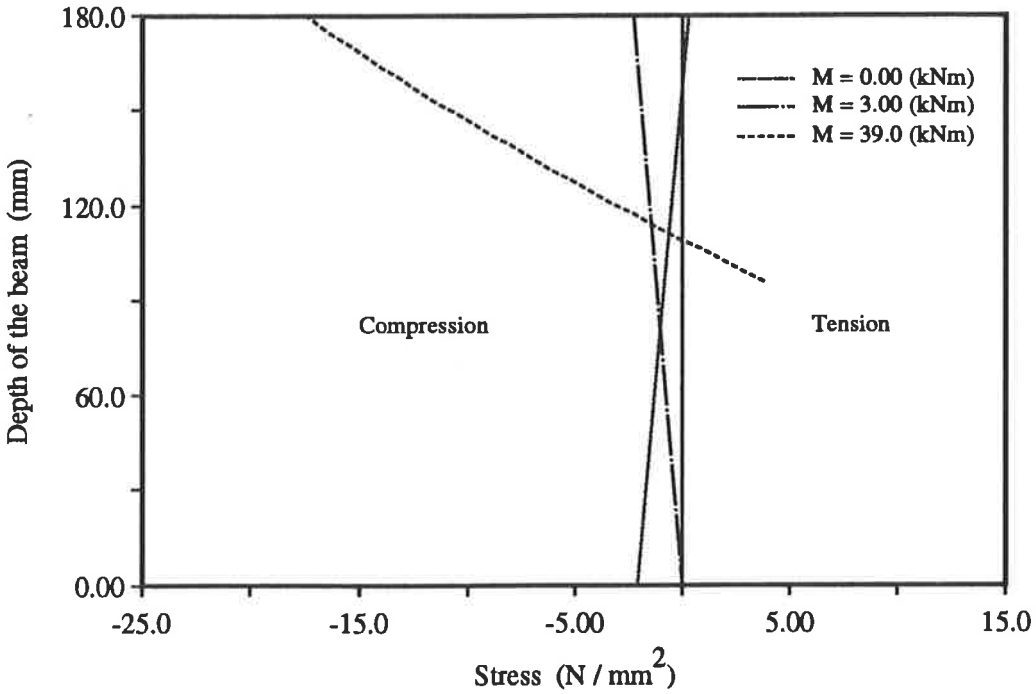

Fig.5-32b The variation of stress profile with the applied moment for Model Four

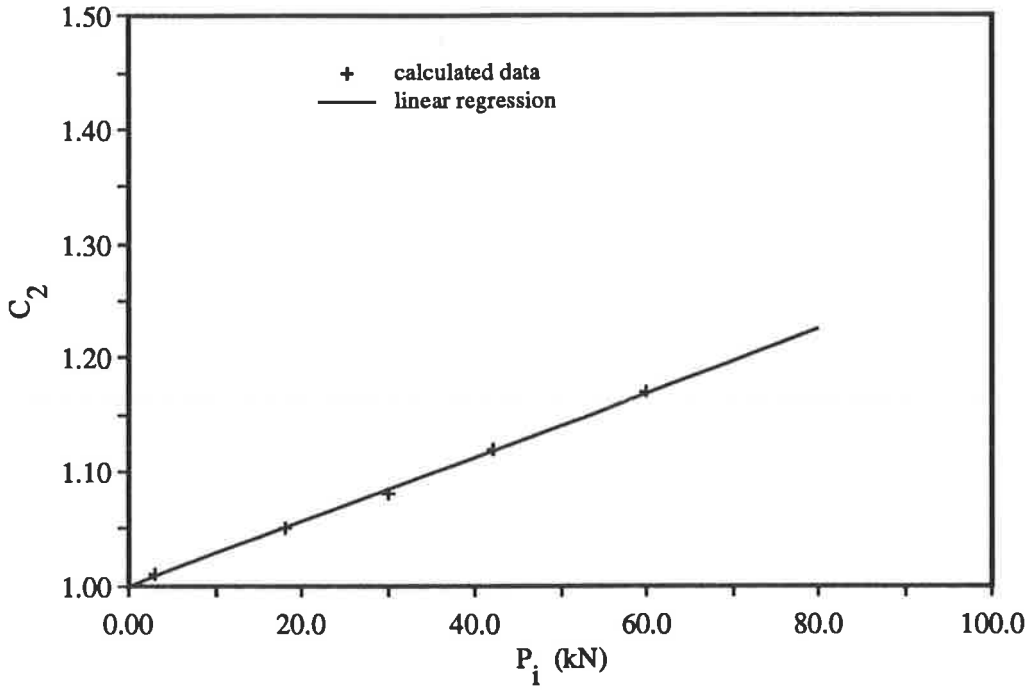

Fig.5-33 The relationship between C_2 and the prestressing forces P_i for Model Four

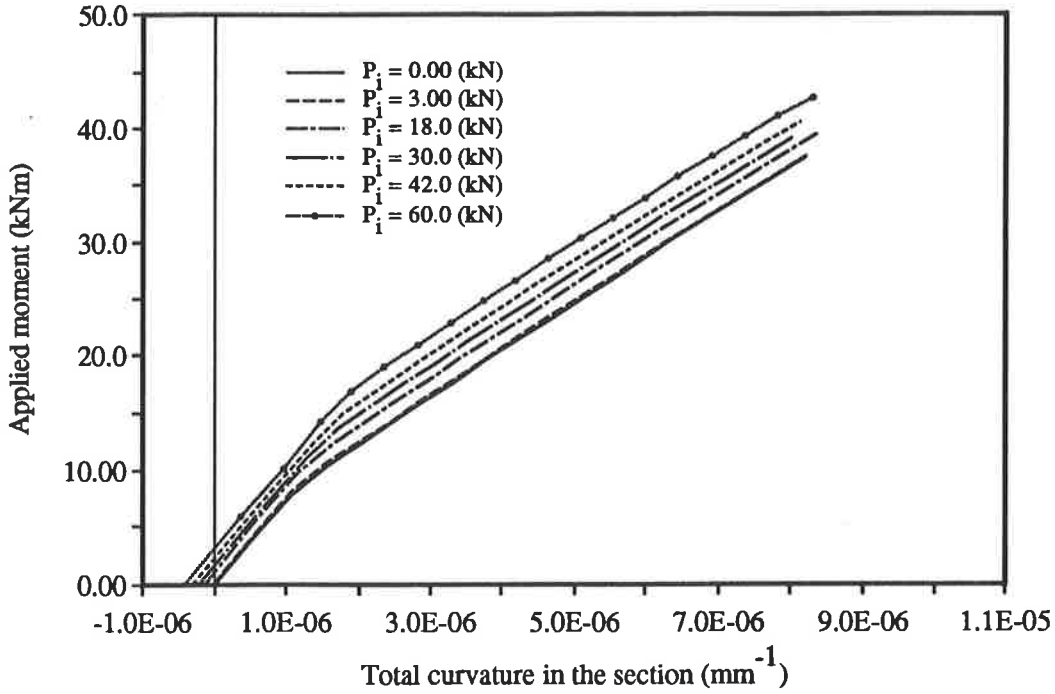

Fig.5-35 Moment versus curvature for Model Five

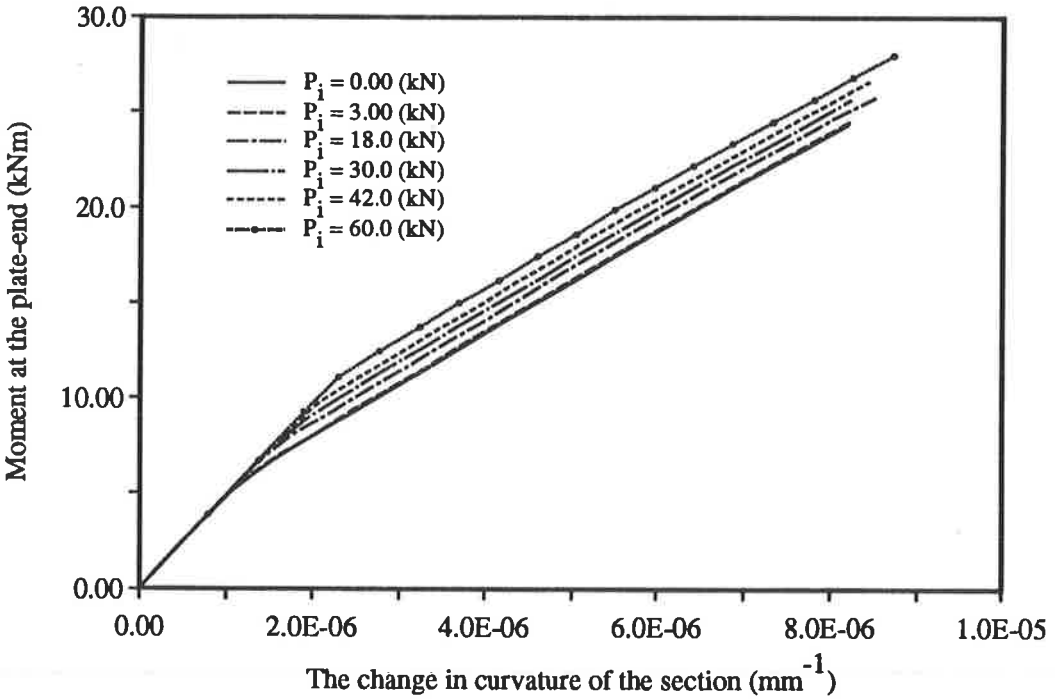

Fig.5-36 Moment versus the change in curvature for Model Five

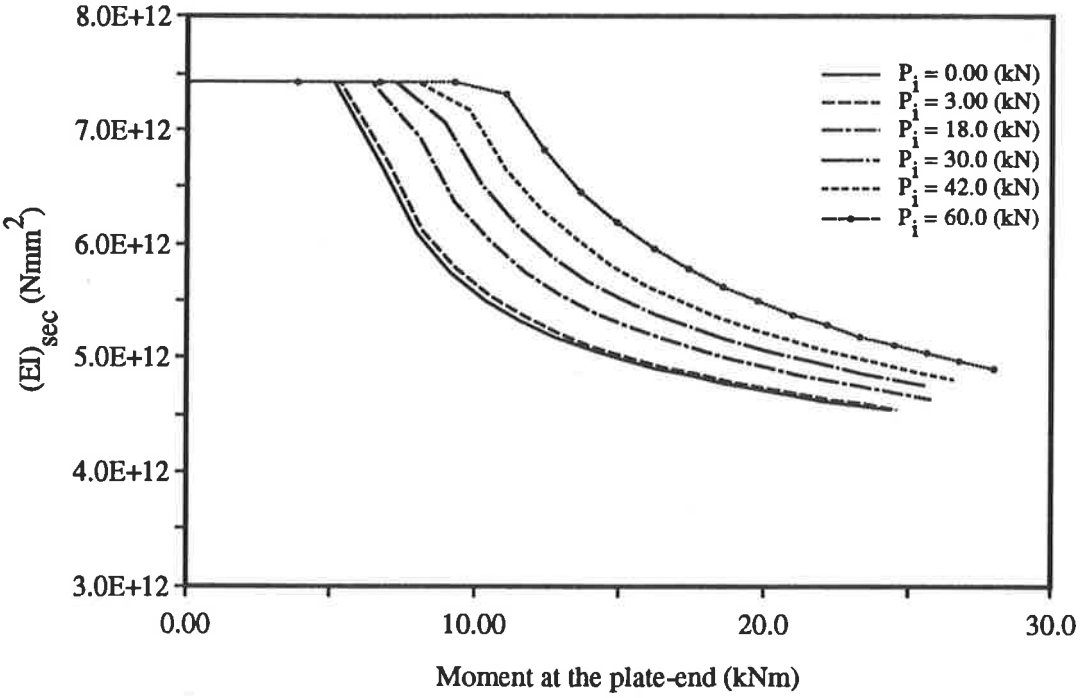

Fig.5-37 The variation of peeling flexural rigidity with moment for Model Five

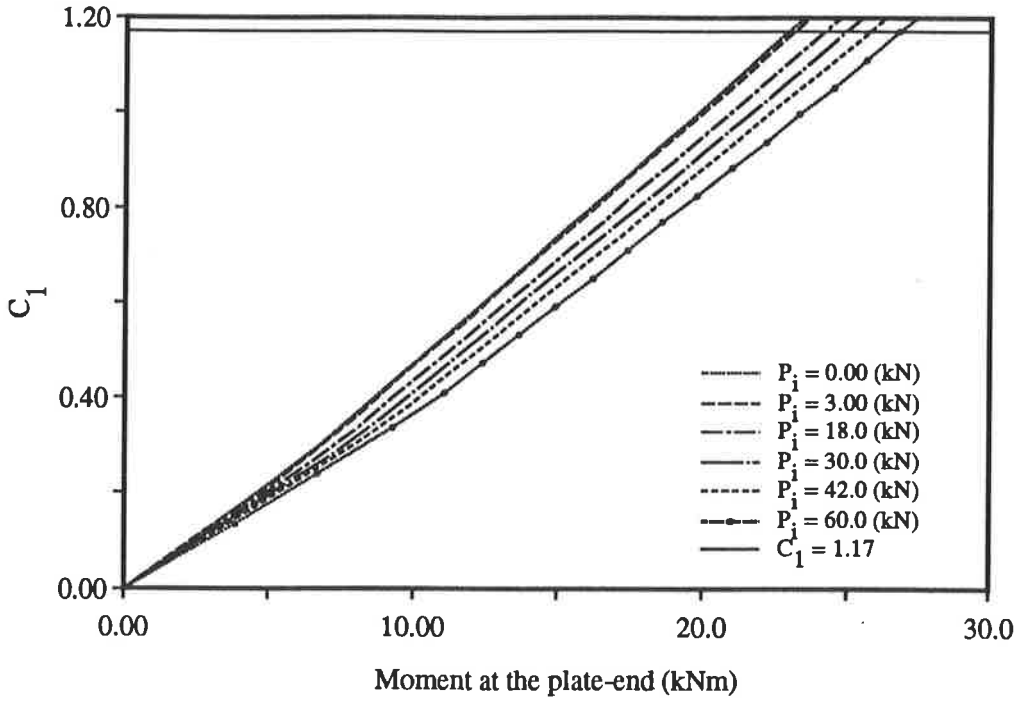

Fig.5-38 The relationship between C_1 and moment at the plate-end M_e for Model Five

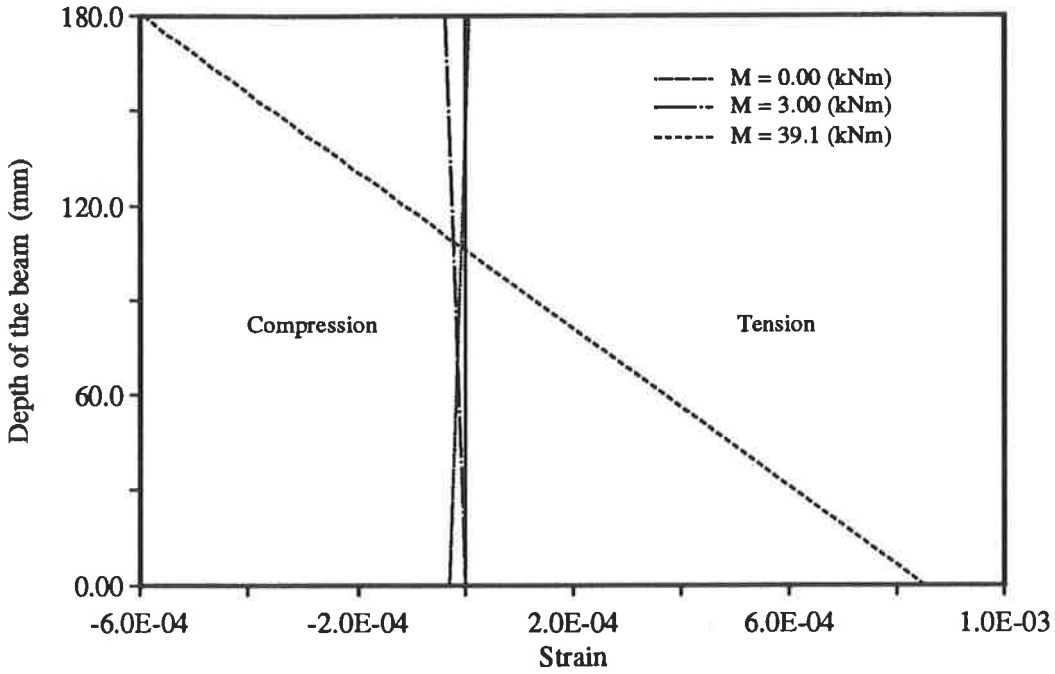

Fig.5-39a The variation of strain profile with the applied moment for Model Five

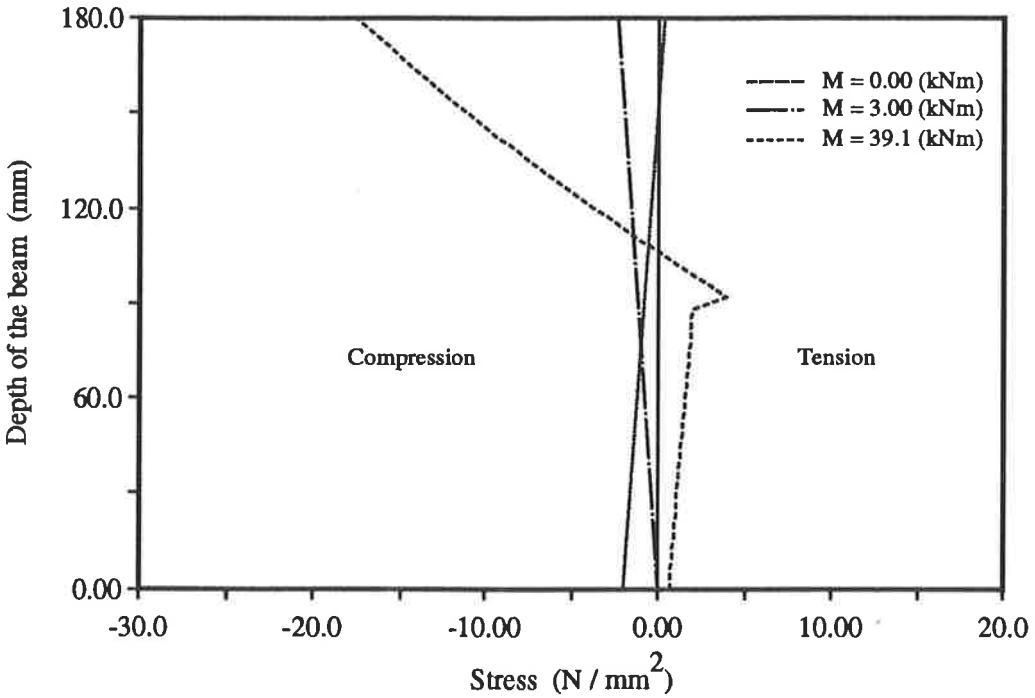

Fig.5-39b The variation of stress profile with the applied moment for Model Five

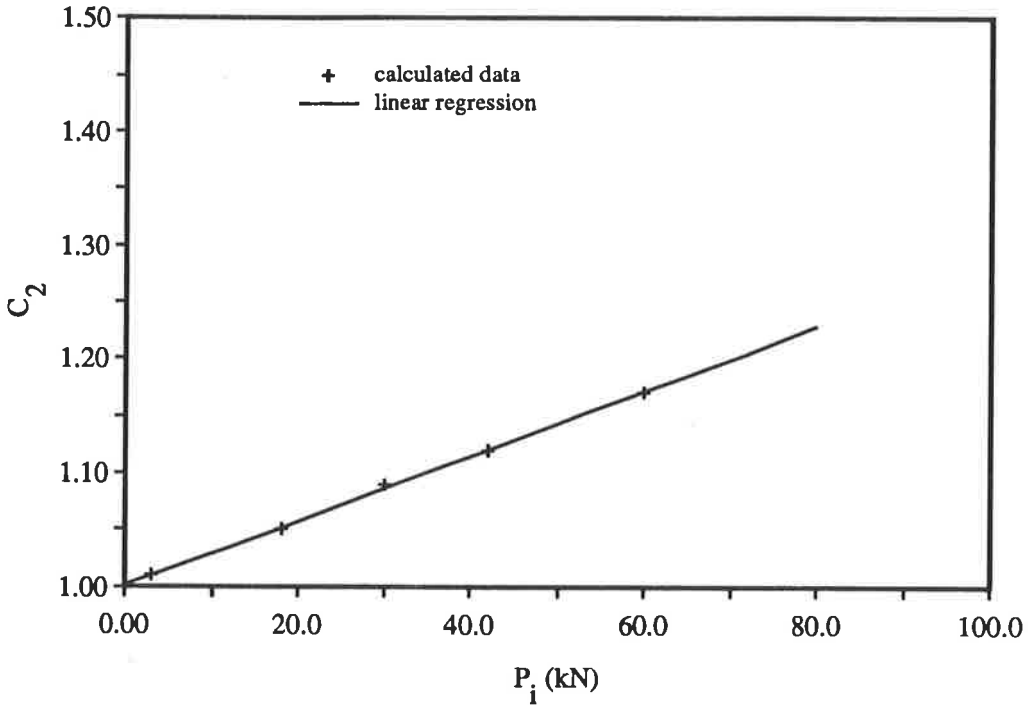

Fig.5-40 The relationship between C_2 and the prestressing forces P_i for Model Five

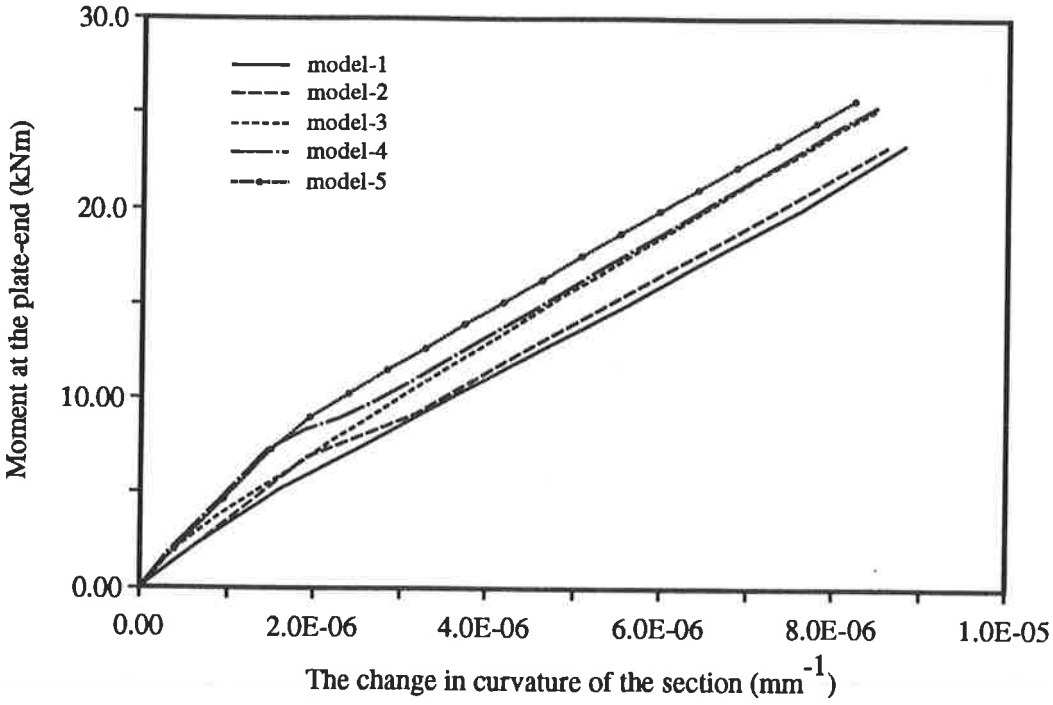

Fig.5-41 Moment versus the change in curvature

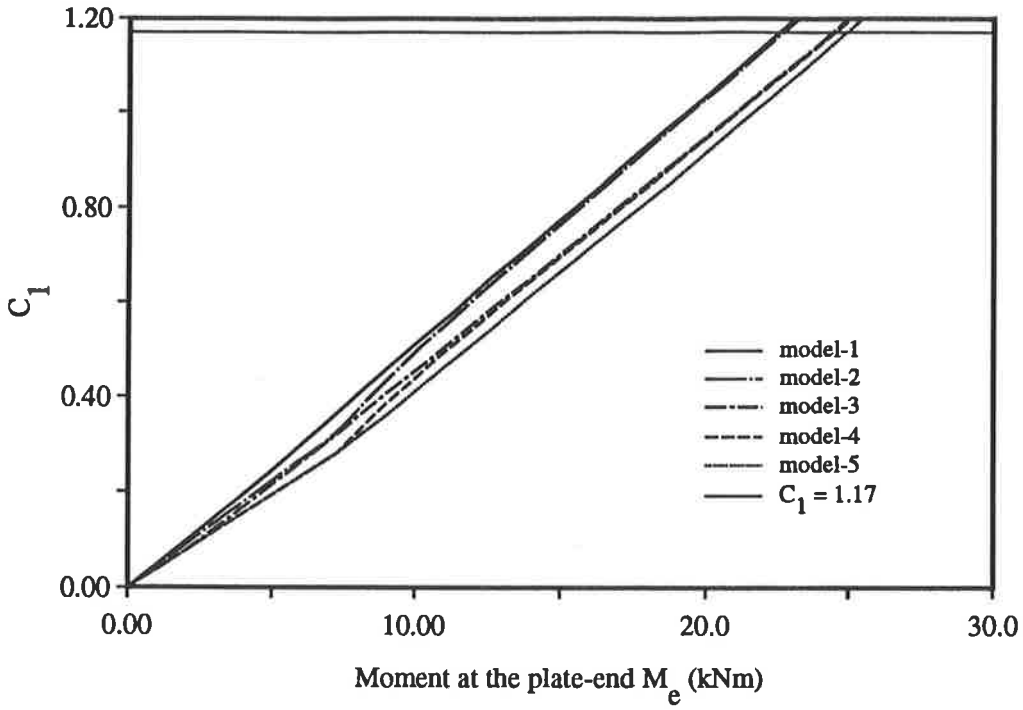

Fig.5-42 The variation of C_1 with the moment at the plate-end M_e

Chapter Six

Analysis of Experimental Tests

6.1 Introduction

The purpose of this chapter is to analysis the experimental data described in Chapter 3. For the plated post-tensioned beams, the results from the experimental tests are compared with the results from the computer analyses as described in Chapter 5. Details of the specimens and the tests are given in Chapters 2 and 3.

6.2 Analysis experimental data

6.2.1. Shear strength of reinforced concrete beams without shear reinforcement

To determine the shear strength of the reinforced concrete beams without shear reinforcement, two specimens in series 1 (SP-S1-L and SP-S2-L) and three specimens beam in series 4 (SP-S5-L, SP-S6-L and SP-S7-L) were tested to failure in shear. The results of the tests are given in Table 6.1:

Table 6.1

Specimen	A_{st} (mm^2)	$(V_{uc})_{exp}$ (kN)	$\frac{(V_{uc})_{exp}}{(V_{up})_o}$	failure mode
SP-S1-L	402	33.4	1.08	shear
SP-S2-L	402	27.5	0.89	shear
SP-S5-L	402	27.9	0.91	shear
SP-S6-L	402	33.1	1.07	shear
SP-S7-L	402	32.0	1.04	shear

where, A_{st} is areas of longitudinal tensile reinforcement, $(V_{up})_o$ is the average shear strength of the test beams.

The average shear strength, $(V_{up})_o$, of the reinforced concrete beams without shear reinforcement was 30.8 kN. This result is used in the following analysis to determine the effect of plating on the shear strength.

6.2.2 Shear strength of reinforced concrete beams with full soffit plating

The shear strength of the fully plated reinforced concrete beams in which the length and width of the soffit plates are as same as that of the beam, are determined from experimental test. Also the shear strength of the fully plated reinforced concrete beams are derived from AS 3600 [24] and the results compared with the experimental tests.

6.2.2.1 Shear strength of the fully plated reinforced concrete beam determined from experimental tests

To investigate the ultimate shear strength, $(V_{up})_{st}$, of the fully plated reinforced concrete beam, six specimens in series 2, in which the thickness of the soffit plate varied from 3.0 to 10.0 mm, were tested. The test results are given in Table 6.2.

Table 6.2

Specimen	t_p (mm)	$(V_{up})_{st}$ (kN)	S_1	$(V_{in})_{st}$ (kN)	S_2
FP/B2/L	3.0	46.80	1.52	16.00	0.52
FP/B2/R	3.0	50.03	1.62	19.23	0.62
FP/B3/L	5.0	64.17	2.08	33.37	1.08
FP/B3/R	5.0	70.76	2.30	39.96	1.30
FP/B4/L	10.0	85.00	2.76	54.20	1.76
FP/B4/R	10.0	78.70	2.56	47.90	1.56

where

t_p = the thickness of the soffit plate

$(V_{in})_{st}$ = $(V_{up})_{st}$ - $(V_{up})_o$, ie., the increase in shear strength of the reinforced concrete beam due to the full soffit plating

$S_1 = \frac{(V_{up})_{st}}{(V_{up})_o}$, ie., ratio of the shear strength of the reinforced concrete beam with full soffit plating to the shear strength of the unplated reinforced concrete beam

$S_2 = \frac{(V_{in})_{st}}{(V_{up})_o}$, ie., ratio of the increase in the shear strength due to the soffit plate to the shear strength of the unplated beam

The relationship between S_1 and t_p are shown in Fig.6-1. The relationship between $(V_{in})_{st}$ and t_p are illustrated in Fig.6-2. It can be seen in Fig.6-1 that the shear strength of the fully plated reinforced concrete beam increases with the thickness of the soffit plate, as given by the following equation:

$$(V_{up})_{st} = (1.0 + k_1 t_p)(V_{up})_o \qquad (6\text{-}1)$$

in which, $k_1 = 1.77\ mm^{-1}$, the coefficient of correlation in linear regression is 0.94. Therefore the shear strength of the fully plated reinforced concrete beam is a function of the area of the external soffit steel plate. The increase in the shear strength due to full plating is from 52 to 176 per cent.

6.2.2.2 Shear strength of reinforced concrete beams with full soffit steel plating in terms of AS 3600

The ultimate shear strength, V_{uc}, of a reinforced concrete beam without shear reinforcement may be determined by the following equation in AS 3600.

$$V_{uc} = \beta_1\beta_2\beta_3 b_v d_o \left[\frac{A_{st} f_c'}{b_v d_o}\right]^{1/3} \quad (6\text{-}2)$$

where

$\beta_1 = 1.4 - \frac{d_o}{2000} \geq 1.1$

$\beta_2 = 1.0$ or

$= 1.0 - (N^*/3.5A_g) \geq 0$ for members subject to significant tension; or

$= 1.0 + (N^*/14A_g)$ for members subject to significant axial compression

A_g = the gross cross-sectional area of a beam

N^* = the axial compressive or tensile force on a cross-section

$\beta_3 = 1.0$

A_{st} = area of the longitudinal tensile reinforcement in the section excluding the area of soffit steel plate

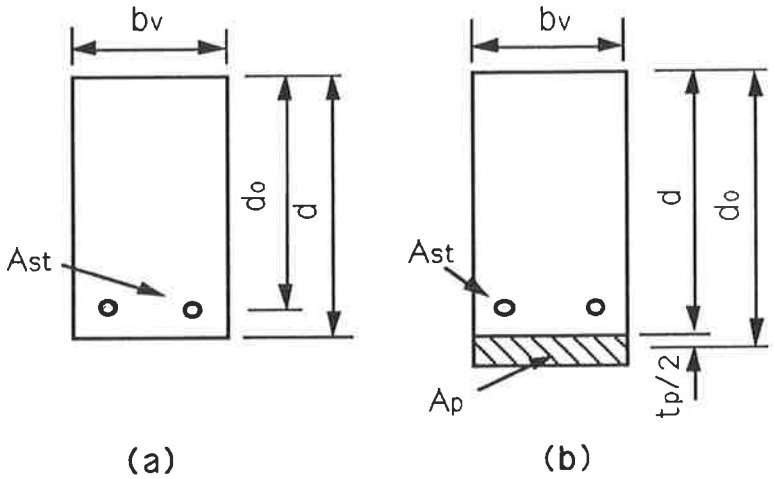

Fig.6-3 Cross-section

The geometric properties of the cross-section that are required in Eq.(6-2) are illustrated in Fig.6-3(a). It can be seen in Eq.(6-2) that the shear strength of the reinforced concrete beam is a function of the area of the longitudinal tensile reinforcement in the section.

For the fully plated reinforced concrete beam, the shear strength, $(V_{uc})_p$, of the beam may also be a function of the total area of the tensile reinforcement ie. the external soffit plate acting as part of the tensile reinforcement of the section, as shown in Fig.6-3(b). Therefore, the ultimate shear strength of the fully plated reinforced concrete beam may be determined by the following equation:

$$(V_{uc})_p = \beta_1\beta_2\beta_3 b_v d_o \left[\frac{(A_{st})_p f_c'}{b_v d_o}\right]^{1/3} \qquad (6\text{-}3)$$

where $(A_{st})_p = A_{st} + A_p$, ie., is the total area of the tensile reinforcement.

The area of the longitudinal tensile reinforcement A_{st}, the ultimate shear strength of the reinforced concrete beam without shear reinforcement V_{uc}, the area of the longitudinal tensile reinforcement including the areas of the soffit plate $(A_{st})_p$, the shear strength of the fully plated reinforced concrete beam $(V_{uc})_p$, and the parameters S_1, S_3, S_4 as well as $(A_1)^{1/3}$ that are defined below are given in Table 6.3.

$$S_1 = \frac{(V_{up})_{st}}{(V_{up})_o}, \text{ as defined in section 6.2.2.1}$$

$$S_3 = \frac{(V_{uc})_p}{V_{uc}}, \text{ ie., shear ratio calculated in terms of AS 3600}$$

$$S_4 = \frac{S_1 - S_3}{S_3}$$

$$A_1 = \frac{(A_{st})_p}{A_{st}}$$

Table 6.3

Specimen	A_{st} (mm^2)	V_{uc} (kN)	$(A_{st})_p$ (mm^2)	$(V_{uc})_p$ (kN)	S_1	S_3	S_4	$(A_1)^{1/3}$
FP/B2/L	402	24.1	792	32.6	1.52	1.35	0.13	1.25
FP/B2/R	402	24.1	792	32.6	1.62	1.35	0.20	1.25
FP/B3/L	402	24.1	1052	36.0	2.08	1.49	0.40	1.38
FP/B3/R	402	24.1	1052	36.0	2.30	1.49	0.54	1.38
FP/B4/L	402	24.1	1702	42.6	2.76	1.77	0.56	1.62
FP/B4/R	402	24.1	1702	42.6	2.56	1.77	0.45	1.62

The relationships between the shear ratios S_3 and S_1 and $(A_{st})_p^{1/3}$ are shown in Fig.6-4. The relationships between the shear ratios S_3 S_1, and $(A_1)^{1/3}$ is shown in Fig.6-5. The dash line represents the value calculated from the Codes and the solid line and curve represent regression analyses of the experimental tests. The relationship between the shear ratio S_4 and $(A_1)^{1/3}$ is shown in Fig.6-6.

It can be seen in Fig.6-4 that the shear strengths of the beams increases with the greater area of longitudinal tensile reinforcement. The increase in the shear strength that was obtained in the experimental tests is larger than that calculated from the Code. The increase is given by the following equation:

$$S_1 = k_2(A_{st})_p^{1/3} \qquad (6\text{-}4)$$

where, $k_2 = 0.39$ ($mm^{-2/3}$) the coefficient of correlation is 0.94. The curvilinear variation of S_1 with $(A_1)^{1/3}$ as shown in Fig.6-5 is given by the following equation:

$$S_1 = [(A_1)^{\frac{1}{3}}]^{k_3} \qquad (6\text{-}5)$$

in which, $k_3 = 2.07$ and the coefficient of correlation of the curvilinear regression is 0.96. The variation of S_4 with $(A_1)^{1/3}$ as shown in Fig.6-6 is given by the following equation:

$$S_4 = k_4 \ln[(A_1)^{1/3}] \qquad (6\text{-}6)$$

where, $k_4 = 1.15$ $(mm^{-1/3})$ and the coefficient of correlation of the curvilinear regression is 0.79.

A comparison of the shear strengths of the fully plated reinforced concrete beam between the experimental tests and the Code in terms of AS 3600, shows that the actual shear strength of the beams is greater than that calculated from the Codes; this increase in the shear strengths is from 13 to 56 %, as described in Table 6.3 and in Fig.6-6. Therefore, the ultimate shear strength of the fully plated reinforced concrete beam without shear reinforcement can be determined from AS 3600 as this gives a conservative value compared with the experimental tests.

6.2.3 Shear strength of the reinforced concrete beam with the external side plates (thickness t_{sp} of the side plate varied)

To investigate the shear strength, V_{sp}, of reinforced concrete beams with external side plates, three beams in series 4 were tested, in which the thickness of the side plates varied from 1 mm to 3 mm. The results of the tests are given in Table 3.4 in Chapter 3.

The shear strength with side plates V_{sp} was determined indirectly from the analysis of the debonding of the soffit plates by applying Eq.(5-7) in the form shown in Eq.(6-7). The shear strength with side plates V_{sp} is now the unknown parameter and

M_{sp} is the pure peeling moment in terms of the properties of the beam with the side and soffit plates.

$$\frac{M_e}{M_{sp}} + \frac{V_e}{V_{sp}} = 1.17 \qquad (6\text{-}7)$$

where

$M_e \not> M_{sp}$ if $M_e > M_{sp}$, than $M_{sp} = M_e$

$V_e \not> V_{sp}$ if $V_e > V_{sp}$, than $V_{sp} = V_e$

M_e = the moment at the end of plate when debonding occurred

$M_{sp} = \frac{(EI)_{sp} f_t}{0.474 E_p t_p}$, the ultimate peeling moment, ie., debonding moment of reinforced concrete beam with both soffit and side plates

$(EI)_{sp}$ = flexural rigidity of reinforced concrete beam with both soffit and side plates based on the linear elastic analysis, ie., the tensile strength of concrete is zero

V_e = the shear forces at the end of plate when debonding occurred

V_{sp} = shear strength of reinforced concrete beams with side plates, but without the shear reinforcement stirrups

Therefore by rearranging Eq.(6-7), the shear strength of a plated reinforced concrete beam with side plates, V_{sp}, may be derived from the following equation:

$$V_{sp} = \frac{V_e}{1.17 - \frac{M_e}{M_{sp}}} \qquad (6\text{-}8)$$

The geometric properties of the beams in series 4 are given in Table 6.4

Table 6.4

Specimen	t_{sp} (mm)	L_{sp} (mm)	d_{cn} (mm)	I_{csp} 1.0E+7(mm^4)	$(EI)_{csp}$ 1.0E+12	d_{ucn} (mm)	I_{usp} 1.0E+8(mm^4)	$(EI)_{usp}$ 1.0E+12
SP-S5-R	1.0	1250	88.0	8.76784	2.99860	104.1	1.10938	3.79406
SP-S6-R	2.0	1250	88.2	9.36549	3.20298	103.2	1.17316	4.01222
SP-S7-R	3.0	1250	88.4	9.62904	3.40731	102.4	1.23646	4.22870
SP-S4-L	4.0	690	88.6	10.5603	3.61161	101.7	1.29935	4.44378

where

$(EI)_{csp}$ = the flexural rigidity of a plated cracked reinforced concrete beam with both side and soffit plates

$(EI)_{usp}$ = the flexural rigidity of a plated uncracked reinforced concrete beam with both side and soffit plates

t_{sp} = the thickness of side plates

L_{sp} = length of the side plate

d_{ucn} = depth from the neutral axis to the center of the soffit plate in the plated uncracked section

d_{cn} = depth from the neutral axis to the center of the soffit plate in the plated cracked section

I_{usp} = second moment of area of the plated uncracked section with the reinforcement transformed to an equivalent area of concrete

I_{csp} = second moment of area of the plated cracked section with the reinforcement transformed to an equivalent area of concrete

The calculated values of M_{csp}, M_{usp}, V_{csp} and V_{usp} are given in Table 6.5.

Table 6.5

Specimen	M_{sp} (kNm)	M_{usp} (kNm)	V_e (kN)	M_e (kNm)	V_{csp} (kN)	V_{usp} (kN)
SP-S5-R	21.7	27.4	54.6	2.73	52.3	51.0
SP-S6-R	23.2	29.0	64.7	3.24	62.8	61.1
SP-S7-R	24.7	30.6	72.6	3.63	71.0	69.1
SP-S4-L	26.1	32.1	60.6	3.03	57.5	56.3

where

M_{sp} = ultimate pure peeling moment based on the flexural rigidity , $(EI)_{csp}$, of plated cracked section with both side and soffit plates

M_{usp} = ultimate pure peeling moment based on the flexural rigidity ,$(EI)_{usp}$, of plated uncracked section with both side and soffit plates

V_{csp} = shear strength of reinforced concrete beam with side plates derived from Eq.(6-8), which is based on the flexural rigidity of plated cracked section

V_{usp} = shear strength of reinforced concrete beam with both side plates derived from Eq.(6-8), which is based on the flexural rigidity of plated uncracked section

It can be seen in Table 6.5 that the shear strengths V_{csp} and V_{usp} are less than the experimental shear force at failure V_e at which debonding of the soffit plate occurred in the experimental test. Therefore, it can be assumed that these specimens debonded due to the shear peeling and hence the shear loads at failure V_e are the shear strengths of the specimens with side plates V_{sp} as listed in Table 6.6

Table 6.6

Specimen	M_{sp} (kNm)	V_{sp} (kN)	$(V_{in})_{sp}$ (kN)	S_5	S_6
SP-S5-R	21.7	54.6	23.8	1.77	0.77
SP-S6-R	23.4	64.7	33.9	2.10	1.10
SP-S7-R	24.7	72.6	41.8	2.36	1.36

where

M_{sp} = ultimate peeling moment based on the flexural rigidity, $(EI)_{csp}$, of plated cracked section with both side and soffit plates, it is based on the linear elastic analysis and tensile strength of concrete is zero

$(V_{in})_{sp}$ = V_{sp} - $(V_{up})_o$, ie., the increase in shear strength due to the side plates

$$S_5 = \frac{V_{sp}}{(V_{up})_o}$$

$$S_6 = \frac{(V_{in})_{sp}}{(V_{up})_o}$$

The relationship between the shear strength, V_{sp}, of the reinforced concrete beam with the side plates and the thickness, t_{sp}, of the side plates is shown in Fig.6-7. The relationship between $(V_{in})_{sp}$ and t_{sp} is shown in Fig.6-8. The relationship between S_5 and t_{sp} is illustrated in Fig.6-9. The relationship between S_6 and t_{sp} is given in Fig.6-10.

It can be seen in Fig.6-7 that the shear strength of the reinforced concrete beams with the side plates increases with the thickness of the side plates. The correlation is given by the following equation:

$$V_{sp} = (V_{up})_o + k_5 t_{sp}^{0.4} \quad (6\text{-}9)$$

where $k_5 = 25.0$ ($kNmm^{-2/5}$) and the coefficient of correlation is 0.95. The results of the analysis of the increase in the shear strength induced by the side plates, as shown in Fig.6-8, are given by the following equation:

$$(V_{in})_{sp} = k_6 t_{sp}^{0.50} \quad (6\text{-}10)$$

in which $k_6 = 23.8$ ($kNmm^{-1/2}$) and the coefficient of correlation is 0.99. The results of the analysis of the relationship between S_5 and t_{sp}, as shown in Fig.6-9, are given by the following equation:

$$S_5 = k_7 t_{sp}^{0.25} \quad (6\text{-}11)$$

where $k_7 = 1.77$ ($mm^{-1/4}$) and the coefficient of correlation is 0.98. The results of the analysis of the relationship between S_6 and t_{sp}, as shown in Fig.6-10, are given by the following equation:

$$S_6 = k_8 t_{sp}^{0.53} \quad (6\text{-}12)$$

in which $k_8 = 0.77$ ($mm^{-0.53}$) and the coefficient of correlation is 0.98.

It can be seen from Fig.6-7 to Fig.6-10 that there is a correlation between the experimental data and the regression.

6.2.4 Shear strength of the reinforced concrete beam with the external side plates (length L_{sp} of the side plates varied)

To investigate the effect of varying the length of the side plates on debonding of the soffit plates, the length of the side plates L_{sp} was varied from 0.0 to 690 mm; eight specimens in series 1 were tested and the results are given in Table 3.1 and the tests described in Chapter 3.

The shear strength of the reinforced concrete beam without shear reinforcement $(V_{up})_o$ was determined from the experimental tests as described in section 6.2.1. The shear strength of the reinforced concrete beams with full side plates of thickness 4.0 mm V_{sp} can be derived from section 6.2.3 and it is equal to 74.3 kN. The flexural rigidity $(EI)_{csp}$ of the plated reinforced concrete beam and the ultimate pure peeling moment and M_{csp} are given in Table 6.7. The parameter C_3 is derived from the following equations:

$$C_3 = \frac{M_e}{M_{csp}} + \frac{V_e}{V_{sp}} \qquad (6\text{-}13)$$

in which $M_{csp} = \frac{(EI)_{csp} f_t}{0.474 E_p t_p}$, ie. ultimate peeling moment based on the flexural rigidity, $(EI)_{csp}$, of the plated cracked section with the side plates and $(EI)_{csp}$ is the flexural rigidity of a plated cracked reinforced concrete beam with side plates

Equation (6-13) is based on the strength of the beam with full side plates. It is assumed that the ultimate shear strength of the reinforced concrete beam with the side plates can be reached when the parameter C_3 is equal to 1.17. Therefore the length of the side plates required to achieved V_{sp} can be determined from that experimental tests.

Table 6.7

Specimen	L_{sp} (mm)	$\frac{L_{sp}}{d}$ (kN)	$(EI)_{csp}$ 1.0E+12	M_{csp} (kNm)
SP-S1-L	0.0	0.0	3.61162	26.1
SP-S2-L	0.0	0.0	3.61162	26.1
SP-S3-L	90	0.5	3.61162	26.1
SP-S2-R	180	1.0	3.61162	26.1
SP-S4-R	270	1.5	3.61162	26.1
SP-S1-R	360	2.0	3.61162	26.1
SP-S3-R	540	3.0	3.61162	26.1
SP-S4-L	690	3.8	3.61162	26.1

The parameters C_3 and S_7 are given in Table 6.8.

Table 6.8

Specimen	L_{sp} (mm)	$\frac{L_{sp}}{d}$ (kN)	V_e (kN)	M_e (kNm)	C_3	S_7
SP-S1-L	0.0	0.0	33.4	1.67	0.50	1.08
SP-S2-L	0.0	0.0	26.4	1.32	0.40	0.86
SP-S3-L	90	0.5	30.8	1.54	0.46	1.00
SP-S2-R	180	1.0	37.0	1.85	0.56	1.20
SP-S4-R	270	1.5	35.0	1.75	0.53	1.14
SP-S1-R	360	2.0	43.2	2.16	0.65	1.40
SP-S3-R	540	3.0	50.0	2.50	0.75	1.62
SP-S4-L	690	3.8	60.6	3.03	0.91	1.97

where

$$S_7 = \frac{V_e}{(V_{up})_o}$$

The relationship between C_3 and $L_{sp}d$ is shown in Fig.6-11. The relationship between S_7 and L_{sp}/d is shown in Fig.6-12.

The variation of the parameter C_3 with L_{sp}/d as shown in Fig.6-11 is given by the following equation:

$$C_3 = 0.424 + k_9\left(\frac{L_{sp}}{d}\right) \qquad (6\text{-}14)$$

where $k_9 = 0.118$ and the coefficient of correlation is 0.93. The variation of the parameter S_7 with L_{sp}/d as shown in Fig.6-12 is given by the following equation:

$$S_7 = 0.97 e^{0.185 \frac{L_{sp}}{d}} \qquad (6\text{-}15)$$

where the coefficient of correlation is 0.92.

The length of side plates L_{sp}/d required to prevent premature failure due to debonding of the side plates before debonding of the soffit plate can be determined from Fig.6-11 and Eq.(6-14) and is equal to L_{sp}/d when $C_3 = 1.17$. Hence, the minimum length L_{sp}/d required is 6.3 ie. the length of the side plate must be equal to 6.3 times the depth of the beam.

6.2.5 Interface shear strength of plated reinforced concrete beams

The longitudinal shear strength at the interface of the soffit steel plate and the concrete beam, when the plated reinforced concrete beam failed in shear or shear peeling, can be determined from standard elastic formula as

$$S_s = \frac{V_p A_p m y_p}{I_p b_p} \qquad (6\text{-}16)$$

where, V_p = shear force acting on the plated section, A_p = areas of the soffit plate, m = modular ratio, y_p = distance from centroid of the soffit plate to neutral axis of the plated section, I_p = the second moment of area of the plated section with the reinforcement transformed to an equivalent area of concrete, b_p = width of the soffit plate, as shown in Fig.6-13.

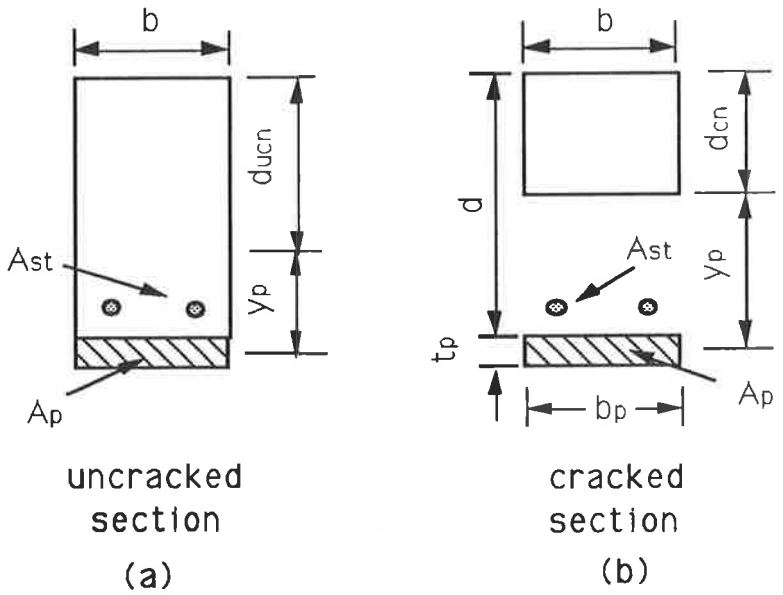

Fig.6-13

For the fully plated reinforced concrete beams in series 2 in section 2.2.2, the section properties, shear stress S_s and S_s/f_t are given in Table 6.9 and Table 6.10,

respectively; this series will be referred to as Group A. For those plated reinforced concrete beams without the side plates, the section properties, shear stress S_s and S_s/f_t are given in Table 6.11 and Table 6.12, respectively and will be referred to as Group B. For the plated reinforced concrete beams with the side plates in series 1, which will be referred to as Group C, the section properties, shear stress S_s and S_s/f_t are given in Table 6.13 and Table 6.14, respectively. Also, the previous results of the plated reinforced concrete beams tested by D.J. Oehlers[4] and J.P. Moran[3] are referred to as Group D and Group E, respectively and the section properties, shear stress S_s and S_s/f_t are given in Table 6.15, Table 6.16, Table 6.17 and Table 6.18, respectively.

Table 6.9 Group A (plated cracked section)

Specimen	t_p (mm)	b_p (mm)	A_p (mm^2)	d_{cn} (mm)	y_p (mm)	I_p 10^7 (mm^4)	V_p (kN)	S_s (N/mm^2)	S_s/f_t
FP/B2/L	3.0	130	390	77.9	103.6	6.44462	46.8	1.35	0.38
FP/B2/R	3.0	130	390	77.9	103.6	6.44462	50.0	1.45	0.40
FP/B3/L	5.0	130	650	87.8	94.7	8.17006	64.2	2.28	0.63
FP/B3/R	5.0	130	650	87.8	94.7	8.17006	70.8	2.52	0.70
FP/B4/L	10.0	130	1300	104.6	80.4	11.4545	85.0	3.66	1.02
FP/B4/R	10.0	130	1300	104.6	80.4	11.4545	78.7	3.39	0.94

Table 6.10 Group A (plated uncracked section)

Specimen	t_p (mm)	b_p (mm)	A_p (mm^2)	d_{ucn} (mm)	y_p (mm)	I_p 10^7 (mm^4)	V_p (kN)	S_s (N/mm^2)	S_s/f_t
FP/B2/L	3.0	130	390	100.5	81.0	9.32862	46.8	0.73	0.20
FP/B2/R	3.0	130	390	100.5	81.0	9.32862	50.0	0.78	0.22
FP/B3/L	5.0	130	650	105.1	77.4	10.4499	64.2	1.46	0.41
FP/B3/R	5.0	130	650	105.1	77.4	10.4499	70.8	1.61	0.45
FP/B4/L	10.0	130	1300	114.7	70.3	12.8384	85.0	2.86	0.79
FP/B4/R	10.0	130	1300	114.7	70.3	12.8384	78.7	2.65	0.74

Table 6.11 Group B (plated cracked section)

Specimen	t_p (mm)	b_p (mm)	A_p (mm^2)	d_{cn} (mm)	y_p (mm)	I_p $10^7(mm^4)$	V_p (kN)	S_s (N/mm^2)	S_s/f_t
SP/S1/L	5.0	130	650	87.8	94.7	8.17006	33.4	1.19	0.33
SP/S2/L	5.0	130	650	87.8	94.7	8.17006	26.4	0.94	0.26
SP/S5/L	5.0	130	650	87.8	94.7	8.17006	27.9	0.99	0.28
SP/S6/L	5.0	130	650	87.8	94.7	8.17006	33.1	1.18	0.33
SP/S7/L	5.0	130	650	87.8	94.7	8.17006	32.7	1.16	0.32
SP/S8/L	5.0	130	650	81.3	101.2	7.31654	33.0	1.40	0.39
SP/S9/L	5.0	130	650	92.7	89.8	8.84356	31.5	0.98	0.27

Table 6.12 Group B (plated uncracked section)

Specimen	t_p (mm)	b_p (mm)	A_p (mm^2)	d_{ucn} (mm)	y_p (mm)	I_p $10^7(mm^4)$	V_p (kN)	S_s (N/mm^2)	S_s/f_t
SP/S1/L	5.0	130	650	105.1	77.4	10.4499	33.4	0.76	0.21
SP/S2/L	5.0	130	650	105.1	77.4	10.4499	26.4	0.60	0.17
SP/S5/L	5.0	130	650	105.1	77.4	10.4499	27.9	0.63	0.18
SP/S6/L	5.0	130	650	105.1	77.4	10.4499	33.1	0.75	0.21
SP/S7/L	5.0	130	650	105.1	77.4	10.4499	32.7	0.74	0.21
SP/S8/L	5.0	130	650	102.7	79.8	10.0540	33.0	0.80	0.22
SP/S9/L	5.0	130	650	107.1	75.4	10.7869	31.5	0.68	0.19

Table 6.13 Group C (plated cracked section)

Specimen	L_{sp} (mm)	t_p (mm)	b_p (mm)	A_p (mm^2)	d_{cn} (mm)	y_p (mm)	I_p $10^7(mm^4)$	V_p (kN)	S_s (N/mm^2)	S_s/f_t
SP/S3/L	90.0	5.0	130	650	87.8	94.7	8.17006	30.8	1.10	0.31
SP/S2/R	180	5.0	130	650	87.8	94.7	8.17006	37.0	1.32	0.37
SP/S4/R	270	5.0	130	650	87.8	94.7	8.17006	35.0	1.25	0.35
SP/S1/R	360	5.0	130	650	87.8	94.7	8.17006	43.2	1.54	0.43
SP/S3/R	540	5.0	130	650	87.8	94.7	8.17006	50.0	1.78	0.49
SP/S4/L	690	5.0	130	650	81.3	101.2	7.31654	60.6	2.16	0.60

Table 6.14 Group C (plated uncracked section)

Specimen	L_{sp} (mm)	t_p (mm)	b_p (mm)	A_p (mm^2)	d_{ucn} (mm)	y_p (mm)	I_p $10^7(mm^4)$	V_p (kN)	S_s (N/mm^2)	S_s/f_t
SP/S3/L	90.0	5.0	130	650	105.1	77.4	10.4499	30.8	0.70	0.19
SP/S2/R	180	5.0	130	650	105.1	77.4	10.4499	37.0	0.84	0.23
SP/S4/R	270	5.0	130	650	105.1	77.4	10.4499	35.0	0.80	0.22
SP/S1/R	360	5.0	130	650	105.1	77.4	10.4499	43.2	0.98	0.27
SP/S3/R	540	5.0	130	650	105.1	77.4	10.4499	50.0	1.14	0.32
SP/S4/L	690	5.0	130	650	105.1	77.4	10.4499	60.6	1.38	0.38

Table 6.15 Group D (plated cracked section)

Specimen	t_p (mm)	b_p (mm)	A_p (mm^2)	d_{cn} (mm)	y_p (mm)	I_p $10^7(mm^4)$	V_p (kN)	S_s (N/mm^2)	S_s/f_t
1/2/S	5.0	130	650	97.1	80.4	9.59922	29.6	1.18	0.37
1/2/N	5.0	130	650	97.1	80.4	9.59922	32.5	1.30	0.41
1/3/S	5.0	130	650	97.1	80.4	9.59922	25.8	1.03	0.32
1/3/N	5.0	130	650	97.1	80.4	9.59922	23.1	0.92	0.29
1/4/S	5.0	130	650	97.1	80.4	9.59922	41.0	1.64	0.51
2/1/S	5.0	130	650	82.7	94.8	6.74051	41.0	1.35	0.31

Table 6.16 Group D (plated uncracked section)

Specimen	t_p (mm)	b_p (mm)	A_p (mm^2)	d_{ucn} (mm)	y_p (mm)	I_p $10^8(mm^4)$	V_p (kN)	S_s (N/mm^2)	S_s/f_t
1/2/S	5.0	130	650	107.6	69.9	1.10451	29.6	0.89	0.28
1/2/N	5.0	130	650	107.6	69.9	1.10451	32.5	0.98	0.31
1/3/S	5.0	130	650	107.6	69.9	1.10451	25.8	0.78	0.24
1/3/N	5.0	130	650	107.6	69.9	1.10451	23.1	0.70	0.22
1/4/S	5.0	130	650	107.6	69.9	1.10451	41.0	1.21	0.38
2/1/S	5.0	130	650	100.6	76.9	0.895675	41.0	0.95	0.22

Table 6.17 Group E (plated cracked section)

Specimen	t_p (mm)	b_p (mm)	A_p (mm^2)	d_{cn} (mm)	y_p (mm)	I_p $10^7(mm^4)$	V_p (kN)	S_s (N/mm^2)	S_s/f_t
7-1	5.0	120	600	94.33	108.2	9.9333	19.4	0.66	0.21
7-2	5.0	120	600	94.33	108.2	9.9333	23.5	0.80	0.25
7-3	5.0	120	600	98.22	104.3	10.9248	33.1	1.14	0.36
7-4	5.0	120	600	98.22	104.3	10.9248	33.9	1.17	0.37
8-1	5.0	120	600	90.97	111.5	9.13992	19.4	0.66	0.22
8-2	5.0	120	600	90.97	111.5	9.13992	27.9	0.94	0.31
8-3	5.0	120	600	103.2	99.26	12.3409	21.2	0.74	0.27
8-4	5.0	120	600	103.2	99.26	12.3409	26.1	0.91	0.34

Table 6.18 Group E (plated uncracked section)

Specimen	t_p (mm)	b_p (mm)	A_p (mm^2)	d_{ucn} (mm)	y_p (mm)	I_p $10^8(mm^4)$	V_p (kN)	S_s (N/mm^2)	S_s/f_t
7-1	5.0	120	600	114.8	87.7	1.33894	19.4	0.40	0.13
7-2	5.0	120	600	114.8	87.7	1.33894	23.5	0.48	0.15
7-3	5.0	120	600	116.5	86.0	1.41816	33.1	0.73	0.23
7-4	5.0	120	600	116.5	86.0	1.41816	33.9	0.74	0.23
8-1	5.0	120	600	113.4	89.0	1.27774	19.4	0.37	0.12
8-2	5.0	120	600	113.4	89.0	1.27774	27.9	0.54	0.18
8-3	5.0	120	600	118.9	83.6	1.53613	21.2	0.50	0.18
8-4	5.0	120	600	118.9	83.6	1.53613	26.1	0.62	0.23

For all the beams considered to have plated cracked sections, the relationship between S_s and V_p is given in Fig.6-14 and the relationship between S_s/f_t and V_p is shown in Fig.6-15. For all the beams considered to have the plated uncracked section, the relationship between S_s and V_p is given in Fig.6-16 and the relationship between S_s/f_t and V_p is illustrated in Fig.6-17.

The longitudinal shear forces shown in Figs 6-14 - 6-17 are a lower bond to the shear strength at the interface between the plate and R.C. beam because none of these beams failed by debonding due to the shear flow. It can be seen in Fig.6-17 that shear stress up to 80% of the tensile strength of the concrete f_t have been resisted without shear flow failure.

6.2.6 Debonding of the plated post-tensioned beams with varying degrees of the initial prestressing forces

As a preliminary study of the effect of post-tensioning on debonding, four plated post-tensioned beams were tested. Also a computer program was developed in Chapter 4 to simulate the actual flexural behaviour of the beam and a parametric study was carried out in Chapter 5. The results of the experimental test are compared with the results of the analysis model.

6.2.6.1 Experimental results

Four beams in series 5 were tested as described in Chapter 3. The results of the experimental tests are given in Table 6.19.

The relationship between the cracking moment $(M_{cr})_{exp}$ and the initial prestressing forces P_i is illustrated in Fig.6-18 together with a linear regression analysis. The

variation of debonding moment at the plate-end $(M_e)_{exp}$ with the initial prestressing forces P_i is shown in Fig.6-19 also with a nonlinear regression analysis of the results.

Table 6.19

Specimen No.	P_i (kN)	$(M_{cr})_{exp}$ (kNm)	$(M_e)_{exp}$ (kNm)
PT1	3.00	11.2	18.2
PT3	18.0	11.8	20.1
PT2	30.0	12.5	21.2
PT4	42.0	13.2	20.8

where, $(M_{cr})_{exp}$ = the cracking moment obtained from the experimental test, $(M_e)_{exp}$ = moment at the plate-end when debonding of the soffit plate occurred, P_i = the initial prestressing forces applied to the section.

The results of the linear regression analysis of the cracking moment $(M_{cr})_{exp}$ with the initial prestressing forces P_i as shown in Fig.6-18 is given by the following equation:

$$(M_{cr})_{exp} = 11.0 + k_{10}P_i \qquad (6\text{-}17)$$

where k_{10} = 5.166E-02 (m) and the coefficient of correlation is 0.99. It can be seen in Fig.6-18 that the cracking moment increases with increasing prestressing force. Also, debonding moment increases with increasing prestressing force, as shown in Fig.6-19. The variation of the debonding moment with the initial prestressing forces P_i as shown in Fig.6-19 is given by the following equation:

$$(M_e)_{exp} = 17.0 + k_{11} \ln(P_i) \qquad (6\text{-}18)$$

in which k_{11} = 1.1 (m) and the coefficient of correlation is 0.94.

In conclusion the experimental results show that both the cracking moment and the debonding moment are increased due to prestressing.

6.2.6.2 Comparison of the results between the tests and analytical models

The predicted data in the five different models described in Chapter 5 are compared with the data obtained from the experimental tests. A comparison between the theoretical and experimental cracking moments is given in Table 6.20 and shown in Fig.6-20.

Table 6.20 A comparison of the cracking moments

P_i	$(M_{cr})_{exp}$	$\frac{M_{cr}}{(M_{cr})_{exp}}$		
(kN)	(kNm)	model-2	model-4	model-5
3.00	11.2	0.76	0.84	0.94
18.0	11.8	0.78	0.87	1.04
30.0	12.5	0.83	0.90	1.09
42.0	13.2	0.89	0.93	1.13

in which, M_{cr} = the cracking moment calculated from the analysis described in Chapter 5.

Considering the cracking moment, the predicted data from the three different models, in which the tensile strength of concrete was taken account in the analysis,

are compared with the experimental results. It can be seen in Fig.6-20 that the predicted data calculated from both Model Two and Model Four are lower than that in the experimental test. However Model Five gave the best fit with the experimental tests.

A comparison of the debonding moments are given in Table 6.21 and shown in Fig.6-21.

Table 6.21 A comparison of the debonding moments

P_i	$(M_e)_{exp}$	$\frac{M_e}{(M_e)_{exp}}$				
(kN)	(kNm)	model-1	model-2	model-3	model-4	model-5
3.00	18.2	1.17	1.17	1.25	1.25	1.27
18.0	20.1	1.10	1.11	1.18	1.18	1.20
30.0	21.2	1.08	1.09	1.15	1.16	1.18
42.0	20.8	1.13	1.15	1.21	1.22	1.24

in which, M_e = the debonding moment calculated from analyses, as described in Chapter 5.

It can be seen in Fig.6-21 that the predicted data from all the models are slightly larger than the results obtained from the experimental tests. However the variation of predicted results in the five different models is not significant. Therefore, all models gives reasonable results for the debonding moment.

6.3 Summary

For the fully plated reinforced concrete beams, the shear strength of the beams without shear reinforcement, can be determined from Codes in terms of AS 3600 by assuming the plate is part of the tensile reinforcement. Experimental test have shown that this procedure will underestimate the increase in the shear strength due to the plates. Longitudinal shear stress at the plate/concrete interface up to 80% of the tensile strength of the concrete were achieved without debonding due to shear flow.

For the plated reinforced concrete beams with the external side plates, the shear strength of the beams, without stirrups increased with increases in the thickness and increases in the length of the side plates. Debonding of the side plate can be prevented by ensuring that the length of the side plates is greater than 6.3 times the depth of the beam.

For the plated post-tensioned beams with varying degrees of the initial prestressing forces, the analytical models gave reasonable representation of the behaviour.

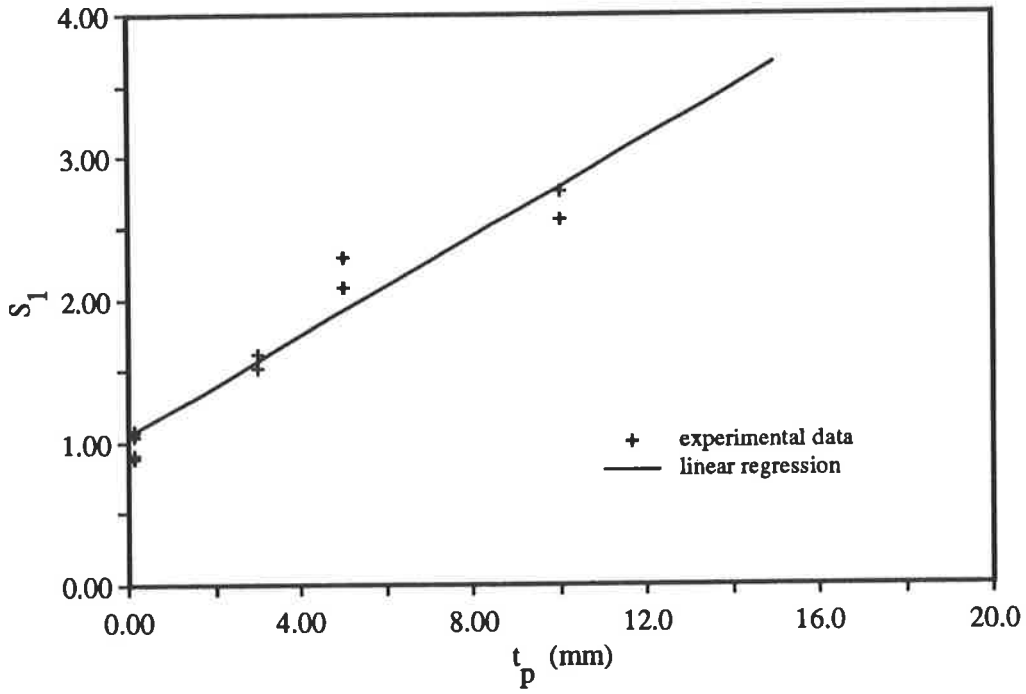

Fig.6-1 The variation of S_1 with t_p

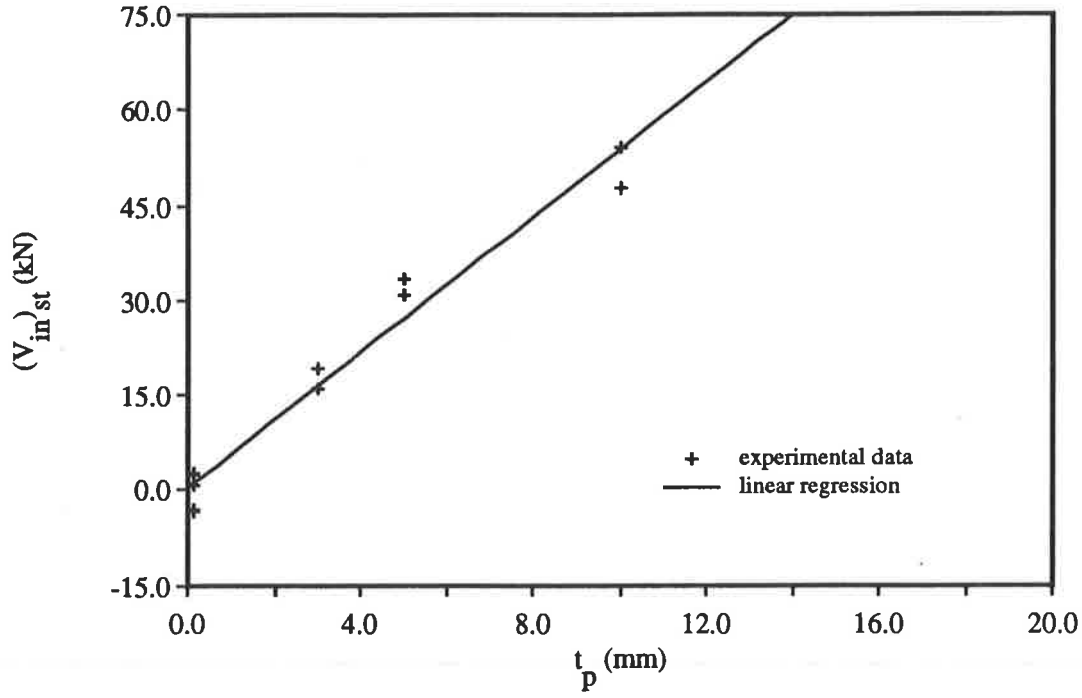

Fig.6-2 The variation of $(V_{in})_{sp}$ with t_p

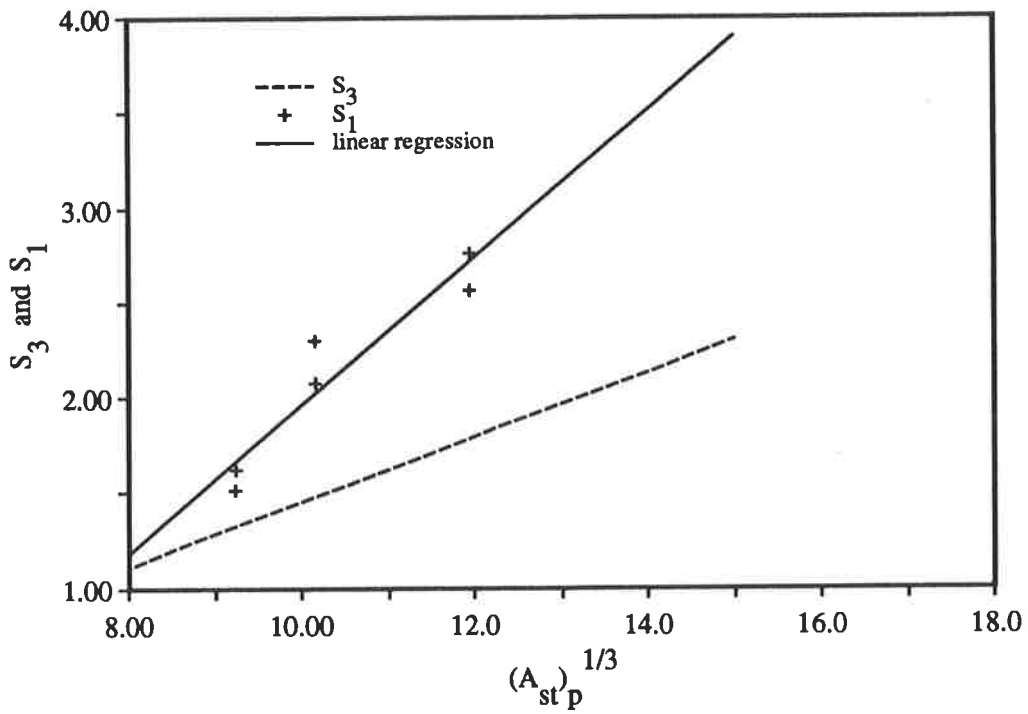

Fig.6-4 The relationship between S_1 and S_3 and $(A_{st})_p^{1/3}$

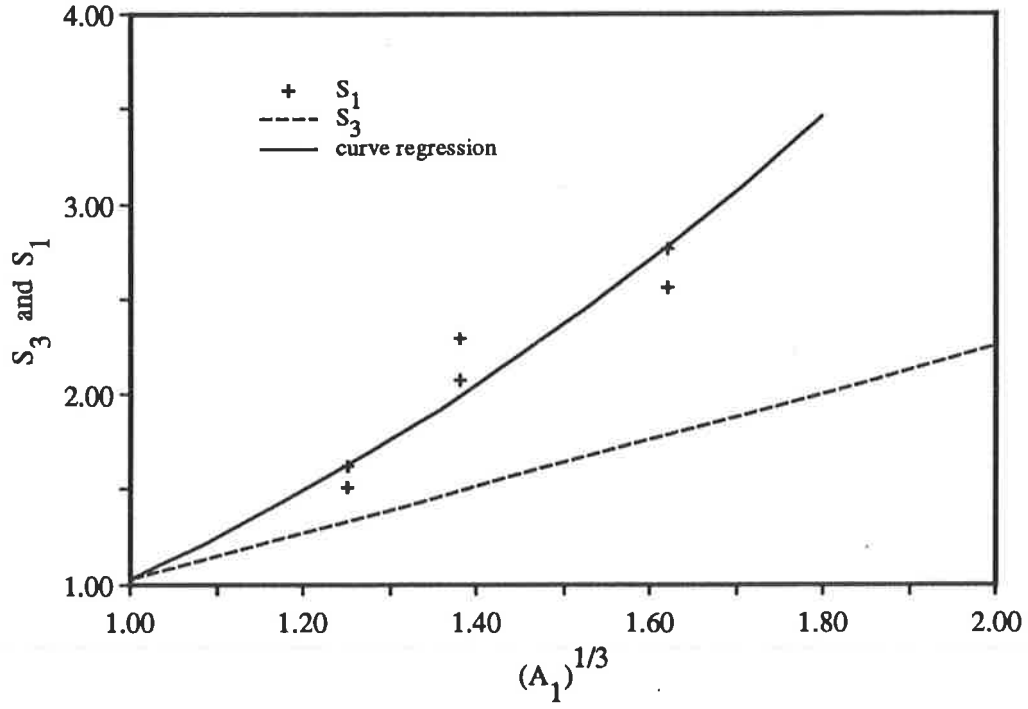

Fig.6-5 The relationship between S_1 and S_3 and $(A_1)^{1/3}$

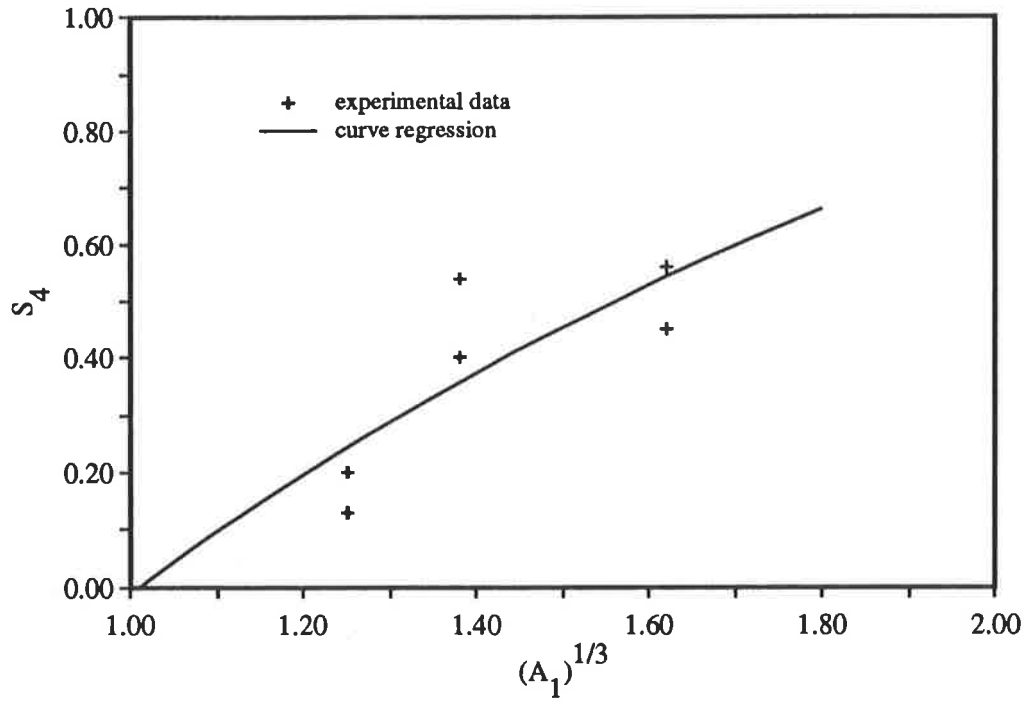

Fig.6-6 The relationship between S_4 and $(A_1)^{1/3}$

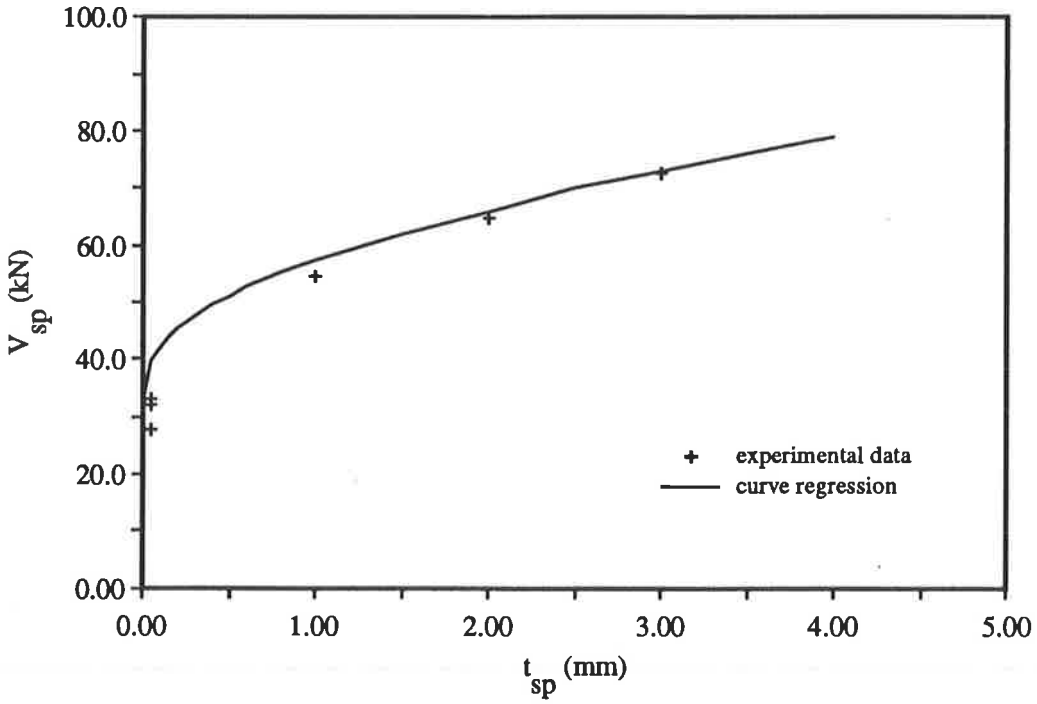

Fig.6-7 The variation of V_{sp} with t_{sp}

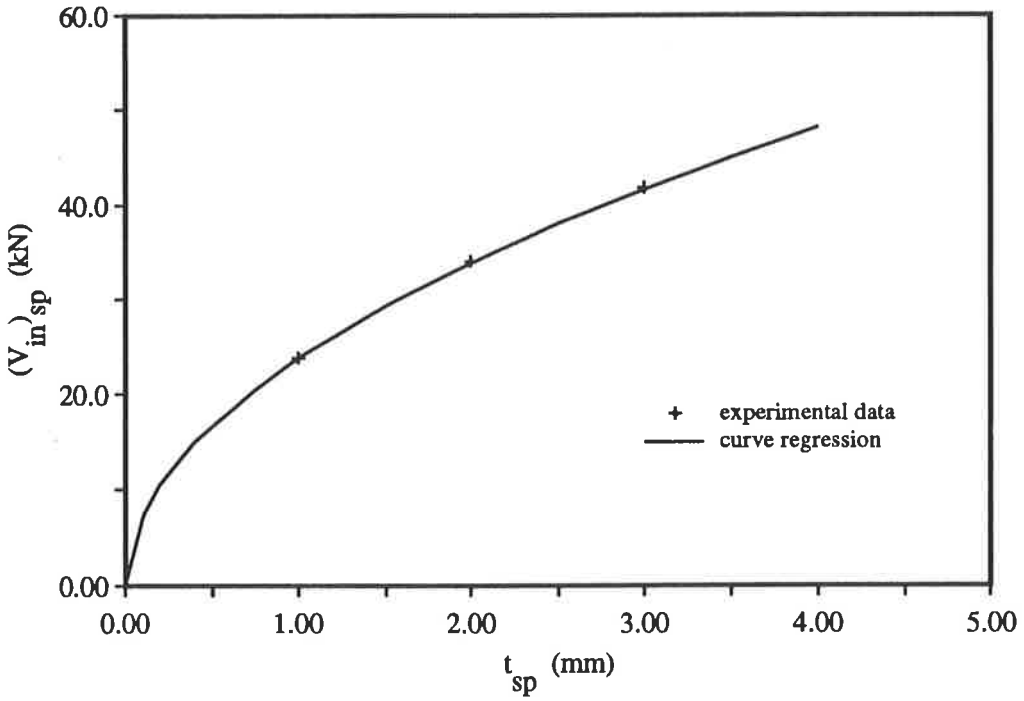

Fig.6-8 The variation of $(V_{in})_{sp}$ with t_{sp}

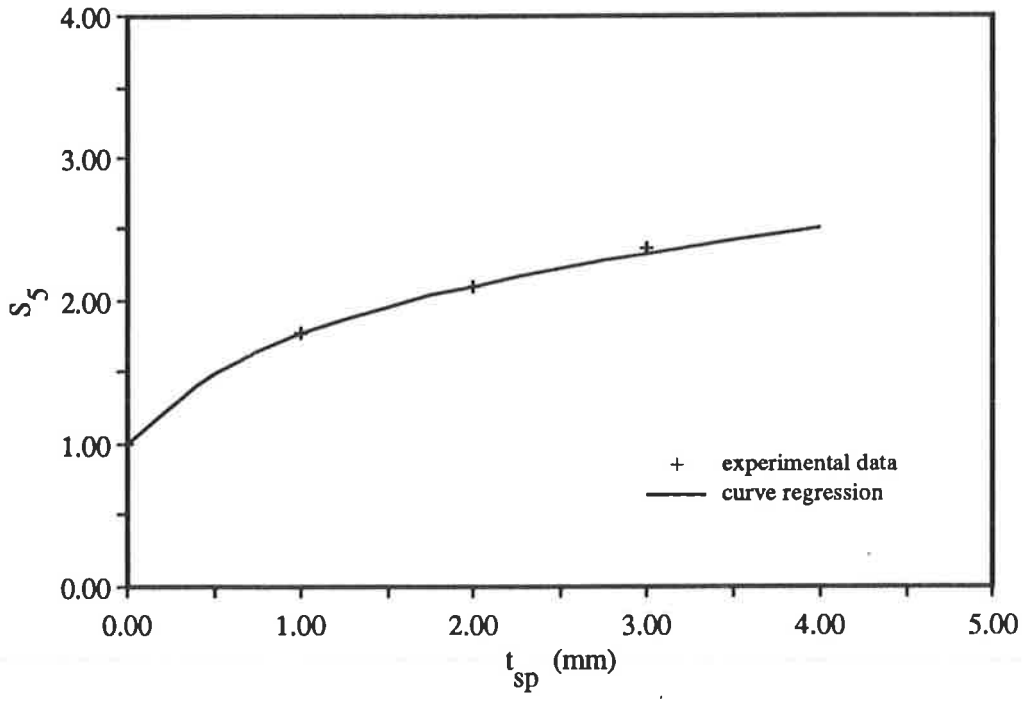

Fig.6-9 The variation of S_5 with t_{sp}

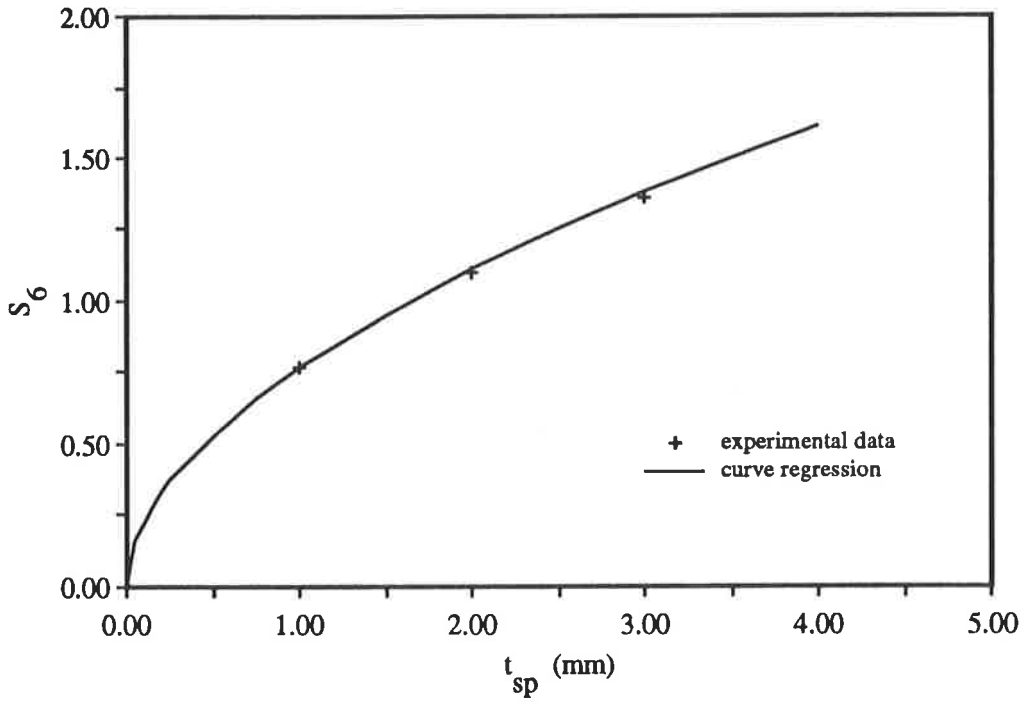

Fig.6-10 The relationship between S_6 and t_{sp}

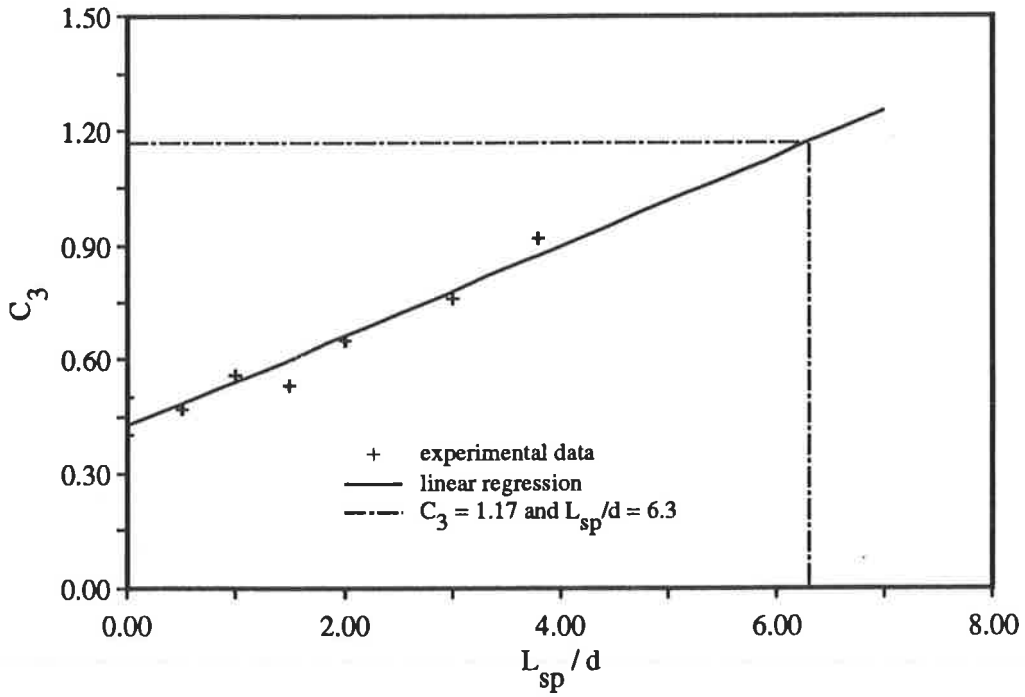

Fig.6-11 The relationship between C_3 and L_{sp}/d

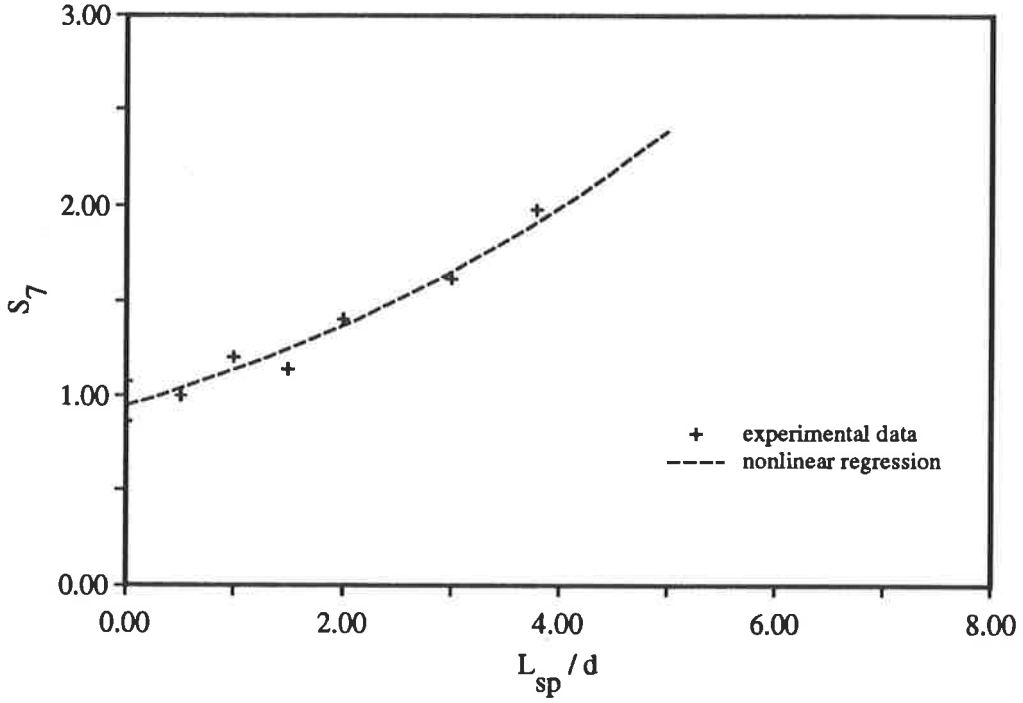

Fig.6-12 The relationship between S_7 and L_{sp}/d

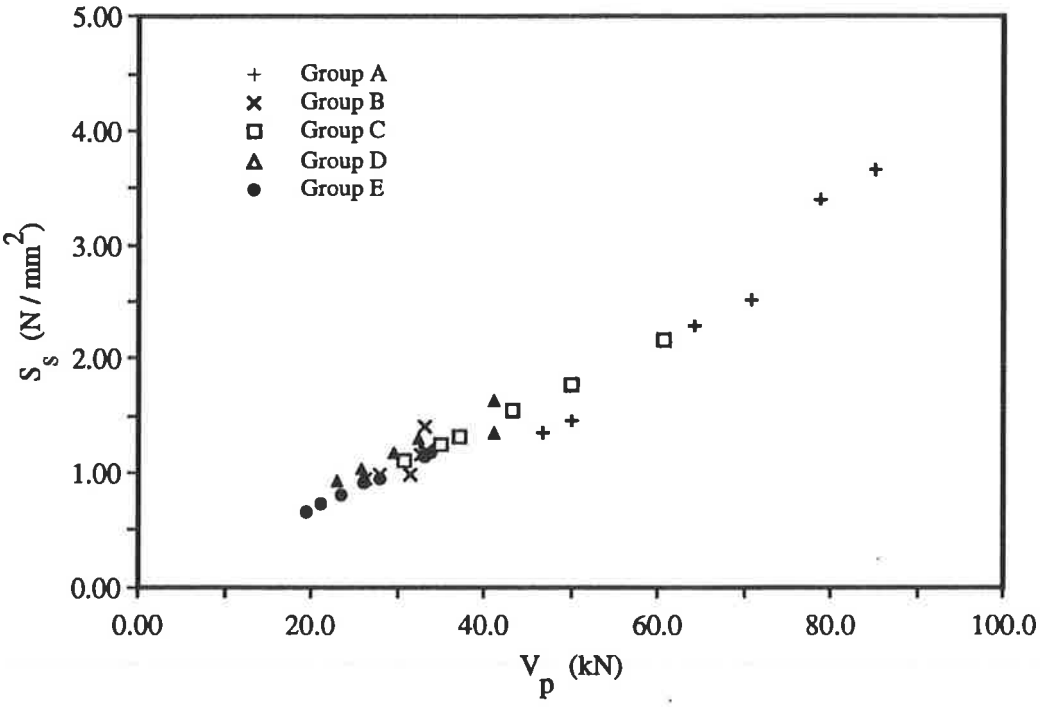

Fig.6-14 The variation of S_s with V_p for plated cracked section

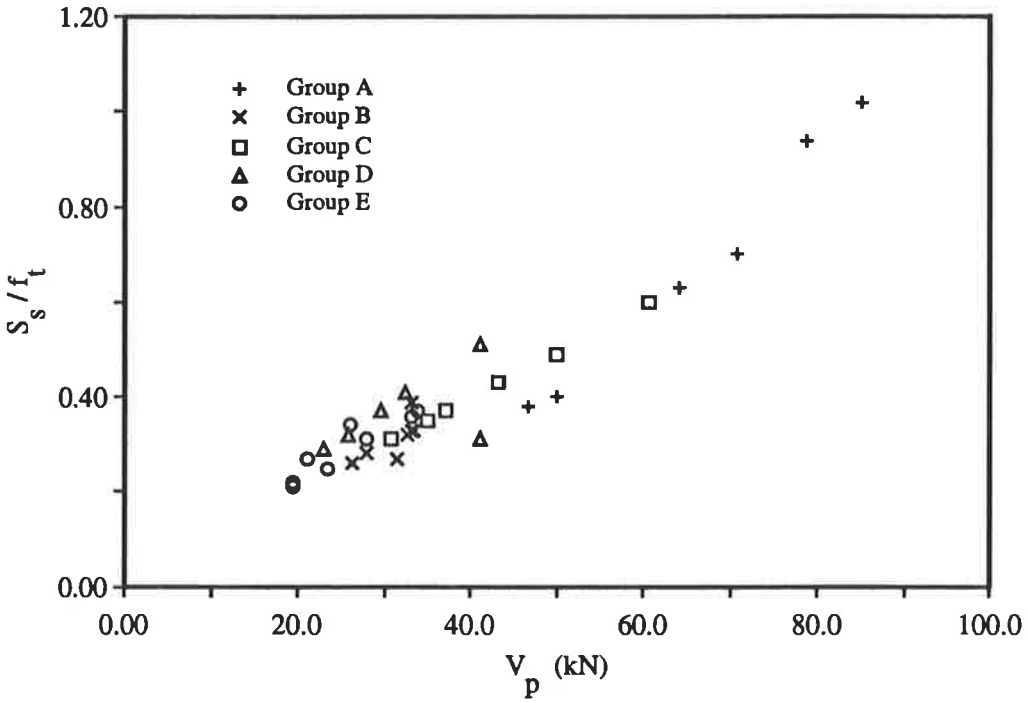

Fig.6-15 The variation of S_s/f_t with V_p for plated cracked section

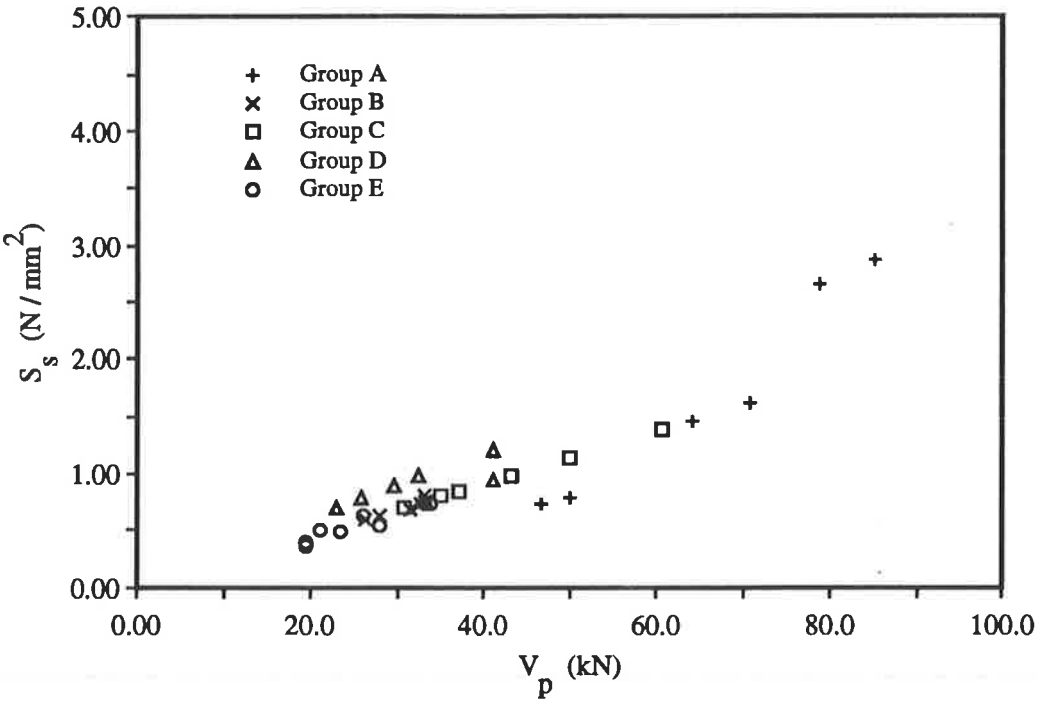

Fig.6-16 The variation of S_s with V_p for plated uncracked section

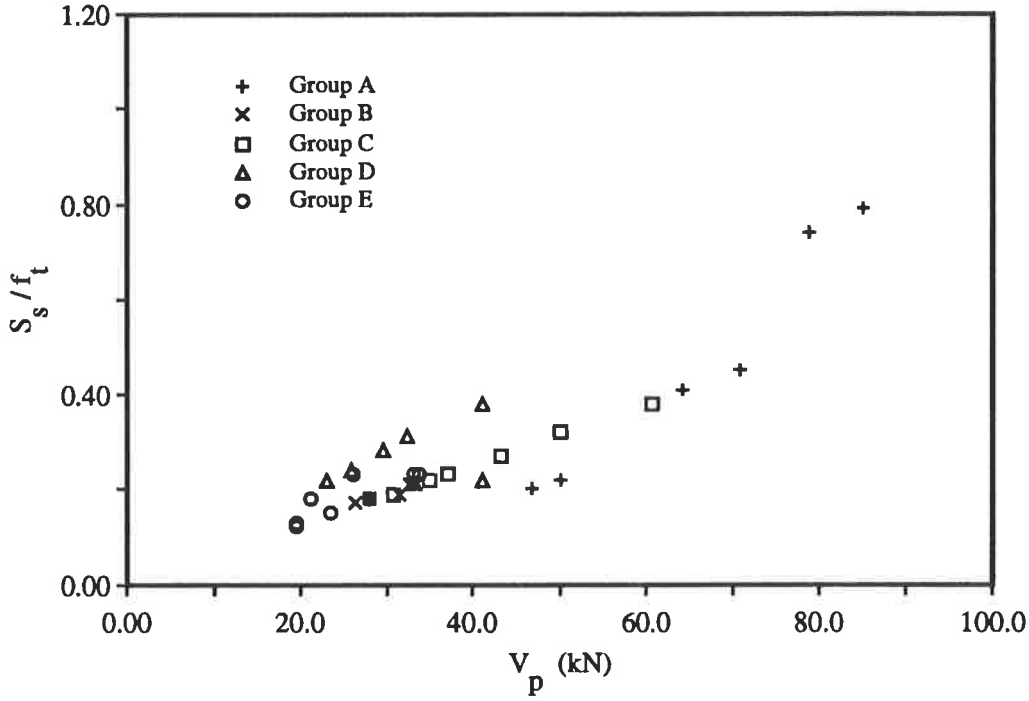

Fig.6-17 The variation of S_s/f_t with V_p for plated uncracked section

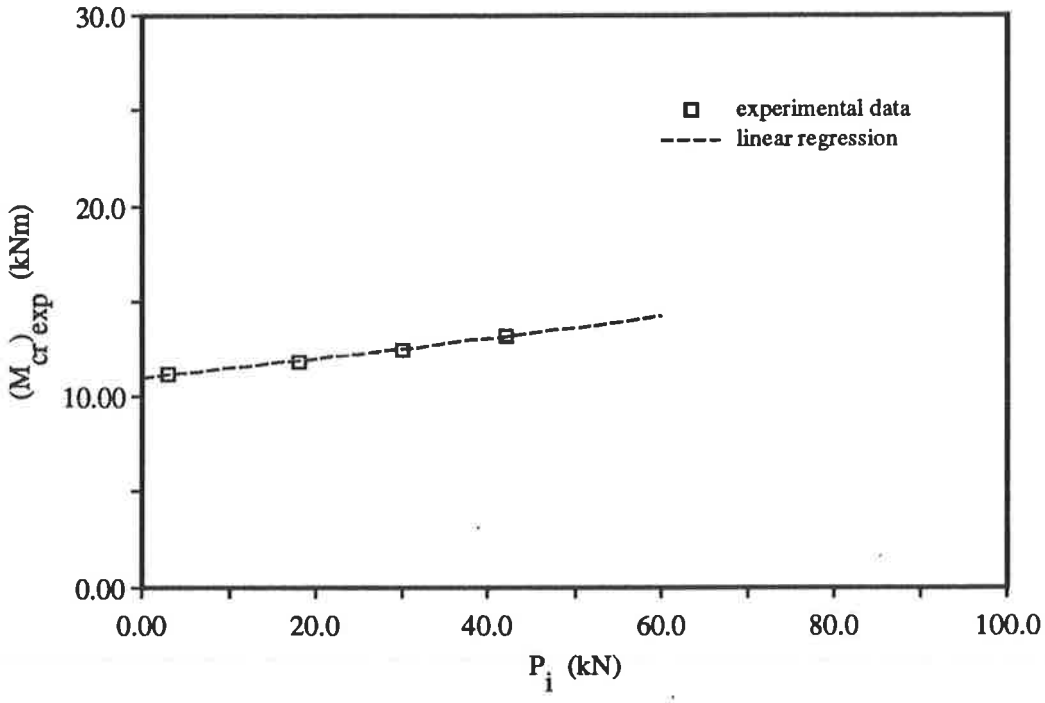

Fig.6-18 The relationship between $(M_{cr})_{exp}$ and P_i

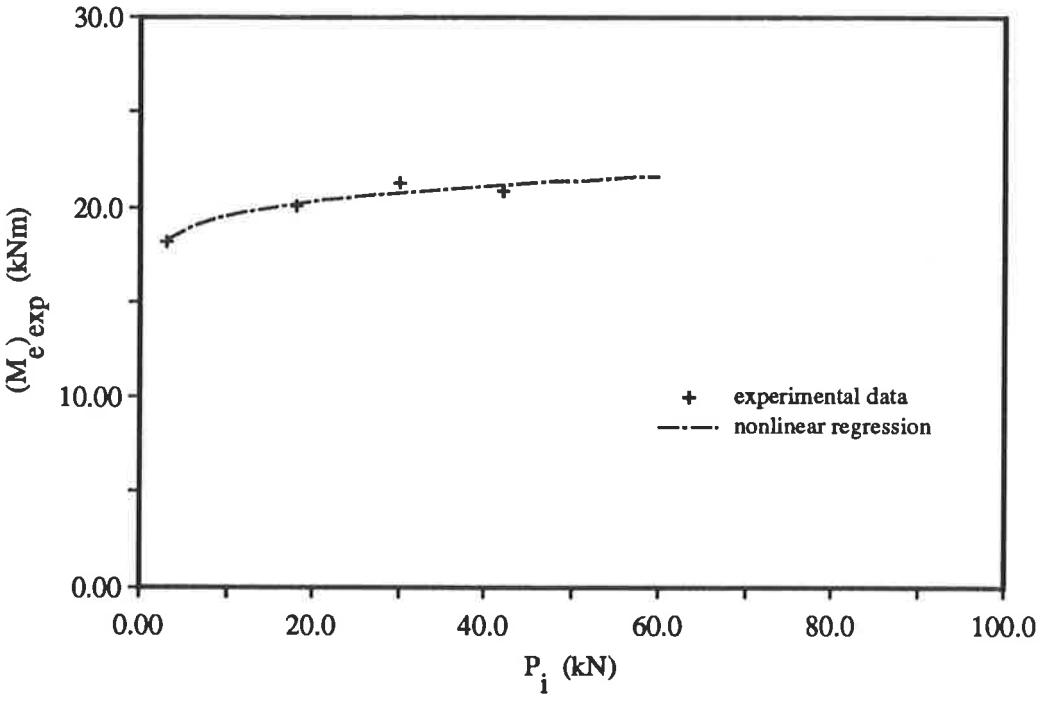

Fig.6-19 The relationship between $(M_e)_{exp}$ and P_i

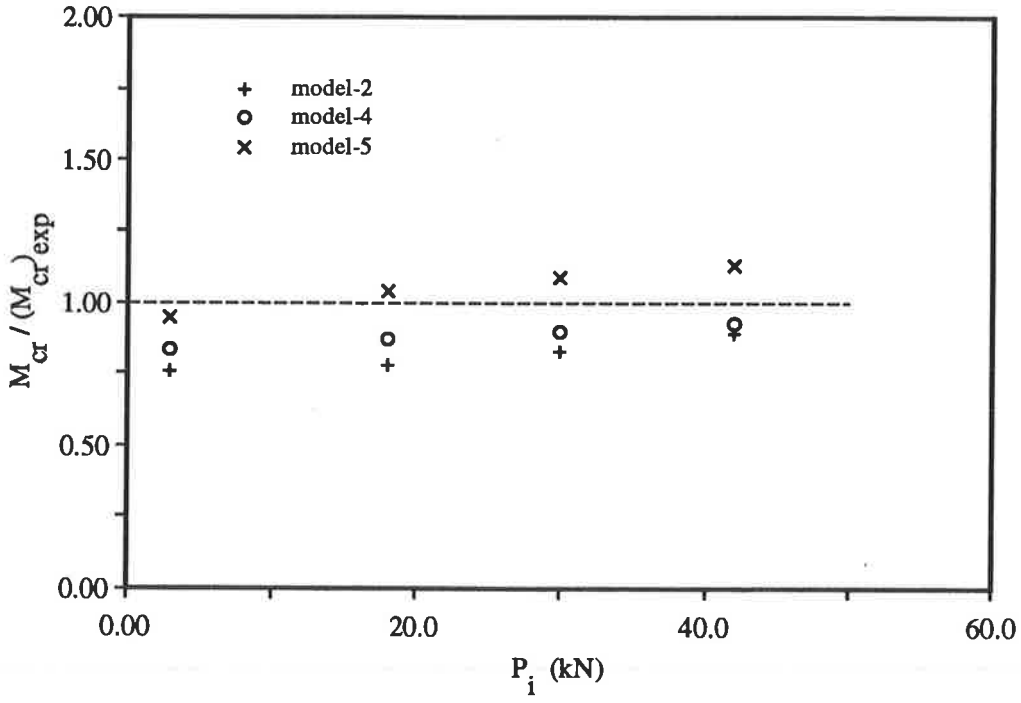

Fig.6-20 A comparison of the cracking moments

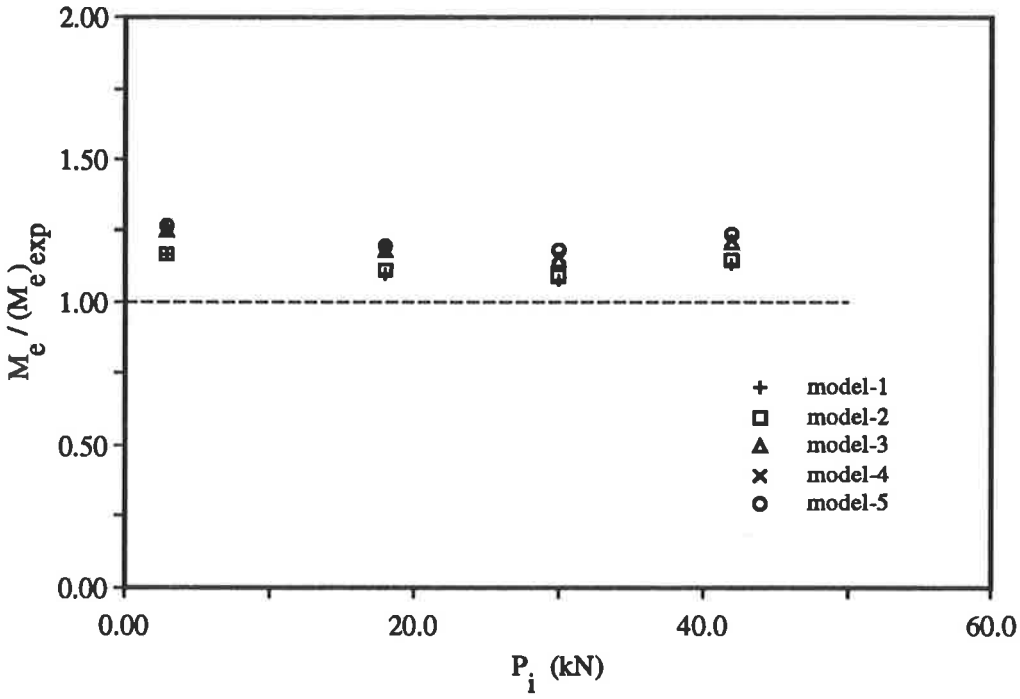

Fig.6-21 A comparison of the debonding moments

Chapter Seven

Conclusions

The following conclusions were drawn from the results of this investigation:

1. Adding steel plates to the sides of reinforced concrete beams increased not only the shear strength of the beams by up to 97% but also increased the debonding moment of the plated reinforced concrete beams by up to 105%.
2. The longer and thicker the side steel plates that were glued to the reinforced concrete beams with, the greater the increase in both the shear strength and the debonding moment of the beams. For this reason, debonding of the soffit plate, in plated reinforced concrete beams, due to shear peeling could be prevented using side plates. Experimental tests showed that this can be achieved by using a length of the side plate of 6.3 times depth of beam. The use of that length of the side plates also restricts the formation of inclined shear cracks in the vicinity of the soffit plate-end.
3. The fully soffit plates can substantially increase the shear strength of the reinforced concrete beam by up to 56 % and debonding is prevented. If the plate is assumed to act as the longitudinal tensile reinforcement being from Codes such as AS3600 give a conservative estimate of the strength of the fully plated reinforced concrete beam.
4. In the experimental tests longitudinal shear stress of up to 80 % of the tensile strength of the concrete were achieved without any signs of debonding due to shear peeling.
5. A computer program was developed to predict the the debonding moment of the soffit plate for the plated reinforced concrete beams with varying degrees of the initial prestressing force. A parametric study showed that the debonding moment increases with increasing initial prestressing forces. The increase in the debonding moment at the plate-end is proportional to the initial prestressing force.

6. A comparison of experimental tests with the results of five analytical models in which the models of simulating the material properties was varied,found that there was not a significant difference to the predicted debonding moment. Also the tension-stiffening effect is small in predicting debonding. This is because the external steel plates act as part of the longitudinal tensile reinforcement and the value of $m\rho$ in the plated beams is much higher than that in the reinforced concrete beams.

References

1. Yacadani, N. and Albrecht, "Risk analysis of fatigue failure of highway steel bridges", ASCE Journal of Structural Engineering, Vol. 113, No. 3, march 1987.
2. R.N. Swamy, R. Jones and J.W. Bloxham, "Structural behaviour of reinforced concrete beams strengthened by epoxy-bonded steel plates", The structural Engineer, Vol. 65, No. 2, Feb. 1987, pp 59-68
3. Deric John Oehlers and John Paul Moran, "Premature failure of externally plated reinforced concrete beams", J. Struct Engrg, ASCE, 116(4), pp 978-995.
4. D.J. Oehlers, "Reinforced concrete beams with plates glued to their soffits", Submitted for publication.
5. T. M. Roberts and H. Haji-Kazemi, "Theoretical study of the behaviour of reinforced concrete beams strengthened by externally bonded steel plates", Proc. Instn Civ. Engrs, Part 2, 89, March, pp 39-55
6. T.M. Roberts, "Approximate analysis of shear and normal stress concentrations in the adhesive layer of plated RC beams", The structural Engineer, Vol. 67, No. 12/20, June 1989, pp 229-233.
7. T.M. Roberts and H. Haji-Kazemi, "Strengthening of under-reinforced concrete beams with mechanically attached steel plates", The international Journal of Cement Composites and Lightweight Concrete, Vol. 11, No.1, Feb. 1989, pp 21-27.
8. G. F. K. Moloney, "The repair and strengthening of reinforced concrete beams with externally bonded mild steel plates", Thesis submitted to the National University of Ireland, June 1986.
9. R.P. Johnson and C. J. Tait, "The strength in combined bending and tension of concrete beams with externally bonded reinforcing plates", Build. Environ , 16(4), pp 287-299

10. ACI-ASCE Task Committee 426, "The shear strength of reinforced concrete members", Proc. ACSE, Vol.99, No.ST6, June 1973, pp 1091-1187.

11. R. Jones, R.N. Swamy, J. Bloxham and A. Bouderbalah, "Composite behaviour of concrete beams with epoxy bonded external reinforcement", International Journal of Cement Composites, Vol.2, No.2, May 1980, pp 91-107.

12. R. Jones, R.N. Swamy and T.H. Ang, "Under and over-reinforced concrete beams with glued steel plates", International Journal of Cement Composites and Lightweight Concrete, Vol.4, No.1, Feb. 1980, pp 19-32

13. R. Jones, R.N. Swamy and J. Bloxham, "Crack control of reinforced concrete beams through epoxy bonded steel plates", Pro. International Conf. on Adhesion between Polymers and Concrete, Aix-en-Provence, Sep. 1986, pp 542-555

14. R.Jones, R.N. Swamy and A. Charif, "Plate separation and anchorage of reinforced concrete beams strengthened by epoxy-bonded steel plates", The Structural Engineer, Vol. 66, No.5/1, March, 1988, pp 85-91

15. M.D. Macdonald, "The flexural performance of 3.5 m concrete beams with various bonded external reinforcements", Supp. Report No. 728, Dept. of the Environment, TRRL, Crowtorne, England, 1982.

16. Warner, R.F. and Faulkes, K.A. (1988). "Prestressed Concrete 2nd Edition", Longman Cheshire, Melbourne, Australia

17. Hogestad E. " A Study of Combined Bending Axial Load in Reinforced Concrete Members," Univ. of Illinois, Eng. Expt. Station Bull, No. 399

18. R.I. Gilbert and R.F. Warner, "Tension Stiffening in Reinforced Concrete Slabs", Proceeding, ASCE, Vol.104, Dec. 1987, pp.1885-1900

19. Domingo J. Carreira and Kuang-Hua Chu, "Stress-Strain Relationship for Reinforced Concrete in Tension", ACI Journal, Proceedings, Vol.83, No.3, Jan.-Feb. 1986, pp.21-28

20. Ajaya K. Gapta and Sergio R. Maestrini, "Tension-Stiffness Model For Reinforced Concrete Bars", Journal Struct. Div., ASCE, Vol.116, No.3, March, 1990, pp.769-790

21. Helmut Floegl and Herbert A. Mang, "Tension Stiffening Concept Based On Bond Slip", Proceeding, ASCE, Vol.108, No. ST112, Dec. 1982, pp.2681-2701

22. D.H. Jiang, S.P. Shah and A.T. Andonian (1984), "Study of the transfer of tensile forces by bond", J.Amer. Concr. Inst., 81(3), pp.251-259

23. D.Z. Yankelevsky (1985), "Bond action between concrete and a deformed bar-A new model", J. Amer. Concr. Inst., 82(2), pp.154-161

24. Australian Standard 3600 - 1988, Concrete Structures, Sydney, Australia